CIVIL ENGINEERING STUDIES
Illinois Center for Transportation Series No. 18-015
UILU-ENG-2018-2015
ISSN: 0197-9191

SEISMIC PERFORMANCE OF SEAT-TYPE ABUTMENT HIGHWAY BRIDGES IN ILLINOIS

Prepared By
James M. LaFave
Larry A. Fahnestock
Jie Luo
Derek L. Kozak

University of Illinois at Urbana-Champaign

Research Report No. FHWA-ICT-18-013

A report of the findings of

ICT PROJECT R27-133
Calibration and Refinement of Illinois' Earthquake Resisting System Bridge Design Methodology: Phase II

Illinois Center for Transportation

August 2018

TECHNICAL REPORT DOCUMENTATION PAGE

1. Report No. FHWA-ICT-18-013	**2. Government Accession No.** N/A	**3. Recipient's Catalog No.** N/A
4. Title and Subtitle Seismic Performance of Seat-Type Abutment Highway Bridges in Illinois		**5. Report Date** August 2018 **6. Performing Organization Code** N/A
7. Author(s) James M. LaFave, Larry A. Fahnestock, Jie Luo, and Derek L. Kozak		**8. Performing Organization Report No.** ICT-18-015 UILU-ENG-2018-2015
9. Performing Organization Name and Address Illinois Center for Transportation Department of Civil and Environmental Engineering University of Illinois at Urbana-Champaign 205 North Mathews Avenue, MC-250 Urbana, IL 61801		**10. Work Unit No.** N/A **11. Contract or Grant No.** R27-133
12. Sponsoring Agency Name and Address Illinois Department of Transportation (SPR) Bureau of Research 126 East Ash Street Springfield, IL 62704		**13. Type of Report and Period Covered** Final Report 10/1/2013 – 8/31/2018 **14. Sponsoring Agency Code** FHWA

15. Supplementary Notes

Conducted in cooperation with the U.S. Department of Transportation, Federal Highway Administration.

16. Abstract

This study assesses the seismic performance of quasi-isolated highway bridges with seat-type abutments, validates the current IDOT design strategy, and provides recommendations for improving a bridge's seismic behavior. To encompass common configurations of highway bridges with non-seismically designed bearing components employed as sacrificial connections between superstructures and substructures, a suite of prototype bridges with variations in span arrangement, girder type, skew angle, pier column height, and foundation soil condition were studied. Detailed three-dimensional nonlinear finite-element models were developed for the bridges, incorporating various critical structural components and geotechnical mechanisms. Multi-mode adaptive pushover analyses were conducted to investigate bridge response characteristics in terms of the force distribution among substructures, the sequence of limit state occurrences, the fusing of sacrificial connections, and the vulnerability of critical bridge components. Eigenvalue modal analyses were also performed in the elastic and inelastic deformation states to reveal modal response characteristics of the bridges. The study culminated in an extensive seismic performance assessment of quasi-isolated bridges, for which thousands of nonlinear dynamic time-history analyses were carried out. The bridges were subjected to a suite of site-specific earthquake ground motions, taking into account the site condition and the regional seismicity of Cairo, Illinois. Assessment results validated that the current quasi-isolation bridge design strategy is generally effective, and the majority of the studied prototype bridges are unlikely to fail in global collapse when subjected to horizontal earthquake ground motions with a 1,000-year return period in deep southern Illinois. Although most of the prototype bridges exhibited satisfactory seismic performance, the response of a small number of them demonstrated a risk of bearing unseating and severe pier column damage. With the aim of improving the seismic performance of these bridges, preliminary recommendations for calibrating the current design strategy were proposed, and their efficacy was demonstrated by comparative studies.

17. Key Words Earthquake engineering; highway bridges; bridge bearings; seismic isolation; quasi-isolation; skew bridges; multi-column piers; soil structure interaction	**18. Distribution Statement** No restrictions. This document is available through the National Technical Information Service, Springfield, VA 22161.

19. Security Classif. (of this report) Unclassified	**20. Security Classif. (of this page)** Unclassified	**21. No. of Pages** 66 pp + appendices	**22. Price** N/A

Form DOT F 1700.7 (8-72) **Reproduction of completed page authorized**

ACKNOWLEDGMENT, DISCLAIMER, MANUFACTURERS' NAMES

This publication is based on the results of **ICT-R27-133, Calibration and Refinement of Illinois' Earthquake Resisting System Bridge Design Methodology: Phase II**. ICT-R27-133 was conducted in cooperation with the Illinois Center for Transportation (ICT); the Illinois Department of Transportation (IDOT); and the U.S. Department of Transportation, Federal Highway Administration (FHWA). Grid resources from the Texas Advanced Computing Center (TACC) at the University of Texas at Austin were used to generate research results reported on within this report.

Members of the Technical Review panel were the following:

- Mark Shaffer, TRP Chair, IDOT
- Nick Barnett, IDOT
- Justin Belue, IDOT
- Dan Brydl, FHWA
- John Ciccone, IDOT
- Patrik Claussen, IDOT
- Chad Hodel, WHKS
- William Kramer, IDOT
- Carl Puzey, IDOT
- Kevin Riechers, IDOT
- Jayme Schiff, IDOT
- Dan Tobias, IDOT

EXECUTIVE SUMMARY

Seismic isolation is one of the most popular strategies to protect civil engineering structures against earthquake hazards. For highway bridges, isolation physically decouples a bridge superstructure from its substructures resting on a shaking ground, leading to a significant reduction in seismic forces transmitted from the superstructure to the substructure and foundation. The isolation technique has conventionally been employed in protecting highway bridges in high-seismic zones, and the decoupling is typically realized by interposing specially designed isolators between bridge superstructures and substructures.

In recent years, bridge engineers at the Illinois Department of Transportation (IDOT) developed an innovative "quasi-isolation" strategy to improve bridge seismic resilience in geographical regions with low-to-moderate seismicity, such as southern Illinois. Different from conventionally isolated bridges, non-seismically designed commonplace bearing components are employed as sacrificial connections between superstructures and substructures of quasi-isolated bridges. During a major earthquake, fusing actions of the sacrificial connections, as well as subsequent bearing deformation and sliding, can reduce seismic demands on bridge substructures and foundations. In conjunction with the sacrificial connections, conservatively designed bearing seat widths at substructures are relied upon to accommodate the displacement demands of bridge superstructures and eventually prevent span loss.

The objectives of this study were to assess the seismic performance of prototype quasi-isolated highway bridges with seat-type abutments, validate the current design strategy, and provide recommendations for improving a bridge's seismic performance. To encompass common configurations of quasi-isolated highway bridges, a suite of prototype bridges with variations in the span arrangement, girder type, skew angle, pier column height, and foundation soil condition were computationally studied. Detailed, yet efficient, three-dimensional nonlinear finite-element models were developed for the bridges, incorporating various critical structural components and geotechnical mechanisms.

Multi-mode adaptive pushover analyses were conducted to investigate bridge response characteristics in terms of the force distribution among substructures, the sequence of limit state occurrences, the fusing of sacrificial connections, and the vulnerability of critical bridge components. Additionally, eigenvalue modal analyses were performed in the elastic and inelastic bridge deformation states to reveal modal response characteristics of the bridges. The study culminated in a comprehensive and extensive seismic performance assessment of prototype quasi-isolated bridges, for which thousands of nonlinear dynamic time-history analyses were carried out using a supercomputer. The bridges were subjected to a suite of site-specific earthquake ground motions, taking into account the site condition and the regional seismicity of Cairo, Illinois.

The assessment results validated that the current quasi-isolation bridge design strategy is generally effective, and the majority of the studied prototype bridges are unlikely to fail in global collapse when subjected to horizontal earthquake ground motions with a 1,000-year return period in deep southern Illinois. Although many of the prototype bridges exhibited satisfactory seismic performance, the

response of a small number of them demonstrated a high risk of bearing unseating and severe pier column damage. With the aim of improving the seismic performance of these bridges, preliminary recommendations for calibrating the current design strategy were proposed, and their efficacy was demonstrated by comparative studies.

TABLE OF CONTENTS

LIST OF FIGURES

LIST OF TABLES

CHAPTER 1: BACKGROUND

1.1 MOTIVATION

In early 2008, the American Association of State Highway and Transportation Officials (AASHTO) published revised standards for the design of earthquake-resistant highway bridges, namely the AASHTO Load and Resistance Factor Design (LRFD) Bridge Design Specifications (AASHTO 2008a) and AASHTO Guide Specifications for LRFD Seismic Bridge Design (AASHTO 2008b). In the revised standards, the return period of the design earthquake was increased from 500 years to 1,000 years for the first time. The longer return period represents a significant increase in design accelerations for highway bridges in the West Coast with high seismicity and some regions in the Midwest and East Coast. This includes the southern Illinois area, where high-magnitude low-probability seismic hazards have also been a primary concern for the safety of transportation infrastructures.

In response to the increased demand on seismic design and the construction of highway bridges, bridge engineers of the Illinois Department of Transportation (IDOT) developed an innovative framework for the design, the construction, and the retrofit of earthquake resisting system (ERS) highway bridges in the state of Illinois (Tobias et al. 2008; IDOT 2012a). Conventional bridge isolation strategies using seismically designed isolators, restrainers, and dampers are typically employed in regions with high seismicities, such as the Western United States. Friction pendulum bearings (Dao et al. 2013) and lead-rubber bearings (Robinson 1982) are typically used for conventionally isolated structures. In contrast, the quasi-isolated bridge system features a simplified and economical design and construction process, yet it is expected to protect the highway bridges in regions with moderate seismicities, such as southern Illinois in the Midwestern United States, from excessive seismic damage and collapse.

The quasi-isolation strategy employs non-seismically designed sacrificial connections between bridge superstructures and substructures in conjunction with conservatively designed bearing seat widths at substructures. During a major earthquake, damage and the failure of these fuse-like connections are expected to limit superstructure inertia forces transferred down to substructures and foundations, dissipate seismic energy, and elongate structural periods. This results in protecting bridge substructures and foundations from severe seismic damage. After the fusing of the sacrificial connections during a major earthquake, bridge superstructures may slide onto substructures with only weak restraints comprised mainly of frictions at bearing-substructure interfaces. Sliding and the displacement response of superstructures and bearings is accommodated by the conservatively designed bearing seat width at substructures. As the primary objective of IDOT's ERS bridge design strategy, the conservative seat width is relied upon to prevent the loss of bridge span (IDOT 2012a), which can directly result in the disruption of transportation lifelines and cause loss of life.

In the quasi-isolation bridge design strategy of Illinois, three tiers of seismic structural redundancy are strategically employed to prevent excessive seismic damage and span loss during major earthquakes (Tobias et al. 2008). The first tier consists of sacrificial superstructure-

substructure connections, such as Type I elastomeric expansion bearings, bearing transverse retainers, low-profile steel fixed bearings, and steel dowel connections. These connections are designed as the weakest fuses with relatively small fusing capacities in the entire bridge system. The second tier is the conservatively designed bearing seat width at substructures. This tier is intended to prevent bridge span loss by accommodating large superstructure and bearing displacements after fusing of the first tier. As the last tier of seismic structural redundancy, limited yielding and damage of the substructure and foundation components, such as reinforced-concrete (RC) pier columns, foundation piles, and backfill/embankment soil, is allowed to occur. Preferably, the capacity of these components should be larger than that of the sacrificial superstructure-substructure connections in the first tier.

Based on the motivations described, the objectives of this research were to assess the seismic performance of prototype quasi-isolated highway bridges with seat-type abutments, reveal the seismic response characteristics of bridges with various permutations of typical configurations, identify deficient performance and potential risks of severe damage to critical components and global bridge collapse, and recommend practical strategies for seismic performance improvement. These objectives were accomplished through an extensive and comprehensive computational investigation on a suite of prototype quasi-isolated bridges. The bridges are supported by non-skew and skew seat-type abutments in conjunction with reinforced concrete (RC) multi-column intermediate piers.

1.2 REPORT ORGANIZATION

The primary goal of this research was to investigate the seismic behavior of typical seat-type abutment bridges in Illinois, assess their performance, and identify any potential risks in their seismic design which should be addressed. The report presents the results of computational modeling of typical IDOT IAB configurations, conducted from 2013 through 2017 in the Department of Civil & Environmental Engineering at the University of Illinois at Urbana-Champaign. The following is a summary of the contents of this report.

Chapter 1 discusses the motivation for the research and provides an overview of past seat-type abutment bridge studies and past computational modeling of seat-type abutment bridges.

Chapter 2 discusses the parametric variations of the prototype bridges explored in this study. This chapter also details the computational modeling procedure for the bridge models.

Chapter 3 outlines the procedure used to perform dynamic analyses.

Chapter 4 presents overall dynamic results for the 80 bridge variants described in Chapter 2.

Chapter 5 explores potential design recommendations to enhance the seismic behavior of seat-type abutment bridges in Illinois.

Chapter 6 summarizes the key results and design recommendations determined. Recommendations for further research are also provided.

1.3 LITERATURE REVIEW

1.3.1 Prior Research on Quasi-Isolated Highway Bridges in Illinois

In order to calibrate and refine the earthquake resisting system (ERS) bridge design methodology, IDOT and the Illinois Center for Transportation (ICT) sponsored a research project with the University of Illinois at Urbana-Champaign. During its first phase (Project No. ICT-R27-070) that was completed in 2013, experimental and computational investigations were carried out primarily in the following research areas:

- Laboratory experimental tests on full-scale specimens of typical bearing components for quasi-isolation
- Computational modeling of bearing components validated and calibrated using full-scale experimental results
- Computational modeling of complete bridge systems
- Parametric studies employing complete bridge models and synthetic ground motions to explore system-level seismic performance for a suite of prototype Illinois bridges
- Recommendations for improving seismic design of quasi-isolated ERS bridges based on experimental and computational results

Detailed results of these investigations have been documented in published technical reports (LaFave et al. 2013a,b) and journal articles (Steelman et al. 2013, 2014, 2016; Filipov et al. 2013a,b). Summarized approaches and important findings and conclusions are reviewed below.

The experimental testing program on full-scale specimens of typical bridge bearing components in Illinois was conducted in the Newmark Civil Engineering Laboratory at the University of Illinois at Urbana-Champaign (LaFave et al. 2013a; Steelman 2013). The experimental setup was designed to simulate real seismic loading conditions for the bearing components installed in bridges. Full-scale specimens of three types of non-seismically designed bridge bearings were tested, namely steel-reinforced laminated elastomeric expansion bearings (IDOT Type I bearings), bearings comprised of a steel-reinforced laminated elastomer and a stainless steel-on-Teflon sliding surface (IDOT Type II bearings), and low-profile steel fixed bearings. These bearing components were tested under various monotonic and cyclic, quasi-static and dynamic displacement protocols in the longitudinal and transverse bridge directions. These experiments yielded valuable information concerning the behavior of bearings and retainers under dynamic loads.

Filipov et al. (2013a) developed a coupled bi-directional nonlinear element to capture the shear and sliding behavior of Type I and II elastomeric bearings using experimentally tested bearing response data. The model captures a number of distinct phases of bearing shear and sliding behavior by using multiple coefficients of friction, namely an initial static coefficient of friction μ_{SI}, a kinetic coefficient of friction, μ_K, and a stick-slip coefficient of friction μ_{SP}. Figure 1.1a shows

the schematic of shear and sliding behavior of the bearing element. The model has been validated and calibrated using results of experimental tests on full-scale bearing specimens.

A coupled bi-directional nonlinear element was developed to capture the elasto-plastic behavior of the steel anchor bolts securing low-profile steel fixed bearing into concrete when subjected to horizontal shear demands (LaFave et al. 2013b; Filipov et al. 2013b). Figure 1.1b schematically illustrates the force-displacement relation of the model. Additionally, the model for sliding behavior of elastomer on concrete is superimposed to the steel anchor model, in order to simulate the post-fusing sliding at the elastomeric pad-concrete interface. This combination of two different types of models was also validated against experimental results.

Yielding and the rupture of the retainer anchor bolt under lateral forces were modeled using a unidirectional elasto-plastic computational model (LaFave et al. 2013b; Filipov et al. 2013b). Figure 1.1c schematically illustrates the force-displacement relation of the model.

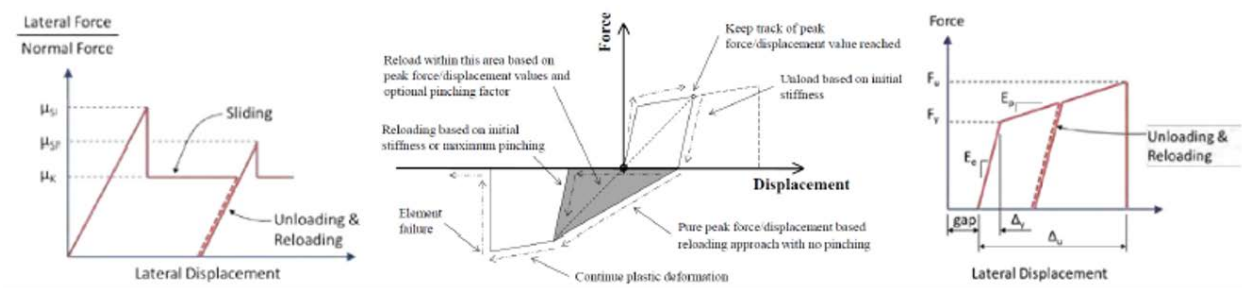

(a) (b) (c)

Figure 1.2: Schematic of computational model for (a) stick-slip and friction behavior of elastomeric bearings (after LaFave et al. 2013b; Filipov et al. 2013a), (b) elasto-plastic shear behavior of steel fixed bearing anchors (after LaFave et al. 2013a; Filipov et al. 2013b), and (c) elasto-plastic behavior of bearing retainer anchors (after LaFave et al. 2013b; Filipov et al. 2013a).

In the computational parametric study conducted in the first phase of the research project, a suite of 48 quasi-isolated highway bridges with three-span continuous superstructures, non-seismically designed bearing components, and non-skew seat-type abutments were developed (LaFave et al. 2013b; Filipov et al. 2013b). A suite of 20 synthetic ground motions developed by (Fernandez and Rix 2008) with an approximately 1,000-year return period were employed in nonlinear dynamic bridge analyses. A number of important observations were made from the nonlinear dynamic bridge analysis results and are briefly summarized as follows:

- Most of the bridges did not experience bearing unseating under design-level earthquake excitations.
- Bridges equipped with Type I elastomeric bearings demonstrated reliable behavior in preventing bridge span loss. For bridges equipped with Type I bearings, unseating was not observed when the bridges were subjected to longitudinal earthquake ground

motions. However, unseating was observed when the bridges were subjected to MCE-level transverse earthquake ground motions.

- Bridges equipped with Type II elastomeric bearings were shown to be more prone to unseating than those with Type I bearings.
- The displacement response of bridges with tall piers and Type II bearings was significantly larger than the other bridges.
- The response of a few bridges under bi-directional seismic excitation was found to be smaller than their response under uni-axial ground motions.

Based on the dynamic analysis results, a few recommendations were made for improving the quasi-isolation strategy:

- The use of Type II elastomeric bearings should be limited to regions of low or moderate seismicity due to their high risk of unseating.
- Type I bearings are appropriate for use in regions of all different seismic hazard levels.
- Using the contribution from the abutment backwall to limit bridge longitudinal response should be considered in seismic bridge design.

1.3.2 Modeling of Seat-Type Bridge Abutments for Seismic Analysis

Seat-type abutments are commonly used for highway bridges in many regions of the United States. The structural components of a typical seat-type abutment may include a backwall, two wingwalls, a stem wall (pile cap) and piles, an approach slab, and bearing components. A primary feature that distinguishes seat-type bridge abutments from integral and semi-integral abutments is that an expansion joint is set between the abutment backwall and the adjacent superstructure end to accommodate thermally induced bridge deformation by separating the superstructure from abutments.

The abutment backwall and wingwalls are traditionally designed to withstand the active pressure of backfill soil and maintain the integrity of the abutment. The design of abutments for service conditions is relatively straightforward, which typically ensures that the reinforced concrete walls, foundation, and connections can withstand the gravity load of the bridge superstructure and the traveling vehicles, as well as the active pressure of backfill soil. However, complications arise when seismic demands are considered. Seat-type abutments and their foundations provide considerable resistance to the longitudinal seismic displacements of bridge superstructures and, in return, are subjected to large seismic force demands brought by the superstructures. A number of post-earthquake reconnaissance reports have indicated seismic bridge damage and failures caused by superstructure-abutment-foundation interactions under moderate to strong earthquakes. This includes the unseating of superstructures at abutments (Buckle 1994; Elnashai et al. 2010; Kawashima et al. 2011; Lee and Loh 2000; Yen et al. 2011), overturning and large residual displacements of abutment foundations (Jennings

1971; Sardo et al. 2006), local pounding damage and the global failure of concrete backwall (Lee and Loh 2000; Sardo et al. 2006; Yen et al. 2011), excessive deformation of the backfill and embankment soil (Lee and Loh 2000), as well as shear key failure (Shamsabadi 2007; Kawashima et al. 2011; Yen et al. 2011).

In view of the seismic damage and failures of bridge abutments, researchers have conducted various investigations to better understand and properly model abutment response characteristics and superstructure-abutment-foundation interactions under seismic demands. In recent years, a number of large-scale field experimental tests on the capacity and stiffness properties of seat-type abutments in passive conditions were carried out (e.g. Stewart et al. 2007; Bozorgzadeh et al. 2008; Wilson and Elgamal 2010). In addition to experimental tests, analytical studies (Wilson 1988; Shamsabadi et al. 2005, 2007) were also conducted to estimate the stiffness and capacity characteristics of bridge abutments for seismic performance-based bridge design and analysis.

Besides the experimental and analytical investigations, numerical simulations (Crouse et al. 1987; Martin et al. 1997; Rollins et al. 2010b) and system identifications (Werner et al. 1987; Wilson and Tan 1990; Goel and Chopra 1997) were also conducted to investigate the stiffness and capacity characteristics of bridge abutments during earthquakes and the implications for seismic bridge response.

1.3.3 Seismic Response Analysis of Highway Bridges with Seat-Type Abutments

The seismic response of seat-type abutment highway bridges has been extensively studied by many researchers over the past several decades using various analytical, numerical, and experimental approaches. A number of representative computational and analytical studies published in the 21st century are reviewed herein. Among all the studies on the seismic response analysis of highway bridges, these studies are most relevant to the present research, in terms of the methodology or conclusion.

Zhang and Makris (2002) employed a stick-spring bridge model and a more sophisticated finite element model to compute the seismic response of two instrumented highway bridges in California, taking into account the soil-structure interaction at bridge embankments. It was concluded that the seismic bridge response can be reliably estimated with the stick-spring bridge model under certain conditions.

Nielson and DesRoches (2007) conducted seismic evaluations for a multi-span simply supported and a multi-span continuous girder bridge with typical configurations in the Central and Southeastern United States. It was concluded that the response of multi-span continuous-girder bridges was found to be predominant in the longitudinal direction, and a 2-D longitudinal model may be used for assessing the seismic risk of this type of bridge. The multi-span simply-supported bridge was found to sustain a similar degree of bearing deformations in the longitudinal and transverse directions.

Kalantari and Amjadian (2010) developed an analytical method for the dynamic analysis of skewed highway bridges with a continuous rigid deck. It was claimed by the authors that this method can be used by bridge engineers for the preliminary seismic design of skew bridges.

Mitoulis (2012) performed a comparative study on the seismic response of three real seat-type abutment bridges with various total length, expansion joint opening width, and backfill models. The author claimed that the seismic participation of seat-type abutments and backfill soil can lead to cost-effective bridge design as the participation of seat-type abutments can reduce the member size of pier columns, bearings, and foundations or be utilized as a second line of defense against seismic demands.

Kaviani et al. (2012) conducted extensive seismic analyses on reinforced concrete highway bridges with skew-angled seat-type abutments. The analysis results indicated that the seismic response of skew bridges, such as deck rotation and column drift, was higher than the equivalent non-skew bridges under the same seismic excitation, and that skew bridges are more prone to collapse then non-skew ones. It was also found that the seismic response of skew bridges was largely affected by the bridge skew and column height, but appeared to be insensitive to the span arrangement.

Kwon and Jeong (2013) studied one-and two-span skew highway bridges supported by elastomeric bearings. The bridge skew was found to have important effects on deck end displacements in the abutment-normal direction. It was also concluded that the minimum seat width specified by AASHTO may not be conservative enough for preventing deck unseating of bridges when subjected to near-fault ground motions.

Through reviewing the existing studies, it was learned that the computational bridge model should at least incorporate reasonably developed nonlinear models for bearing components, pier columns, and abutments. Specifically, the superstructure-abutment interaction effect needs to be sufficiently accounted for by the abutment model, so that the dynamic pounding forces between abutments and deck ends, the unseating of deck ends at abutments, the rotation of skew bridge decks, and other critical seismic responses of seat-type abutment bridges can be captured. In contrast, the bridge superstructure is typically modeled using linear elastic beam or shell elements to save computational cost, as it is not expected to sustain excessive seismic damage.

CHAPTER 2: COMPUTATIONAL MODELING OF PROTOTYPE QUASI-ISOLATED BRIDGES

To comprehensively investigate the seismic response characteristics of quasi-isolated seat-type abutment highway bridges in Illinois, a suite of prototype bridges were computationally modeled for subsequent studies. The suite encompasses three-span and four-span bridges with steel-plate and prestressed-precast-concrete (PPC) girders, which are categorized into four major types of bridges based on the span arrangement and girder type. For each of the four major bridge types, 20 bridge variants that differ in the skew angle, pier column height, and foundation soil condition were included, in order to investigate the effect of these parameters on bridge seismic response. The 80 bridge variants in total were intended to represent both the common existing quasi-isolated bridges and the design trends for future bridges in the state of Illinois.

The nonlinear finite-element package Open System for Earthquake Engineering Simulation (*OpenSees*) was employed to computationally model the bridges. Detailed three-dimensional (3-D) finite-element models were created for all the 80 prototype bridge variants. The finite-element bridge model includes various nonlinear materials and elements for modeling critical structural components and geotechnical mechanisms of the bridges.

2.1 PROTOTYPE QUASI-ISOLATED HIGHWAY BRIDGES

In this study, a suite of 80 prototype quasi-isolated highway bridges was computationally modeled. The bridges comprise permutations of configurations including three and four spans, steel-plate and PPC girders, five bridge skew angles 0°, 15°, 30°, 45°, and 60°), and pier columns with two different clear heights (4.6 m (15 ft) and 12.2 m (40 ft)), as well as soft and hard foundation soil conditions, as shown in Table 2.1. The design of these bridges, complied with AASHTO and IDOT bridge design specifications (AASHTO, 2010, 2011; IDOT, 2012a), is intended to represent existing quasi-isolated bridges in Illinois and bridges that are planned for future construction. Each of the prototype bridges is uniquely referred to using nomenclature comprised of eight characters, as illustrated in Figure 2.1. For instance, “3S45P15H” refers to the three-span steel-plate-girder (3S) bridge with a skew of 45°, pier columns with a clear height of 4.6-m (15-ft) (P15), and hard foundation soil (H). The first two characters denote the four basic bridge types (3S, 4S, 3C and 4C), which are defined based on the bridge superstructure.

Table 2.7: Prototype Quasi-Isolated Bridge Variants for Computational Studies

Component	Alternatives	3-span steel (3S)				4-span steel (4S)				3-span concrete (3C)				4-span concrete (4C)				Variants
		1	2	3	4	5	6	7	8	9	10	11	12	13	14	15	16	
Span length [m (ft)]	24.4-36.6-24.4 (80-120-80)	✓	✓	✓	✓					✓	✓	✓	✓					4
	44.2-48.8-48.8-44.2 (145-160-160-145)					✓	✓	✓	✓					✓	✓	✓	✓	
Pier column height [m (ft)]	4.57 (15)	✓		✓		✓		✓		✓		✓		✓		✓		2
	12.19 (40)		✓		✓		✓		✓		✓		✓		✓		✓	
Foundation soil condition	Hard	✓	✓			✓	✓			✓	✓			✓	✓			2
	Soft			✓	✓			✓	✓			✓	✓			✓	✓	
Skew angle	0°, 15°, 30°, 45°, 60°	5 skew angles are considered for each of the above 16 combinations.																5
Total number of bridge variants		**80**																

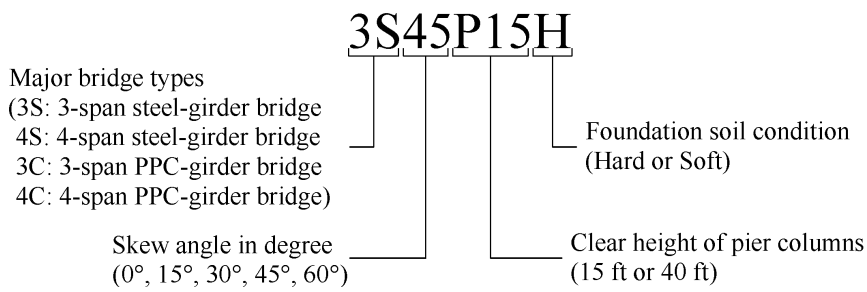

Figure 2.3: Nomenclature for prototype bridge variants.

Figure 2.2 depicts the three- and four-span prototype bridges with their critical components annotated. The three-span continuous superstructure comprises six girders, transverse diaphragms, and a concrete slab on top of the girders. The four-span continuous superstructure consists of the same components, but the number of girders is increased to seven. The superstructure is supported by two seat-type abutments and two or three intermediate reinforced-concrete (RC) multi-column piers. The piers and abutments are supported by steel H piles. Table 2.2 provides detail information for the critical bridge components.

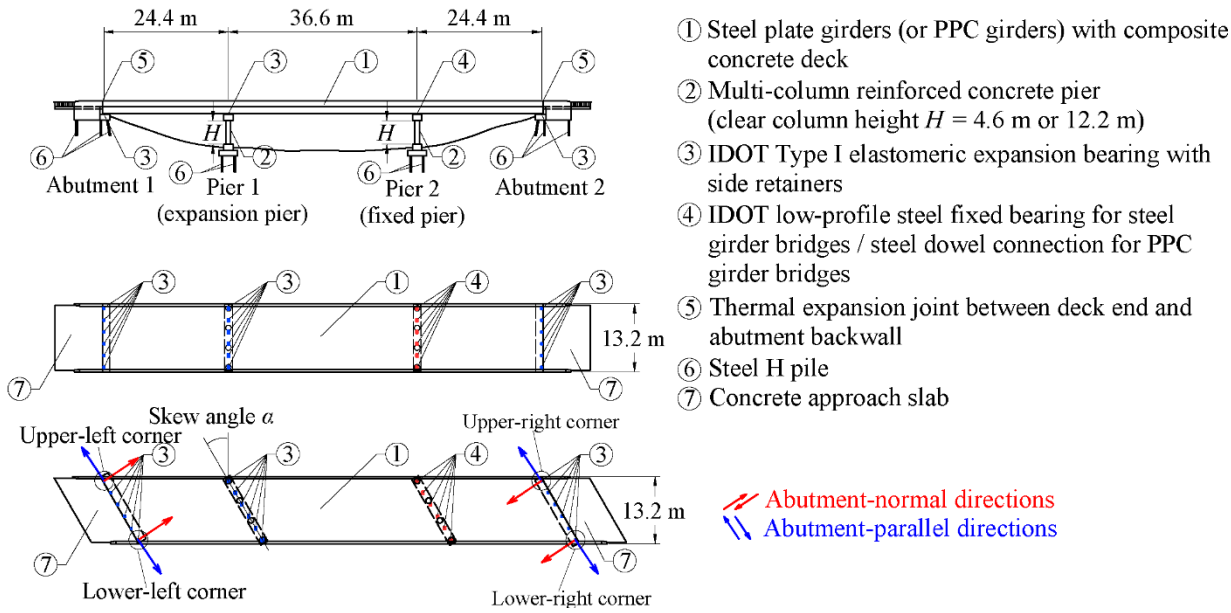

(a). Three-span prototype bridges

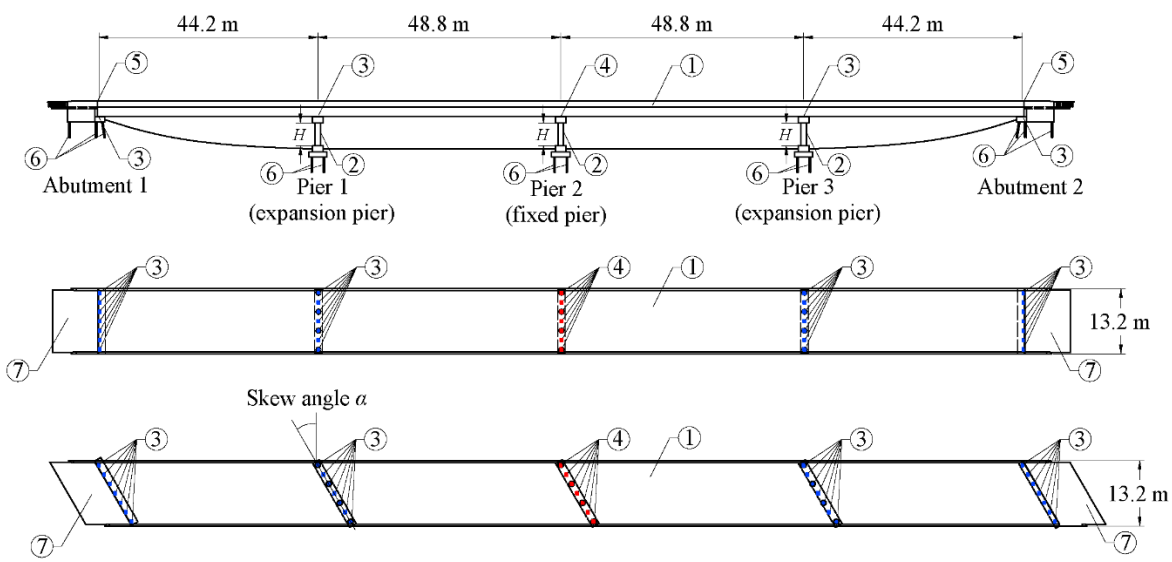

(b). Four-span prototype bridges

Figure 2.4: Configuration and dimensions of (a) three-span and (b) four-span prototype quasi-isolated bridges.

Table 2.8: Design Parameters of Critical Structural Components for Prototype Quasi-Isolated Bridges

Bridge type	**3-span steel-girder (3S) bridges**	**4-span steel-girder (4S) bridges**	**3-span concrete-girder (3C) bridges**	**4-span concrete-girder (4C) bridges**
Span length [m (ft)]	24.4-36.6-24.4 (80-120-80)	44.2-48.8-48.8-44.2 (145-160-160-145)	24.4-36.6-24.4 (80-120-80)	44.2-48.8-48.8-44.2 (145-160-160-145)
Skew angle	0°, 15°, 30°, 45°, 60°	0°, 15°, 30°, 45°, 60°	0°, 15°, 30°, 45°, 60°	0°, 15°, 30°, 45°, 60°
Superstructure				
No. of girders	6	7	6	7
Girder depth [mm (in.)]	1,067 (42)	1,676 (66)	1,372 (54)	1,829 (72)
Girder spacing [m (ft)]	2.29 m (7.5)	1.88 m (6.2)	2.29 m (7.5)	1.88 m (6.17)
Deck width [m (ft)]	13.15 (43.2)	13.15 (43.2)	13.15 (43.2)	13.15 (43.2)
Deck thickness [mm (in.)]	210 (8.25)	210 (8.25)	210 (8.25)	210 (8.25)
Bearing components				
Bearings at abutments	Type I, 11-d	Type I, 15-e	Type I, 12-e	Type I, 15-e
Elastomer planar dimensions [mm (in.)]	280 × 406 (11 × 16)	381 × 610 (15 × 24)	305 × 457 (12 × 18)	381 × 610 (15 × 24)
Elastomer thickness [mm (in.)]	89 (3.50)	133 (5.25)	100 (3.94)	133 (5.25)
No. of anchor per retainer	1	1	1	1
Retainer anchor dia. [mm (in.)]	25.4 (1.0)	31.8 (1.25)	31.8 (1.25)	38.1 (1.5)
Retainer anchor steel	A36	A36	A36	A36
Bearings at expansion pier(s)	Type I, 18-a	Type I, 20-a	Type I, 13-b (two rows)	Type I, 15-b (two rows)
Elastomer planar dimensions [mm (in.)]	457 × 610 (18 × 24)	508 × 610 (20 × 24)	330 × 508 (13 × 20)	381 × 610 (15 × 24)
Elastomer thickness [mm (in.)]	76 (3.0)	83 (3.25)	64 (2.5)	76 (3.0)
No. of anchor per retainer	1	1	1	1
Retainer anchor dia. [mm (in.)]	38.1 (1.5)	50.8 (2)	31.8 (1.25)	38.1 (1.5)
Retainer anchor steel	A36	A36	A36	A36
Sacrificial connections at fixed pier	Steel fixed bearing	Steel fixed bearing	#8 (U.S.) steel dowel bars	#8 (U.S.) steel dowel bars
Anchor diameter [mm (in.)]	38.1 (1.5)	31.8 (1.25)	25.4 (1.0)	25.4 (1.0)
No. of anchor per girder line	2	4	3 bars at an exterior girder 6 bars at an interior girder	3 bars at an exterior girder 6 bars at an interior girder
Anchor steel grade	A36	A36	A36	A36
Multi-column pier				
Column clear height [mm (ft)]	4.57 (15) / 12.19 (40)	4.57 (15) / 12.19 (40)	4.57 (15) / 12.19 (40)	4.57(15) / 12.19 (40)
Column diameter [m (ft)] (4.57-m- / 12.19-m-tall columns)	1.07 (3.5) / 1.22 (4.0)	1.07 (3.5) / 1.22 (4.0)	1.07 (3.5) / 1.22 (4.0)	1.07 (3.5) / 1.22 (4.0)

Table 2.2 (cont.): Design Parameters of Critical Structural Components for Prototype Quasi-Isolated Bridges

Bridge type	3-span steel-girder (3S) bridges	4-span steel-girder (4S) bridges	3-span concrete-girder (3C) bridges	4-span concrete-girder (4C) bridges
No. of columns for different skews	4 (0°, 15°, 30°) 5 (45°) 6 (60°)	4 (0°, 15°, 30°) 5 (45°) 6 (60°)	4 (0°, 15°, 30°) 5 (45°) 6 (60°)	4 (0°, 15°, 30°) 5 (45°) 6 (60°)
Concrete nominal strength [MPa (ksi)]	24 (3.5)	24 (3.5)	24 (3.5)	24 (3.5)
Reinforcement ratio	2 %	2 %	2 %	2 %
Reinforcement yield strength [MPa (ksi)]	414 (60)	414 (60)	414 (60)	414 (60)
Pier cap cross-sectional width and height [m (ft)]	1.52 × 1.22 (5 × 4)	1.52 × 1.22 (5 × 4)	1.52 × 1.22 (5 × 4)	1.52 × 1.22 (5 × 4)
Pile cap cross-sectional width and height [m (ft)]	3.66 × 1.07 (12 × 3.5)	3.66 × 1.07 (12 × 3.5)	3.66 × 1.07 (12 × 3.5)	3.66 × 1.07 (12 × 3.5)
Steel pile	HP12 × 84 (U.S.)	HP12 × 84 (U.S.)	HP12 × 84 (U.S.)	HP12 × 84 (U.S.)
No. of piles at a pier for different skews	14 (0°, 15°) 16 (30°) 18 (45°) 22 (60°)	16 (0°, 15°, 30°) 18 (45°) 22 (60°)	14 (0°, 15°) 16 (30°) 18 (45°) 22 (60°)	20 (0°, 15°, 30°, 45°) 22 (60°)
Seat-type abutment				
Expansion joint width for different skews (normal to joint edge) [mm (in.)]	44.5 (1.75) (0°, 15°, 30°) 38.1 (1.5) (45°) 31.8 (1.25) (60°)	57.2 (2.25) (0°, 15°) 50.8 (2.0) (30°) 44.4 (1.75) (45°) 38.1 (1.5) (60°)	44.5 (1.75) (0°, 15°, 30°) 38.1 (1.5) (45°) 31.8 (1.25)	57.2 (2.25) (0°, 15°) 50.8 (2.0) (30°) 44.4 (1.75) (45°) 38.1 (1.5) (60°)
Backwall cross-section [m (in.)]	1.14 × 0.61 (45 × 24)	1.81 × 0.61 (71 × 24)	1.42 × 0.61 (56 × 24)	1.91 × 0.61 (75 × 24)
Pile cap cross-section [m (in.)]	1.98 × 1.07 (78 × 42)	1.98 × 1.07 (78 × 42)	1.98 × 1.07 (78 × 42)	1.98 × 1.07 (78 × 42)
Steel pile	HP12 × 84 (U.S.)	HP12 × 84 (U.S.)	HP12 × 84 (U.S.)	HP12 × 84 (U.S.)
No. of piles at an abutment for different skews	9 (0°, 15°, 30°) 11 (45°) 13 (60°)	9 (0°, 15°, 30°) 11 (45°) 13 (60°)	9 (0°, 15°, 30°) 11 (45°) 13 (60°)	11 (0°, 15°, 30°, 45°) 13 (60°)
Approach slab length × width × thickness [m (ft)]	9.14 × 12.19 × 0.38 (30 × 40 × 1.25)	9.14 × 12.19 × 0.38 (30 × 40 × 1.25)	9.14 × 12.19 × 0.38 (30 × 40 × 1.25)	9.14 × 12.19 × 0.38 (30 × 40 × 1.25)

Table 2.3 lists the seismic mass of the bridge superstructures. The superstructure mass does not change much in the non-skew and skew bridge variants of the same type. The 4C bridges have the heaviest superstructures of a bridges, while the 3S bridges have the lightest superstructures. The superstructure mass is directly related to the seismic force demand on the bridge.

Table 2.9: Seismic Mass of Bridge Superstructure (10^3 kg)

Skew (°)	3S bridges	4S bridges	3C bridges	4C bridges
0	1,197	2,758	1,680	3,949
15	1,197	2,766	1,726	4,024
30	1,198	2,766	1,767	4,091
45	1,198	2,772	1,823	4,180
60	1,199	2,773	1,948	4,390

A 3-D nonlinear finite-element model was created for each of the 80 prototype bridges using *OpenSees*. The full-bridge model includes a superstructure and several substructures, as well as all bearings/retainers and foundation piles. In addition to structural components, geotechnical mechanisms such as backfill passive resistance at the abutments and pile caps of intermediate

piers, as well as lateral and axial soil-pile interaction, are also incorporated in the model. Figure 2.3 shows two examples of the 3-D bridge models, one of which is a highly skewed three-span bridge supported by short piers and the other is a non-skew four-span bridge supported by tall piers.

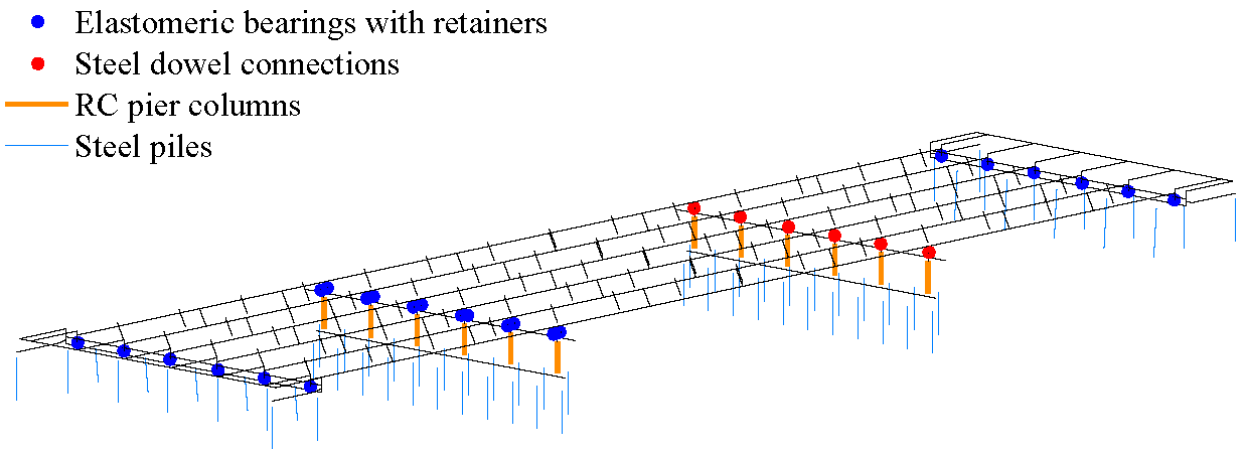

(a). 3C60P15H bridge

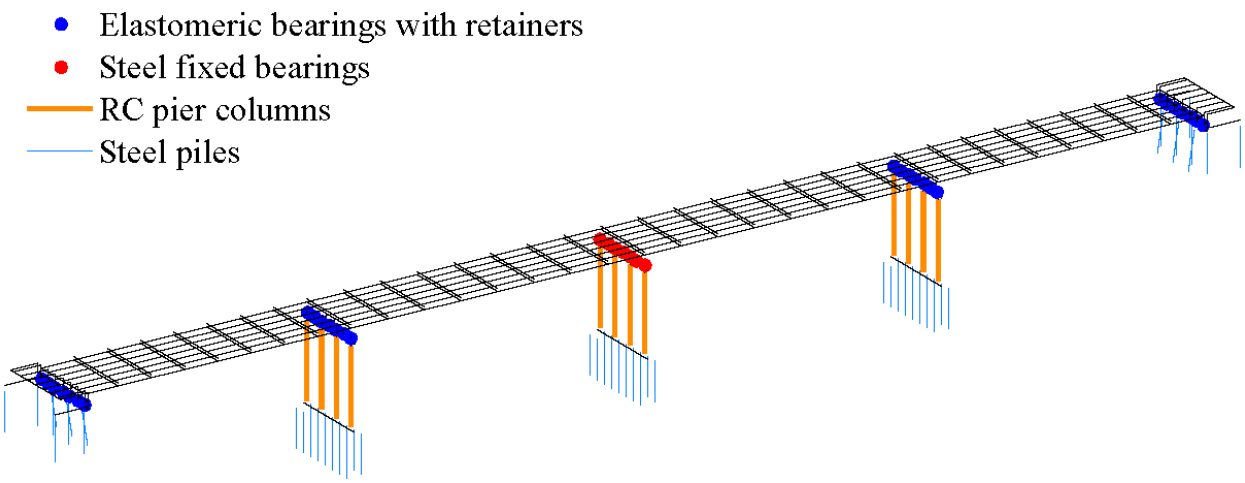

(b). 4S00P40S bridge

Figure 2.5: Examples of 3-D finite-element bridge models.

2.2 COMPUTATIONAL MODELING AND BRIDGE DETAILS

2.2.1 Bridge Superstructure Model

The bridge superstructure was modeled using a grillage modeling approach (O'Brien et al. 2015), as illustrated in Figure 2.4. The grillage superstructure model consists of longitudinal and transverse elastic beam elements. The elastic beam elements were laid out in a grid pattern and the members were rigidly connected to each other at the nodes. The longitudinal beam elements were used to model the composite behavior of girders with associated concrete slabs connected to the girder top flanges. The properties of the longitudinal beam elements were

determined using composite sectional properties of girders with associate concrete slab. In the transverse direction, elastic beam elements were used to model the concrete slab and diaphragms between the girders. The sectional properties of the beam elements modeling the concrete slab were determined based on the tributary slab area, the slab thickness [21.0 cm (8.25 in.)], and the elastic modulus of the concrete material. The diaphragm using C-or MC-shaped structural steel was modeled using a transverse beam element whose elastic stiffness was determined based on the sectional properties of the corresponding steel shape. Stiffness properties of the cross-frame in 4S bridges were determined using an equivalent beam approach introduced by AASHTO/NSBA Steel Bridge Collaboration (2014). In this approach, the cross-frame is simplified into an equivalent Euler-Bernoulli beam.

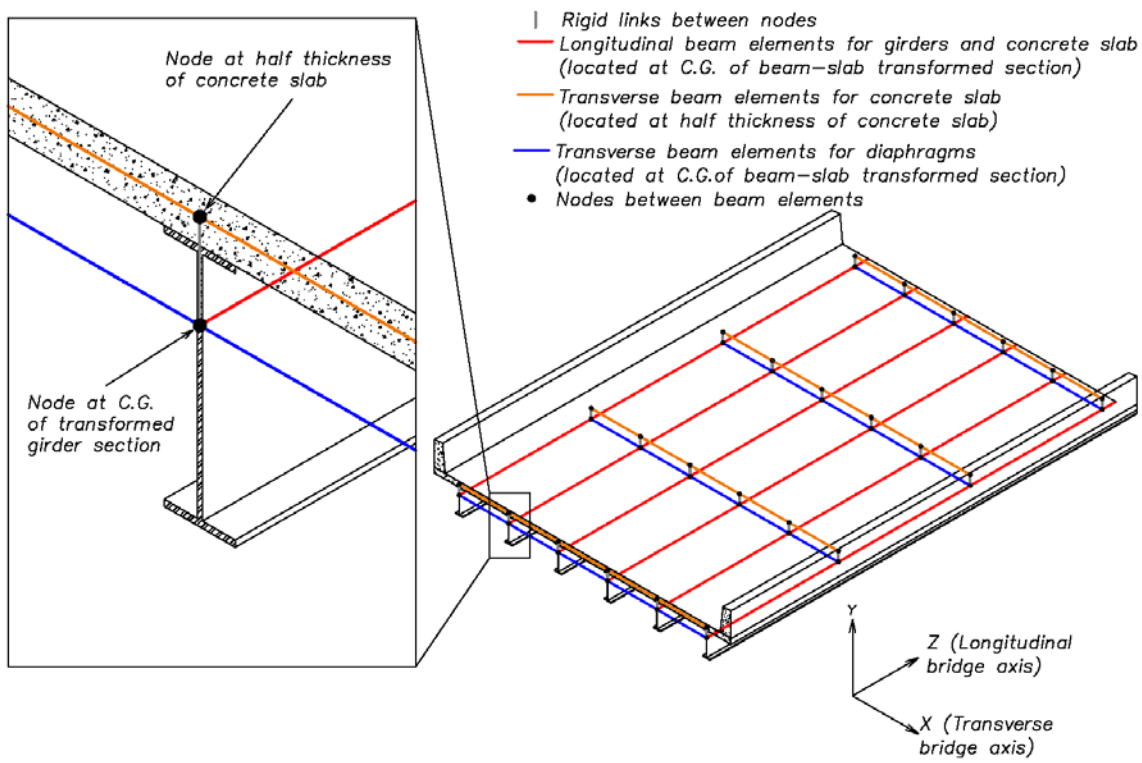

Figure 2.6: Schematic of grillage superstructure model.

2.2.2 Bridge Substructure Model

The multi-column RC intermediate piers were modeled using a combination of linear elastic and nonlinear inelastic beam elements, as illustrated in Figure 2.5a. While the pier cap and pile cap are modeled elastically, the circular pier columns standing between the pier and pile caps are modeled using nonlinear beam elements with distributed plasticity (Neuenhofer & Filippou, 1997). Each pier column was discretized into ten such nonlinear beam elements of equal length, and each element had three integration points for Legendre-Gauss quadrature. At each integration point, a fiber-discretized RC section was utilized to determine the element stiffness matrix, considering the nonlinear constitutive relation of concrete and steel materials under combined axial and flexural loads. Figure 2.5b illustrates the mesh of the RC section. Fibers of three types of materials were used for modeling the unconfined concrete cover, confined

concrete core, and vertical reinforcing steel. Constitutive properties of the confined concrete core were determined using the model proposed by Mander et al. (1988), per Article 8.8.4 of the AASHTO specification (AASHTO, 2011). While the axial and flexural stiffness's of the column were captured by the fiber-discretized sections, shear stiffness of the column section was determined as $0.8G_cA_g$, where G_c is the shear modulus of concrete and A_g is the gross cross-sectional area of the column, per Article 8.6.2 of the same AASHTO specification. Per Article 5.6.5 of the same specification (AASHTO, 2011), the effective torsional moment of inertia of the column cross-section was determined as $0.2J_g$, where J_g is the gross torsional moment of inertia of the column cross-section. More details about the intermediate pier model can be found in Luo et al. (2017a,b).

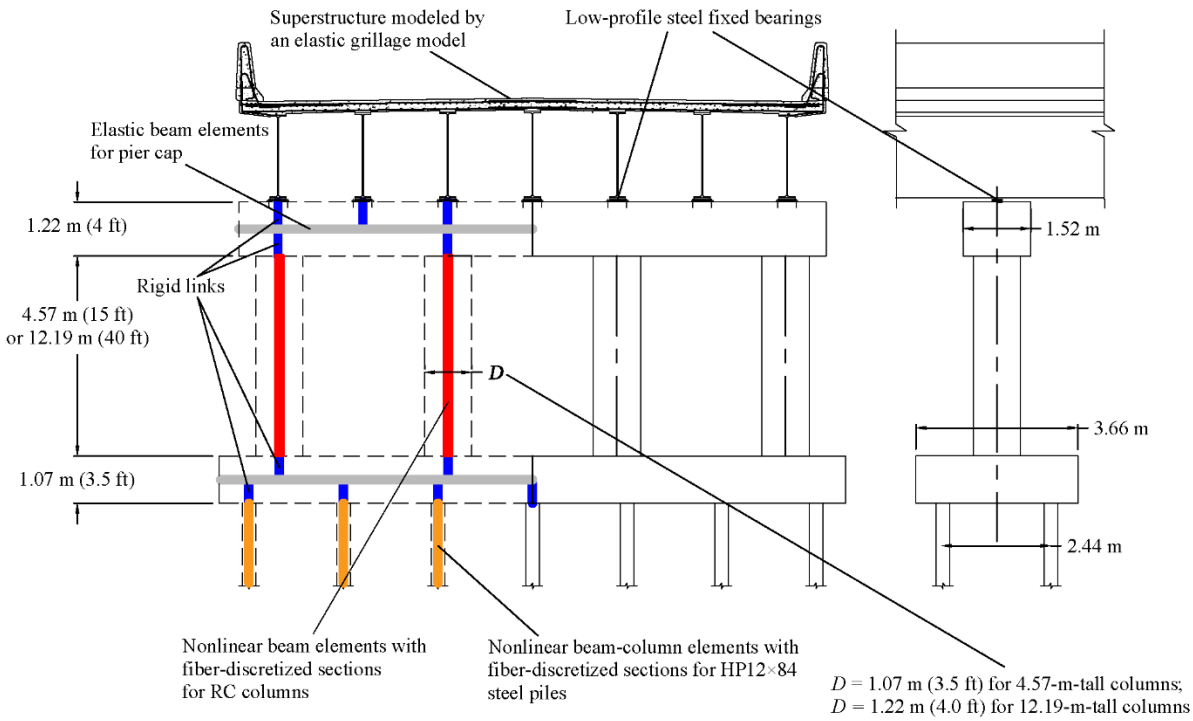

(a). Model for intermediate pier substructure

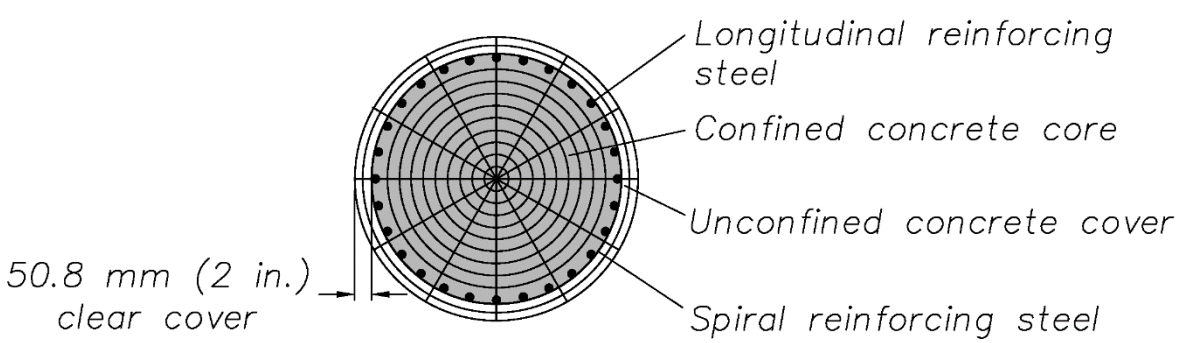

(b). Fiber-discretized section of RC pier columns

Figure 2.7: Computational model of multi-column intermediate pier.

2.2.3 Bridge Foundation Model

Steel H piles supporting the abutments and piers were also modeled using nonlinear fiber beam elements with distributed plasticity (Neuenhofer & Filippou, 1997), to capture their nonlinear material behavior. The number and size of the elements were determined to have at least five elements for the top pile portion (of ten diameters) and at least five elements for the rest of the pile, as recommended by Kornkasem et al. (2001).

Figure 2.6 shows the two actual foundation soil profiles used to model the substructure foundations. The two profiles were selected as the softest and hardest from a pool consisting of 20 sets of geotechnical boring logs for bridge construction projects in the southernmost 10 counties in Illinois, which possess the highest seismicity of the entire state. In the two selected soil profiles, the portion between the ground surface and a depth of 14.6 m (48 ft) was considered, as it was assumed that the steel H piles of the prototype bridges were driven to bedrock at this depth. These two soil profiles will hereafter be referred to as the "soft foundation soil condition" and "hard foundation soil condition." Through static lateral analyses performed on the pier and abutment pile foundation models, it was found for both soil profiles that even if a large lateral deflection occurred at the pile cap level, the pile deflection at a depth greater than 6.1 m (20 ft) was nearly zero. Therefore, to reduce the number of pile elements in the model and save computational costs, the pile bodies were cut off at the fixity depth of 6.1 m (20 ft) and a pinned boundary condition was imposed at the pile end at that depth.

Interactions between the pile body and surrounding soil were modeled with the beam on a nonlinear Winkler foundation method that is a widely used modeling strategy for pile foundations under axial and lateral loads (Matlock et al., 1978; Novak and Sheta, 1980; Nogami et al., 1992). At each node between two pile elements, a nonlinear *p-y* spring and a nonlinear *t-z* spring developed by Boulanger et al. (1999) for use in *OpenSees* were employed to simulate lateral soil resistance to the pile and vertical skin friction between the pile and surrounding soil, respectively. The backbone curves of the *p-y* springs for soft clay and sand approximate the analytical models proposed by Matlock (1970) and API (1987), respectively. For stiff clay, the *p-y* spring in *OpenSees* developed by Boulanger et al. (1999) was modified to approximate the analytical backbone curve proposed by Reese and Van Impe (2011).

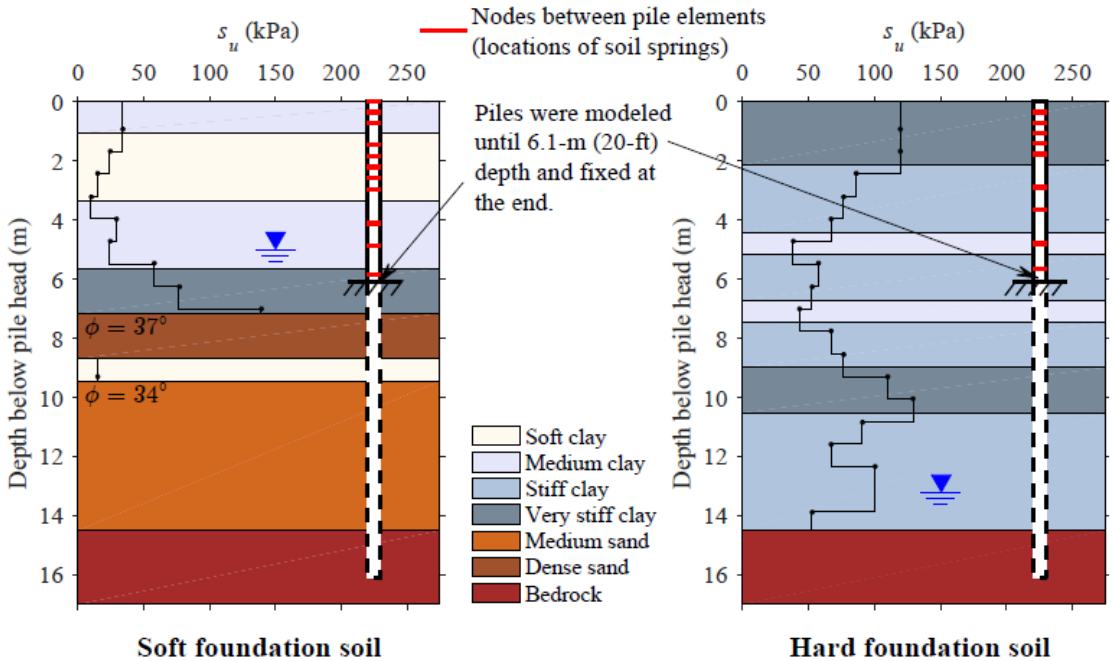

Figure 2.8: Soft and hard foundation soil profiles for modeling bridge pile foundations.

Figure 2.7a shows the fiber-discretized pile section at each integration point of the nonlinear beam element. Through static analyses performed on the pier and abutment pile foundations, it was found that even if a large lateral deflection occurred at the pile cap level, the pile deflection at the depth of 6.1 m (20 ft) was nearly zero. Therefore, to reduce the number of pile elements included in the model and save computational costs, the pile bodies were cut off at the fixity depth of 6.1 m (20 ft) and a fixed boundary condition was imposed at this depth. The pile bodies beyond this fixity depth were neglected in the foundation model. Interactions between the pile body and surrounding soil were modeled using the beam on a nonlinear Winkler foundation method that is a widely used modeling strategy for pile foundation under axial and lateral loads (Matlock et al. 1978; Novak and Sheta 1980; Nogami et al. 1992). At each node between two pile elements, a nonlinear *p-y* spring and a nonlinear *t-z* spring developed by Boulanger et al. (1999) for use in *OpenSees* were employed to simulate the lateral soil resistance to the pile and the vertical skin friction between the pile and surrounding soil, respectively. A schematic of the pile model with nonlinear springs is shown in Figure 2.7b. The backbone curves of the *p-y* springs for soft clay and sand approximate the analytical models proposed by Matlock (1970) and API (1987), respectively. For stiff clay, the *p-y* spring developed by Boulanger et al. (1999) was modified to approximate the analytical backbone curve proposed by Reese and Van Impe (2011).

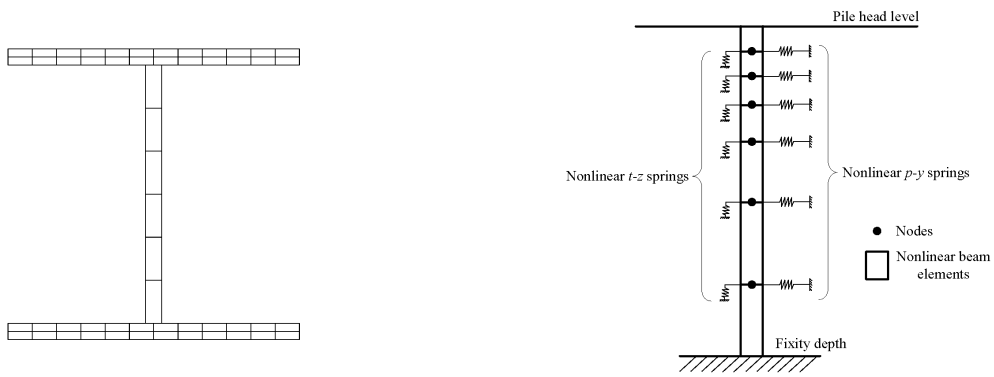

(a) (b)

Figure 2.9: (a) Fiber discretized section of foundation piles, (b) schematic of pile model with *p-y* and *t-z* springs.

2.2.4 Bridge Superstructure-Substructure Connection Model

Non-seismically designed elastomeric expansion bearings, transverse bearing retainers, low-profile steel fixed bearings, and steel dowel connections are employed in the quasi-isolated bridges as sacrificial superstructure-substructure connections. In the last phase of the research project, numerical models for these components were developed on the basis of experimentally measured response characteristics. The configurations, experimental behaviors, and computational models of these components are briefly reviewed below and more details can be found elsewhere (Filipov et al. 2013a,b; LaFave et al. 2013a,b; Steelman et al. 2013, 2014, 2016).

Figure 2.8a shows the configuration of IDOT Type I elastomeric expansion bearings (IDOT 2012a) placed at the abutments and expansion piers of quasi-isolated bridges. Figure 2.8b illustrates the computational model for the shear and sliding behavior of the steel shim reinforced bearing elastomer. The bearing elastomer is directly placed on top of the concrete substructure. When the bridge is subjected to seismic demands, the bearing elastomer may experience shear deformation and subsequent sliding on the substructure. Shear and stick-slip sliding behavior of the elastomer was simulated using a coupled bi-directional stick-slip friction model (Filipov et al. 2013a). In this model, the initial static coefficient of friction of μ_I = 0.6 and the kinematic coefficient of friction of μ_K = 0.45 were used to model the initial static and kinematic friction between the elastomer and concrete substructure. The coefficients of friction were determined through experimental tests on full-scale bearing specimens (Steelman et al. 2013). The shear stiffness of the elastomer (the slope in Figure 2.8b) was estimated as the material shear modulus multiplied by the plan area of the elastomer and then divided by the thickness of the elastomer (Filipov et al. 2013a). A shear modulus of 586 kPa (85 psi) was determined by experimental tests (Steelman et al. 2013).

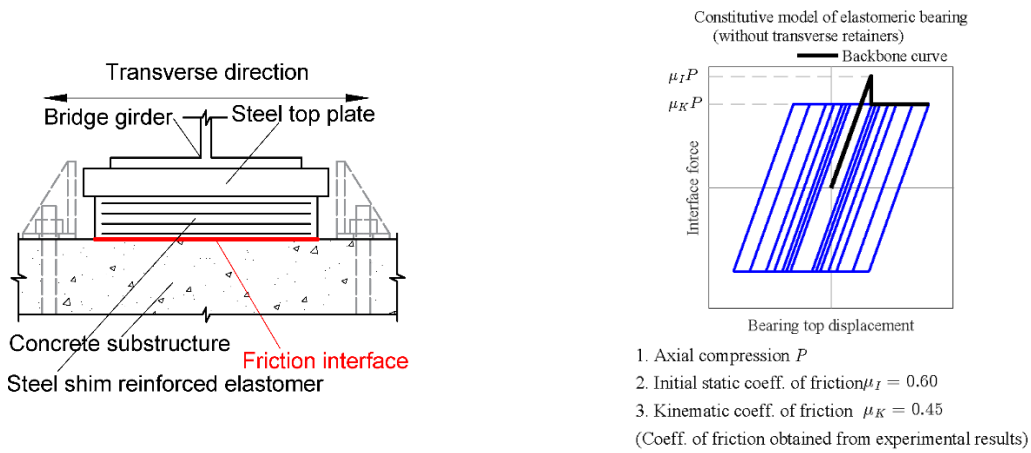

(a) (b)

Figure 2.10: (a) Configuration and (b) computational model of IDOT Type I elastomeric expansion bearings employed in quasi-isolated bridges (IDOT 2012a; Filipov et al. 2013a; LaFave et al. 2013b; Steelman et al. 2013).

While shear and sliding of the elastomeric bearing in the longitudinal bridge direction is only restrained by elastomer-concrete interface friction, a pair of bearing retainers is placed on the two transverse sides of each elastomeric expansion bearing to restrain its shear deformation and sliding in the transverse bridge direction, in conjunction with the elastomer-concrete friction at the bearing bottom. Figure 2.9a shows the configuration of the bearing retainers. A steel anchor bolt secures each single retainer into the concrete substructure.

The IDOT Bridge Manual (IDOT 2012a) provides a method for nominally proportioning the anchor bolts of bearing retainers. The retainer anchors of the prototype bridges were proportioned on the basis of the IDOT Bridge Manual method. The IDOT Bridge Manual also provides a number of available options for the anchor diameter (0.625 in., 0.75 in., 1.0 in., 1.25 in., 1.5 in., 2 in., and 2.5 in.). 3C bridges use one A36 grade 1 in. diameter anchor bolt per retainer, 4S and 3C use one A36 grade 1.25 in. diameter anchor bolt per retainer, and 4C bridges use one A36 grade 1.5 in. diameter anchor bolt per retainer.

The experimentally measured retainer anchor behavior, when subjected to seismic demands, was simulated using a uni-directional elasto-plastic computational model that considers the initial gap, yielding, strain hardening, and ultimate rupture responses (Filipov et al. 2013a). Figure 2.9b schematically illustrates the computational model. In this model, the expected ultimate and yielding capacities of a single retainer anchor bolt, *Ru* and *Ry*, were determined using the nominal cross-sectional area of the anchor bolt and the ultimate tensile strength of the anchor bolt material. The behavior was calibrated against experimentally measured retainer anchor response data (Filipov et al. 2013b; LaFave et al. 2013a,b).

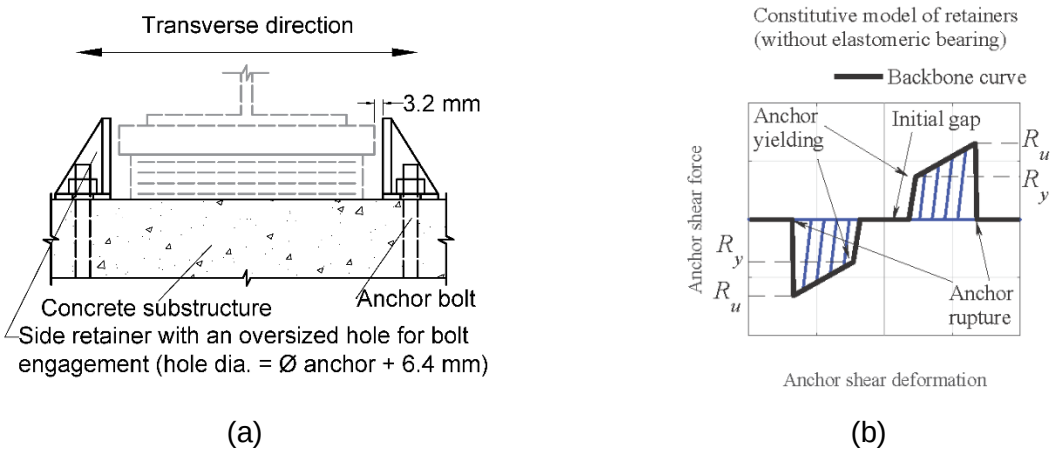

(a) (b)

Figure 2.11: (a) Configuration and (b) computational model of transverse bearing retainers employed in quasi-isolated bridges (IDOT 2012a; Filipov et al. 2013a; LaFave et al. 2013b; Steelman et al. 2013).

For the quasi-isolated bridges with steel-plate girders, IDOT low-profile steel fixed bearings (IDOT 2012a) are typically installed on one intermediate pier (the so-called "fixed pier") to compensate for the flexibility of the elastomeric expansion bearings and resist superstructure motions caused by vehicle braking forces. Figure 2.10a shows the configuration of the low-profile steel fixed bearing. The bottom steel plate of the bearing is secured into the supporting concrete substructure by anchor bolts. An elastomeric neoprene leveling pad is placed between the bearing bottom plate and the top surface of the concrete substructure. The top steel plate is mated to the bottom plate via two steel pintles.

By inspection of the plans of many recently constructed quasi-isolated highway bridges in Illinois, it was found that the specified nominal fusing capacity of low-profile steel fixed bearing anchors, namely 20% of the superstructure dead load on the bearing, is typically over-designed. A primary potential reason for this design trend in practice may be that bridge designers tend to regard the specified fusing capacity as a minimum requirement and use larger or more anchor bolts for conservatism. A secondary potential reason is that a fusing capacity in the close vicinity of 20% of the dead load on the bearing is not always available in actual design due to the limited options for anchor diameters. In this situation, bridge designers may round the anchor diameter up to the nearest available size and result in over-designed nominal fusing capacity. In the prototype bridges, this trend of over-designed fixed bearing anchors has been considered. The 3S bridges use two A36 grade 1.5 in. diameter steel anchor bolts per girder line while the 4S bridges use four A36 grade 1.25 in. diameter steel anchor bolts per girder line.

Through full-scale experimental studies, it was found that a properly proportioned steel fixed bearing can achieve predictable and reliable behavior of anchor rupture and subsequent sliding, when subjected to seismic demands (Steelman et al. 2014). Shear behavior of the anchor bolts was simulated using a coupled bi-directional model possessing a similar elasto-plastic behavior to the model for retainer anchors (Filipov et al. 2013b; LaFave et al. 2013b), as shown in Figure 2.10b. The behavior was validated by experimentally measured steel-fixed bearing response

data (Filipov et al. 2013b; Steelman et al. 2014). Additionally, the interface friction between the bearing bottom plate and elastomeric leveling pad was simulated using the same model as the elastomeric expansion bearings, but with different coefficients of friction ($\mu_I = \mu_K = 0.30$).

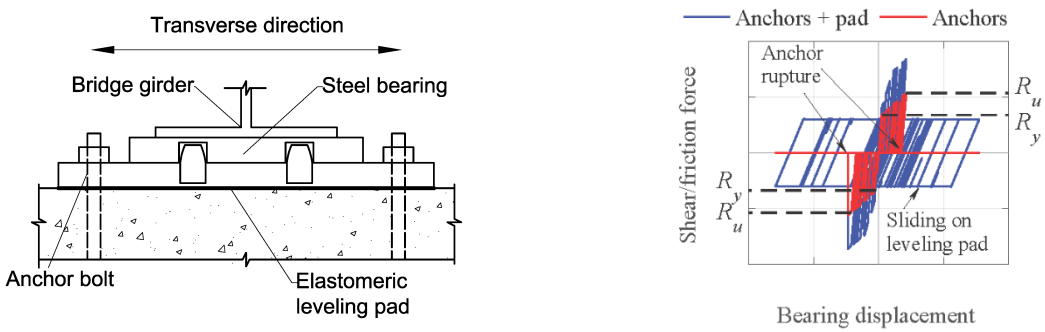

(a) (b)

Figure 2.12: (a) Configuration and (b) computational model of low-profile steel fixed bearings employed in quasi-isolated bridges (IDOT 2012a; Filipov et al. 2013b; LaFave et al. 2013b; Steelman et al. 2014).

Different from the steel-plate-girder bridges, the prototype PPC-girder bridges employ steel dowel connections between superstructures and fixed piers. #8 (U.S.) steel dowel bars with a nominal diameter of 25.4 mm (1.0 in.) are used to connect the pier cap to the diaphragm and PPC girder bottom flanges. On each face of the pier between two adjacent girders, the minimum required number of dowel bars, denoted by *N*, is given by the following equation

$$N = \frac{1}{2}\left[\frac{0.2DL}{28.3S} - 2\right] \geq 2 \tag{2.1}$$

where *DL* is the sum of all superstructure dead loads at the given pier under consideration in kips; *S* is the number of beam spaces. Except for the *N* dowel bars on each face between two adjacent girders, additional dowels are placed at each girder line to connect the girder bottom flange to the pier cap (one bar for each exterior girder and two bars for each interior girder). In additional to the dowels, a 12.5-mm (0.5-in.)-thick layer of preformed joint filler is placed between the PPC girder bottom and concrete pier cap.

Like the steel fixed bearing anchors, the steel dowel bars embedded in concrete tend to be subjected to shear forces during seismic events and friction tends to develop between the preformed joint filler and concrete. Due to these similarities and a lack of experimental data on these steel dowel connections, they were simulated using the same computational models as the low-profile steel fixed bearings, but with different parameters to account for the number and size of the steel dowels.

2.2.5 Seat-Type Bridge Abutment Components

Seat-type abutments are also commonly used in quasi-isolated highway bridges in the state of Illinois, besides integral abutments and semi-integral abutments. Figure 2.11 depicts the sectional view of a typical non-skew seat-type bridge abutment in Illinois. Skew seat-type abutments have similar configurations to the non-skew one, except that the approach slab is skewed, and the two pieces of wingwalls are not perpendicular to the backwall and pile cap. A primary feature that distinguishes seat-type bridge abutments from integral and semi-integral abutments is that an expansion joint is set between the abutment backwall and adjacent superstructure end to accommodate thermally induced bridge deformation by separating the superstructure from abutments.

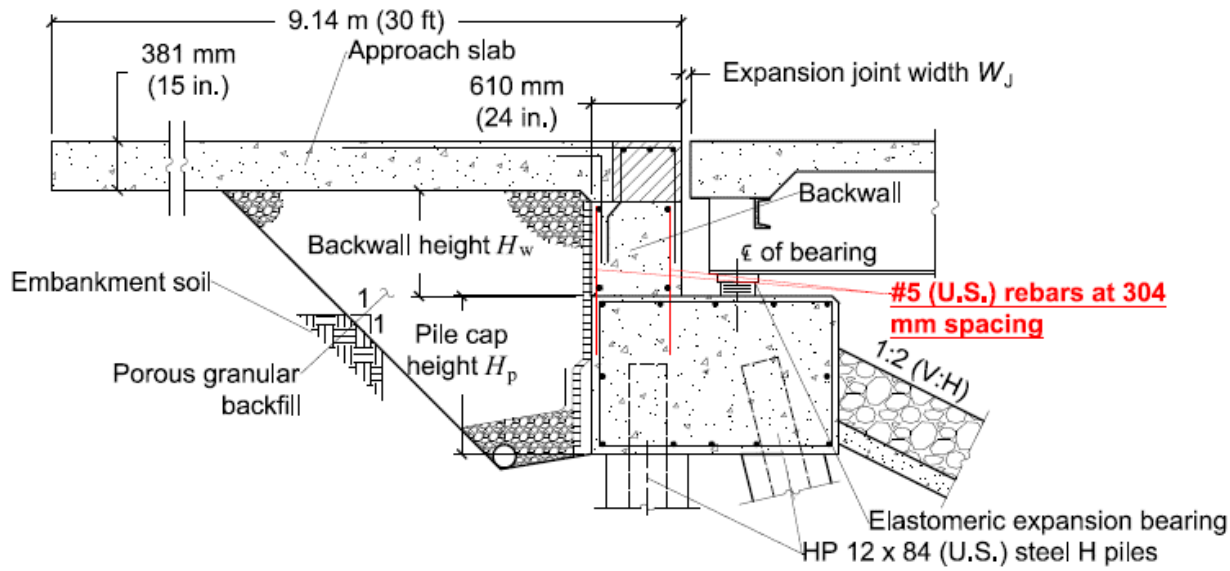

Figure 2.13: A typical seat-type bridge abutment for quasi-isolated highway bridges in Illinois (IDOT 2012a).

During major earthquakes, a critical response characteristic of quasi-isolated bridges with seat-type abutments is the sliding of superstructures on supporting substructures after sufficient fusing of the sacrificial superstructure-substructure connections. In this situation, bridge superstructures may act somewhat as “floating bridges” with only limited frictional resistance at the superstructure-substructure interface (Steelman et al. 2014). The superstructure sliding that is only weakly restrained by the friction may result in significant dynamic interactions between deck ends and seat-type abutments. Displacements of bridge superstructures are limited by the abutments to varying degrees, while the abutments are in turn subjected to impact forces from superstructures. The impact of superstructure ends will cause force and deformation demands on the abutment and its foundation buried in the embankment. To reasonably model bridge seismic response, the superstructure-abutment-foundation interaction (SAFI) needs to be taken into account in the computational bridge model.

The abutment model incorporates a few structural components and geotechnical mechanisms that are critical to capture the seismic SAFIs. Figure 2.12 illustrates the nonlinear finite-element

model of the typical seat-type abutment shown in Figure 2.11. Several critical structural connections and geotechnical mechanisms were modeled using nonlinear springs. In addition, elastic beam elements were used to model some reinforced concrete members, including the pier cap, backwall body, wingwalls, and approach slab. For these massive concrete members, seismic damage is most likely to occur only at their joints and connections, rather than anywhere else along their length. Thus, for the sake of saving computational cost, elastic beam elements were used to model these members, in lieu of nonlinear beam elements. To capture the nonlinear material response of steel piles, nonlinear beam elements with fiber-discretized sections were employed. The following sections introduce the modeling approaches for the pile foundation, expansion joint, backwall, backwall-wingwall connection, backfill passive resistance, wingwall, and pile cap.

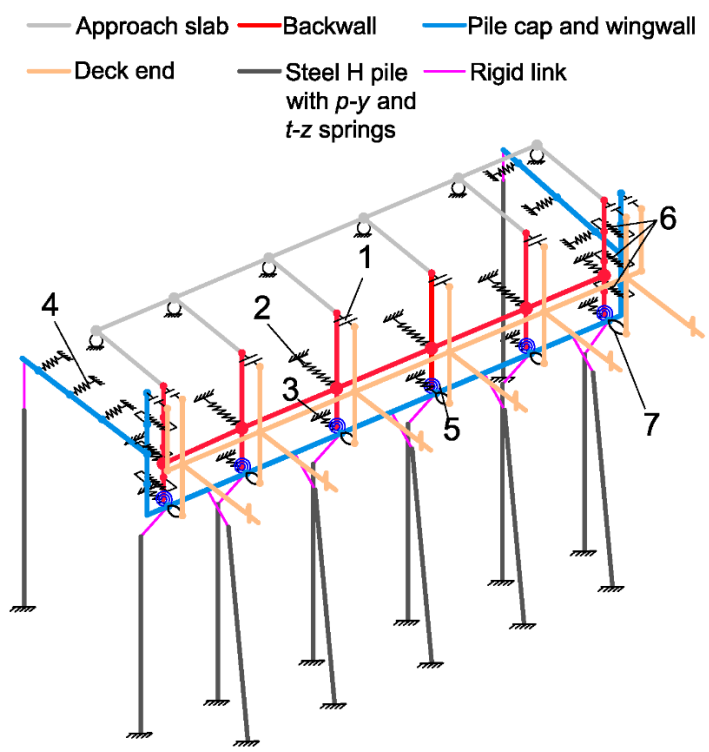

Figure 2.14: A 3-D finite-element model for the typical seat-type bridge abutment shown in Figure 2.11.

2.2.5.1 Abutment Pile Foundation Model

The abutments of different bridge variants differ in the layout of foundation piles, due to different dead and live gravity loads from the superstructures, as well as different pile cap lengths of bridges with various skews. For bridges with a skew angle of α, the length of the abutment pile cap is increased by a factor of $\frac{1}{\cos\alpha}$ as compared to non-skew bridges, as illustrated in Figure 2.13. In this situation, to meet the maximum pile spacing of 2.43 m (8.0 ft) specified by IDOT (2012a), more piles may be needed for skew abutments than for non-skew abutments.

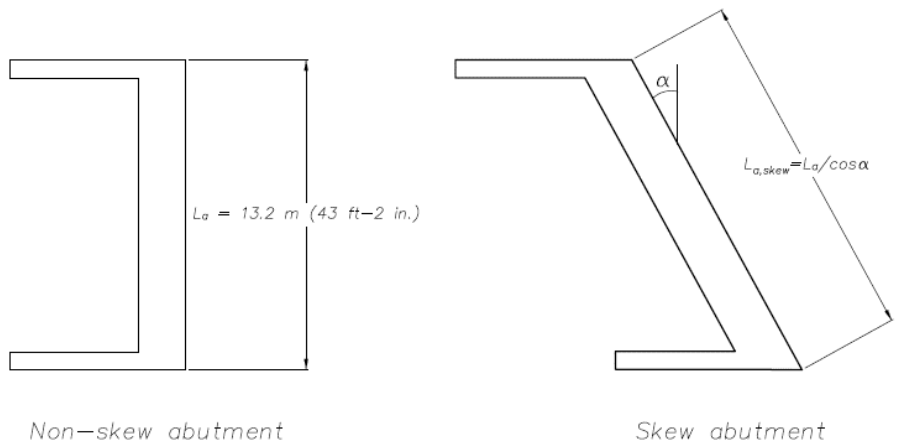

Figure 2.15: Pile cap length of non-skew and skew abutments.

Batter piles with a slope of 152.4 mm (6 in.) of vertical rise for every 25.4 mm (1 in.) of horizontal run are placed in the front row (the row near the deck end). The angle of batter (the angle made by the batter pile with the vertical) is 9.5°. The direction of the batter is to the deck end. Vertical piles are placed in the back row (the row near the embankment). In addition to these two rows, a single pile supports the end of each piece of wingwall. Table 2.4 indicates the pile number and spacing at the abutments of various prototype bridges. Similar to the pile layout at intermediate piers, the abutment piles are also widely spaced (spacing is greater than four times of pile width). Thus, pile group effect was not considered in the model. The soil profile and modeling approach for vertical abutment piles are the same as those for the pier piles, which were introduced earlier.

Table 2.10: Pile Number and Spacing at an Abutment

Major bridge type	Skew (°)	Pile member size	No. of batter pile N_{ab}	No. of vertical pile N_{av}	Center-to-center Pile spacing S_a [m (ft)]	Spacing normalized to pile width S_a / b_p
3S, 4S, 3C	0	HP 12×84	3	4	1.98 (6.5)	6.3
	15		3	4	2.13 (7)	6.8
	30		3	4	2.43 (8)	7.8
	45		5	4	2.26 (7.5)	7.3
	60		5	6	2.43 (8)	7.8
4C	0	HP 12×84	5	4	1.52 (5)	4.9
	15		5	4	1.52 (5)	4.9
	30		5	4	1.83 (6)	5.9
	45		5	4	2.29 (7.5)	7.3
	60		5	6	2.43 (8)	7.8

Under seismic excitations, the abutment batter piles may act as both in-batter and out-batter piles, due to the cyclic seismic forces. However, the dominant longitudinal seismic force demand on the abutment piles results from the impact of superstructure ends on the abutments. In this loading scenario, the abutment batter piles behave as in-batter piles. Studies for the behavior of batter piles under lateral loads have been sparse in literature. Kubo (1964) proposed values of *p*-multipliers for modifying the *p*–*y* curves of piles with various batter

angles, based on experimental results. For the in-batter abutment piles in this study ($\vartheta = -9.5^{o}$), a *p*-multiplier of 1.2 was proposed by Kubo (1964). However, the experimental results of Awoshika and Reese (1971) demonstrated that there is little difference between the behavior of a vertical pile and an in-batter pile under later loads, which essentially implies a *p*-multiplier of unity. Considering both studies, a *p*-multiplier of 1.1 was employed to modify the *p*−*y* springs of abutment batter piles. In the abutment model, the ultimate lateral resisting force of the *p*−*y* springs connected to the batter piles, denoted as p_{ult}, was multiplied by 1.1. Then, the amplified ultimate lateral resisting force, $1.1p_{ult}$, is plugged in to the nonlinear formula for determining the *p*-*y* curve. Plugging $1.1p_{ult}$ into the formula results in 10% more soil resistance, than that of the *p*-*y* curve determined with p_{ult}, at any compressive deformation up to the ultimate value. More details regarding the *p*-multiplier can be found in Reese and Van Impe (2011).

Under generic cyclic loads, the batter piles may switch between in-batter and out-batter conditions. Ideally, the *p*-*y* spring for batter piles should have unsymmetrical behavior for the two conditions. However, the *p*-*y* spring elements used in the model only support symmetrical behavior. Under earthquakes in the longitudinal direction, the most significant lateral force demand on the abutment piles comes from the pounding between the deck end and abutment backwall. In this situation, the abutment is pushed by the bridge deck, and the abutment piles therefore work as in-batter piles. In contrast, when the deck moves away from the abutment, the abutment piles work as out-batter piles, but the pulling force on the abutment foundation is capped by bearing friction capacity, which could be much smaller than the pounding force between the deck and abutment backwall. Considering that the piles in the in-batter state could be subjected to much larger force than in the out-batter state, the *p*-*y* multiplier is determined for the in-batter state and then also used for the out-batter state. Except for this *p*-multiplier, the abutment batter piles were modeled using the same approach as the pier piles, which were introduced earlier.

2.2.5.2 Expansion Joint Model

In the typical seat-type bridge abutment, an expansion joint is configured between the backwall and the adjacent superstructure end to accommodate thermally induced bridge deformation by separating the superstructure and abutment and allowing relative displacements between the two. The joint opening width, *W*, is normal to the joint edge. The IDOT Bridge Manual (IDOT 2012a) specifies the design value of *W*.

In the abutment model, a few gap-spring elements were employed to simulate the instantaneous gap opening/closing, contact, and release at each step of a static or dynamic analysis. These elements are labeled as component No. 1 in Figure 2.12. The force-deformation relation of the gap-spring element is shown in Figure 2.14. When the element is subjected to tension or compressive deformation smaller than the joint opening width *W*, the element does not provide any resisting force and has a zero stiffness. When the compressive deformation exceeds the joint opening width *W*, the element becomes very stiff to simulate the hard contact between the deck end and abutment backwall. In the abutment model that is illustrated in Figure 2.12, the gap-spring elements were placed at the girder line and parapet locations. The elements were oriented normal to the edge of the expansion joint.

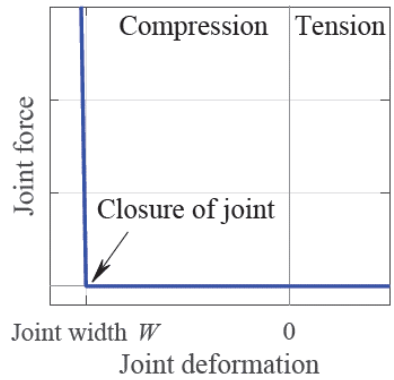

Figure 2.16: Force-deformation relation of gap-spring elements modeling expansion joints.

The RC backwall is connected to the pile cap by two rows of #5 (U.S.) reinforcing steel (15.8-mm diameter) with a 0.3-m (1-ft) spacing along the wall. The reinforcing steel is provided as the shrinkage and temperature reinforcement in concrete walls specified by AASHTO (2010). As shown in Figure 2.11, the thickness of the backwall is 0.61 m (2 ft), which is a standard practice in the state of Illinois (IDOT 2012a).

When the bridge is subjected to longitudinal seismic demands, the backwall that is engaged by the bridge superstructure is subjected to out-of-plane forces. In the abutment model, the backwall was modeled as a cantilever wall whose bottom is connected to the pile cap through an elasto-plastic hinge. To obtain the moment-curvature relation of the backwall section, a sectional analysis was conducted using *SAP2000*. Based on the obtained moment-curvature relation, an equivalent plastic hinge method proposed by Abo-Shadi et al. (2000) for modeling out-of-plane bending behavior of RC walls was employed to determine the moment-rotation relation of backwall bottom. For the non-skew prototype bridges, the computed moment-rotation relation of backwall bottom is shown in Figure 2.15. For skew prototype bridges the abutment backwall is elongated by a factor of $\frac{1}{\cos\alpha}$, where α is the bridge skew angle. Thus, for a skew prototype bridge, the moment-rotation relation of the backwall bottom hinge was obtained through multiplying the hinge moment of the equivalent non-skew bridge shown in Figure 2.15 by a factor of $\frac{1}{\cos\alpha}$. In the finite-element abutment model, the moment-rotation relation shown in Figure 2.15 was distributed into several rotational nonlinear springs at the backwall bottom, one the basis of tributary wall width of each spring. These springs are labeled as component No. 5 in the finite-element abutment model shown in Figure 2.12. The backwall body was modeled using elastic beam elements. The estimated shear capacity of the concrete backwall body is higher than the shear demand that is required to cause flexural failure of the wall-bottom hinge. Thus, shear failure of the backwall body was not explicitly modeled.

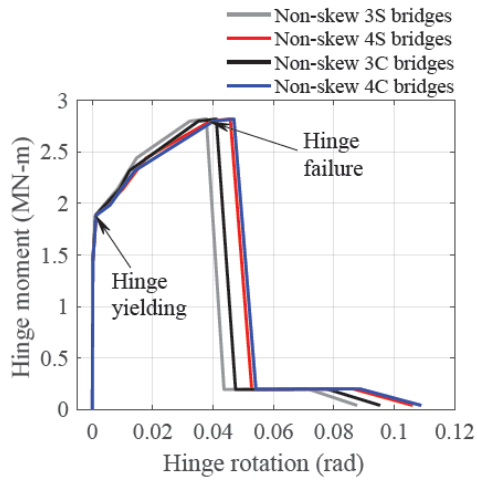

Figure 2.17: Moment-rotation relation of backwall bottom.

2.2.5.3 Backwall-Wingwall Connection Model

In the typical seat-type bridge abutment, pairs of bent steel dowel bars are typically embedded in the concrete at the junction between a backwall and a wingwall, crossing the construction joint between the two (IDOT 2012a). The configuration of these steel dowel bars can be found in Luo et al. (2017a). The purpose of these connections is to strengthen the construction joint between the backwall and wingwall and maintain the integrity of the abutment. During earthquake events, the backwall-wingwall connections help resist the out-of-plane bending response of the abutment back-wall, in conjunction with the backwall-to-pile-cap connections at the wall bottom, which was introduced earlier. In return, the backwall-wingwall connections will be subjected to shear demands from the superstructure-abutment interactions.

The shear force-deformation relation of each pair of steel dowel bars was estimated using an analytical model proposed by Vintzeleou and Tassios (1986). Calibrated by full-scale experimental results, the analytical model was proposed for predicting the shear force-deformation behavior of steel dowel bars embedded in concrete when subjected to interface shear. The idealized shear force-deformation relation of one pair of steel dowel bars is shown in Figure 2.16. In the abutment model shown in Figure 2.12, a nonlinear spring was used to simulate each pair of dowel bars connecting the backwall and wingwall, labeled as component No. 6. The shear force-deformation relation shown in Figure 2.16 was assigned to each nonlinear spring. The dowel model shown in Figure 2.16 has symmetrical force-deformation behavior in two opposite directions, which simulates the full cyclic dowel behavior. However, the dowels are basically only loaded in half cycles when the backwall is pushed by the deck under earthquakes in the longitudinal direction. The dowel model shown in Figure 2.16 supports cyclic response with both full and half loading cycles; the backbone curve for full and half loading cycles remains the same.

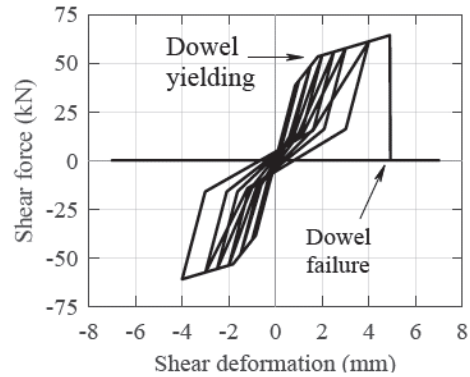

Figure 2.18: Idealized shear force-deformation relation of one pair of steel dowel bars connecting the abutment backwall and wingwall (Vintzeleou and Tassios 1986).

2.2.5.4 Backfill Passive Resistance Model

When the bridge is subjected to seismic demands, sufficiently large superstructure displacement in the longitudinal direction can cause closure of the expansion joint and engagement between the superstructure and abutment backwall. In this situation, the backwall is pushed against the backfill and embankment soil by the superstructure. As a result, passive resistance from the backfill and embankment soil is mobilized and acts as a major resistance to the displacement of the abutment and superstructure, in addition to the resistance of abutment foundation.

The force-displacement relation of the passive soil resistance behind the backwall was determined using an experimentally validated model proposed by Shamsabadi et al. (2005, 2007). This model was developed based on the limit-equilibrium logarithmic-spiral surface, method of slices, and hyperbolic stress-strain behavior of soils (Terzaghi et al. 1996; Shields and Tolunay 1973). As claimed by Shamsabadi et al. (2005, 2007), the passive force-displacement response of cohesive and cohesionless backfill soils predicted by this model is in good agreement with small-and full-scale experimental test results.

For the prototype bridges, as shown in Figure 2.11 and Figure 2.17, a nearly isosceles right triangular region of porous granular material is placed adjacent to the abutment backwall and pile cap. Figure 2.17 illustrates a typical logarithmic-spiral soil failure surface in passive conditions (Terzaghi et al. 1996). Stewart et al. (2007) and Bozorgzadeh et al. (2008) performed large-scale experimental tests on the passive response of bridge abutment backfill and found that the length of the passive soil failure wedge, labeled as L_{wedge} in Figure 2.17, was usually greater than twice the height of the soil wedge, H_{wedge} labeled in Figure 2.17. For the prototype bridge abutment, this wedge shape means that the soil failure surface tends to develop in the embankment soil outside the porous granular material, as shown in Figure 2.17. The embankment soil was assumed to be compacted clean sand, as compaction of road embankment soil is required by the Standard Specifications for Road and Bridge Construction of IDOT (2012b). The soil properties for compacted clean sand (Rollins et al. 2010a; Shamsabadi et al. 2007) were used in determining the backwall passive resistance.

In addition to the soil properties, the other critical factor for determining backfill passive resistance is the backwall and pile cap height. The backwall height, labeled as H_w in Figure 2.17, is the summation of the girder depth and bearing height, and varies in different major bridge types. The abutment pile cap height, labeled as H_p in Figure 2.17, remains the same for bridges of different major types. Table 2.5 summarizes H_w and Hp for the four major bridge types. The summation of H_w and Hp was regarded as the height of the passive soil wedge, H_{wedge}, for computing the backfill passive resistance.

For the non-skew prototype bridges, the computed force P versus backwall top displacement D of backfill passive resistance is shown in Figure 2.18. The ascending branch of the backbone curves exhibits a hyperbolic shape and is flattened after the ultimate passive capacity is reached. The unloading/reloading response was assumed to be linear based on the experimental results of Stewart et al. (2007). The force-displacement relation, $P(D)$, shown in Figure 2.18 was then distributed to the backwall and pile cap based on a triangular soil pressure distribution and a trapezoidal one (Terzaghi et al. 1996). The resistance on the backwall, P_{BW}, and that on the pile cap, P_{PC}, were further distributed into a number of nonlinear springs in the abutment model, on the basis of tributary backwall width of each spring. The springs for P_{BW} and P_{PC} are labeled as components No. 2 and 3 in Figure 2.12.

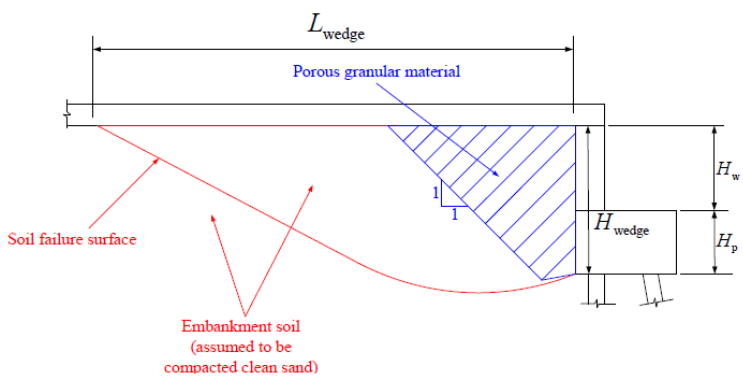

Figure 2.19: Logarithmic-spiral soil failure surface in passive conditions (Terzaghi et al. 1996).

Table 2.11: Height of Abutment Backwall and Pile Cap Defined in Figure 2.11 and Figure 2.17

Major bridge type	3S	4S	3C	4C
Backwall height H_w [m (ft)]	1.14 (3.75)	1.81 (5.94)	1.42 (4.66)	1.91 (6.27)
Pile cap height H_p [m (ft)]	1.07 (3.5)	1.07 (3.5)	1.07 (3.5)	1.07 (3.5)
Total height $H_w + H_p$ [m (ft)]	2.21 (7.25)	2.88 (9.44)	2.49 (8.16)	2.98 (9.77)

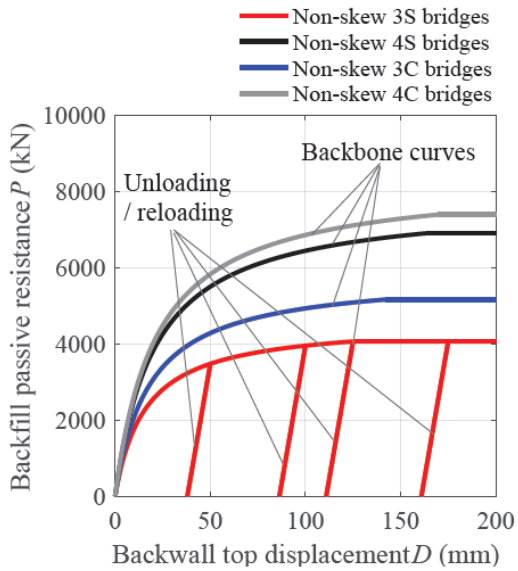

Figure 2.20: Passive resistance of abutment backfill of non-skew prototype bridges.

The backfill passive resistance normal to the backwall of a skew abutment, *P*skew, was computed using the backfill resistance *P* of a counterpart non-skew abutment with the same width W_a. Marsh (2013) investigated backfill passive resistance of skew abutments through large-scale experimental tests, and proposed the following equations:

$$P_{skew} = R(\theta)P \tag{2.3a}$$

$$R(\theta) = 8 \times 10^{-5}\theta^{2} - 0.0181\theta + 1 \tag{2.3b}$$

where P_{skew} and P are the ultimate passive resistance of skew and non-skew abutments, and ϑ is the bridge skew angle in degree. The *R* factor defined in Equation (2.3) is plotted in Figure 2.19. The *R* factor of skew bridges is always smaller than unity, which means that the ultimate backfill passive resistance of a skew abutment is smaller than that of the counterpart non-skew abutment. For the prototype skew bridges, the passive resistance *P* of non-skew bridges shown in Figure 2.18 was multiplied by the *R* factor defined in Equation (2.3). Additionally, in the finite-element model of skew abutments, the nonlinear springs for backfill passive resistance (components No. 2 and 3 in Figure 2.12) were oriented normal to the abutment backwall and pile cap.

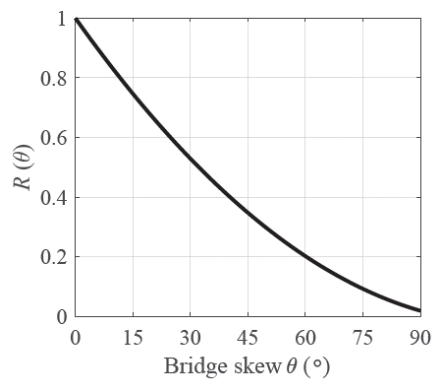

Figure 2.21: Reduction factor *R* for backfill passive resistance of skew abutments (Marsh 2013).

2.2.5.5 Wingwall Model

The backfill/embankment passive resistance applied to the abutment wingwalls was modeled using the same approach as that applied to the backwall. The nonlinear springs for passive soil resistance on wingwalls are labeled as component No. 4 in the abutment model shown in Figure 2.12. For many bridge embankments in Illinois, the top width of the embankment is close to the abutment width and there is not sufficient soil outside the two wingwalls for developing a passive soil failure wedge. Thus, the passive resistance from the soil enclosed by the abutment was considered, but that from the soil outside the wingwalls was neglected. This means that the nonlinear springs for passive soil resistance to wingwalls, labeled as component No. 4 in Figure 2.12, can only subjected to compression.

2.2.5.6 Approach Slab Model

As shown in Figure 2.11, a concrete approach slab is connected to the top of abutment backwall. In the prototype bridges, the length of the approach slab is typically 9.14 m (30 ft), the width is 12.19 m (40 ft), and the thickness is 0.38 m (1.25 ft). The weight of an approach slab is around 1,000 kN (225 kips). In order not to neglect this large amount of mass in the bridge seismic analysis, the approach slab was included in the abutment model. As shown in Figure 2.12, the slab body is modeled using a grid of elastic beam elements. The total slab mass was distributed into a number of nodal masses lumped to the boundary nodes of the beam elements.

2.2.5.7 Global Validation of Bridge Model

So far, large-scale shake-table tests on the seismic performance of full quasi-isolated bridges have not been conducted. A global validation of the finite-element bridge model could only be available after large-to full-scale shake-table tests are performed on quasi-isolated bridges. Although large-scale shake-table tests on other types of highway bridges have been very sparsely reported in the literature (e.g. Cruz-Noguez and Saiidi 2010), these test results cannot provide a reliable and comprehensive validation of the quasi-isolated bridge model, due to the inherent differences between the different types of bridges.

Alternatively, seismic response data collected from field-instrumented quasi-isolated bridges during real earthquakes would also be used for global validation of the quasi-isolated bridge model. However, such data has not been collected in the current stage. Although seismic response data has been collected for a few instrumented bridges during historical earthquakes (e.g. Zhang and Makris 2002), the ability of this data to validate the quasi-isolated bridge model is very limited, due to the inherent differences between the instrumented bridges and quasi-isolated bridges.

Although a global model validation is not available in the current state due to the lack of shake-table and field test data on quasi-isolated bridges, numerical models of many of the critical bridge components have been validated either by the author or the developer of the component models that were employed in the global bridge model.

CHAPTER 3: NONLINEAR DYNAMIC ANALYSIS DETAILS

3.1 SEISMIC PERFORMANCE ASSESSMENT PROCEDURE

To provide a comprehensive and extensive assessment of the seismic performance of the prototype quasi-isolated bridges, each of the 80 bridge variants was subjected to a suite of 20 earthquake ground motion time histories applied in the four horizontal incident directions. This led to 1,600 nonlinear dynamic analyses for each of the four major bridge types and 6,400 analyses in total for all the bridges.

In the nonlinear dynamic analyses, stiffness-proportional viscous damping was employed. At each step of a dynamic analysis, the viscous damping matrix is constructed using the tangential global stiffness matrix. This was multiplied by a constant coefficient that was determined by using a targeted viscous damping ratio for the fundamental mode of 5% and the initial elastic fundamental period of the bridge. Pant et al. (2013) concluded that the stiffness-proportional damping with a constant coefficient determined using the frequency of the entire base-isolated building rather than the superstructure alone provides a reasonable estimate of the peak structural response. The use of tangential-stiffness-proportioned damping in nonlinear dynamic structural analyses was also recommended by Petrini et al. (2008) and Charney (2008), and, thus, it was adopted in this study.

In the nonlinear dynamic analyses, the equations of motion were solved by the Trapezoidal Rule with the second-order Backward Difference Formula (TRBDF2) integration scheme proposed by Bathe (2007). It is a direct implicit time-integration scheme with second-order accuracy and unconditional stability. Different from the Newmark-β and HHT-α schemes, this scheme has no parameter to choose or adjust by the analyst. A five-millisecond default time step size was used in the analyses. At each time step, the Krylov Subspace accelerated Newton algorithm proposed by (Scott and Fenves 2010) was employed as the default iterative algorithm for solving the nonlinear system of equations. Whenever convergence difficulties were encountered at a time step, alternative iterative algorithms (e.g., the Newton's method with line search) and a smaller step size were relied upon to achieve convergence at this step. After the convergence was achieved, the default iterative algorithm and time step size were resumed in the next step.

Considering the large number of nonlinear dynamic analyses to perform, the supercomputer "Stampede" at the Texas Advanced Computing Center (TACC), the University of Texas at Austin, was utilized to process the computational jobs in parallel. The multi-processor interpreter of *OpenSees*, *OpenSeesMP* (McKenna and Fenves 2008), was compiled and configured on Stampede for running analyses. Multiple computing nodes can be requested for one multi-threaded job. In this study, each bridge variant was subjected to the suite of 20 ground motions applied in the four incident directions. Therefore, five computing nodes with 80 CPU cores in total were requested for one multi-threaded job in which all the 80 dynamic analyses of one bridge variant were included.

3.2 EARTHQUAKE GROUND MOTION TIME HISTORIES

A suite of 20 site-specific earthquake accelerograms was employed for the nonlinear response-history analyses performed on the bridge models. These accelerograms were developed by modifying historical bedrock motions recorded from other geographic regions to match the site-specific seismic hazard level at Cairo, Illinois. Located in the center of the New Madrid Seismic Zone, Cairo, possesses the highest seismicity in the entire state of Illinois. The accelerograms represent a seismic hazard level of 5% probability of exceedance in 50 years (1,000-year return period), as AASHTO has increased the specified return period for design earthquakes from 500 years to 1,000 years since 2008 (AASHTO, 2008b). The geotechnical site conditions at Cairo were also considered in development of the accelerograms. Figure 3.1 shows the pseudo-acceleration response spectra. The peak ground acceleration of the accelerograms ranges from 0.26 g to 0.40 g. The procedure for developing the accelerograms has been reported in detail by Kozak et al. (2017). More information about the ground motions can be found in Appendix B and in LaFave et al. (2018).

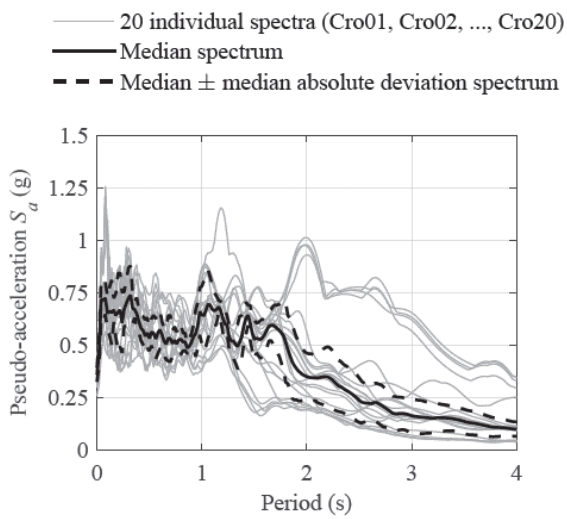

Figure 3.1: 5%-damping elastic pseudo-acceleration response spectra of seismic ground motions employed for nonlinear dynamic time-history analysis.

In the nonlinear dynamic bridge analyses, the suite of 20 accelerograms was applied to each prototype bridge in four horizontal incident directions, namely the pure longitudinal (0°) and transverse (90°), as well as 45° and 135°, directions, as shown in Figure 3.2. The earthquake ground motions applied in four directions is an attempt to reduce the uncertainty of ground motion incident direction in the assessment program while still maintaining an affordable number of response-history analyses. By acting on the nodal masses of a finite-element bridge model, an accelerogram induces inertia forces to the bridge. It is important to note that the effects of vertical ground acceleration are not included in the current study.

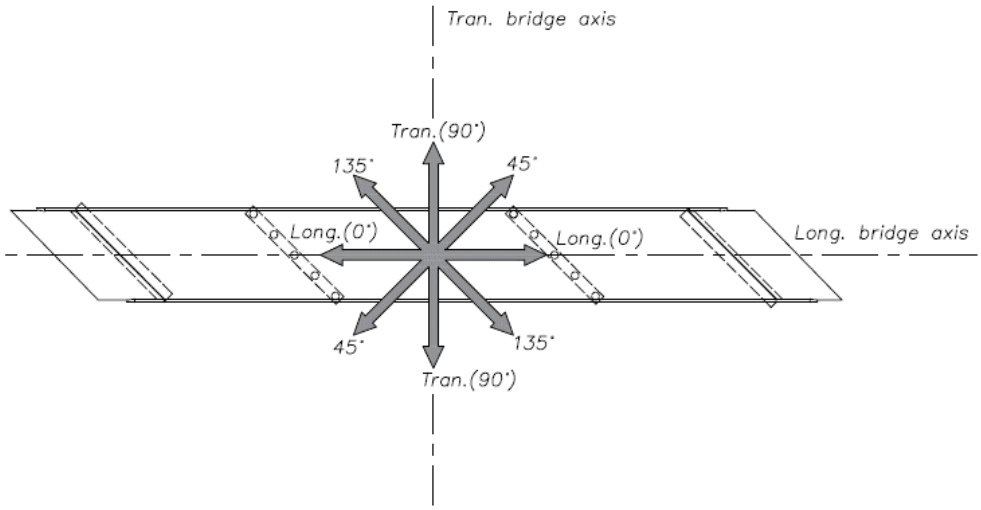

Figure 3.2: Four horizontal incident directions (0°, 45°, 90°, and 135°) of earthquake ground motion time histories for nonlinear dynamic bridge analyses.

3.3 IDENTIFICATION OF COMPONENT LIMIT STATE OCCURRENCES

Table 3.1 lists the limit states of critical bridge components that were monitored during analysis, which are used as measures indicating bridge seismic performance. Some of the limit states are desired fusing actions, such as the sliding of elastomeric bearings and the rupture of bearing anchors or dowel bars, while others represent component damage, such as the yielding of reinforcing steel and the crushing of concrete cover at pier column bases, as well as the unseating of bearings at substructures. As observed during post-earthquake reconnaissances (e.g. Yen et al. 2011), unseating of bearings can be a major cause of a global bridge collapse, and so it is regarded as an unacceptable damage limit state.

In the response-history analysis, the unseating of bearings is not explicitly simulated, but rather it is identified by comparing maximum bearing sliding distance with the bearing seat width at the substructure during post-processing. Figure 2.2a illustrates abutment-normal and -parallel sliding directions toward unseating of the four exterior abutment bearings. The four deck corners supported by these bearings will be referred to as the “upper-left corner”, “lower-left corner”, “upper-right corner”, and “lower-right corner”, as shown in Figure 2.2. For both skew and non-skew bridges, the four exterior abutment bearings are subject to a higher risk of unseating than the other interior bearings at the abutments, due to a shorter seat width in the abutment-parallel direction. Sliding limits in the abutment-parallel and -normal directions are conservatively calculated assuming that unseating will occur as long as any part of the elastomer slides and reaches an abutment edge. Sliding limits in the abutment-parallel and -normal directions are denoted as d_p and d_n, respectively, which are conservatively calculated assuming that unseating will occur as long as any part of the elastomer slides and reaches an abutment edge. Figure 3.3 shows schematic diagrams for calculating d_p and d_n. For the bearing support at an acute deck corner, d_p and d_n are calculated as follows (Luo et al. 2017b):

$$d_p = N\cos\alpha + \left(d_e - \frac{W_e}{2}\right)\sin\alpha - \frac{L_e}{2}\cos\alpha \tag{3.1a}$$

$$d_n = \cos\alpha\left(N - d_e - \frac{W_e}{2}\right) - \frac{L_e}{2}\sin\alpha \tag{3.1b}$$

and for the bearing support at an obtuse deck corner, d_p and d_n are determined as follows:

$$d_p = N\cos\alpha - \left(d_e + \frac{W_e}{2}\right)\sin\alpha - \frac{L_e}{2}\cos\alpha \tag{3.2a}$$

$$d_n = \cos\alpha\left(N - d_e - \frac{W_e}{2}\right) - \frac{L_e}{2}\sin\alpha \tag{3.2b}$$

where

d_e = distance between bearing center and girder end;

L_e = length of bearing elastomer;

W_e = width of bearing elastomer;

α = bridge skew angle (°);

N = minimum seat width (in.) at a bridge substructure for a 1000-year seismic event, determined per IDOT Bridge Manual (IDOT 2012).

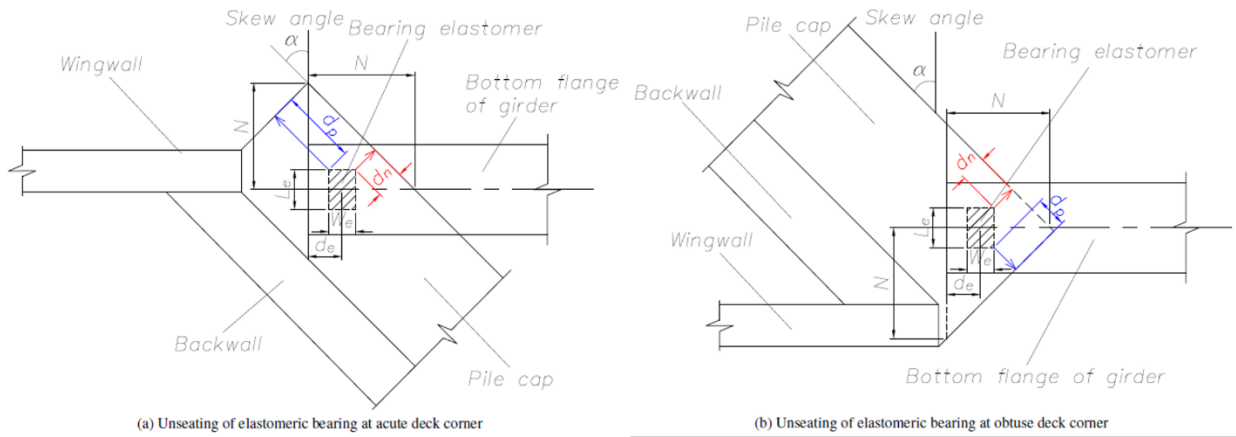

Figure 3.3: Unseating of elastomeric bearings at deck corners: (a) acute deck corner; (b) obtuse deck corner.

Table 3.1: Fusing and Damage Limit States of Critical Bridge Components

Substructure	Limit states	Abbreviation	Category
Abutments (A1 and A2)	Closure of expansion joint	CEJ@A1 and/or A2	Preferred
	Mobilization of backfill ultimate capacity	MBU@A1 and/or A2	Damage, acceptable
	Failure of backwall-to-pile-cap connection	FBP@A1 and/or A2	Fusing, acceptable
	Rupture of retainer anchor	RRA@A1 and/or A2	Fusing, preferred
	Sliding of elastomeric bearing	SEB@A1 and/or A2	Fusing, preferred
	Unseating of elastomeric bearing at acute deck corner	**UBA@A1 and/or A2**	**Damage unacceptable**
	Unseating of elastomeric bearing at obtuse deck corner	**UBO@A1 and/or A2**	**Damage, unacceptable**
	Yielding of pile supporting wingwall	YPW@A1 and/or A2	Damage, acceptable
	Yielding of pile supporting backwall	YPB@A1 and/or A2	Damage, acceptable
Expansion piers (P1 and P3)	Rupture of retainer anchor	RRA@P1 and/or P3	Fusing, preferred
	Sliding of elastomeric bearing	SEB@P1 and/or P3	Fusing, preferred
	Unseating of elastomeric bearing	**UEB@P1 and/or P3**	**Damage, unacceptable**
	Yielding of vertical reinforcing steel at column base	YRS@P1 and/or P3	Damage, acceptable
	Rupture of vertical reinforceing steel at column base	**RRS@P1 and/or P3**	**Damage, unacceptable**
	Crushing of concrete cover at column base	CCC@P1 and/or P3	Damage, acceptable
	Yielding of pile at pier	YPP@P1 and/or P3	Damage, acceptable
Fixed pier (P2)	Rupture of retainer anchor (only for 3C and 4C bridges)	RRA@P2	Fusing, preferred
	Rupture of steel dowel connection (only for 3C and 4C bridges)	RSD@P2	Fusing, preferred
	Rupture of steel fixed bearing anchor (only for 3S and 4S bridges)	RFA@P2	Fusing, preferred
	Unseating of steel fixed bearing	**USB@P2**	**Damage, unacceptable**
	Yielding of vertical reinforcing steel at column base	YRS@P2	Damage, acceptable
	Rupture of vertical reinforcing steel at column base	**RRS@P2**	**Damage, unacceptable**
	Crushing of concrete cover at column base	CCC@P2	Damage, acceptable
	Yielding of pile at pier	YPP@P2	Damage, acceptable

Damage to pier columns is classified into four levels based on the tensile strain of the vertical reinforcing steel and the compressive strain of unconfined concrete cover, both of which are measured at the column base. Table 3.2 shows the ranges of peak strain for these damage levels (Kowalsky 2001 and Revell 2013).

Table 3.2: Classification of Pier Column Damage

Damage level	Peak strain range	
	Vertical reinforcing steel (tension)	Unconfined concrete cover (compression)
Undamaged	0 ~ 0.0021	-0.002 ~ 0
Lightly damaged (unlikely requiring repair)	0.0021 ~ 0.015	-0.005 ~ -0.002
Moderately damaged (repairable)	0.015 ~ 0.06	-0.018 ~ 0.005
Severely damaged (not easily repairable)	≥ 0.06	≤ - 0.018

CHAPTER 4: SEISMIC PERFORMANCE ASSESSMENT VIA NONLINEAR DYNAMIC ANALYSES

Component limit states introduced in Chapter 3 were identified for each of the 6,400 analyses, and the occurrences of these limit states were statistically studied. In addition to limit states, peak values of some critical structural responses parameters were also recorded in each analysis, such as the tensile strain of reinforcing steel and the compressive strain of concrete cover at pier column bases, as well as the displacement and rotation of bridge superstructures. For a specific structural response, the median of the 20 peak values excited by the 20 individual ground motions applied in the same incident direction was employed to statistically measure the response amplitude, as shown in Eq. (4.1)

$$\text{median}(u) = \underset{GM = \text{Cro01, Cro02, …, Cro20}}{\text{median}} \left(\max_t \left| u(t;\ GM) \right| \right) \tag{4.1a}$$

$$\text{MAD}(u) = \underset{GM = \text{Cro01, Cro02, …, Cro20}}{\text{median}} \left(\max_t \left| u(t;\ GM) \right| - \text{median}(u) \right) \tag{4.1b}$$

where $u(t;\ GM)$ denotes the time series of a specific structural response, $u(t)$, excited by a ground motion *GM*. The statistical measure determined by Eq. (4.1) is hereafter referred to as "median peak response". Because each bridge model can be highly nonlinear and may sustain many damage and rupture events in an analysis, some of the peak responses in a data set can be significantly away from the other observations and are viewed as outliers. Therefore, the median was preferred over the mean in this study because the median is generally more robust against outliers than is the mean (Ryan 2006). To measure the statistical dispersion of response data, the median absolute deviation (MAD) was employed. As a robust statistic, the MAD is generally less sensitive to outliers than is the standard deviation (Sheskin 2011). The MAD of peak values of a structural response was calculated using Eq. (4.1b).

4.1 OVERALL BRIDGE SEISMIC PERFORMANCE

An overview of the analysis results reveals that the bridges exhibited two primary performance deficiencies that could potentially result in extensive seismic damage and even losses of bridge spans during a major earthquake. One deficiency is the unseating of abutment bearings of highly skewed bridges supported by tall piers, and the other is the damage to short pier columns of non-skew or lightly skewed bridges, especially the heavy 4C bridges. Except for these two primary deficiencies, occurrences of the other limit states are less likely to cause global bridge failure and are generally accepted by the quasi-isolation design strategy. More details of the bridge seismic response can be found in Appendix C.

4.2 SLIDING AND UNSEATING OF ELASTOMERIC BEARINGS

The limit state of bearing unseating was identified by comparing the peak bearing sliding distance with the corresponding seat width at substructures. Figure 4.1 illustrates the peak sliding ratios of the four exterior abutment bearings supporting four deck corners. For each bearing, the peak sliding distance normalized to the corresponding abutment seat width in both the abutment-normal and abutment-parallel directions are recorded. For each of the 1,600 analyses, peak bearing sliding distances in the two directions were plotted as a dot in the two-dimensional figure. In 11 out of the 1,600 analyses, exterior abutment bearing unseating was observed, all of which occurred at 45°- and 60°-skew bridges supported by tall pier columns. Most of the unseating cases occurred at acute deck corners in the abutment-normal direction. The unseating of abutment bearings was not observed in any of the 3S bridge analyses, while it occurred in only 1 and 2 analyses of 4S and 3C bridges, respectively. Bearing unseating at intermediate piers was not observed in any analysis.

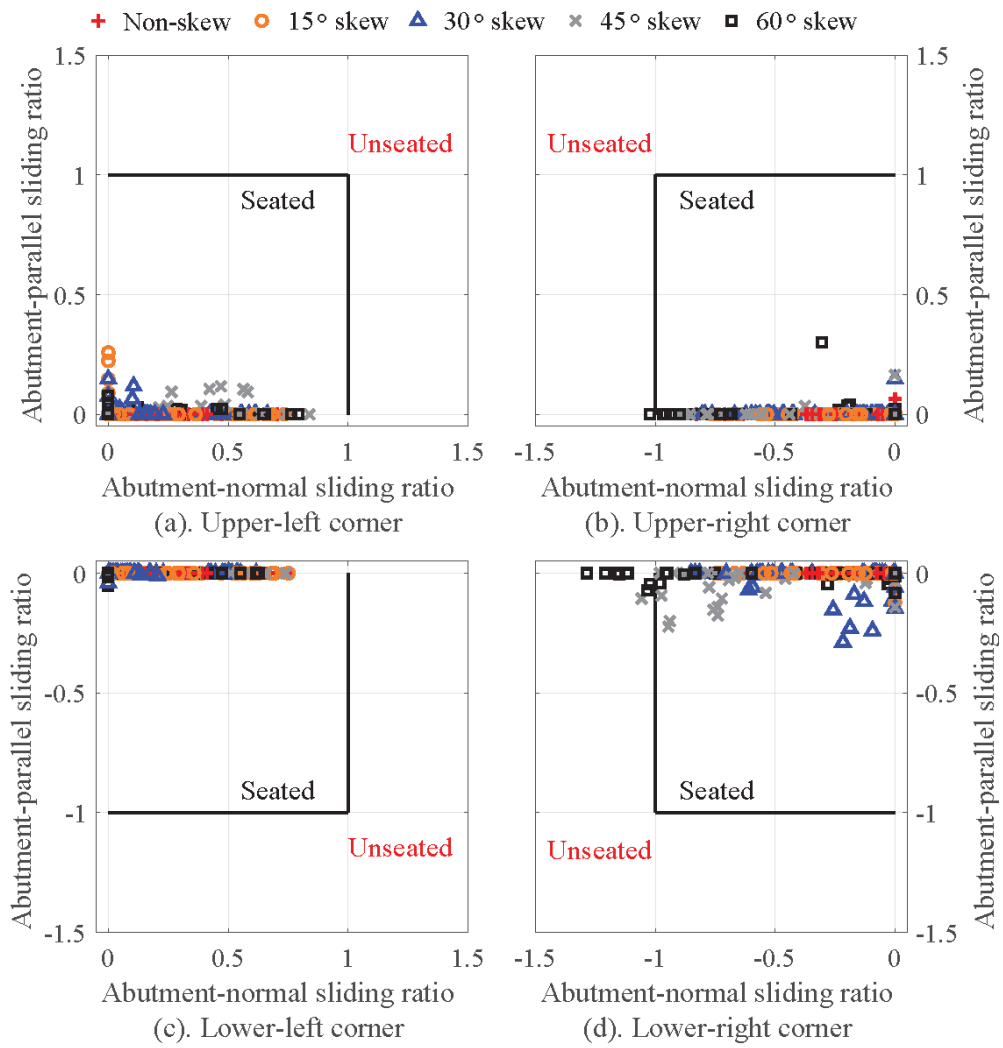

Figure 4.1: Peak sliding ratios of elastomeric bearings at deck corners of 4C bridges.

4.3 FUSING PERFORMANCE OF SACRIFICIAL SUPERSTRUCTURE-SUBSTRUCTURE CONNECTIONS

Table 4.1 statistically summarizes the fusing performance of steel fixed bearings (3S and 4S bridges) and the steel dowel connections (3C and 4C bridges) on top of fixed piers (Pier 2). For 3S and 4S bridges, fusing of Pier 2 connections occurred only in 4.4% and 11.8% of the 1,600 analyses for each basic bridge type, respectively. For 3C and 4C bridges, the percentage of occurrences is larger (19.3% and 32.7%) than that of 3S and 4S bridges. Relative contribution of each parametric variation to total occurrences was also studied. It was found that bridges with larger skews, short pier columns, and hard foundation soil sustained much more fusing of Pier 2 connections than their equivalent bridges with small skews, tall pier columns, and soft foundation soil. For example, 100% of the fusing occurred at 3S bridges with 45°- and 60°-skews; 89.9% of the fusing occurred at 4S bridges with hard foundation soil; 82.6% of the fusing occurred at 4C bridges supported by short pier columns. For each of the four basic bridge types, the rupturing of bearing retainer anchors was not observed in any analysis.

Table 4.1: Fusing performance of Steel Fixed Bearings (3S and 4S bridges) and Steel Dowel Connections (3C and 4C bridges) on Top of Fixed Piers (Pier 2)

Basic bridge type	No. of analyses with limit state occurrences[1]	Skew angle (°)[2]					Foundation soil[2]		Pier column height[2]	
		0	15	30	45	60	Hard	Soft	Short (4.6 m)	Tall (12.2 m)
3S	71 (4.4%)	0 (0%)	0 (0%)	0 (0%)	16 (22.5%)	55 (77.5%)	65 (91.5%)	6 (8.5%)	57 (80.3%)	14 (19.7%)
3C	309 (19.3%)	0 (0%)	1 (0.3%)	20 (6.5%)	111 (35.9%)	177 (57.3%)	231 (74.8%)	78 (25.2%)	231 (74.8%)	78 (25.2%)
4S	188 (11.8%)	0 (0%)	1 (0.5%)	10 (5.3%)	43 (22.9%)	134 (71.3%)	169 (89.9%)	19 (10.1%)	152 (80.9%)	36 (11.1%)
4C	523 (32.7%)	26 (5.0%)	37 (7.1%)	75 (14.3)	163 (31.2%)	222 (42.4%)	353 (67.5%)	170 (22.5%)	432 (82.6%)	91 (17.4%)

1. Percentage in brackets equals to no. of analyses with limit state occurrences out of 1,600 analyses.
2. Percentage in bracekts indicates contribution of each parameter to no. of analyses with limit state occurrences.

Table 4.2 summarizes the fusing performance of bearing retainer anchors at the two abutments. A clear trend for all the four basic bridge types is that tall-pier bridges sustained significantly more fusing of abutment bearing retainers than their equivalent short-pier bridges. The fusing limit state occurred more at bridges with hard foundation soil than those with soft soil, but the difference is less significant than that between tall and short-pier bridges. The bridges with large skews experienced more bearing retainer fusing at abutments than those with small skews.

Table 4.2: Fusing Performance of Bearing Retainer Anchors at Bridge Abutments

Basic bridge type		No. of analyses with limit state occurrences[1]	Skew angle (°)[2]					Foundation soil[2]		Pier column height[2]	
			0	15	30	45	60	Hard	Soft	Short (4.6 m)	Tall (12.2 m)
3S	Abut. 1	662	61 (9.2%)	103 (15.6%)	155 (23.4%)	176 (26.6%)	167 (25.2%)	378 (57.1%)	284 (42.9%)	144 (21.8%)	518 (78.2%)
	Abut. 2	391	17 (4.3%)	32 (8.2%)	107 (27.4%)	132 (33.8%)	103 (26.3%)	236 (60.4%)	155 (39.6%)	15 (3.8%)	376 (96.2%)
3C	Abut. 1	446	39 (8.7%)	61 (13.7%)	96 (21.5%)	122 (27.4%)	128 (28.7%)	241 (54.0%)	205 (46.0%)	23 (5.2%)	423 (94.8%)
	Abut. 2	329	12 (3.6%)	19 (5.8%)	76 (23.1%)	108 (32.8%)	114 (34.7%)	205 (62.3%)	124 (37.7%)	10 (3.0%)	319 (97.0%)
4S	Abut. 1	269	15 (5.6%)	20 (7.4%)	47 (17.5%)	83 (30.9%)	104 (38.7%)	174 (64.7%)	95 (35.3%)	1 (0.4%)	268 (99.6%)
	Abut. 2	225	14 (6.2%)	20 (8.9%)	41 (18.2%)	66 (29.3%)	84 (37.3%)	162 (72.0%)	63 (28.0%)	0 (0.0%)	225 (100.0%
4C	Abut. 1	259	22 (8.5%)	25 (9.7%)	50 (19.3%)	74 (28.6%)	88 (34.0%)	188 (72.6%)	71 (27.4%)	18 (6.9%)	241 (93.1%)
	Abut. 2	304	21 (6.9%)	22 (7.2%)	58 (19.1%)	85 (28.0%)	118 (38.8%)	185 (60.9%)	119 (39.1%)	34 (11.2%)	270 (88.8%)

1. Percentage in brackets equals to no. of analyses with limit state occurrences out of 1,600 analyses.
2. Percentage in bracekts indicates contribution of each parameter to no. of analyses with limit state occurrences.

4.4 DAMAGE TO PIER COLUMNS

Table 4.3 summarizes the pier column damage levels of each major bridge type. The column damage was classified in accordance with Table 3.2. The short pier columns of 4S and 4C bridges sustained moderate to severe damage. The short fixed-pier columns sustained more severe damage than the short expansion-pier columns. On the contrary, damage to the tall columns is similar at the fixed and expansion piers. In general, the three-span bridges sustained much less pier column damage than the four-span bridges.

Table 4.3: Summary of Pier Column Damage

Pier column type		Major bridge type			
		3S	3C	4S	4C
Short columns (3.5 ft dia., 2% reinforcing ratio)	Expansion pier	Undamaged	Undamged	Undamaged to light	Moderate to severe
	Fixed pier	Undamaged to light	Light to moderate	Moderate	Moderate to severe
Tall columns (4 ft dia., 2% reinforcing ratio)	Expansion pier	Undamaged	Undamaged to light	Light	Light
	Fixed pier	Undamaged	Undamaged to light	Light	Light

4.5 OTHER LIMIT STATES

The yielding of abutment piles was quite commonly observed for all the four basic bridge types. For 3S bridges, the yielding of abutment piles was observed in about 60% of the analyses, but this percentage increased to 80% and 90% for the other three types of bridges, as shown in Table 4.4. The yielding of pier piles was rarer than that of abutment piles, while the yielding of piles supporting expansion piers occurred less that of fixed-pier piles. Table 4.4 shows the occurrence percentage of pile yielding at intermediate piers. The piles supporting intermediate piers in the soft foundation soil were more susceptible to yielding than those in the hard soil, as shown in Table 4.6. At bridge abutments, closure of the expansion joint between the deck end and backwall was observed in over 90% of the analyses for each basic bridge type. In contrast, the failure of backwall-to-pile-cap connections and the mobilization of ultimate passive resistance for the backfill very rarely occurred in all the analyses.

4.6 THE EFFECT OF SUPERSTRUCTURE SEISMIC MASS

The mass of bridge superstructures played an important role in the bridge seismic response and limit state occurrence. The superstructure mass of the four basic bridge types are listed in Table 2.3. The 3S bridges have the lightest superstructures while the 4C bridges have the heaviest ones. Table 4.4 summarizes the component damage limit states that show positive correlation with bridge superstructure mass. The occurrence of the tabulated limit states increases with superstructure mass.

Table 4.4: Damage Limit States Showing Positive Correlation With Superstructure Mass (Superstructure Masses of 3S, 3C, 4S, and 4C Bridges Rank in Ascending Order)

Substructure	Damaging limit state	3S bridges	3C bridges	4S bridges	4C bridges
Abutment 1	Mobilization of backfill ultimate capacity (MBU@A1)	1%	3%	3%	9%
	Yielding of pile supporting wingwall (YPW@A1)	61%	81%	80%	88%
	Yielding of pile supporting backwall (YPB@A1)	64%	92%	88%	98%
Abutment 2	Mobilization of backfill ultimate capacity (MBU@A2)	1%	3%	3%	8%
	Yielding of pile supporting wingwall (YPW@A2)	60%	77%	79%	90%
	Yielding of pile supporting backwall (YPB@A2)	58%	83%	87%	97%
Pier 1 (expansion pier)	Yielding of vertical reinforcing steel at column ends (YRS@P1)	10%	27%	57%	76%
	Crushing of concrete cover at column ends (CCC@P1)	0%	0%	2%	26%
	Yielding of piles (YSP@P1)	17%	37%	39%	54%
Pier 3 (expansion pier)	Yielding of vertical reinforcing steel at column ends (YRS@P3)	N/A	N/A	55%	76%
	Crushing of concrete cover at column ends (CCC@P3)	N/A	N/A	4%	29%
	Yielding of piles (YSP@P3)	N/A	N/A	39%	52%
Pier 2 (fixed pier)	Yielding of vertical reinforcing steel at column ends (YRS@P2)	42%	63%	89%	92%
	Crushing of concrete cover at column ends (CCC@P2)	0%	9%	34%	43%
	Yielding of piles (YSP@P2)	32%	54%	73%	64%

4.7 THE EFFECT OF BRIDGE SKEW

The highly skewed bridges of all the four types typically sustained more fusing of bearing retainers at abutments and steel bearings or dowels at fixed piers than the bridges with smaller skews. This is largely due to the bi-directional translation and rotation of the skew superstructure. Directly resulted from rupture of abutment bearing retainers, the highly skewed bridges were more susceptible to bearing unseating at abutments than those with small skews. As indicated in Section 4.3, the observed bearing unseating at abutments exclusively occurred in bridges with 45° and 60° skews supported by tall pier columns. For many bridges with high skews, the peak bearing sliding distance was quite close to the abutment seat width, although bearing unseating did not occur. For highly skewed bridges, the closure of expansion joints occurred in almost all the analyses due to the bi-directional deck displacement, regardless of ground motion incident direction.

Field reconnaissances of the 1971 San Fernando earthquake and the 2010 Chile earthquake found that skew bridges experienced in-plane deck rotation and their acute deck corners

tended to drop off the abutment under strong earthquake ground motions (Yen et al. 2011). As an example for this response characteristic, Figure 4.2 shows the collapse of a 40°-skew bridge during the 2010 Chile earthquake. The failure pattern of the two curtain walls (walls on the two transverse sides of an abutment, acting as side restrainers to the deck end) at one abutment demonstrated that the acute deck corner knocked off the curtain wall adjacent to it and dropped off from the abutment. This caused a global collapse of the bridge, while the curtain wall adjacent to the obtuse deck corner was intact. This observed seismic response characteristic of skew bridges is generally consistent with the response observed herein. In both the longitudinal and transverse analyses, the acute deck corner of highly skewed bridges tended to drop off the abutment in either the abutment-parallel or abutment-normal direction.

It has been concluded that the oblique contact between the skew deck end and abutment is a major cause of the deck rotation and bearing unseating (Kawashima et al. 2011). Figure 4.3a shows a schematic of the in-plane deck rotation of a skew bridge during a longitudinal pushover analysis. As the right deck end engages with Abutment 2 after the closure of the expansion joint, the skew abutment causes a resultant resistance R of the normal contact resistance Rn and the tangential friction resistance R_t. This resultant force causes the bridge superstructure to rotate in the clockwise direction and the acute deck corner at Abutment 2 tends to drop off the abutment. This behavior can actually be explained by an analogy to the classical kinematics problem of the sliding of a mass block on a slope, as shown in Figure 4.3b. Under the gravity force, the block will slide along the slope when the tangential friction is too insufficient to resist the component of the gravity force along the slope. The sliding of the skew deck end at the abutment under a longitudinal seismic force behaves similarly to the sliding of the block on the slope. When the component of the seismic force along the abutment exceeds resistance provided by the abutment, which includes the restraints from the bearing retainers and friction at the bearing bottom, then the deck end will slide along the abutment. Figure 4.3c illustrates the unseating mechanism of a skew bridge under transverse seismic forces. As the bridge is pushed transversely, the expansion joint at Abutment 1 is closed and the deck end is restrained from large transverse displacement by the normal contact and tangential friction at the closed joint. However, the expansion joint at Abutment 2 becomes wider and wider, and the acute deck corner will drop off from Abutment 2 after the transverse bearing retainers are fused.

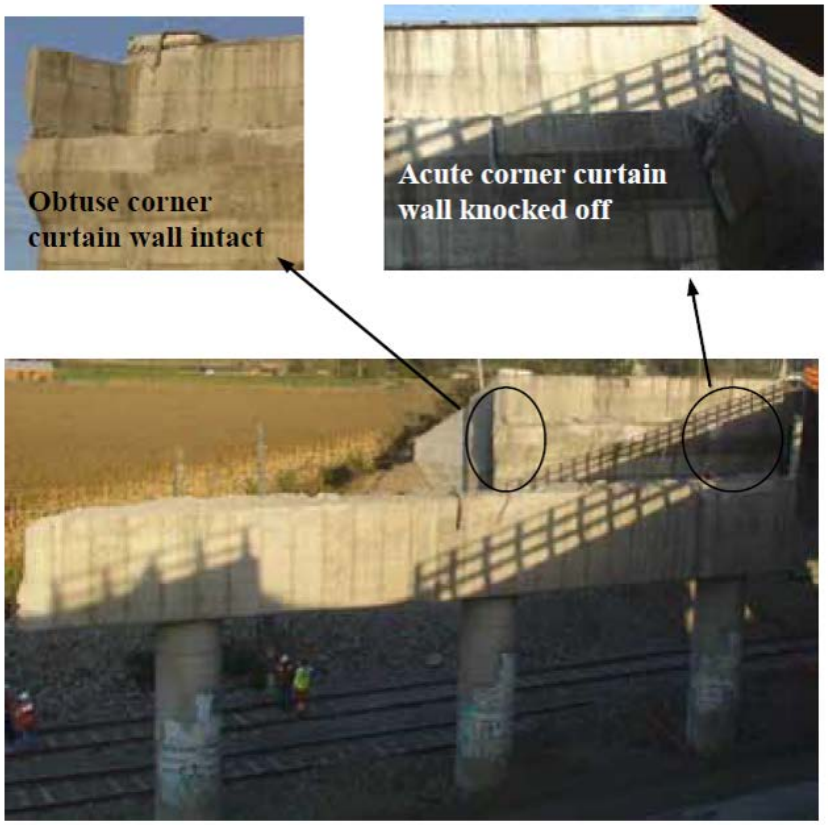

Figure 4.2: Collapse of a Route 5 overcrossing at Hospital during the 2010 Chile earthquake (Figure Source: Yen et al. 2011).

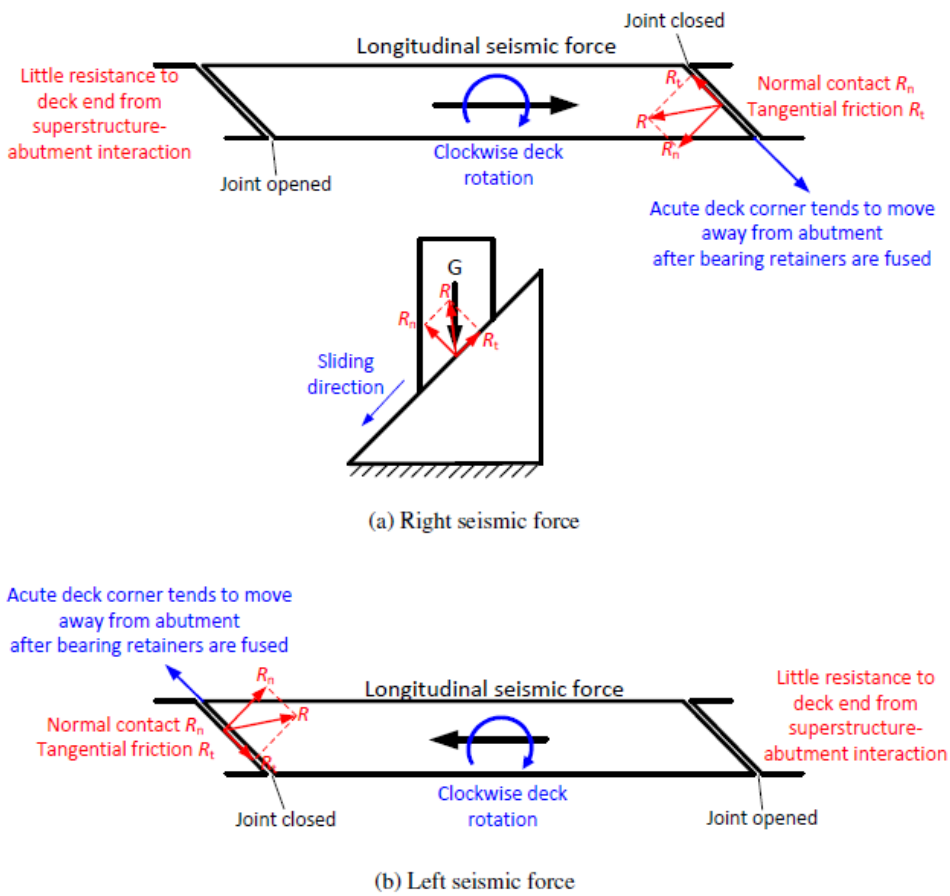

Figure 4.3: Rotation of bridge superstructure subjected to longitudinal seismic forces.

4.8 THE EFFECT OF PIER COLUMN HEIGHT

For each of the four types of bridges, the taller pier columns resulted in significantly larger deck displacement and rotation than did the shorter ones. The most undesirable consequence of the large deck displacement and rotation is the unseating of bearings, which occurred exclusively at the abutments of tall-pier bridges. Besides bearing unseating, the tall-pier bridges of all the four types are more susceptible to a few component limit states than their short-pier equivalents, as shown in Table 4.5. The high occurrences of these limit states are essentially a direct consequence of the large deck displacement and rotation. In contrast, some other limit states occurred more in short-pier bridges than in their tall-pier equivalents. These limit states are all associated with the fixed pier (Pier 2), as shown in Table 4.5. In the short-pier bridges, the fixed pier has much larger lateral stiffness than the expansion piers. As a result, the stiff fixed pier incurred considerable seismic forces and resulted in damage to the connections, columns and piles at Pier 2.

4.9 THE EFFECT OF FOUNDATION SOIL CONDITION

For each of the four types of bridges, the peak deck displacements were generally higher in the presence of the soft soil. However, the deck rotations appeared to be insensitive to the

foundation soil condition. As summarized in Table 4.6, the sacrificial superstructure-to-substructure connections at abutments and fixed piers fused easier at bridges with the soft foundation soil than those with the hard soil. The hard soil increases the lateral stiffness of the substructures and provides the required forces to rupture the anchors, which eventually helps the fusing of these sacrificial components. On the contrary, the mobilization of full backfill resistance occurred more at bridges with the soft soil. The large deck displacement resulting from the soft foundation soil caused considerable deformation of abutment backfill.

Table 4.5: Effect of Pier Column Height on Occurrence of Limit States

Occurrence of limit state	Substructure	Limit state	3S bridges		4S bridges		3C bridges		4C bridges	
			Short pier	Tall pier	Short pier	Tall pier	Short pier	Tall pier	Short pier	Tall pier
More in tall-pier bridges	Abutment 1	Rupture of retainer anchor (RRA@A1)	22%	78%	0%	100%	5%	95%	7%	93%
		Mobilization of backfill ultimate capacity (MBU@A1)	0%	100%	0%	100%	2%	98%	19%	81%
		Slidng of elastomeric bearing (SEB@A1)	5%	95%	19%	81%	2%	98%	9%	91%
	Abutment 2	Rupture of retainer anchor (RRA@A2)	4%	96%	0%	100%	3%	97%	11%	89%
		Mobilization of backfill ultimate capacity (MBU@A2)	0%	100%	0%	100%	3%	97%	8%	92%
		Slidng of elastomeric bearing (SEB@A2)	1%	99%	17%	83%	1%	99%	13%	87%
		Unseating of bearing at obtuse corner of deck (UBO@A2)	N/A	N/A	N/A	N/A	N/A	N/A	0%	100%
		Unseating of bearing at acute corner of deck (UBA@A2)	N/A	N/A	0%	100%	0%	100%	0%	100%
	Pier 1 (expansion	Yielding of vertical reinforcing steel at column base (YRS@P1)	2%	98%	35%	65%	8%	92%	47%	53%
	Pier 3 (expansion	Yielding of vertical reinforcing steel at column base (YRS@P3)	N/A	N/A	34%	66%	N/A	N/A	46%	54%
More in short-pier bridges	Pier 2 (fixed pier)	Rupture of steel fixed bearing anchors (RFA@P2)	80%	20%	81%	19%	N/A	N/A	N/A	N/A
		Rupture of steel dowel connection (RSD@P2)	N/A	N/A	N/A	N/A	75%	25%	83%	17%
		Yielding of vertical reinforcing steel at column base (YRS@P2)	67%	33%	51%	49%	56%	44%	51%	49%
		Crushing of concrete cover at column base (CCC@P2)	100%	0%	81%	19%	93%	7%	67%	33%
		Yielding of pile (YSP@P2)	56%	44%	56%	44%	58%	42%	60%	40%

Table 4.6: Effect of Foundation Soil on Occurrence of Limit States

Occurrence of limit state	Substructure	Limit state	3S bridges		4S bridges		3C bridges		4C bridges	
			Hard soil	Soft soil	Hard soil	Soft soil	Hard soil	Soft soil	Hard soil	Soft soil
More in bridges with hard foundation soil	Abutment 1	Rupture of retainer anchor (RRA@A1)	57%	43%	65%	35%	54%	46%	73%	27%
	Abutment 2	Rupture of retainer anchor (RRA@A2)	60%	40%	72%	28%	62%	38%	61%	39%
	Pier 2 (fixed pier)	Rupture of steel fixed bearing anchors (RFA@P2)	92%	8%	90%	10%	N/A	N/A	N/A	N/A
		Rupture of steel dowel connection (RSD@P2)	N/A	N/A	N/A	N/A	69%	31%	67%	33%
		Rupture of retainer anchor (RRA@P2)	N/A	N/A	N/A	N/A	100%	0%	93%	7%
More in bridges with soft foundation soil	Abutment 1	Mobilization of backfill ultimate capacity (MBU@A1)	0%	100%	19%	81%	7%	93%	31%	69%
	Abutment 2	Mobilization of backfill ultimate capacity (MBU@A2)	0%	100%	7%	93%	10%	90%	28%	72%
	Pier 1 (expansion pier)	Yielding of pile (YSP@P1)	14%	86%	23%	77%	22%	78%	28%	72%
	Pier 3 (expansion pier)	Yielding of pile (YSP@P3)	N/A	N/A	22%	78%	N/A	N/A	28%	72%
	Pier 2 (fixed pier)	Yielding of pile (YSP@P2)	20%	80%	43%	57%	29%	71%	35%	65%

CHAPTER 5: RECOMMENDATIONS FOR IMPROVING BRIDGE SEISMIC PERFORMANCE

To improve the deficient bridge seismic performance, two adjustments to the current bridge design are proposed. Specifically, strengthening bearing retainer anchorage at abutments to prevent bearing unseating after the rupture of the retainer anchors. The other adjustment is weakening the sacrificial connections at fixed piers to reduce superstructure seismic forces that can be transferred to pier columns. In addition to the discussion in this chapter, more detailed results from comparative studies between the original bridges and bridges with the proposed adjustments are included in Appendix D.

5.1 STRENGTHENING OF BEARING RETAINER ANCHORAGE AT ABUTMENTS

As introduced in Section 4.2, a few highly skewed bridges supported by tall pier columns sustained bearing unseating at the abutments. Table 5.1 shows these bridges along with their original and strengthened bearing retainer anchors at the abutments. The shear capacity of the bearing retainer anchors specified by the IDOT Bridge Manual (IDOT, 2012) is 20% of the superstructure dead load at the bearing under consideration. By reviewing the plans of many existing bridges in Illinois, it was found that the bearing retainer anchors are typically over-designed with a shear capacity higher than the specified value. To take this common practice into account, the anchor shear capacity of the five prototype bridges tabulated in Table 5.1 was originally designed to be around 30% of the superstructure dead load on the bearing. To determine the required anchor strength for preventing bearing unseating, additional response-history analyses were performed on the five bridges using the same suite of earthquake ground motions applied in the four incident directions. The only difference between these additional analyses and those discussed in previous sections is the strengthened retainer anchorage at abutments. Through these additional analyses, it was found that in order to completely prevent bearing unseating at the abutments of these bridges, the shear capacity of the retainer anchors needs to be increased to about 90% of the dead load on the bearing.

Table 5.1: Comparison of Retainer Anchor Rupture and Bearing Unseating in Bridges With Original and Strengthened Retainer Anchorage

Bridge variant	No. of anchor per retainer		Anchor diameter [mm (in.)]		Shear capacity / bearing dead load	
	Original	Strengthened	Original	Strengthened	Original	Strengthened
4S60P40S	1	2	31.8 (1.25)	38.1 (1.5)	30%	88%
3C60P40S	1	2	31.8 (1.25)	38.1 (1.5)	30%	88%
4C45P40H	1	2	38.1 (1.50)	50.8 (2.00)	27%	96%
4C60P40H	1	2	38.1 (1.50)	50.8 (2.00)	27%	96%
4C60P40S	1	2	38.1 (1.50)	50.8 (2.00)	27%	96%

Figure 5.1 compares the peak sliding distance and the unseating of the elastomeric bearings at the deck corners of the 4C60P40S bridge between the cases with original and strengthened retainer anchorage. This bridge sustained the most occurrences of bearing unseating at abutments among all the bridges and, thus, it is selected as an example to show the efficacy of

the strengthening strategy. At each of the four deck corners, the peak bearing sliding in the abutment-normal direction was effectively reduced and bearing unseating was completed prevented by the strengthened retainer anchors.

Figure 5.2 compares the retainer and bearing responses at the lower-right deck corner (acute deck corner supported by Abutment 2) of the 4C60P40S bridge when subjected to a transverse ground motion. As shown in Figure 5.2a, the strengthened anchor didn't rupture in the analysis but the original one did. Consequently, shear deformation and sliding of the bearing was significantly suppressed and unseating was prevented, as shown in Figure 5.2b.

As the bearing retainer anchors are used as structural fuses to protect substructures and their foundations, strengthening the abutment retainer anchors may cause increased force demands on the abutment and its pile foundation. Figure 5.3 compares the peak pile strain of the 4C60P40S bridge with the original and strengthened bearing retainer anchors at its abutments. As expected, the peak strain of the abutment piles is generally increased due to the strengthened bearing retainers. However, Article 5.2.4 of the AASHTO Guide Specifications for LRFD Seismic Bridge Design (AASHTO 2011) indicates that for earthquake-resisting system with abutment contribution, "pile-supported foundations shall be designed to sustain the design earthquake displacements; inelastic behavior of the piles at the abutments shall be considered acceptable." In line with the AASHTO provision, the inelastic response of the foundation piles is utilized as the Tier 3 seismic structural redundancy of the quasi-isolation strategy and it is preferred to bearing unseating.

As demonstrated by the comparative analysis in this section, a practical and effective approach to prevent abutment bearing unseating for highly skewed tall-pier bridges is to strengthen the abutment bearing retainers. However, the potentially increased lateral force demands on the abutment foundation should also be considered in the foundation design.

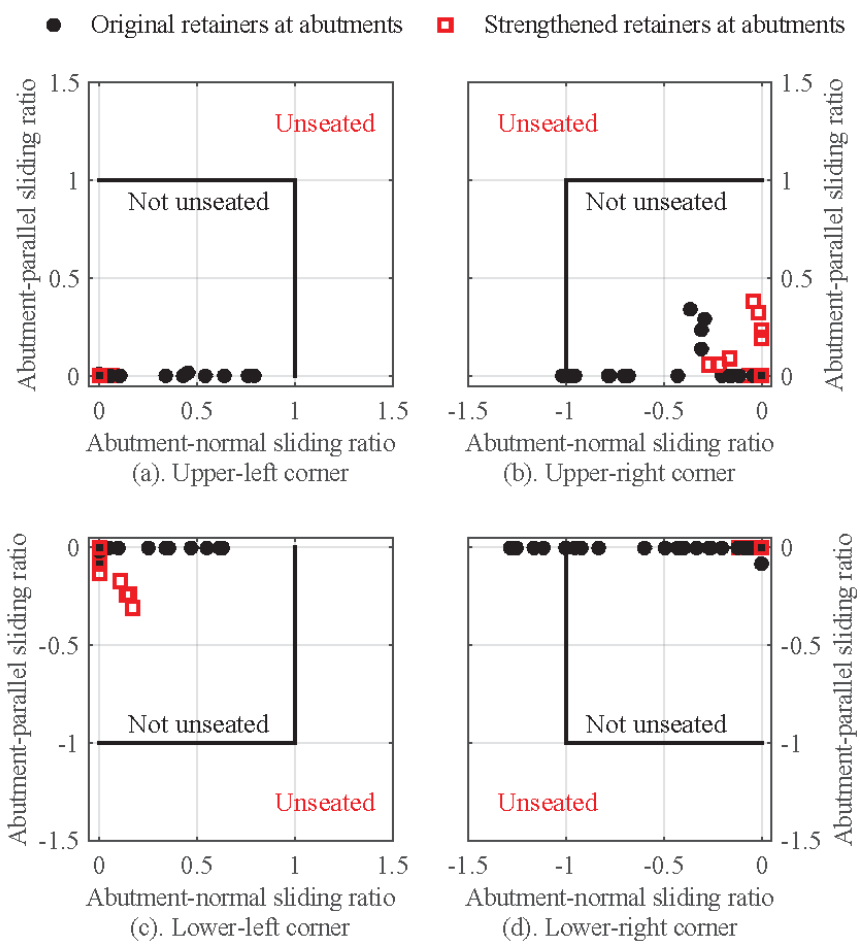

Figure 5.1: Comparison of peak sliding ratios of elastomeric bearings at the deck corners of the 4C60P40S bridge variant with original and strengthened retainer anchorage at the abutments.

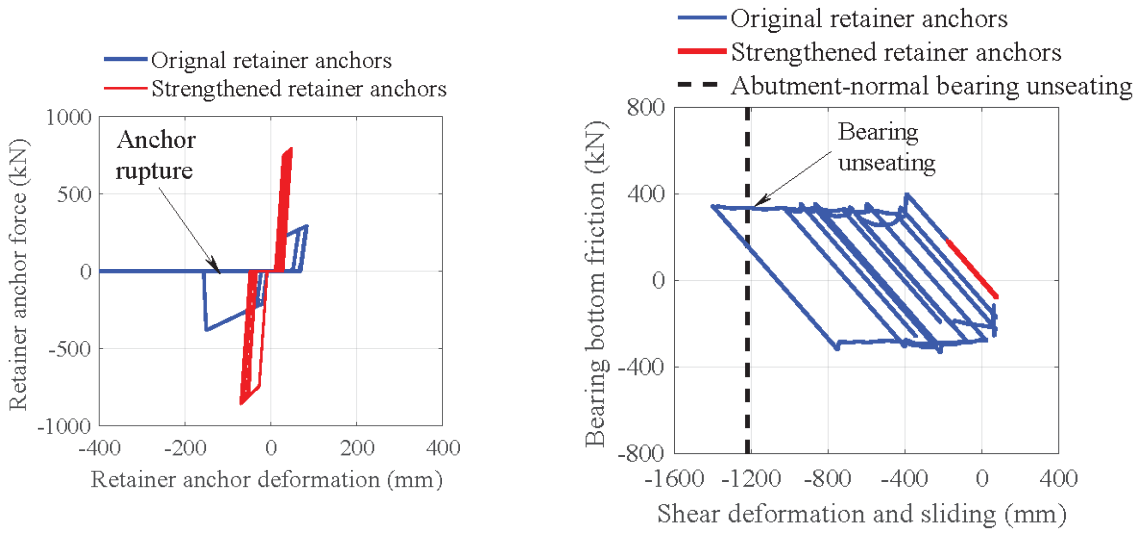

(a) (b)

Figure 5.2: Comparison of retainer anchor and elastomeric bearing response at the lower-right deck corner of the 4C60P40S bridge when subjected to a transverse ground motion (anchor rupture and bearing unseating were prevented by strengthening retainer anchors).

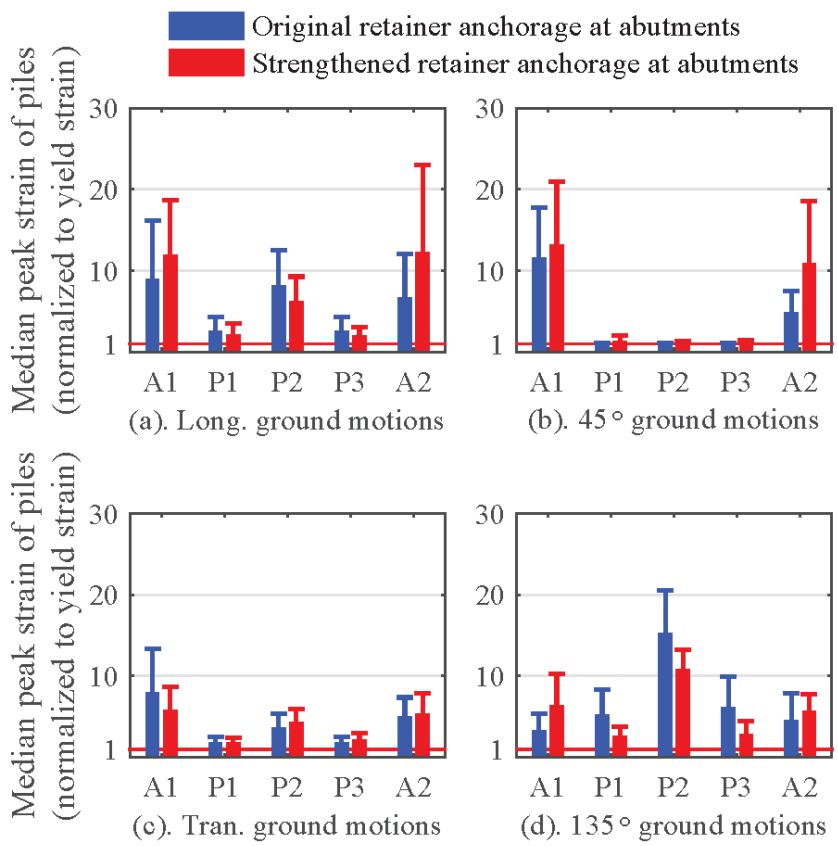

Figure 5.3: Comparison of peak pile strain (median + median absolute deviation) of the 4C60P40S bridge variant with original and strengthened retainer anchorage at abutments: (a) response under longitudinal ground motions; (b) response under 45° ground motions; (c) response under transverse ground motions; and (d) response under 135° ground motions.

5.2. WEAKENING CONNECTIONS BETWEEN SUPERSTRUCTURE AND FIXED PIER

Installed on top of the fixed pier, anchors of low-profile steel fixed bearings (in steel-plate-girder bridges) and steel dowels (in PPC-girder bridges) are intended to act as structural fuses that should rupture during major earthquake events. Similar to the bearing retainer anchors, the shear capacity of steel-fixed bearing anchors specified by the IDOT Bridge Manual (IDOT 2012) is 20% of the superstructure dead load on the bearing under consideration. Through the inspection of the plans of many recently constructed highway bridges in Illinois, it was found that the specified nominal fusing capacity of low-profile steel fixed bearing anchors is typically over-designed. A primary reason for this design trend in practice may be that bridge engineers tend to regard the specified fusing capacity as a minimum requirement and use larger or more anchor bolts for conservatism. However, because the anchor bolts are intended to act as structural fuses during earthquake events, this “conservatism” may prevent the anchor bolts from rupture, and incur more seismic damage to pier columns. A secondary reason may be that fusing capacity in the close vicinity of 20% of the dead load on the bearing is not always

available in actual design due to the limited options for anchor diameters. In this situation, bridge designers may round the anchor diameter up to the nearest available size, which results in over-designed fusing capacity.

For the PPC-girder bridges, the minimum required number of #8 (U.S.) steel dowels on each face of the pier between two adjacent girders, denoted by *N*, is given by the following equation:

$$N = \frac{1}{2}\left[\frac{0.2DL}{28.3S} - 2\right] \geq 2 \tag{5.1}$$

where *DL* is the sum of all superstructure dead loads at the given pier under consideration (kips); *S* is the number of beam spaces. The 28.3, in kips, is the nominal shear capacity of a #8 (U.S.) steel dowel with a yield strength of 60 ksi. As seen in Figure 5.4b, except these dowels between adjacent girders, additional dowels are used at each girder line to connect the bottom girder angle to the pier cap (one dowel for each exterior girder and two dowels for each interior girder). Although Eq. (5.1) aims to provide a total fusing capacity of the dowels between girders equal to 20% of the superstructure dead load imposed on the fixed pier, there are two potential sources leading to over-designed fusing capacity at this fixed pier connection. First, as seen in Figure 5.4b, a minimum value of 2 is specified for *N*, which can be much larger than the *N* value calculated by Eq. (5.1). Second, the dowels at girder lines provide extra shear capacity to the global fixed pier connection.

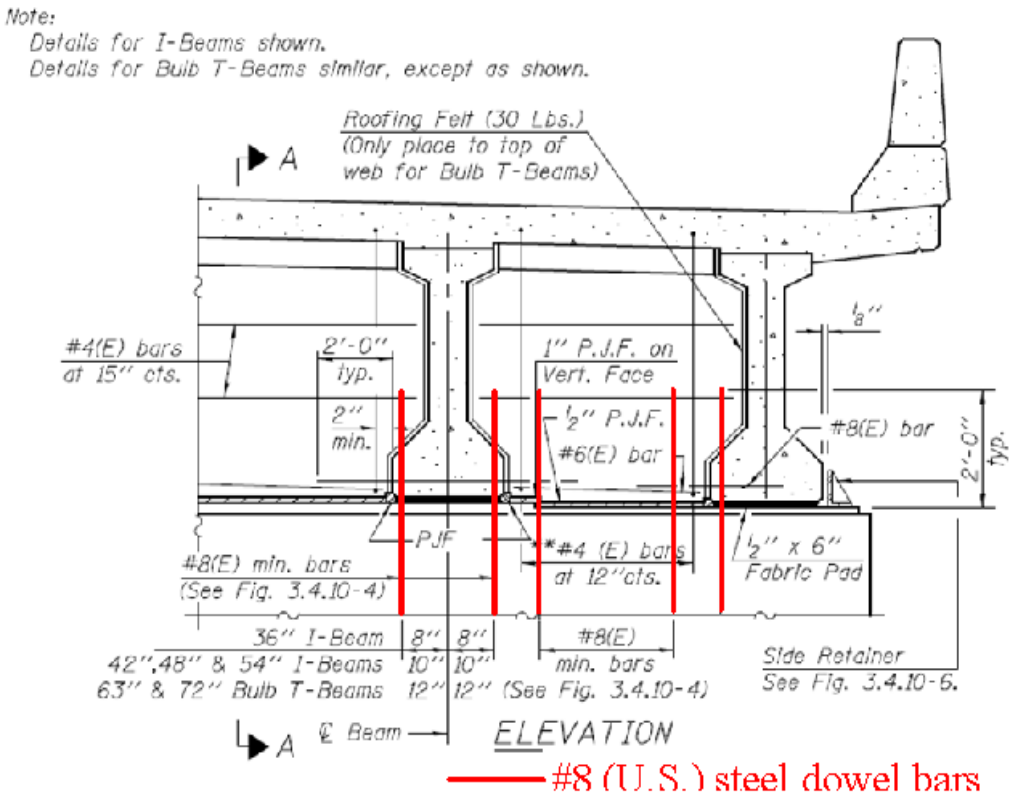

(a). Elevation view

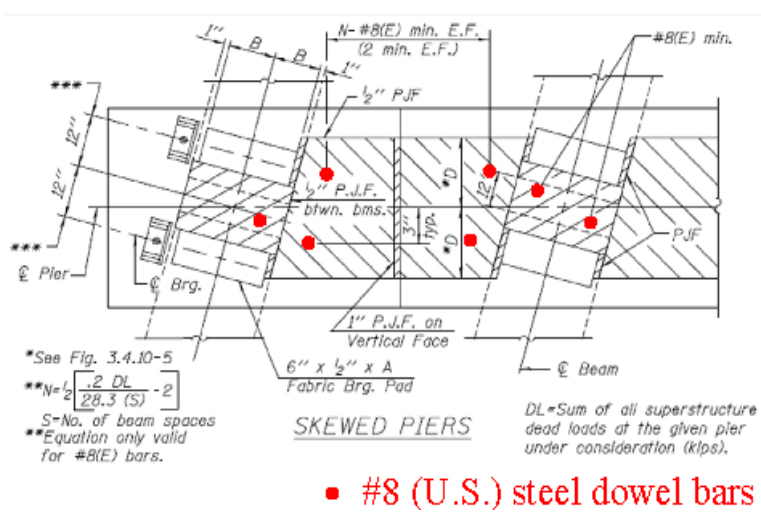

(b). Plan view

Figure 5.4: Details of superstructure-to-fixed-pier connections in PPC girder bridges (after IDOT 2012).

As indicated in Table 5.2, the steel fixed bearing anchors and steel dowels are weakened to improve the fusing performance of these components and reduce damage to pier columns. Besides the overdesigned connections, two additional design cases are considered, namely

specified and weakened designs. The connection in the specified design possesses a fusing capacity around 20% of the superstructure dead load at the considered bearing, while the fusing capacity of the weakened design is around 10% to 15% of the superstructure dead load. Using bridge 4S30P15S as an example, Figure 5.5 comparatively demonstrates the effect of weakening the superstructure-to-fixed-pier connections on mitigating seismic damage to pier columns, measured by the peak strain of reinforcing steel and the concrete cover at the column bases of the fixed pier (P2). The comparison clearly shows that weakening the fixed bearing anchorage leads to reduced inelastic strain of the vertical reinforcements of pier columns.

Table 5.2: Different Designs of Connections Between Superstructure and Fixed Pier

Bridge	Design cases	No. of anchor per girder	Anchor diameter [mm (in.)]	Shear capacity / bearing dead load
[3S00P15S,	Over-designed	2	38.1 (1.5)	44%
3S15P15S,	Specified	2	25.4 (1.0)	20%
3S30P15S]	Further weakened	2	19.1 (0.75)	11%
[4S00P15S,	Over-designed	4	31.8 (1.25)	46%
4S15P15S,	Specified	2	31.8 (1.25)	23%
4S30P15S]	Further weakened	2	25.4 (1.0)	15%
[3C00P15S,	Over-designed	3 (exterior), 6 (interior)	25.4 (1.0)	64%
3C15P15S,	Specified	2 (exterior), 3 (interior)	19.1 (0.75)	19%
3C30P15S]	Further weakened	2 (exterior), 3 (interior)	15.9 (0.625)	13%
[4C00P15S,	Over-designed	3 (exterior), 6 (interior)	25.4 (1.0)	45%
4C15P15S, 4C30P15S]	Weakened	2 (exterior), 3 (interior)	19.1 (0.75)	13%

Using bridge 4S30P15S as an example, Figure 5.5 comparatively demonstrates the effect of weakening the superstructure-to-fixed-pier connections on mitigating seismic damage to pier columns, measured by the peak strain of reinforcing steel and the concrete cover at the column bases of the fixed pier (P2). The comparison clearly shows that weakening the fixed bearing anchorage leads to reduced inelastic strain of the vertical reinforcements of pier columns.

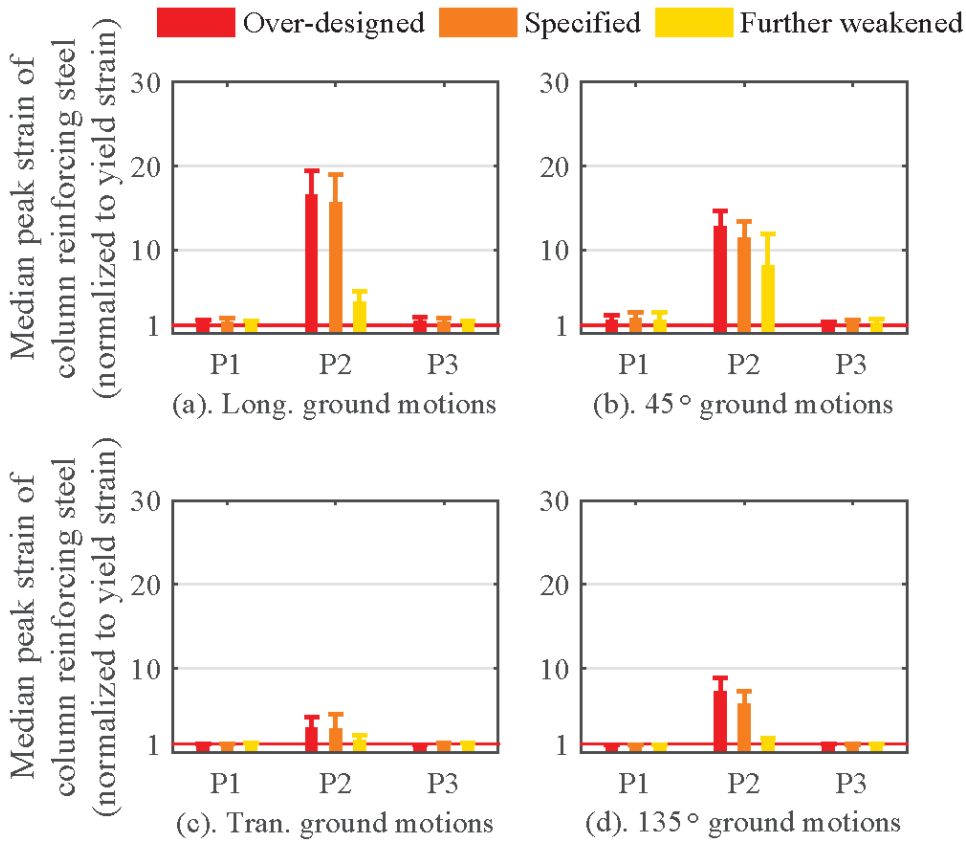

Figure 5.5: Comparison of peak strain (median + median absolute deviation) of reinforcing steel at pier column bases of the 4S30P15S bridge variant with different designs of steel fixed bearing anchorage: (a) response under longitudinal ground motions; (b) response under 45° ground motions; (c) response under transverse ground motions; and (d) response under 135° ground motions.

As an example of the pier column response, Figure 5.6 compares the force-deflection response of Pier 2 columns between the three design cases of fixed bearing anchorage strength. In the over-designed and specified cases, the pier columns exhibit clear inelastic and large-deflection response. In contrast, the column response is essentially elastic and the deflection is the smallest in the case with the further weakened fixed bearing anchorage strength. Although weakening the fixed bearing anchors is effective for the selected 3S, 4S, and 3C bridges, merely using this strategy appeared to be ineffective for some of the 4C bridges. The reason is that for the fixed piers, even after the steel dowels were fused, the post-fusing friction between the performed joint filler and the concrete surface could result in considerable damage to the pier columns. Another reason is due to the large superstructure dead load. The similar situation was also observed at the expansion piers. Therefore, merely weakening the connections at the fixed pier may not be an effective strategy for the long-span massive concrete bridges. In this situation, using larger pier columns in conjunction with weakened connections is necessary to reduce the seismic damage to the pier columns. Table 5.3 lists three cases with different combinations of pier columns and connections between the superstructure and the fixed pier.

Case 1 is the original configuration without any modification of the components. In Case 2, the columns of both the expansion and fixed piers are enlarged, but the steel dowel connections on top of the fixed pier is not weakened. In Case 3, enlarged pier columns are used in conjunction with weakened connections. In Cases 2 and 3, except the larger column diameter, the reinforcing ratio, 2%, and grade of the steel and concrete material of the pier column remain the same as Case 1.

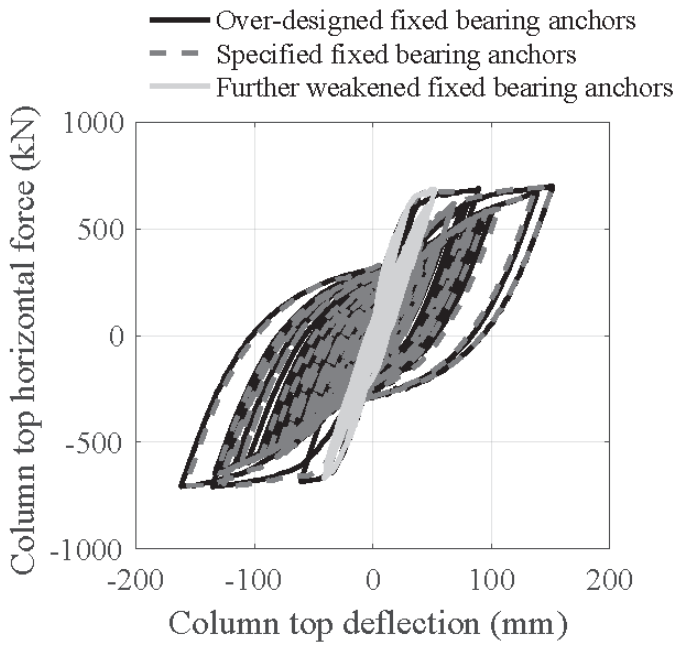

Figure 5.6: Comparison of column response at Pier 2 of 4S30P15S bridge when subjected to a longitudinal ground motion (pier-normal response averaged over four columns at Pier 2).

Table 5.3: Different Designs of Connections Between Superstructure and Fixed pier

Bridge	Case	No. of dowels per girder	Dowel diameter [mm (in.)]	Pier column diameter [m (ft)]
[4C00P15S, 4C15P15S, 4C30P15S]	1	3 (exterior) 6 (interior) (over-designed, 45% dead load)	25.4 (1.0)	1.07 (3.5) (original)
	2	3 (exterior) 6 (interior) (over-designed, 45% dead load)	25.4 (1.0)	1.37 (4.5) (enlarged)
	3	2 (exterior) 3 (interior) (weakened, 13% dead load)	19.1 (0.75)	1.37 (4.5) (enlarged)

Figure 5.7 compares mitigation effects of column damage between Cases 1 and 2. It can be seen that enlarging the pier column diameter significantly reduces the peak steel and concrete strain at both the expansion and fixed piers. Figure 5.8 demonstrates that when the enlarged pier columns are used in conjunction with the weakened connections, additional reduction of peak steel and concrete strain at the fixed pier is achieved. Therefore, for the heavy 4C bridges

with small skew and short pier columns, the seismic damage to pier columns can be mitigated by increasing column size in conjunction with weakened superstructure-to-fixed-pier connections.

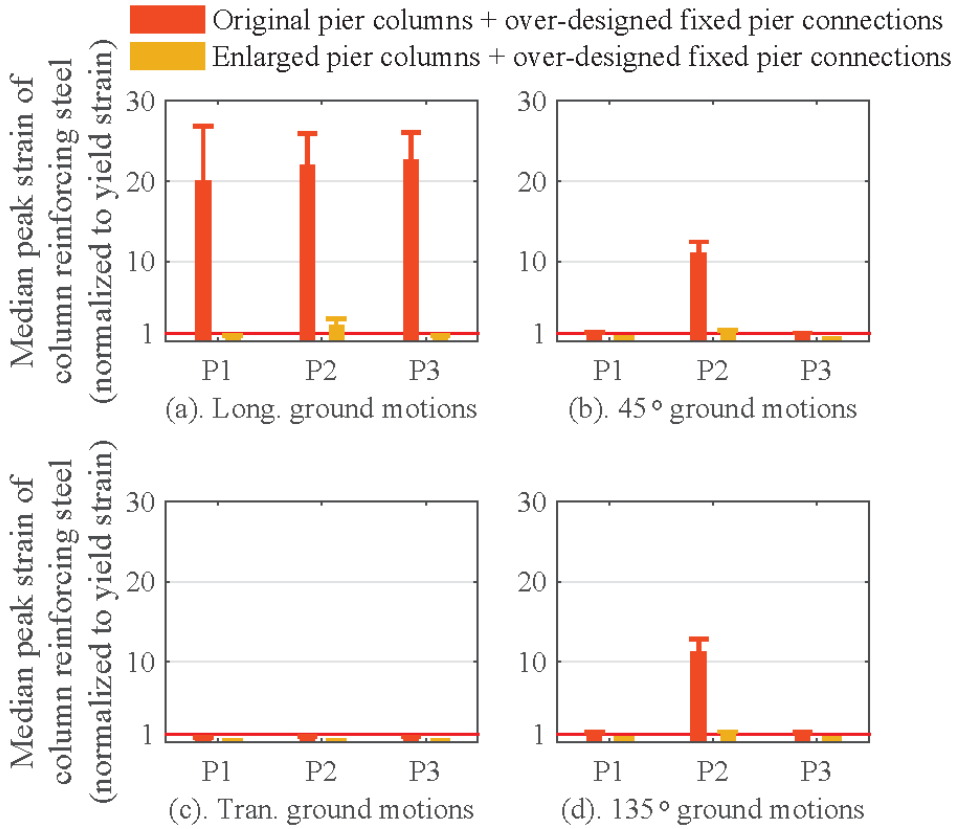

Figure 5.7: Comparison of peak strain (median + median absolute deviation) of reinforcing steel at pier column bases of 4C00P15S bridge between Cases 1 and 2 of Table 5.3: (a) response under longitudinal ground motions; (b) response under 45° ground motions; (c) response under transverse ground motions; and (d) response under 135° ground motions.

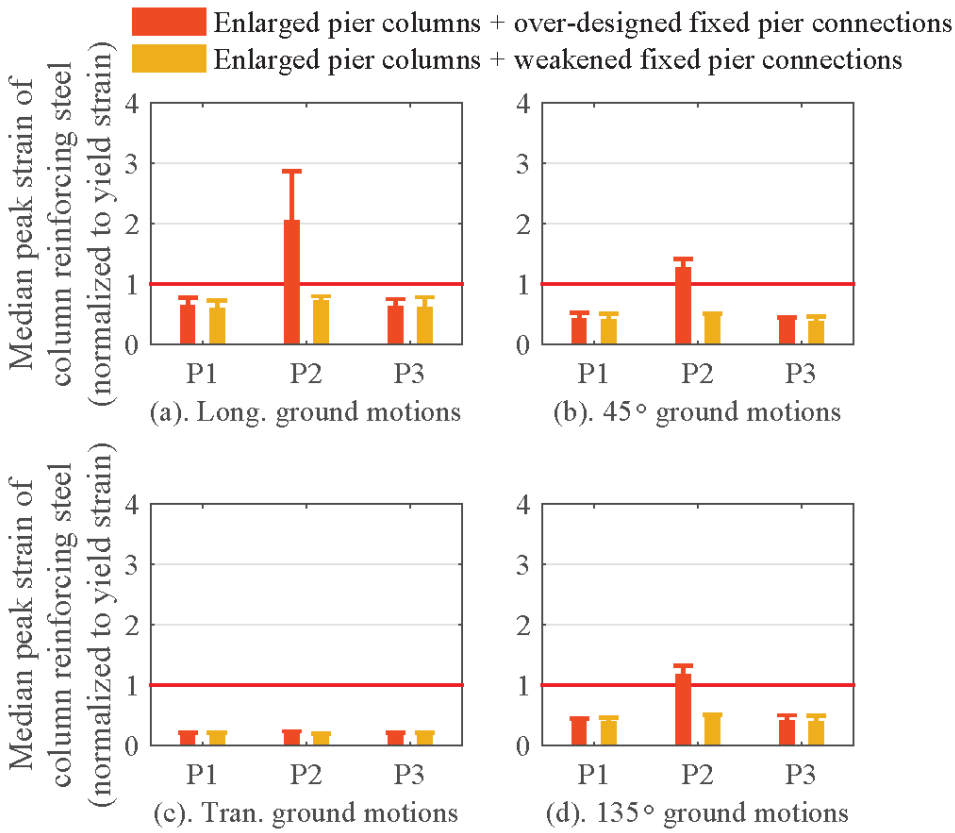

Figure 5.8: Comparison of peak strain (median + median absolute deviation) of reinforcing steel at pier column bases of 4C00P15S bridge between Cases 2 and 3 of Table 5.3: (a) response under longitudinal ground motions; (b) response under 45° ground motions; (c) response under transverse ground motions; (d) response under 135° ground motions.

CHAPTER 6: SUMMARY AND CONCLUSIONS

This report presents a comprehensive seismic performance assessment program for Illinois highway bridges designed by the quasi-isolation strategy. A matrix of eighty prototype bridges encompassing permutations of various bridge configurations was computationally modeled and then subjected to a suite of eighty site-specific earthquake accelerograms having a 1,000-year return period. For each bridge, the accelerograms were applied in four horizontal incident directions. Based on the eighty bridge models and the twenty ground motions applied in four directions, 6,400 response-history analyses were performed using a supercomputer.

The seismic performance assessment presented in this report demonstrated that the majority of the prototype quasi-isolated bridges only sustained limited local damage and were unlikely to collapse when subjected to earthquake ground motions with a 1,000-year return period in southern Illinois. Despite the overall satisfactory performance, abutment bearing unseating occurred in the analyses of several highly skewed bridges supported by tall piers. All of the bearing unseating occurred after the fusing of the bearing retainers at the abutments of these bridges. In addition to the bearing unseating, a small number of non-skew or lightly skewed bridges supported by short piers sustained moderate to severe damage to the pier columns.

To improve bridge seismic performance in these two aspects, two recommendations for adjusting the current design strategy were proposed. The first is to strengthen the bearing retainer anchorage at abutments of highly skewed bridges supported by tall piers. In the few bridges that experienced bearing unseating at their abutments, the fusing capacity of the retainer anchors was improved from the original 30% of the superstructure dead load on the bearing to around 90%. Comparative response-history analyses were performed to evaluate the proposed strengthening strategy and the results demonstrated that bearing unseating at the abutments of these bridges were prevented by strengthening the retainer anchorage. The other adjustment was to weaken the commonly over-designed superstructure-to-fixed-pier connections of non-skew or lightly skewed bridges supported by short pier columns, in order to mitigate pier column damage. Comparative response-history analysis results demonstrated that when the connection fusing capacity was reduced from more than 40% to around 10% to 15% of the superstructure dead load on the connection, effective mitigation of column damage was achieved in many bridges. For the heaviest four-span PPC-girder bridges, enlarged pier columns in conjunction with weakened connections were found to significantly mitigate pier column seismic damage. For these long-span massive bridges, merely weakening the sacrificial connections seemed to be insufficient in protecting pier columns.

REFERENCES

AASHTO. (2008a). *LRFD bridge design specifications and interim specifications*, Washington, D.C.

AASHTO. (2008b). *Guide specifications for LRFD seismic bridge design*, Washington, D.C.

AASHTO. (2010). *LRFD bridge design specifications*, Washington, D.C.

AASHTO. (2011). *Guide specification for LRFD seismic bridge design*, Washington, D.C.

AASHTO/NSBA Steel Bridge Collaboration. (2014). "Guidelines for Steel Girder Bridge Analysis.", *G13.1*, 2nd Ed., Washington, D.C.

Abo-Shadi, N., Saiidi, M., and Sanders, D. (2000). "Seismic response of reinforced concrete bridge pier walls in the weak direction." *Rep. No. MCEER-00-0006*, Univ. of Nevada, Reno, NV.

API. (1987). "Recommended practice for planning, designing and constructing fixed offshore platforms." *API Recommended practice 2A (RP 2A)*, 17th Ed., Washington, D.C.

Awoshika, K. and Reese, L. C. (1971) "Analysis of foundation with widely spaced batter piles." *Rep. No. 117-3F*, Center for Highway Research, Univ. of Texas at Austin, Texas.

Bathe, K. (2007). "Conserving energy and momentum in nonlinear dynamics: A simple implicit time integration scheme." *Comput. Struct*., 85(7-8), 437–445.

Boulanger, R., Curras, C., Kutter, B., Wilson, D., and Abghari, A. (1999). "Seismic soil-pile-structure interaction experiments and analyses." *J. Geotech. Geoenviron. Eng*., 10.1061/(ASCE)1090-0241(1999)125:9(750), 750-759.

Bozorgzadeh, A., Ashford, S. A., Restrepo, J. I., and Nimityongskul, N. (2008) "Experimental and analytical investigation on stiffness and ultimate capacity of bridge abutments." *Rep. No. UCSD/SSRP-07/12*, Univ. of California, San Diego, La Jolla, CA.

Buckle, I. G. (1994). "The Northridge, California earthquake of January 17, 1994: performance of highway bridges." *Rep. No. NCEER-94-0008*, State Univ. of New York at Buffalo, NY.

Castilla, F., Martin, P., and Link, J. (1984). "Fixity of members embedded in concrete." *Rep. No. CERL M-339*, U.S. Army Corps of Engineers, Champaign, IL.

Charney, F. A. (2008). "Unintended consequences of modeling damping in structures." *J. Struct. Eng.*, 10.1061/(ASCE)0733-9445(2008)134:4(581), 581-592.

Crouse, C. B., Hushmand, B., and Martin, G. R. (1987). "Dynamic soil-structure interaction of a single-span bridge." *Earthq. Eng. Struct. D*., 15(6), 711–729.

Cruz-Noguez, C. and Saiidi, M (2010). "Experimental and Analytical Seismic Studies of a Four-Span Bridge System with Innovative Materials." *Rep. No. CCEER-10-4*, Univ. of Nevada, Reno, NV.

Dao, N. D., Ryan, K. L., Sato, E., and Sasaki, T. (2013). "Predicting the displacement of triple pendulum™ bearings in a full-scale shaking experiment using a three-dimensional element." *Earthq. Eng. Struct. D*., 42(11), 1677–1695.

Elnashai, A. S., Gencturk, B., Kwon, O., Al-Qadi, I. L., Hashash, Y., Roesler, J. R., and Valdivia, A. (2010). "The Maule (Chile) earthquake of February 27, 2010: consequence assessment and case studies." *Rep. No. 10-04*, MAE Center, Univ. of Illinois at Urbana-Champaign, Champaign, IL.

Fernandez, J., and Rix, G. (2008). Seismic Hazard Analysis and Probabilistic Ground Motions in the Upper Mississippi Embayment. *Geotech. Earthq. Eng. Soil Dyn*. IV:pp. 1-10. doi: 10.1061/40975(318)8

Filipov, E. T., Fahnestock, L. A., Steelman, J. S., Hajjar, J. F., and LaFave, J. M. (2013a). "Evaluation of quasi-isolated seismic bridge behavior using nonlinear bearing models." *Eng. Struct*., 49(0), 168–181.

Filipov, E. T., Revell, J. R., Fahnestock, L. A., LaFave, J. M., Hajjar, J. F., Foutch, D. A., and Steelman, J. S. (2013b). "Seismic performance of highway bridges with fusing bearing components for quasi-isolation." *Earthq. Eng. Struct. D*., 42(9), 1375–1394.

Goel, R. K. and Chopra, A. K. (1997). "Evaluation of bridge abutment capacity and stiffness during earthquakes." Earthq. Spectra, 13(1), 1–23.

IDOT (Illinois Dept. of Transportation). (2012a). *Bridge manual*, Springfield, IL.

IDOT (Illinois Dept. of Transportation). (2012b). *Standard specifications for road and bridge construction*, Springfield, IL.

IDOT (Illinois Dept. of Transportation). (2015). "ABD 15.2: New Precast Prestressed Concrete IL-Beam Sections and Revisions to the I-Beams and Bulb T-Beams." <http://www.idot.illinois.gov/Assets/uploads/files/Doing-Business/Memorandums-&-Letters/Highways/Bridges/ABD-Memos/ABD152.pdf>.

IDOT (Illinois Dept. of Transportation). (n.d.). *Illinois Department of Transportation Bridge Information website*. <http://apps.dot.illinois.gov/bridgesinfosystem/main.aspx>.

Jennings, P. C. (1971). "Engineering features of the San Fernando earthquake of February 9, 1971." *Rep. No. EERL-71-02*. California Institute of Technology, Pasadena, CA.

Kalantari, A., and Amjadian, M. (2010). "An approximate method for dynamic analysis of skewed highway bridges with continuous rigid deck." *Eng. Struct*., 32(9), 2850–2860.

Kawashima, K., Unjoh, S., Hoshikuma, J., and Kosa, K. (2011). "Damage of Bridges due to the 2010 Maule, Chile, earthquake." *J. Earthq. Eng*., 15(7), 1036–1068.

Kaviani, P., Zareian, F. and Ertugrul, T. (2012). "Seismic behavior of reinforced concrete bridges with skew-angled seat-type abutments." *Eng. Struct*., 45, 137–150.

Kornkasem, W., Foutch, D. A., and Long, J. H. (2001). "Seismic behavior of pile-supported bridges." *Rep. No. 03-05*. Mid-America Earthquake Center, Univ. of Illinois at Urbana-Champaign, Champaign, IL.

Kowalsky, J. (2001). "Deformation limit states for circular reinforced concrete bridge columns." *J. Struct. Eng*., 10.1061/(ASCE)0733-9445(2000)126:8(869), 869-878.

Kozak, D. L., Luo, J., Olson, S. M., LaFave, J. M., and Fahnestock, L. A. (2017). "Modification of ground motions for use with dynamic structural analyses in Central North America." *J. Earthq. Eng*., 10.1080/13632469.2017.1387190.

Kubo, K. (1964). "Experimental study of the behavior of laterally loaded piles." *Rep. No. 12(2)*. Transportation Technology Research Institute, Japan.

Kwon, O., and Jeong, S. (2013). "Seismic displacement demands on skewed bridge decks supported on elastomeric bearings." J. Earthq. Eng., 17(7), 998–1022.

LaFave, J., Fahnestock, L., Foutch, D., Steelman, J., Revell, J., Filipov, E., and Hajjar, J. (2013a). "Experimental investigation of the seismic response of bridge bearings." *Rep. No. FHWA-ICT-13-002*. Illinois Center for Transportation, Springfield, IL.

LaFave, J., Fahnestock, L., Foutch, D., Steelman, J., Revell, J., Filipov, E., and Hajjar, J. (2013b). "Seismic performance of quasi-isolated highway bridges in Illinois." *Rep. No. FHWA-ICT-13-015*. Illinois Center for Transportation, Springfield, IL.

LaFave, J. M., Fahnestock, L. A., and Kozak, D. L. (2018). "Seismic Performance of Integral Abutment Highway Bridges in Illinois." *Rep. No. FHWA-ICT-18-012*. Illinois Center for Transportation, Springfield, IL.

Lee, G. C. and Loh, C. (2000). "The Chi-chi, Taiwan earthquake of September 21, 1999: reconnaissance report." *Rep. No. MCEER-00-0003*. State Univ. of New York at Buffalo, Buffalo, NY.

Luo, J., Fahnestock, L. A., Kozak, D. L., and LaFave, J. M. (2017a). "Seismic analysis incorporating detailed structure-abutment-foundation interaction for quasi-isolated highway bridges." *Struct. Infrastructure E.*, 13(5), 581-603.

Luo, J., Fahnestock, L. A., and LaFave, J. M. (2017b). Nonlinear static pushover and eigenvalue modal analyses of quasi-isolated highway bridges with seat-type abutments. *Structures*, 12, 145-167.

Mander, J., Priestley, M., and Park, R. (1988). "Theoretical stress-strain model for confined concrete." *J. Struct. Eng*., 10.1061/(ASCE)0733-9445(1988)114:8(1804), 1804-1826.

Marsh, A. (2013). "Evaluation of passive force on skewed bridge abutments with large-scale tests," M.S. Thesis, Brigham Young Univ., Provo, UT.

Martin, G. R., Yan, L., and Lam, I. P. (1997). "Development and implementation of improved seismic design and retrofit procedures for bridge abutments." Univ. of Southern California, Los Angeles, CA.

Matlock, H. (1970). "Correlations for design of laterally loaded piles in soft clay." *Proc., 2nd Annu. Offshore Technol. Conf*., Vol. 1, 577-594.

Matlock, H., Foo, S. H., and Bryant, L. L. (1978). "Simulation of lateral pile behavior." *Proc., Earthq. Eng. and Soil Dyn*., ASCE, New York, 600-619.

McKenna, F., and Fenves, G. (2008, April 17). *OpenSees Interpreter on Parallel Computers*. <http://opensees.berkeley.edu/OpenSees/parallel/TNParallelProcessing.pdf>.

Mitoulis, S. A. (2012). “Seismic design of bridges with the participation of seat-type abutments.” *Eng. Struct*., 42 (0), 222–233.

Neuenhofer, A. and Filippou, F. C. (1997). “Evaluation of nonlinear frame finite-element models.” *J. Struct. Eng*., 10.1061/(ASCE)0733-9445(1997)123:7(958), 958-966.

Nielson, B. G. and DesRoches, R. (2007). “Seismic performance assessment of simply supported and continuous multispan concrete girder highway bridges.” *J. Bridge Eng*., 10.1061/(ASCE)1084-0702(2007)12:5(611), 611-620.

Nogami, T., Otani, J., Konagai, K., and Chen, H. (1992). “Nonlinear soil-pile interaction model for dynamic lateral motion.” *J. Geotech. Engrg*., 10.1061/(ASCE)0733-9410(1992)118:1(89), 89-106.

Novak, M., and Sheta, M. (1980). “Approximate approach to contact problems of piles.” *Proc., ASCE Nat. Convention, Dyn. Response of Pile Found: Analytical Aspects*, ASCE, New York, 55-79.

O’Brien, E. J., Keogh, D. L., O’Connor, A. J., and Lehane, B. M. (2015). *Bridge deck analysis*, 2nd Ed., CRC Press, Taylor & Francis Group, Boca Raton, FL.

OpenSees [Computer software]. Pacific Earthquake Engineering Research Center, Univ. of California, Berkeley, CA.

Pant, D. R., Wijeyewickrema, A. C., and ElGawady, M. A. (2013). “Appropriate viscous damping for nonlinear time-history analysis of base-isolated reinforced concrete buildings.” *Earthq. Eng. Struct. D*., 42(15), 2321–2339.

Petrini, L., Maggi, C., Priestley, M. J. N., and Calvi, G. M. (2008). “Experimental verification of viscous damping modeling for inelastic time history analyzes.” *J. Earthq. Eng*., 12(S1), 125–145.

Reese, L. C., and Van Impe, W. F. (2011). *Single piles and pile groups under lateral loading*, 2nd Ed., CRC Press, Taylor & Francis Group, London, U.K.

Revell, J. (2013). “Quasi-isolated highway bridges: influence of bearing anchorage strength on seismic performance,” M.S. Thesis, Univ. of Illinois at Urbana-Champaign, Champaign, IL.

Robinson, W. H. (1982). “Lead-rubber hysteretic bearings suitable for protecting structures during earthquakes.” *Earthq. Eng. Struct. D*., 10(4), 593–604.

Rollins, K. M., Gerber, T. M., Cummings, C. R., and Pruett, J. M. (2010a). “Dynamic passive pressure on abutments and pile caps.” *Rep. No. UT-10.18*. Brigham Young Univ., Provo, UT.

Rollins, K. M., Gerber, and Nasr, M. (2010b). “Numerical analysis of dense narrow backfills for increasing lateral passive resistance.” *Rep. No. UT-10.19*. Brigham Young Univ. Provo, UT.

Ryan, T. P. (2006). *Modern engineering statistics*, John Wiley & Sons, Hoboken, NJ.

SAP2000 [Computer software]. Computers and Structures, Walnut Creek, CA.

Sardo, A. G., Sardo, T. E., and Harik, I. E. (2006). "Post earthquake investigation field manual for the state of Kentucky." *Rep. No. KTC-06-30/SPR2234-01-1F*. Kentucky Transportation Center, Univ. of Kentucky, Lexington, KY.

Scott, M. H. and Fenves, G. L. (2010). "Krylov Subspace accelerated Newton algorithm: Application to dynamic progressive collapse simulation of frames." *J. Struct. Eng*., 10.1061/(ASCE)ST.1943-541X.0000143, 473-480.

Shamsabadi, A., Ashour, M., and Norris, G. (2005). "Bridge abutment nonlinear force-displacement-capacity prediction for seismic design." *J. Geotech. Geoenviron. Eng*., 10.1061/(ASCE)1090-0241(2005)131:2(151), 151-161.

Shamsabadi, A. (2007). "Three-dimensional nonlinear seismic soil-abutment-foundation-structure interaction analysis of skewed bridges," Ph.D. Dissertation, Univ. of Southern California, Los Angeles, CA.

Shamsabadi, A., Rollins, K., and Kapuskar, M. (2007). "Nonlinear soil-abutment-bridge structure interaction for seismic performance-based design." *J. Geotech. Geoenviron. Eng*., 10.1061/(ASCE)1090-0241(2007)133:6(707), 707-720..

Sheskin, D. J. (2011). *Handbook of parametric and nonparametric statistical procedures*. Boca Raton, FL: Chapman & Hall/CRC.

Shields, D. H., and Tolunay, A. Z. (1973). "Passive pressure coefficients by method of slices." *J. Soil Mech. Found. Div*., 99(12), 1043-1053.

Steelman, J. (2013). "Sacrificial bearing components for quasi-isolated response of bridges subjected to high-magnitude, low-probability seismic hazard." Ph.D. Dissertation, Univ. of Illinois at Urbana-Champaign, Champaign, IL.

Steelman, J., Fahnestock, L., Filipov, E., LaFave, J., Hajjar, J., and Foutch, D. (2014). "Shear and friction response of nonseismic laminated elastomeric bridge bearings subject to seismic demands." *J. Bridge Eng*., 10.1061/(ASCE)BE.1943-5592.0000406, 612-623.

Steelman, J., Filipov, E., Fahnestock, L., Revell, J., LaFave, J., Hajjar, J., and Foutch, D. (2014). "Experimental behavior of steel fixed bearings and implications for seismic bridge response." *J. Bridge Eng*., 19 (8), A4014007.

Steelman, J., Fahnestock, L., Hajjar, J., and LaFave, J. (2016). "Performance of nonseismic PTFE sliding bearings when subjected to seismic demands." *J. Bridge Eng*., 10.1061/(ASCE)BE.19435592.0000777, 04015028.

Stewart, J. P. et al. (2007). "Full scale cyclic testing of foundation support systems for highway bridges. Part II: Abutment backwalls." Rep. No. UCLA-SGEL-2007/02, Structural and Geotechnical Engineering Laboratory, Univ. of California, Los Angeles.

Terzaghi, K., Peck, R. B., and Mesri, G. (1996). *Soil mechanics in engineering practice*, 3rd Ed., Wiley, U.K.

Tobias, D., Anderson, R., Hodel, C., Kramer, W., Wahab, R., and Chaput, R. (2008). "Overview of earthquake resisting system design and retrofit strategy for bridges in Illinois." *Pract. Period. Struct. Des. and Constr.*, 10.1061/(ASCE)1084-0680(2008)13:3(147), 147-158.

Werner, S. D., Beck, J. L., and Levine, M. B. (1987). "Seismic response evaluation of Meloland Road overpass using 1979 Imperial Valley earthquake records." *Earthq. Eng. Struct. D.*, 15(2), 249–274.

Wilson, J. C. (1988). "Stiffness of non-skew monolithic bridge abutments for seismic analysis." *Earthq. Eng. Struct. D.*, 16(6), 867–883.

Wilson, P. and Elgamal, A. (2010). "Large-scale passive earth pressure load-displacement tests and numerical simulation." *J. Geotech. Geoenviron. Eng.*, 136 (12), 1634–1643.

Wilson, P. and Tan, B. (1990). "Bridge abutments: Assessing their influence on earthquake response of Meloland Road Overpass." *J. Eng. Mech.*, 10.1061/(ASCE)0733-9399(1990)116:8(1838), 1838-1856.

Vintzeleou, E. N. and Tassios, T. P. (1986). "Mathematical models for dowel action under monotonic and cyclic conditions." *Mag. Concrete res.*, 38(134), 13–22.

Yen, W. P., Chen, G., Buckle, I., Allen, T., Alzamora, D., Ger, J. and Arias, J. G. (2011). "Postearthquake reconnaissance report on transportation infrastructure impact of the February 27, 2010 offshore Maule Earthquake in Chile." *Rep. No. FHWA-HRT-11-030*, Federal Highway Administration, U. S. Department of Transportation, McLean, VA.

Zhang, J. and Makris, N. (2002). "Seismic response analysis of highway overcrossing including soil-structure interaction." *Earthq. Eng. Struct. D.*, 31(11), 1967–1991.

APPENDIX A: PROTOTYPE BRIDGE PARAMETERS

Table A.1: Component Mass of Prototype Bridges (units: 10^3 kg)

Bridge	3S00P15H	4S00P15H	3C00P15H	4C00P15H
Superstructure	1197	2758	1680	3949
Abutments				
Backwall	48	72	58	76
Pile cap	128	128	128	128
Wingwall	54	78	62	81
Approach slab	206	206	206	206
Pile body (6.1 m)	12	14	14	18
Piers				
Pier cap	117	176	117	176
Pier column	79	117	79	117
Pile cap	240	360	240	386
Pile body (6.1 m)	19	38	21	48
Soil around piles	189	280	193	347
Total mass	2289	4227	2798	5532
Total mass in computer model	2288	4231	2797	5535

Table A.2: Girder Reaction and Sizing of Bearing Components of 3S Bridges

	Abutment	Expansion pier	Fixed pier
$R_{DC1} + R_{DC2}$ (kips)	31	130	130
R_{DW} (kips)	15	43	43
R_{LL} (kips)	62	130	130
Expansion length (ft)	200	120	N.A.
Bearing size	11-d	18-a	N.A.
No. of anchor per retainer	1	1	N.A.
Dia. of retainer anchor (in.)	1	1.5	N.A.
No. of anchor per fixed bearing	N.A.	N.A.	2
Dia. of fixed bearing anchor (in.)	N.A.	N.A.	1.5

Table A.3: Girder Reaction and Sizing of Bearing Components of 4S Bridges

	Abutment	Expansion pier	Fixed pier
$R_{DC1} + R_{DC2}$ (kips)	70	180	180
R_{DW} (kips)	17	53	48
R_{LL} (kips)	74	152	175
Expansion length (ft)	305	160	N.A.
Bearing size	15-e	20-a	N.A.
No. of anchor per retainer	1	1	N.A.
Dia. of retainer anchor (in.)	1.25	2	N.A.
No. of anchor per fixed bearing	N.A.	N.A.	4
Dia. of fixed bearing anchor (in.)	N.A.	N.A.	1.25

Table A.4: Girder Reaction and Sizing of Bearing Components of 3C Bridges

	Abutment	Expansion pier (Abut. side)	Expansion pier (Pier side)	Fixed pier
R_{DC1} (kips)	65.5	65.5	98	164
R_{DC2} (kips)	6	7.5	7.5	15
R_{DW} (kips)	15	21.5	21.5	43
R_{LL} (kips)	62	65	65	130
Expansion length (ft)	200	120	120	N.A.
Bearing size	12-e	13-b	13-b	N.A.
No. of anchor per retainer	1	1	1	2
Dia. of retainer anchor (in.)	1.25	1.25	1.25	1.5
No. of anchor per fixed bearing	N.A.	N.A.	N.A.	
Dia. of fixed bearing anchor (in.)	N.A.	N.A.	N.A.	

Table A.5: Girder Reaction and Sizing of Bearing Components of 4C Bridges

	Abutment	Expansion pier (Abut. side)	Expansion pier (Pier side)	Fixed pier
R_{DC1} (kips)	122.5	122.5	135.4	271.5
R_{DC2} (kips)	2.3	3.6	3.6	6.5
R_{DW} (kips)	17	26	26	48
R_{LL} (kips)	74	76	76	175
Expansion length (ft)	305	160	160	N.A.
Bearing size	15-e	15-b	15-b	N.A.
No. of anchor per retainer	1	1	1	2
Dia. of retainer anchor (in.)	1.5	1.5	1.5	1.5
No. of anchor per fixed bearing	N.A.	N.A.	N.A.	
Dia. of fixed bearing anchor (in.)	N.A.	N.A.	N.A.	

Table A.6: Sectional Properties of Longitudinal Beam Elements in Superstructure Models (x-axis is the bridge longitudinal axis, y-axis is the vertical axis)

Major bridge type		3S[1]	4S[1]	3C[2]	4C[2]
Girder type		Steel plate girder	Steel plate girder	PPC girder (IL54-2438)	PPC girder (IL72-3838)
Girder depth [cm (in.)]		116.8 (46)	174 (68.5)	137.2 (54)	182.9 (72)
Flange width [cm (in.)]		30.5 (12)	55.9 (22)	Top: 61.0 (24) Bottom: 96.5 (38)	96.5 (38)
Flange thickness [cm (in.)]		5.1 (2)	3.2 (1.25)	Top: 15.4 (6.1) ~ 31.8 (12.5) Bottom: 17.8 (7) ~ 55.9 (22)	Top: 12.7 (5) ~ 31.8 (12.5) Bottom: 17.8 (7) ~ 55.9 (22)
Web depth [cm (in.)]		106.7 (42)	167.6 (66)	49.5 (19.5)	95.3 (37.5)
Web thickness [mm (in.)]		1.1 (0.44)	1.3 (0.5)	17.8 (7)	17.8 (7)
Concrete slab thickness [mm (in.)]		21.0 (8.25)	21.0 (8.25)	21.0 (8.25)	21.0 (8.25)
Properties of transformed interior girder section	Area [cm^2 ($in.^2$)]	1024 (158.7)	1057 (163.9)	9131 (1415)	9797 (1519)
	Moment of inertia about x-x axis [cm^4 ($in.^4$)]	2.27×10^6 (5.43×10^4)	5.51×10^6 (1.32×10^5)	3.11×10^7 (7.46×10^5)	5.67×10^7 (1.36×10^6)
	Moment of inertia about y-y axis [cm^4 ($in.^4$)]	2.58×10^6 (6.18×10^4)	1.44×10^6 (3.46×10^4)	1.79×10^7 (4.30×10^5)	1.18×10^7 (2.83×10^5)
	Torsional consant [cm^4 ($in.^4$)]	8.57×10^4 (2059)	6.88×10^4 (1653)	1.85×10^6 (4.44×10^4)	1.90×10^6 (4.56×10^4)
Properties of transformed exterior girder section	Area [cm^2 ($in.^2$)]	1138 (176)	1245 (192.9)	9828 (1523)	1.09×10^4 (1695)
	Moment of inertia about x-x axis [cm^4 ($in.^4$)]	2.37×10^6 (5.70×10^4)	5.96×10^6 (1.43×10^5)	3.32×10^7 (7.98×10^5)	4.73×10^7 (1.51×10^6)
	Moment of inertia about y-y axis [cm^4 ($in.^4$)]	4.96×10^6 (1.19×10^5)	3.66×10^6 (8.79×10^4)	2.94×10^7 (7.06×10^5)	2.60×10^7 (6.24×10^5)
	Torsional consant [cm^4 ($in.^4$)]	1.03×10^5 (2467)	9.66×10^4 (2321)	1.95×10^6 (4.68×10^4)	2.06×10^6 (4.96×10^4)

1. Sectional properties are calculated based on the elastic modulus of plate girder steel ($E_{s,\,steel}$ = 200 GPa).
2. Sectional properties are calculated based on the elastic modulus of PPC girder concrete ($E_{c,\,girder}$ = 32.9 GPa).

Table A.7: Configuration of Diaphragms (Cross-Frames) Between Girders

Major bridge type	3S	4S	3C	4C
Member size	C15×50	Top chord: WT7×21.5 Diagnoal members: L8×8×1 Bottom chord: L8×8×1	MC12×31	MC18×42.7
Longitudinal spacing [m (ft)]	6.10 (20)	6.10 (20)	Spans up to 90 ft shall be braced at $0.33L$ and $0.67L$; Spans over 90 ft shall be braced at $0.25L$, $0.5L$, and $0.75L$; where L is the span length (IDOT 2012). Concrete panel diaphragms are used to connect girders between spans.	

Table A.8: Number, Diameter, and Spacing of Columns at an Intermediate Pier

Bridge skew (°)	0	15	30	45	60
Column number per pier	4	4	4	5	6
Diameter of 4.57-m-tall columns [m (ft)]	1.07 (3.5)	1.07 (3.5)	1.07 (3.5)	1.07 (3.5)	1.07 (3.5)
Diameter of 12.19-m-tall columns [m (ft)]	1.22 (4.0)	1.22 (4.0)	1.22 (4.0)	1.22 (4.0)	1.22 (4.0)
Center-to-center column spacing [m (ft)]	3.81 (12.5)	3.94 (12.94)	4.4 (14.43)	4.04 (13.26)	4.57 (14.99)
Spacing normalized to diameter (4.57-m-tall columns)	3.56	3.68	4.11	3.78	4.27
Spacing normalized to diameter (12.19-m-tall columns)	3.12	3.22	3.61	3.31	3.75

Table A.9: Material Properties of Pier Column

Column property		4.57-m-tall pier columns	12.19-m-tall pier columns
Concrete	Clear cover thickness [mm (in.)]	50.8 (2.0)	50.8 (2.0)
	Compressive strength [MPa (ksi)]	24.1 (3.5)	24.1 (3.5)
Vertical reinforcement	Bar diameter [mm (in.)]	28.7 (1.128)	28.7 (1.128)
	No. of bars	28	36
	Yield strength [MPa (ksi)]	414 (60)	414 (60)
	Reinforcement ratio	2%	2%
Transverse reinforcement	Spiral diameter [mm (in.)]	12.7 (0.5)	12.7 (0.5)
	Spiral hoop spacing [mm (in.)]	76.2 (3.0)	76.2 (3.0)
	Yield strength (MPa)	414 (60)	414 (60)

Table A.10: Pile Number and Spacing at an Intermediate Pier

Major bridge type	Skew (°)	Pile member size	Pile number in one row N_p	Center-to-center Pile spacing S_p [m (ft)]	Spacing normalized to pile width S_p / b_p
3S	0	HP 12×84	7	2.13 (7)	6.8
	15		7	2.13 (7)	6.8
	30		8	2.13 (7)	6.8
	45		9	2.29 (7.5)	7.3
	60		11	2.44 (8)	7.8
4S	0	HP 12×84	8	1.83 (6)	5.9
	15		8	1.83 (6)	5.9
	30		8	2.13 (7)	6.8
	45		9	2.29 (7.5)	7.3
	60		11	2.44 (8)	7.8
3C	0	HP 12×84	7	2.13 (7)	6.8
	15		7	2.13 (7)	6.8
	30		8	2.13 (7)	6.8
	45		9	2.29 (7.5)	7.3
	60		11	2.44 (8)	7.8
4C	0	HP 12×84	10	1.52 (5)	4.9
	15		10	1.52 (5)	4.9
	30		10	1.68 (5.5)	5.4
	45		10	1.83 (6)	5.9
	60		11	2.44 (8)	7.8

APPENDIX B: TIME HISTORIES AND RESPONSE SPECTRA OF EARTHQUAKE GROUND MOTIONS

Table B.12: Parameters of Earthquake Ground Motions Employed for Nonlinear Dynamic Bridge Analyses

Individual ground motion	PGA (g)	PGV (m/s)	PGD (m)	Arias Intensity (m/s)	Predominant period (s)
Cro01	0.36	1.00	0.63	6.44	0.08
Cro02	0.40	0.45	0.25	5.69	0.22
Cro03	0.30	0.70	0.34	4.65	1.18
Cro04	0.31	0.47	0.12	2.26	0.30
Cro05	0.38	1.06	0.69	6.45	0.08
Cro06	0.39	0.44	0.26	5.02	0.32
Cro07	0.36	0.46	0.30	2.36	1.32
Cro08	0.31	0.32	0.12	2.34	0.30
Cro09	0.33	0.31	0.12	2.42	0.30
Cro10	0.26	0.45	0.31	2.18	1.36
Cro11	0.40	0.50	0.29	5.33	0.22
Cro12	0.38	1.10	0.72	6.40	0.08
Cro13	0.30	0.31	0.11	2.64	0.30
Cro14	0.35	0.44	0.20	4.30	0.12
Cro15	0.40	0.47	0.27	4.76	0.22
Cro16	0.38	1.06	0.70	6.38	0.08
Cro17	0.35	0.35	0.14	2.96	0.28
Cro18	0.35	0.45	0.20	4.37	0.12
Cro19	0.40	0.51	0.28	4.87	0.22
Cro20	0.39	0.71	0.36	6.21	0.10

A suite of 20 site-specific earthquake ground motion time histories with a 1,000-year return period for Cairo, Illinois was developed by Kozak et al. (2017). The time history, 5%-damping elastic pseudo-acceleration spectrum, pseudo-velocity spectrum, and displacement spectrum of each ground motion are illustrated in this appendix.

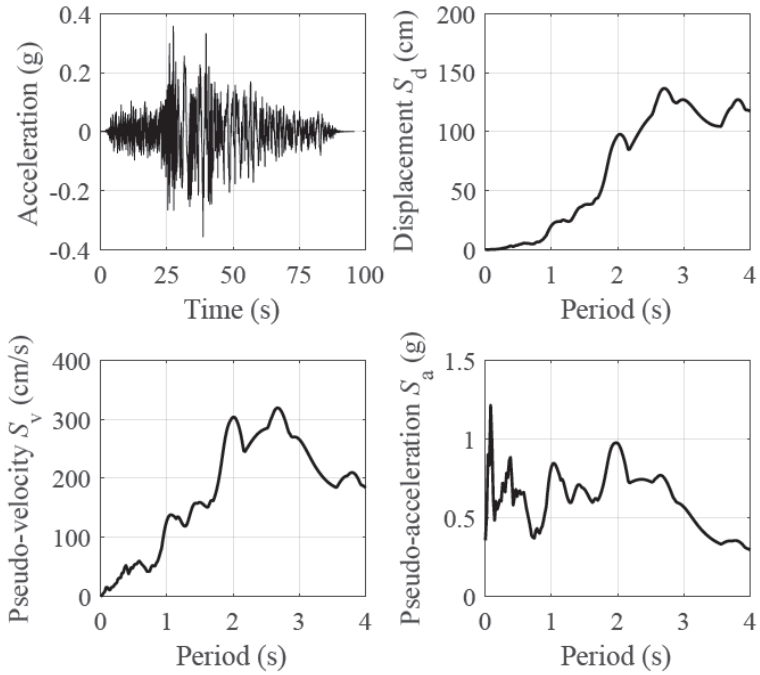

Figure B.1: Time history, 5%-damped pseudo-acceleration spectrum, pseudo-velocity spectrum, and displacement spectrum of earthquake motion Cro01.

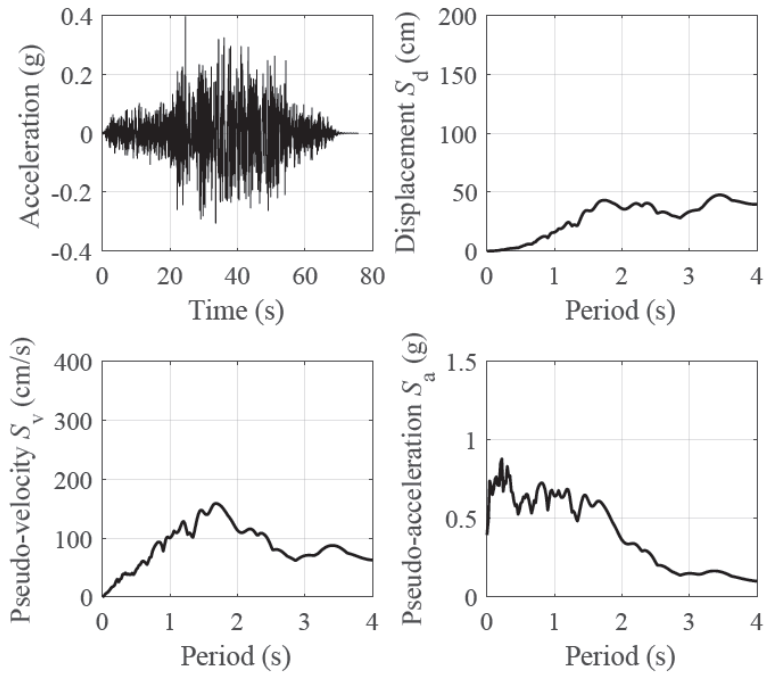

Figure B.2: Time history, 5%-damped pseudo-acceleration spectrum, pseudo-velocity spectrum, and displacement spectrum of earthquake motion Cro02.

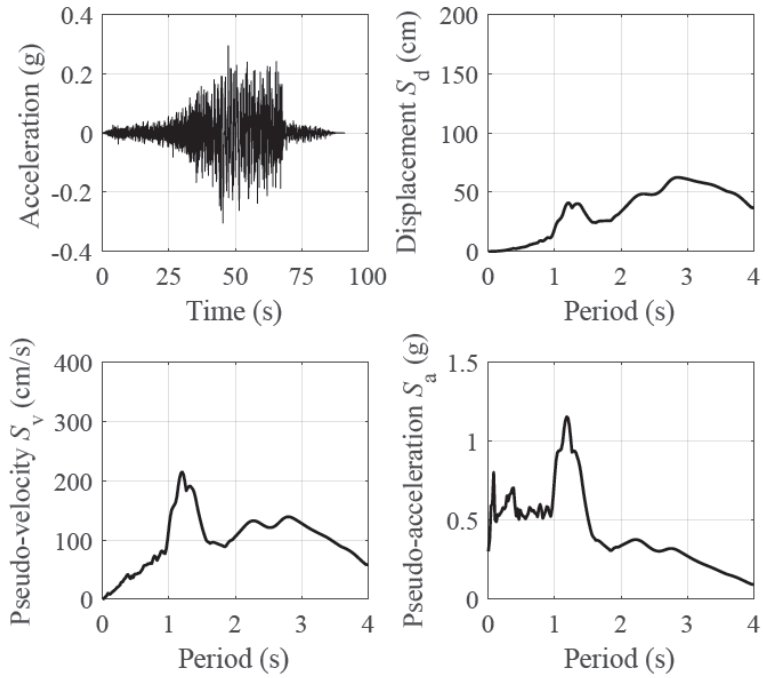

Figure B.3: Time history, 5%-damped pseudo-acceleration spectrum, pseudo-velocity spectrum, and displacement spectrum of earthquake motion Cro03.

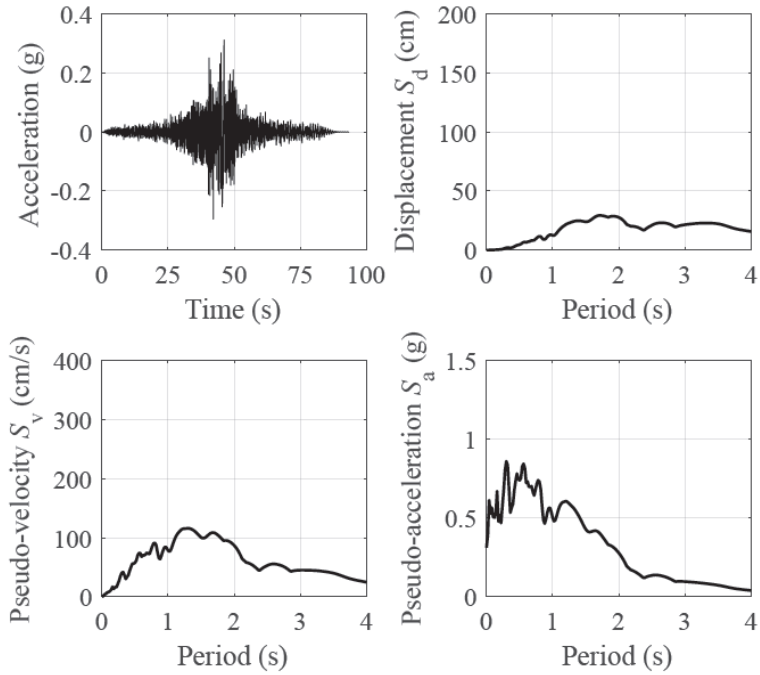

Figure B.4: Time history, 5%-damped pseudo-acceleration spectrum, pseudo-velocity spectrum, and displacement spectrum of earthquake motion Cro04.

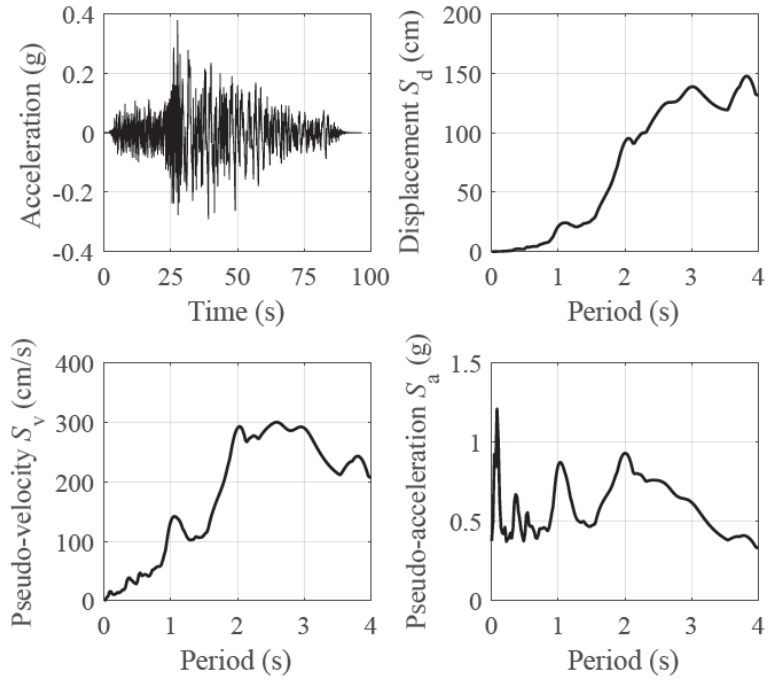

Figure B.5: Time history, 5%-damped pseudo-acceleration spectrum, pseudo-velocity spectrum, and displacement spectrum of earthquake motion Cro05.

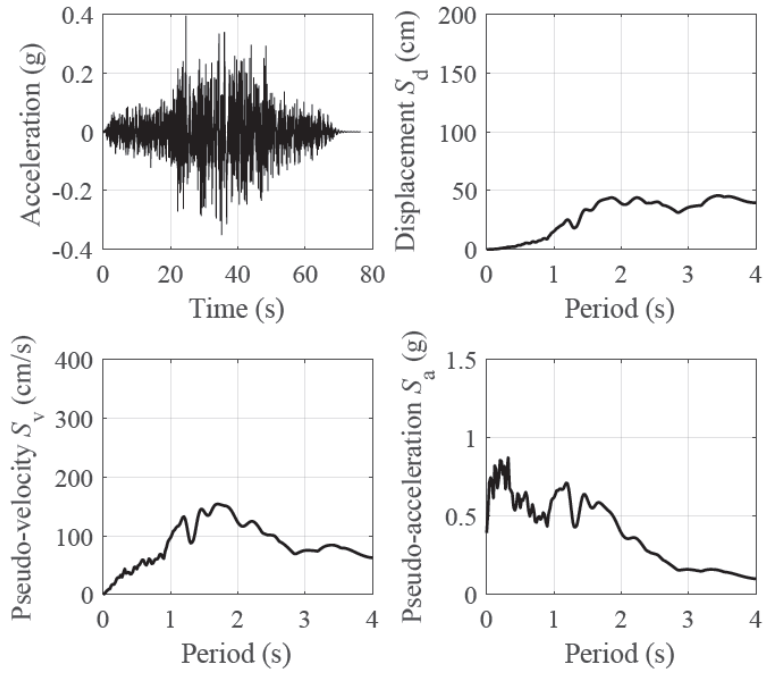

Figure B.6: Time history, 5%-damped pseudo-acceleration spectrum, pseudo-velocity spectrum, and displacement spectrum of earthquake motion Cro06.

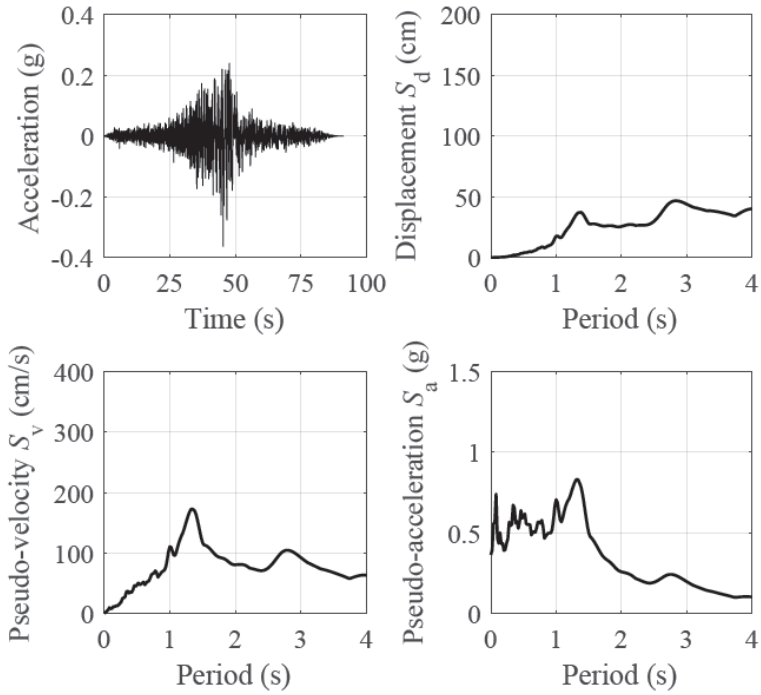

Figure B.7: Time history, 5%-damped pseudo-acceleration spectrum, pseudo-velocity spectrum, and displacement spectrum of earthquake motion Cro07.

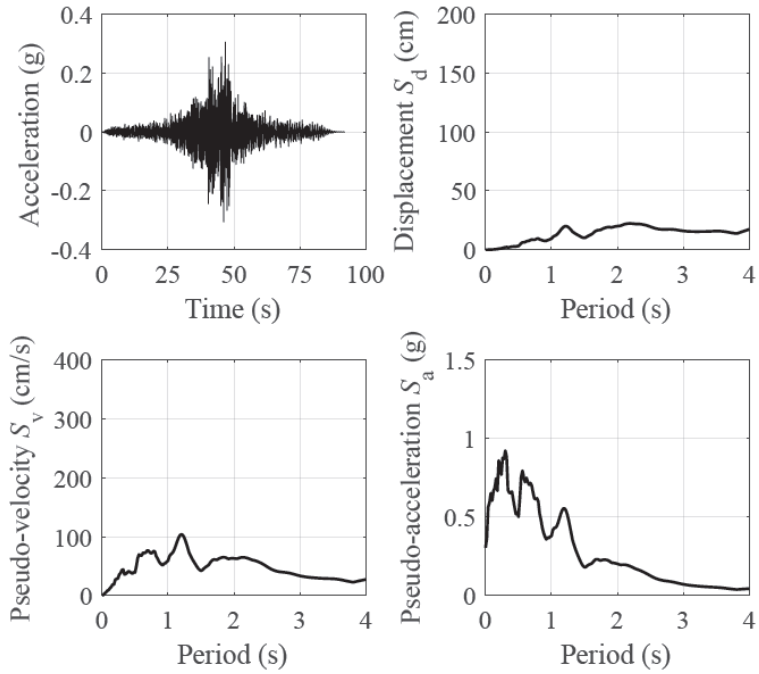

Figure B.8: Time history, 5%-damped pseudo-acceleration spectrum, pseudo-velocity spectrum, and displacement spectrum of earthquake motion Cro08.

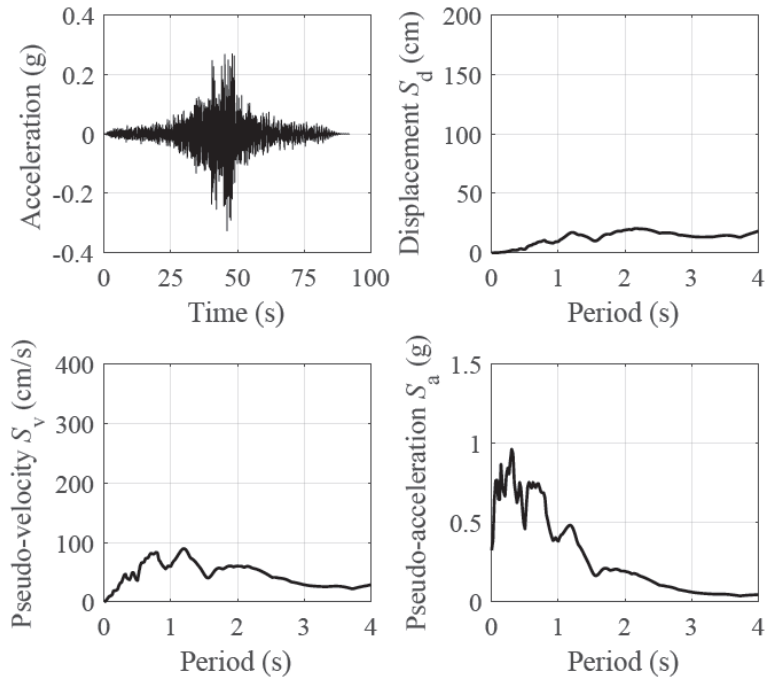

Figure B.9: Time history, 5%-damped pseudo-acceleration spectrum, pseudo-velocity spectrum, and displacement spectrum of earthquake motion Cro09.

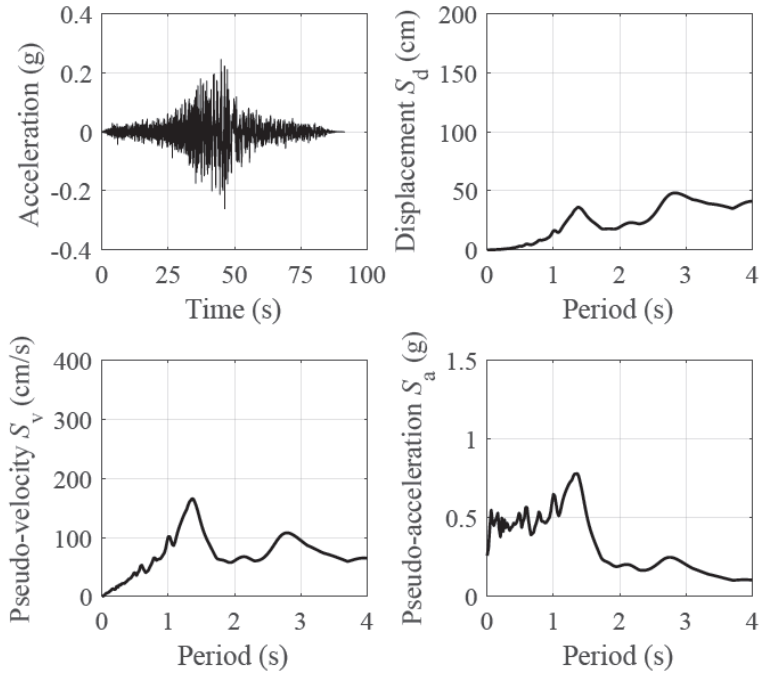

Figure B.10: Time history, 5%-damped pseudo-acceleration spectrum, pseudo-velocity spectrum, and displacement spectrum of earthquake motion Cro10.

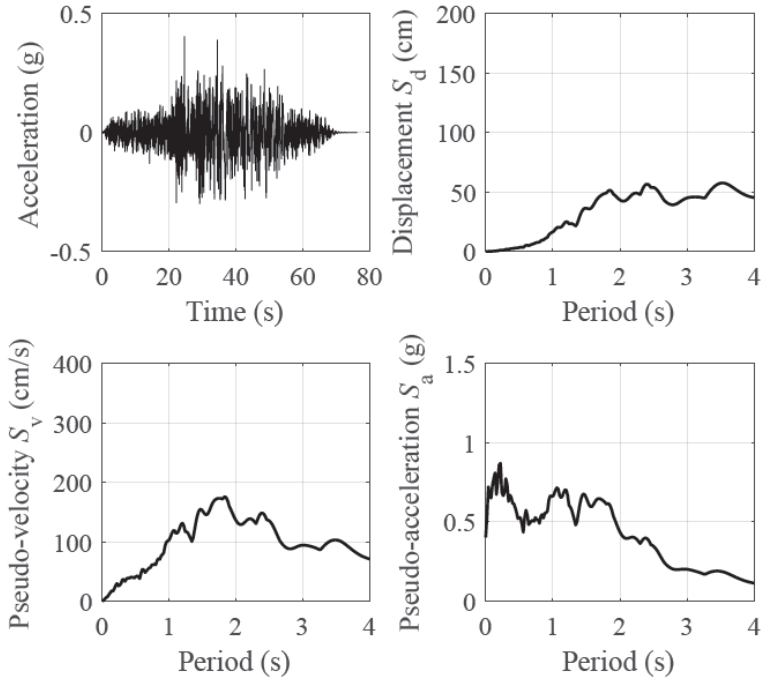

Figure B.11: Time history, 5%-damped pseudo-acceleration spectrum, pseudo-velocity spectrum, and displacement spectrum of earthquake motion Cro11.

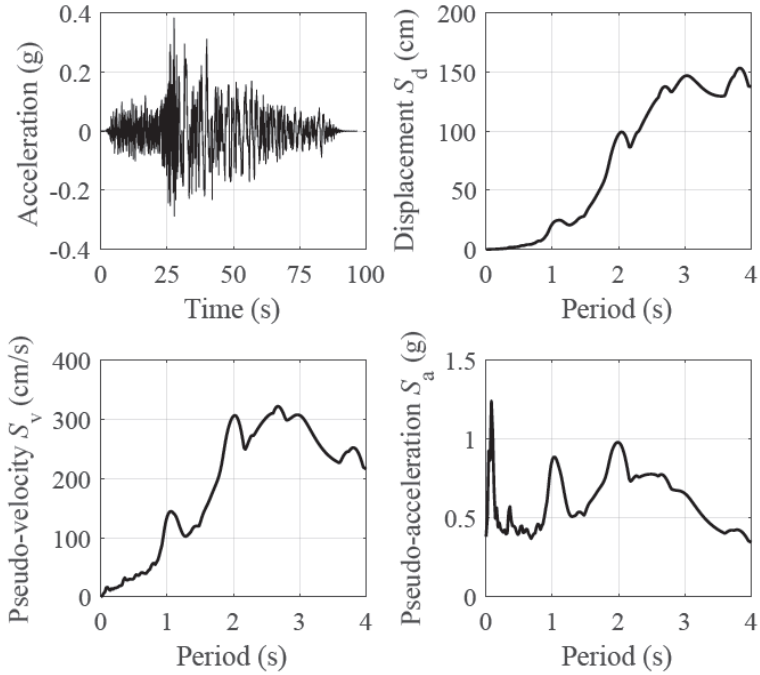

Figure B.12: Time history, 5%-damped pseudo-acceleration spectrum, pseudo-velocity spectrum, and displacement spectrum of earthquake motion Cro12.

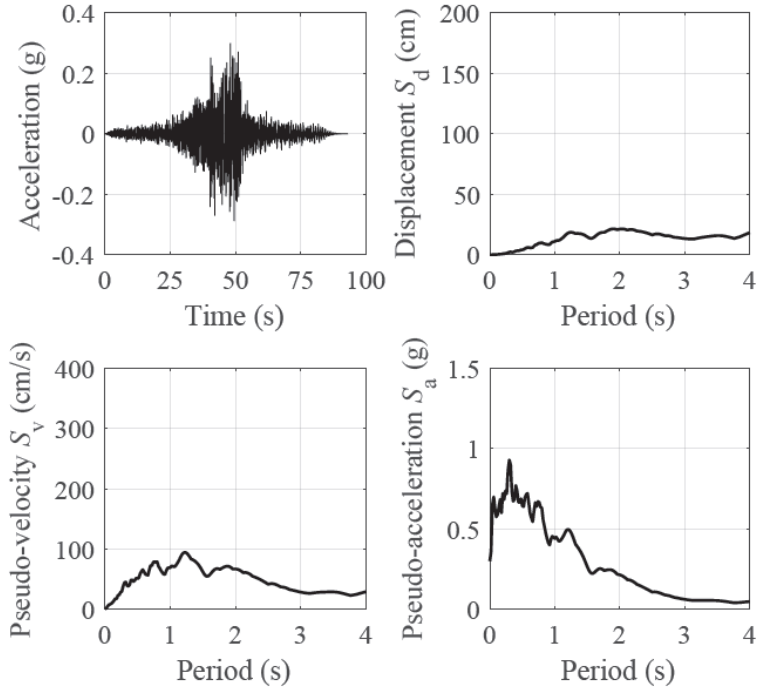

Figure B.13: Time history, 5%-damped pseudo-acceleration spectrum, pseudo-velocity spectrum, and displacement spectrum of earthquake motion Cro13.

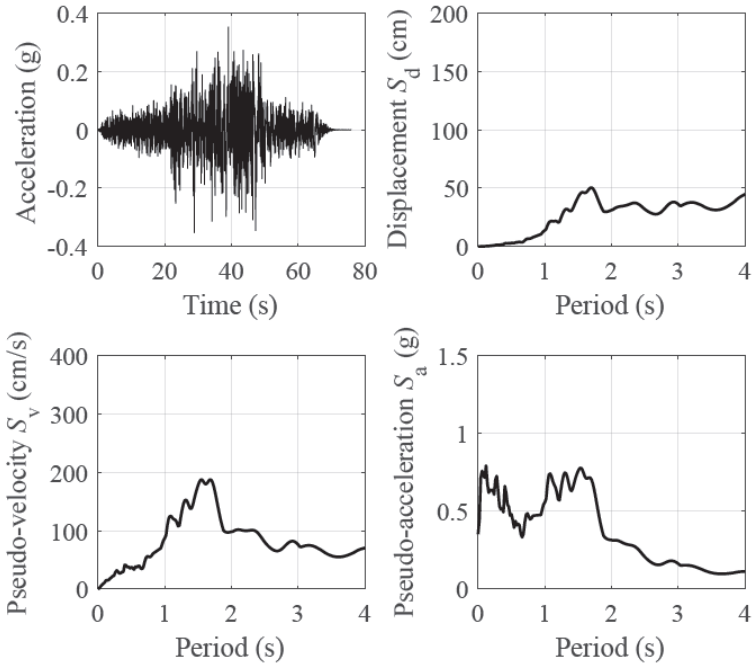

Figure B.14: Time history, 5%-damped pseudo-acceleration spectrum, pseudo-velocity spectrum, and displacement spectrum of earthquake motion Cro14.

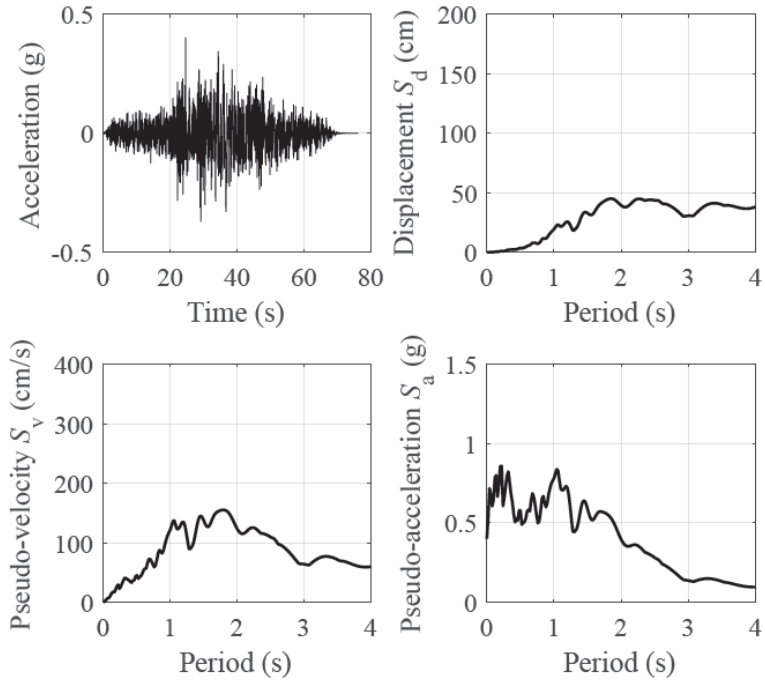

Figure B.15: Time history, 5%-damped pseudo-acceleration spectrum, pseudo-velocity spectrum, and displacement spectrum of earthquake motion Cro15.

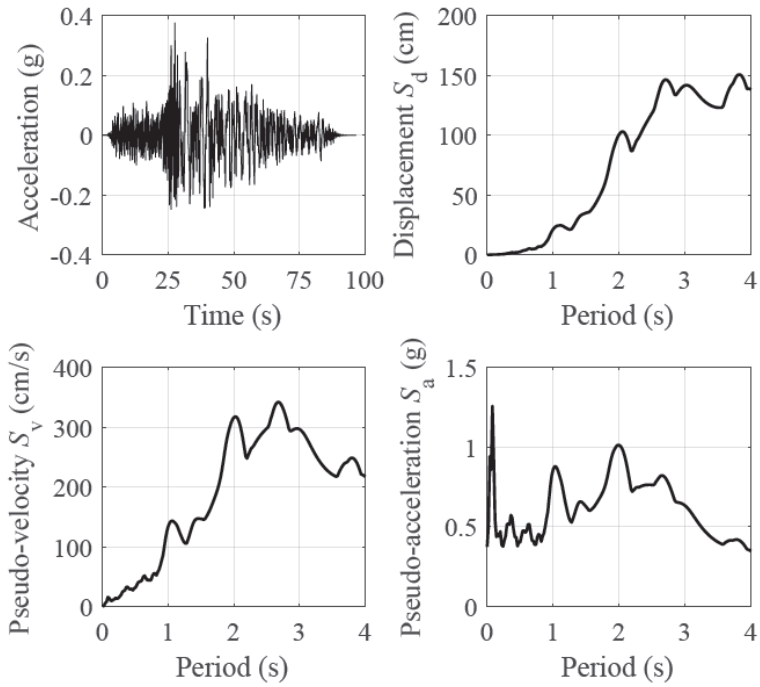

Figure B.16: Time history, 5%-damped pseudo-acceleration spectrum, pseudo-velocity spectrum, and displacement spectrum of earthquake motion Cro16.

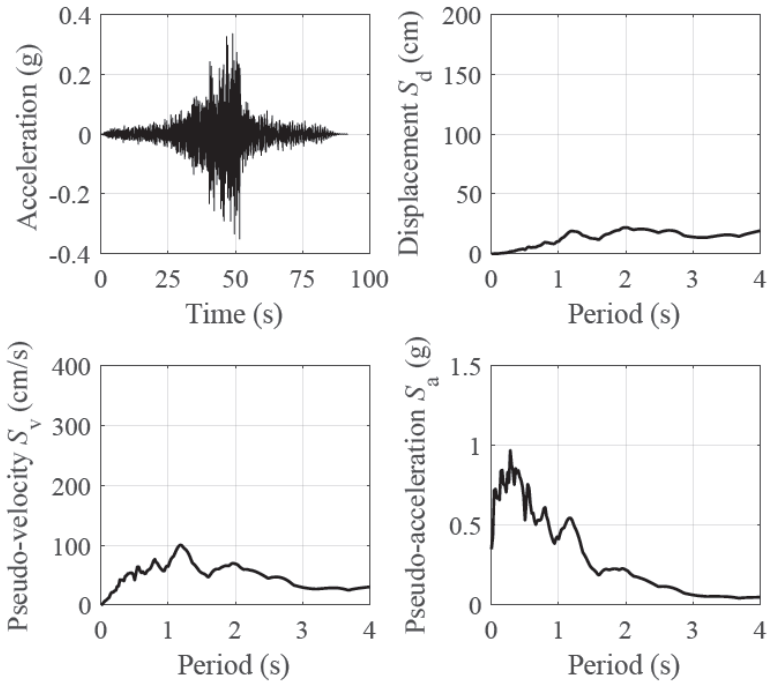

Figure B.17: Time history, 5%-damped pseudo-acceleration spectrum, pseudo-velocity spectrum, and displacement spectrum of earthquake motion Cro17.

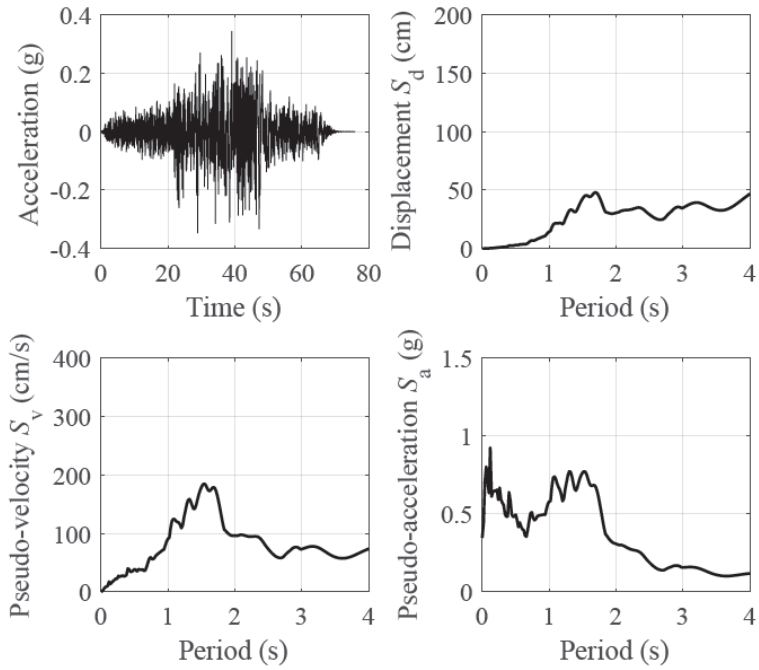

Figure B.18: Time history, 5%-damped pseudo-acceleration spectrum, pseudo-velocity spectrum, and displacement spectrum of earthquake motion Cro18.

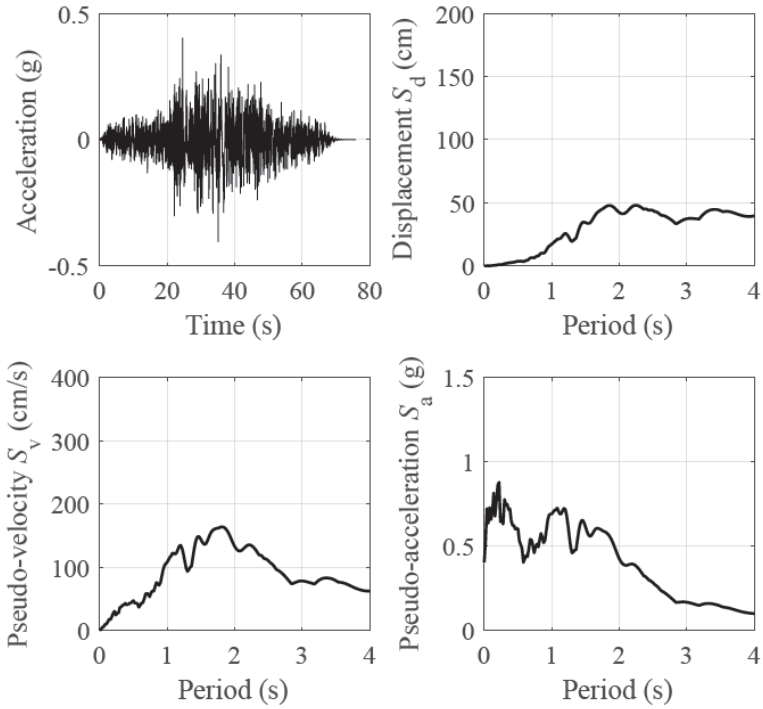

Figure B.19: Time history, 5%-damped pseudo-acceleration spectrum, pseudo-velocity spectrum, and displacement spectrum of earthquake motion Cro19.

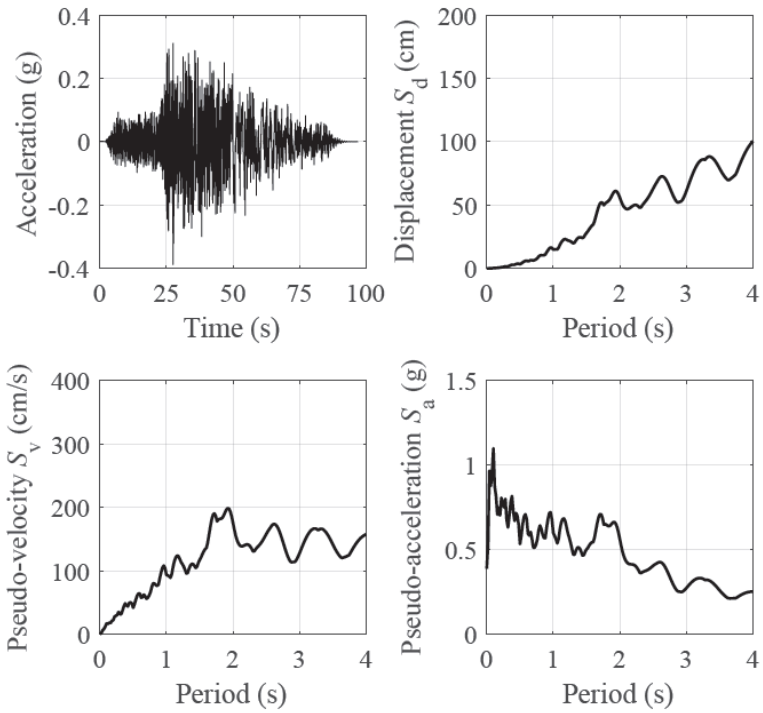

Figure B.20: Time history, 5%-damped pseudo-acceleration spectrum, pseudo-velocity spectrum, and displacement spectrum of earthquake motion Cro2

APPENDIX C: ADDITIONAL RESULTS FOR CHAPTER 4

C.1 ADDITIONAL ANALYSIS RESULTS FOR 3S BRIDGES

Table C1.1: Limit state occurrences of each 3S bridge variant under 0° and 45° ground motions (each percentage indicates the number of analyses with occurrences of a limit state out of the 20 analyses with the ground motions applied to a bridge variant in an incident direction)

Ground motion direction	Bridge variant	Critical limit states																												
		Abutment 1 (A1)									Pier 1 (P1, expansion pier)						Pier 2 (P2, fixed pier)					Abutment 2 (A2)								
		CEJ	MBU	FBP	RRA	SEB	UBA	UBO	YPW	YPB	RRA	SEB	UEB	YRS	CCC	YPP	RFA	USB	YRS	CCC	YPP	CEJ	MBU	FBP	RRA	SEB	UBO	UBA	YPW	YPB
0°	3S00P15H	100%	0	0	0	0	0	0	100%	95%	0	0	0	0	0	0	0	0	100%	0	0	100%	0	0	0	0	0	0	100%	70%
	3S15P15H	100%	0	0	0	0	0	0	100%	95%	0	0	0	0	0	0	0	0	100%	0	0	100%	0	0	0	0	0	0	100%	100%
	3S30P15H	100%	0	0	0	0	0	0	100%	95%	0	0	0	0	0	0	0	0	100%	5%	0	100%	0	0	0	0	0	0	100%	100%
	3S45P15H	100%	0	0	0	0	0	0	100%	45%	0	0	0	0	0	0	60%	0	100%	0	45%	100%	0	0	0	0	0	0	100%	90%
	3S60P15H	100%	0	0	0	0	0	0	10%	0	0	0	0	0	0	0	100%	0	10%	0	75%	100%	0	0	0	0	0	0	35%	0
	3S00P40H	100%	0	0	0	35%	0	0	100%	95%	0	0	0	5%	0	0	0	0	0	0	0	100%	0	0	0	30%	0	0	100%	95%
	3S15P40H	100%	0	0	0	50%	0	0	100%	100%	0	0	0	5%	0	0	0	0	0	0	0	100%	0	0	0	40%	0	0	100%	100%
	3S30P40H	100%	0	0	65%	45%	0	0	100%	100%	0	0	0	5%	0	0	0	0	25%	0	0	100%	0	0	65%	60%	0	0	100%	100%
	3S45P40H	100%	0	0	75%	60%	0	0	100%	80%	0	0	0	0	0	0	0	0	35%	0	0	100%	0	0	75%	70%	0	0	100%	90%
	3S60P40H	100%	0	0	90%	65%	0	0	100%	40%	0	0	0	5%	0	0	10%	0	60%	0	40%	100%	0	0	80%	75%	0	0	100%	75%
	3S00P15S	100%	0	0	0	0	0	0	75%	75%	0	0	0	0	0	0	0	0	100%	0	0	100%	0	0	0	0	0	0	80%	60%
	3S15P15S	100%	0	0	0	0	0	0	85%	95%	0	0	0	0	0	0	0	0	100%	0	15%	100%	0	0	0	0	0	0	95%	100%
	3S30P15S	100%	0	0	0	0	0	0	90%	90%	0	0	0	0	0	0	0	0	100%	15%	90%	100%	0	0	0	0	0	0	95%	100%
	3S45P15S	100%	0	0	0	0	0	0	65%	80%	0	0	0	0	0	0	0	0	80%	0	100%	100%	0	0	0	0	0	0	70%	95%
	3S60P15S	100%	0	0	0	5%	0	0	30%	30%	0	0	0	0	0	0	30%	0	0	0	100%	100%	0	0	5%	10%	0	0	25%	35%
	3S00P40S	100%	25%	0	0	70%	0	0	100%	100%	0	0	0	25%	0	0	0	0	35%	0	0	100%	15%	0	0	75%	0	0	100%	100%
	3S15P40S	100%	25%	0	0	80%	0	0	100%	100%	0	0	0	15%	0	0	0	0	40%	0	0	100%	15%	0	0	80%	0	0	100%	100%
	3S30P40S	100%	0	0	20%	80%	0	0	100%	100%	0	0	0	0	0	0	0	0	55%	0	5%	100%	5%	0	35%	100%	0	0	100%	100%
	3S45P40S	100%	0	0	45%	70%	0	0	100%	100%	0	0	0	0	0	0	0	0	40%	0	80%	100%	0	0	65%	80%	0	0	100%	100%
	3S60P40S	100%	0	0	0	60%	0	0	90%	100%	0	0	0	0	0	30%	0	0	20%	0	100%	100%	0	0	0	80%	0	0	95%	95%
45°	3S00P15H	100%	0	0	0	0	0	0	95%	70%	0	0	0	0	0	0	0	0	100%	0	0	100%	0	0	0	0	0	0	100%	30%
	3S15P15H	100%	0	0	0	0	0	0	100%	80%	0	0	0	0	0	0	0	0	100%	0	0	100%	0	0	0	0	0	0	100%	75%
	3S30P15H	100%	0	0	0	0	0	0	100%	85%	0	0	0	0	0	0	0	0	100%	0	0	100%	0	0	0	0	0	0	100%	85%
	3S45P15H	100%	0	0	0	0	0	0	100%	65%	0	0	0	0	0	0	0	0	100%	0	0	100%	0	0	20%	0	0	0	100%	80%
	3S60P15H	100%	0	0	0	0	0	0	60%	5%	0	0	0	0	0	0	30%	0	80%	0	0	100%	0	0	0	0	0	0	70%	30%
	3S00P40H	100%	0	0	15%	0	0	0	100%	95%	0	0	0	0	0	0	0	0	0	0	0	100%	0	0	0	0	0	0	100%	100%
	3S15P40H	100%	0	0	45%	5%	0	0	100%	100%	0	0	0	5%	0	0	0	0	0	0	0	100%	0	0	35%	0	0	0	100%	100%
	3S30P40H	100%	0	0	80%	35%	0	0	100%	100%	0	0	0	5%	0	0	0	0	10%	0	0	100%	0	0	85%	50%	0	0	100%	100%
	3S45P40H	100%	0	0	90%	75%	0	0	100%	95%	0	0	0	20%	0	0	0	0	40%	0	0	100%	0	0	95%	80%	0	0	100%	85%
	3S60P40H	100%	0	0	75%	75%	0	0	100%	80%	0	0	0	50%	0	0	0	0	75%	0	0	100%	0	0	90%	80%	0	0	100%	75%
	3S00P15S	100%	0	0	0	0	0	0	10%	70%	0	0	0	0	0	10%	0	0	100%	0	75%	100%	0	0	0	0	0	0	25%	50%
	3S15P15S	100%	0	0	0	0	0	0	40%	60%	0	0	0	0	0	0	0	0	100%	0	5%	100%	0	0	0	0	0	0	45%	40%
	3S30P15S	100%	0	0	0	0	0	0	65%	65%	0	0	0	0	0	0	0	0	100%	0	0	100%	0	0	0	0	0	0	70%	75%
	3S45P15S	100%	0	0	5%	0	0	0	30%	55%	0	0	0	0	0	0	0	0	95%	0	5%	100%	0	0	0	0	0	0	25%	40%
	3S60P15S	100%	0	0	10%	0	0	0	0	10%	0	0	0	0	0	0	0	0	40%	0	0	100%	0	0	0	0	0	0	5%	15%
	3S00P40S	100%	0	0	0	5%	0	0	100%	100%	0	0	0	5%	0	65%	0	0	5%	0	15%	100%	0	0	0	10%	0	0	100%	100%
	3S15P40S	100%	0	0	20%	40%	0	0	100%	100%	0	0	0	5%	0	10%	0	0	10%	0	5%	100%	0.05	0	5%	40%	0	0	100%	100%
	3S30P40S	100%	5%	0	70%	70%	0	0	100%	100%	0	0	0	10%	0	0	0	0	35%	0	0	100%	0	0	55%	55%	0	0	100%	100%
	3S45P40S	100%	0	0	85%	75%	0	0	100%	100%	0	0	0	30%	0	0	0	0	60%	0	0	100%	0	0	90%	80%	0	0	100%	100%
	3S60P40S	100%	0	0	75%	75%	0	0	90%	100%	0	0	0	35%	0	0	0	0	75%	0	0	100%	0	0	80%	80%	0	0	75%	90%
Preferred limit states:		0	20%	40%	60%	80%	100%																							
Acceptable limit states:		0	20%	40%	60%	80%	100%																							
Unacceptable limit states:		0	20%	40%	60%	80%	100%																							

Table C1.1 Continued: Limit state occurrences of each 3S bridge variant under 90° and 135° ground motions (each percentage indicates the number of analyses with occurrences of a limit state out of the 20 analyses with the ground motions applied to a bridge variant in an incident direction)

Ground motion direction	Bridge variant	Critical limit states																												
		Abutment 1 (A1)									Pier 1 (P1, expansion pier)						Pier 2 (P2, fixed pier)					Abutment 2 (A2)								
		CEJ	MBU	FBP	RRA	SEB	UBA	UBO	YPW	YPB	RRA	SEB	UEB	YRS	CCC	YPP	RFA	USB	YRS	CCC	YPP	CEJ	MBU	FBP	RRA	SEB	UBO	UBA	YPW	YPB
90°	3S00P15H	0	0	0	50%	5%	0	0	0	5%	0	0	0	0	0	0	0	0	0	0	15%	0	0	0	0	0	0	0	0	0
	3S15P15H	60%	0	0	65%	10%	0	0	0	15%	0	0	0	0	0	5%	0	0	0	0	20%	5%	0	0	0	0	0	0	0	0
	3S30P15H	95%	0	0	80%	15%	0	0	35%	40%	0	0	0	0	0	0	0	0	5%	0	15%	25%	0	0	5%	0	0	0	0	0
	3S45P15H	100%	0	0	70%	15%	0	0	35%	15%	0	0	0	5%	0	0	0	0	0	0	10%	90%	0	0	5%	0	0	0	0	0
	3S60P15H	100%	0	0	55%	10%	0	0	40%	5%	0	0	0	5%	0	0	0	0	10%	0	0	95%	0	0	0	0	0	0	0	0
	3S00P40H	0	0	0	100%	85%	0	0	0	0	0	0	0	65%	0	65%	0	0	15%	0	10%	0	0	0	55%	10%	0	0	0	5%
	3S15P40H	100%	0	0	100%	100%	0	0	70%	55%	0	0	0	70%	0	60%	0	0	20%	0	5%	100%	0	0	60%	10%	0	0	5%	5%
	3S30P40H	100%	0	0	100%	100%	0	0	100%	95%	0	0	0	60%	0	10%	0	0	50%	0	5%	100%	0	0	90%	40%	0	0	75%	50%
	3S45P40H	100%	0	0	100%	100%	0	0	100%	90%	0	0	0	25%	0	0	0	0	15%	0	0	100%	0	0	90%	35%	0	0	95%	40%
	3S60P40H	100%	0	0	100%	80%	0	0	95%	80%	0	0	0	60%	0	0	0	0	35%	0	0	100%	0	0	80%	75%	0	0	75%	45%
	3S00P15S	0	0	0	25%	5%	0	0	0	15%	0	0	0	0	0	95%	0	0	0	0	100%	0	0	0	0	0	0	0	0	0
	3S15P15S	10%	0	0	35%	5%	0	0	0	20%	0	0	0	0	0	95%	0	0	0	0	95%	5%	0	0	0	0	0	0	0	0
	3S30P15S	60%	0	0	40%	0	0	0	0	20%	0	0	0	0	0	70%	0	0	0	0	45%	10%	0	0	0	0	0	0	0	0
	3S45P15S	100%	0	0	65%	15%	0	0	0	20%	0	0	0	0	0	10%	0	0	0	0	25%	40%	0	0	5%	0	0	0	0	0
	3S60P15S	100%	0	0	70%	20%	0	0	0	15%	0	0	0	10%	0	0	0	0	0	0	0	95%	0	0	20%	0	0	0	0	0
	3S00P40S	0	0	0	90%	65%	0	0	0	60%	0	0	0	35%	0	90%	0	0	10%	0	85%	0	0	0	30%	10%	0	0	0	60%
	3S15P40S	95%	0	0	90%	80%	0	0	0	75%	0	0	0	40%	0	95%	0	0	10%	0	95%	90%	0	0	40%	25%	0	0	0	65%
	3S30P40S	100%	0	0	95%	85%	0	0	35%	90%	0	0	0	60%	0	90%	0	0	25%	0	85%	100%	0	0	70%	35%	0	0	0	80%
	3S45P40S	100%	0	0	100%	100%	0	0	65%	100%	0	0	0	15%	0	55%	0	0	10%	0	75%	100%	0	0	85%	50%	0	0	35%	60%
	3S60P40S	100%	0	0	100%	90%	0	0	65%	95%	0	0	0	50%	0	0	0	0	45%	0	35%	100%	0	0	85%	75%	0	0	55%	70%
135°	3S00P15H	100%	0	0	0	0	0	0	100%	55%	0	0	0	0	0	0	0	0	100%	0	0	100%	0	0	0	0	0	0	90%	45%
	3S15P15H	100%	0	0	15%	5%	0	0	65%	30%	0	0	0	0	0	0	0	0	100%	0	10%	100%	0	0	0	0	0	0	80%	20%
	3S30P15H	100%	0	0	30%	5%	0	0	20%	5%	0	0	0	0	0	0	0	0	90%	0	40%	100%	0	0	5%	0	0	0	40%	0
	3S45P15H	90%	0	0	45%	5%	0	0	0	5%	0	0	0	0	0	0	20%	0	5%	0	65%	100%	0	0	5%	0	0	0	5%	0
	3S60P15H	90%	0	0	35%	5%	0	0	0	0	0	0	0	0	0	0	45%	0	0	0	25%	100%	0	0	0	0	0	0	0	0
	3S00P40H	100%	0	0	25%	0	0	0	100%	100%	0	0	0	0	0	0	0	0	0	0	0	100%	0	0	0	0	0	0	100%	95%
	3S15P40H	100%	0	0	85%	40%	0	0	100%	100%	0	0	0	20%	0	10%	0	0	5%	0	0	100%	0	0	15%	5%	0	0	100%	100%
	3S30P40H	100%	0	0	100%	95%	0	0	80%	35%	0	0	0	60%	0	25%	0	0	70%	0	5%	100%	0	0	100%	45%	0	0	95%	80%
	3S45P40H	100%	0	0	100%	95%	0	0	15%	15%	0	0	0	20%	0	15%	0	0	75%	0	55%	100%	0	0	85%	30%	0	0	75%	55%
	3S60P40H	100%	0	0	100%	80%	0	0	10%	35%	0	0	0	10%	0	0	60%	0	75%	0	65%	100%	0	0	40%	20%	0	0	20%	0
	3S00P15S	100%	0	0	0	0	0	0	30%	80%	0	0	0	0	0	10%	0	0	100%	0	75%	100%	0	0	0	0	0	0	10%	50%
	3S15P15S	100%	0	0	0	0	0	0	60%	85%	0	0	0	0	0	50%	0	0	100%	0	100%	100%	0	0	0	0	0	0	45%	80%
	3S30P15S	100%	0	0	0	0	0	0	65%	70%	0	0	0	0	0	50%	0	0	95%	0	100%	100%	0	0	0	0	0	0	55%	65%
	3S45P15S	100%	0	0	0	0	0	0	15%	15%	0	0	0	0	0	50%	0	0	0	0	100%	100%	0	0	5%	0	0	0	20%	25%
	3S60P15S	100%	0	0	25%	0	0	0	0	0	0	0	0	0	0	5%	0	0	0	0	95%	85%	0	0	0	0	0	0	0	0
	3S00P40S	100%	0	0	0	10%	0	0	100%	100%	0	0	0	5%	0	60%	0	0	5%	0	20%	100%	0	0	0	5%	0	0	100%	100%
	3S15P40S	100%	0	0	60%	25%	0	0	95%	100%	0	0	0	5%	0	80%	0	0	5%	0	80%	100%	0	0	5%	15%	0	0	100%	100%
	3S30P40S	100%	0	0	95%	65%	0	0	45%	90%	0	0	0	35%	0	75%	0	0	40%	0	80%	100%	0	0	25%	30%	0	0	80%	80%
	3S45P40S	100%	0	0	100%	70%	0	0	10%	45%	0	0	0	5%	0	75%	0	0	10%	0	100%	100%	0	0	35%	35%	0	0	35%	65%
	3S60P40S	100%	0	0	100%	80%	0	0	30%	75%	0	0	0	0	0	70%	0	0	10%	0	95%	100%	0	0	35%	35%	0	0	5%	20%

Preferred limit states:	0	20%	40%	60%	80%	100%
Acceptable limit states:	0	20%	40%	60%	80%	100%
Unacceptable limit states:	0	20%	40%	60%	80%	100%

Table C1.2: Occurrences of limit states at abutments (A1 and A2) of 3S bridge variants

Limit state	No. of analyses with occurrence [1]	Skew angle [2] (°)					Foundation soil [2]		Column height [2] (m)		Ground motion incident angle [2] (°)			
		0	15	30	45	60	Hard	Soft	4.57	12.19	0	45	90	135
Closure of expansion joint (CEJ@A1)	1480 (93%)	240 (16%)	293 (20%)	311 (21%)	318 (21%)	318 (21%)	747 (50%)	733 (50%)	721 (49%)	759 (51%)	400 (27%)	400 (27%)	284 (19%)	396 (27%)
Mobilization of backfill ultimate capacity (MBU@A1)	11 (1%)	5 (45%)	5 (45%)	1 (9%)	0 (0%)	0 (0%)	0 (0%)	11 (100%)	0 (0%)	11 (100%)	10 (91%)	1 (9%)	0 (0%)	0 (0%)
Failure of backwall-to-pile-cap connection (FBP@A1)	0 (0%)	0	0	0	0	0	0	0	0	0	0	0	0	0
Rupture of retainer anchor (RRA@A1)	662 (41%)	61 (9%)	103 (16%)	155 (23%)	176 (27%)	167 (25%)	378 (57%)	284 (43%)	144 (22%)	518 (78%)	59 (9%)	114 (17%)	306 (46%)	183 (28%)
Slidng of elastomeric bearing (SEB@A1)	528 (33%)	56 (11%)	88 (17%)	119 (23%)	136 (26%)	129 (24%)	259 (49%)	269 (51%)	25 (5%)	503 (95%)	124 (23%)	91 (17%)	197 (37%)	116 (22%)
Unseating of bearing at obtuse corner of deck (UBA@A1)	0 (0%)	0	0	0	0	0	0	0	0	0	0	0	0	0
Unseating of bearing at acute corner of deck (UBO@A1)	0 (0%)	0	0	0	0	0	0	0	0	0	0	0	0	0
Yielding of pile supporting wingwall (YPW@A1)	983 (61%)	202 (21%)	223 (23%)	227 (23%)	187 (19%)	144 (15%)	566 (58%)	417 (42%)	364 (37%)	619 (63%)	349 (36%)	318 (32%)	128 (13%)	188 (19%)
Yielding of pile supporting backwall (YPB@A1)	1020 (64%)	223 (22%)	242 (24%)	236 (23%)	185 (18%)	134 (13%)	460 (45%)	560 (55%)	356 (35%)	664 (65%)	323 (32%)	307 (30%)	182 (18%)	208 (20%)
Closure of expansion joint (CEJ@A2)	1428 (89%)	240 (17%)	280 (20%)	287 (20%)	306 (21%)	315 (22%)	723 (51%)	705 (49%)	670 (47%)	758 (53%)	400 (28%)	400 (28%)	231 (16%)	397 (28%)
Mobilization of backfill ultimate capacity (MBU@A2)	8 (1%)	3 (38%)	4 (50%)	1 (13%)	0 (0%)	0 (0%)	0 (0%)	8 (100%)	0 (0%)	8 (100%)	7 (88%)	1 (13%)	0 (0%)	0 (0%)
Failure of backwall-to-pile-cap connection (FBP@A2)	0 (0%)	0	0	0	0	0	0	0	0	0	0	0	0	0
Rupture of retainer anchor (RRA@A2)	391 (24%)	17 (4%)	32 (8%)	107 (27%)	132 (34%)	103 (26%)	236 (60%)	155 (40%)	15 (4%)	376 (96%)	65 (17%)	111 (28%)	144 (37%)	71 (18%)
Slidng of elastomeric bearing (SEB@A2)	352 (22%)	28 (8%)	43 (12%)	83 (24%)	92 (26%)	106 (30%)	151 (43%)	201 (57%)	2 (1%)	350 (99%)	140 (40%)	95 (27%)	73 (21%)	44 (13%)
Unseating of bearing at obtuse corner of deck (UBO@A2)	0 (0%)	0	0	0	0	0	0	0	0	0	0	0	0	0
Unseating of bearing at acute corner of deck (UBA@A2)	0 (0%)	0	0	0	0	0	0	0	0	0	0	0	0	0
Yielding of pile supporting wingwall (YPW@A2)	961 (60%)	201 (21%)	214 (22%)	222 (23%)	192 (20%)	132 (14%)	552 (57%)	409 (43%)	357 (37%)	604 (63%)	359 (37%)	323 (34%)	68 (7%)	211 (22%)
Yielding of pile supporting backwall (YPB@A2)	927 (58%)	192 (21%)	217 (23%)	223 (24%)	185 (20%)	110 (12%)	424 (46%)	503 (54%)	311 (34%)	616 (66%)	341 (37%)	294 (32%)	96 (10%)	196 (21%)

1 The number above the parentheses indicates the number of analyses with occurrences of a limit state.
The percentage inside the parentheses indicates the ratio of the number above the parentheses to all the 1,600 analyses.
2 The number above the parentheses indicates the number of analyses with occurrences of a limit state contributed by a parametric variation.
The percentage inside the parentheses indicates the relative contribution of a parametric variation to the total occurrences of a limit state.

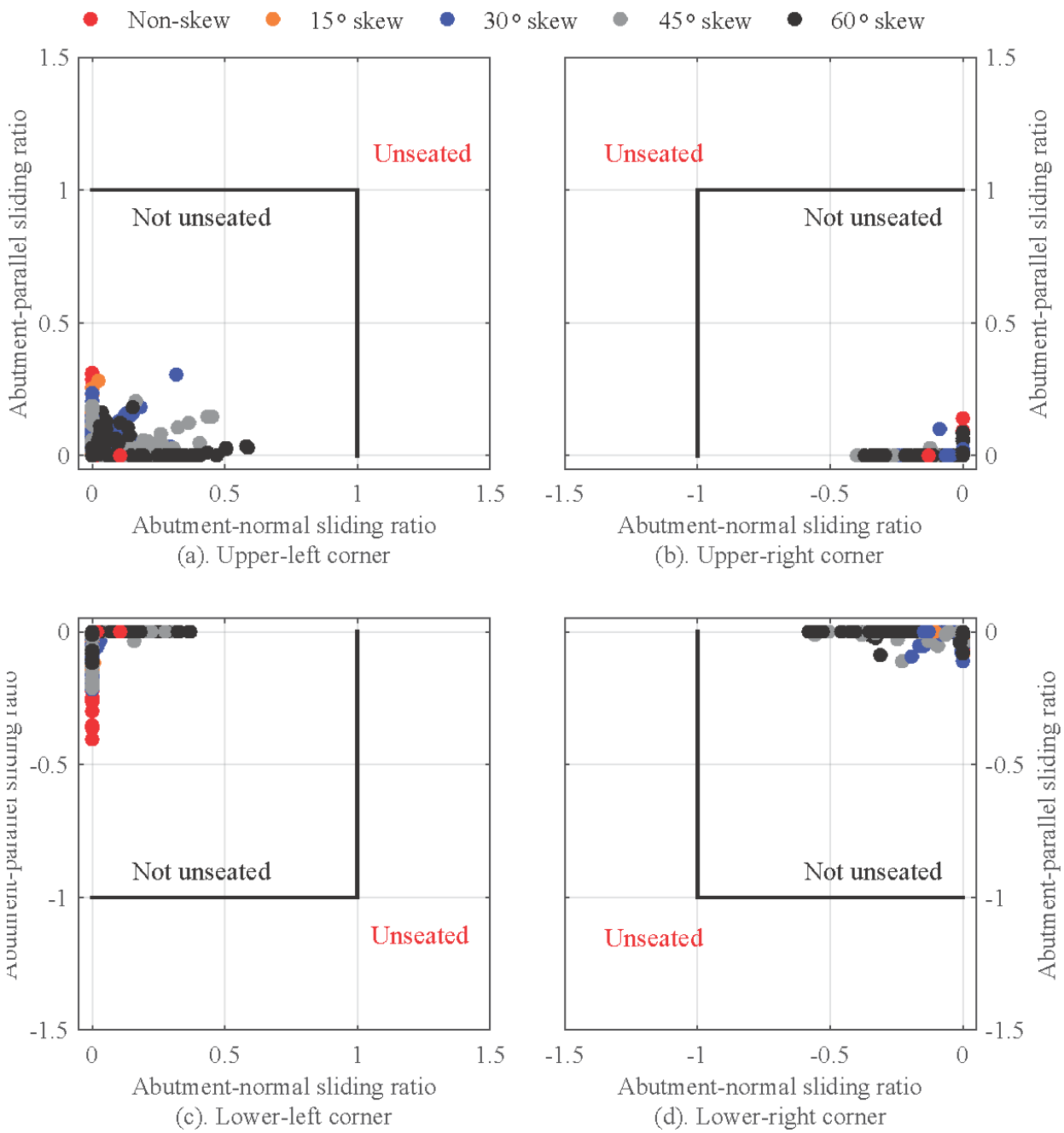

Figure C1.1: Peak sliding ratios of elastomeric bearings at deck corners of 3S bridges.

Table C1.3: Normalized Peak Strains of Steel H Piles Supporting Abutments of 3S Bridges (peak strains are normalized to the yield strain of steel piles, 0.0017; numbers outside and inside the parentheses are medians and median absolute deviations, respectively; data for piles supporting backwalls and wingwalls are placed on the left and right sides of the commas, respectively)

Foundation soil condition		Hard				Soft			
Pier column height (m)		4.57		12.19		4.57		12.19	
Longitudinal (0°) ground motions	Bridge skew (°) 0	1.1 (0.2) ,	2.0 (0.3)	4.4 (1.9) ,	6.0 (2.1)	1.2 (0.3) ,	1.1 (0.2)	6.4 (1.9) ,	5.6 (2.4)
	15	1.7 (0.3) ,	2.4 (0.6)	7.3 (2.4) ,	8.1 (2.3)	2.2 (0.6) ,	1.7 (0.4)	7.9 (1.8) ,	7.1 (1.8)
	30	1.8 (0.6) ,	2.2 (0.7)	6.4 (2.2) ,	7.8 (2.3)	3.0 (0.9) ,	2.5 (0.7)	7.6 (2.7) ,	6.7 (2.5)
	45	1.1 (0.3) ,	1.4 (0.4)	1.7 (0.4) ,	2.9 (0.7)	1.5 (0.4) ,	1.4 (0.4)	5.3 (1.9) ,	5.2 (1.8)
	60	0.6 (0.1) ,	0.7 (0.1)	1.0 (0.2) ,	1.3 (0.2)	0.9 (0.2) ,	0.9 (0.2)	2.8 (1.2) ,	2.7 (1.2)
45° ground motions	Bridge skew (°) 0	1.0 (0.2) ,	1.3 (0.3)	2.3 (0.9) ,	3.2 (1.0)	1.1 (0.2) ,	0.9 (0.1)	4.1 (0.9) ,	3.0 (0.9)
	15	1.2 (0.2) ,	1.6 (0.3)	3.9 (1.6) ,	4.9 (1.5)	1.0 (0.1) ,	1.0 (0.1)	4.4 (1.5) ,	3.4 (1.3)
	30	1.4 (0.3) ,	1.8 (0.5)	5.6 (2.9) ,	7.1 (2.5)	1.6 (0.6) ,	1.3 (0.3)	5.9 (2.2) ,	5.1 (2.0)
	45	1.1 (0.2) ,	1.5 (0.3)	2.4 (0.9) ,	4.5 (1.2)	1.0 (0.2) ,	0.9 (0.1)	5.7 (2.3) ,	4.9 (2.3)
	60	0.8 (0.1) ,	1.0 (0.2)	1.3 (0.4) ,	2.2 (1.0)	0.8 (0.1) ,	0.7 (0.1)	3.0 (1.6) ,	2.5 (1.3)
Transverse (90°) ground motions	Bridge skew (°) 0	0.8 (0.1) ,	0.4 (0.1)	0.9 (0.1) ,	0.5 (0.0)	0.8 (0.1) ,	0.5 (0.1)	1.2 (0.3) ,	0.8 (0.2)
	15	0.8 (0.1) ,	0.5 (0.1)	0.9 (0.1) ,	0.9 (0.2)	0.7 (0.1) ,	0.5 (0.1)	1.2 (0.3) ,	0.8 (0.1)
	30	0.8 (0.1) ,	0.5 (0.2)	1.3 (0.3) ,	1.5 (0.5)	0.7 (0.1) ,	0.6 (0.1)	1.5 (0.4) ,	1.1 (0.2)
	45	0.6 (0.1) ,	0.6 (0.2)	1.1 (0.3) ,	1.9 (0.6)	0.7 (0.1) ,	0.6 (0.1)	1.6 (0.4) ,	1.3 (0.3)
	60	0.5 (0.1) ,	0.6 (0.2)	1.1 (0.3) ,	1.8 (0.6)	0.6 (0.1) ,	0.5 (0.1)	1.6 (0.6) ,	1.3 (0.5)
135° ground motions	Bridge skew (°) 0	1.0 (0.2) ,	1.2 (0.3)	2.1 (0.5) ,	3.1 (0.8)	1.1 (0.1) ,	0.9 (0.1)	4.0 (0.8) ,	3.1 (0.7)
	15	0.9 (0.1) ,	1.0 (0.2)	2.5 (0.8) ,	3.2 (1.1)	1.7 (0.4) ,	1.3 (0.3)	3.4 (1.1) ,	2.5 (0.8)
	30	0.8 (0.1) ,	0.8 (0.1)	1.1 (0.2) ,	1.2 (0.2)	1.4 (0.4) ,	1.2 (0.3)	1.6 (0.6) ,	1.3 (0.4)
	45	0.6 (0.1) ,	0.6 (0.1)	0.8 (0.2) ,	0.9 (0.2)	0.8 (0.1) ,	0.8 (0.1)	1.0 (0.2) ,	0.9 (0.1)
	60	0.4 (0.1) ,	0.4 (0.1)	0.7 (0.2) ,	0.8 (0.2)	0.7 (0.1) ,	0.7 (0.1)	0.9 (0.2) ,	0.8 (0.2)

Unyielded: normalized strain < 1 (unnormalized strain < 0.0017)

Yielded without signficniant strain hardening: 1 ≤ normalized strain < 10 (0.0017 ≤ unnormalized strain < 0.017)

Yielded and significantly strain hardened: 10 ≤ normalized strain (0.017 ≤ unnormalized strain)

Table C1.4: Occurrences of Limit States at Expansion Piers (Pier 1) of 3S Bridge Variants

Limit state	No. of analyses with occurrence [1]	Skew angle [2] (°)					Foundation soil [2]		Column height [2] (m)		Ground motion incident angle [2] (°)			
		0	15	30	45	60	Hard	Soft	4.57	12.19	0	45	90	135
Rupture of retainer anchor (RRA@P1)	0 (0%)	0	0	0	0	0	0	0	0	0	0	0	0	0
Sliding of elastomeric bearing (SEB@P1)	0 (0%)	0	0	0	0	0	0	0	0	0	0	0	0	0
Unseating of elastomeric bearing (UEB@P1)	0 (0%)	0	0	0	0	0	0	0	0	0	0	0	0	0
Yielding of vertical reinforcing steel at column end (YRS@P1)	177 (11%)	28 (16%)	33 (19%)	47 (27%)	24 (14%)	45 (25%)	100 (56%)	77 (44%)	4 (2%)	173 (98%)	12 (7%)	33 (19%)	100 (56%)	32 (18%)
Crushing of concrete cover at column end (CCC@P1)	0 (0%)	0	0	0	0	0	0	0	0	0	0	0	0	0
Yielding of pile at pier (YPP@P1)	267 (17%)	79 (30%)	62 (23%)	64 (24%)	41 (15%)	21 (8%)	38 (14%)	229 (86%)	71 (27%)	196 (73%)	6 (2%)	17 (6%)	129 (48%)	115 (43%)

1 The number above the parentheses indicates the number of analyses with occurrences of a limit state.
The percentage inside the parentheses indicates the ratio of the number above the parentheses to all the 1,600 analyses.

2 The number above the parentheses indicates the number of analyses with occurrences of a limit state contributed by a parametric variation.
The percentage inside the parentheses indicates the relative contribution of a parametric variation to the total occurrences of a limit state.

Table C1.5: Normalized peak strain of Vertical Reinforcing Steel at Pier Column Base of 3S Bridges (peak strains are normalized to the yield strain, 0.0021; numbers outside the parentheses are medians, while those inside are median absolute deviations; data of reinforcing steel at column base of expansion and fixed piers are placed on the left and right sides of the commas, respectively; performance levels in the footnote are defined per Kowalsky (2001) and Revell (2013))

Foundation soil condition			Hard				Soft			
Pier column height (m)			4.57		12.19		4.57		12.19	
Longitudinal (0°) ground motions	Bridge skew (°)	0	0.2 (0.0) ,	2.0 (0.2)	0.6 (0.1) ,	0.6 (0.1)	0.4 (0.0) ,	2.4 (0.4)	0.7 (0.2) ,	0.9 (0.2)
		15	0.2 (0.0) ,	2.3 (0.3)	0.6 (0.1) ,	0.7 (0.1)	0.4 (0.1) ,	3.1 (0.7)	0.7 (0.2) ,	0.9 (0.3)
		30	0.3 (0.0) ,	2.8 (0.9)	0.7 (0.1) ,	0.8 (0.1)	0.4 (0.0) ,	4.2 (1.2)	0.7 (0.1) ,	1.0 (0.2)
		45	0.2 (0.0) ,	1.4 (0.2)	0.5 (0.2) ,	0.9 (0.2)	0.2 (0.0) ,	1.1 (0.1)	0.5 (0.1) ,	1.0 (0.2)
		60	0.2 (0.0) ,	0.8 (0.0)	0.6 (0.1) ,	1.1 (0.4)	0.1 (0.0) ,	0.7 (0.1)	0.4 (0.1) ,	0.8 (0.1)
45° ground motions	Bridge skew (°)	0	0.2 (0.0) ,	1.5 (0.2)	0.6 (0.1) ,	0.5 (0.0)	0.2 (0.0) ,	1.4 (0.1)	0.6 (0.1) ,	0.7 (0.0)
		15	0.3 (0.0) ,	1.8 (0.3)	0.6 (0.1) ,	0.6 (0.1)	0.4 (0.0) ,	1.8 (0.3)	0.6 (0.1) ,	0.7 (0.1)
		30	0.5 (0.1) ,	2.4 (0.7)	0.8 (0.1) ,	0.8 (0.1)	0.6 (0.1) ,	3.0 (1.1)	0.9 (0.1) ,	0.9 (0.2)
		45	0.5 (0.1) ,	1.4 (0.2)	0.9 (0.2) ,	1.0 (0.2)	0.5 (0.1) ,	1.2 (0.1)	0.9 (0.2) ,	1.2 (0.4)
		60	0.6 (0.1) ,	1.1 (0.2)	0.9 (0.2) ,	1.3 (0.7)	0.6 (0.1) ,	0.9 (0.1)	0.9 (0.2) ,	1.5 (0.9)
Transverse (90°) ground motions	Bridge skew (°)	0	0.3 (0.1) ,	0.4 (0.0)	1.2 (0.5) ,	0.8 (0.1)	0.2 (0.0) ,	0.2 (0.0)	0.9 (0.2) ,	0.6 (0.2)
		15	0.4 (0.1) ,	0.4 (0.0)	1.2 (0.2) ,	0.9 (0.1)	0.2 (0.0) ,	0.3 (0.0)	0.9 (0.1) ,	0.7 (0.2)
		30	0.6 (0.1) ,	0.7 (0.1)	1.2 (0.2) ,	1.0 (0.2)	0.5 (0.1) ,	0.5 (0.1)	1.0 (0.1) ,	0.8 (0.2)
		45	0.6 (0.1) ,	0.8 (0.1)	0.9 (0.2) ,	0.9 (0.2)	0.6 (0.1) ,	0.6 (0.1)	0.8 (0.1) ,	0.6 (0.2)
		60	0.7 (0.1) ,	0.7 (0.1)	1.1 (0.3) ,	0.9 (0.3)	0.7 (0.1) ,	0.7 (0.1)	1.0 (0.2) ,	0.9 (0.4)
135° ground motions	Bridge skew (°)	0	0.2 (0.0) ,	1.5 (0.1)	0.6 (0.0) ,	0.6 (0.0)	0.2 (0.0) ,	1.5 (0.1)	0.6 (0.1) ,	0.7 (0.0)
		15	0.3 (0.1) ,	1.3 (0.1)	0.7 (0.1) ,	0.7 (0.2)	0.3 (0.0) ,	1.6 (0.2)	0.6 (0.2) ,	0.7 (0.1)
		30	0.4 (0.1) ,	1.2 (0.1)	1.1 (0.2) ,	1.2 (0.2)	0.3 (0.0) ,	1.5 (0.2)	0.9 (0.2) ,	0.9 (0.2)
		45	0.5 (0.1) ,	0.7 (0.1)	0.9 (0.1) ,	1.2 (0.2)	0.3 (0.1) ,	0.8 (0.1)	0.7 (0.2) ,	0.8 (0.1)
		60	0.5 (0.0) ,	0.5 (0.0)	0.7 (0.1) ,	1.3 (0.2)	0.4 (0.1) ,	0.5 (0.1)	0.6 (0.2) ,	0.7 (0.1)

Undamaged (unyielded):	normalized strain < 1 (unnormalized strain < 0.0021)
Lightly damaged (unlikely requiring repair):	1 ≤ normalized strain < 7.1 (0.0021 ≤ unnormalized strain < 0.015)
Moderately damaged (repairable):	7.1 ≤ normalized strain < 28.6 (0.015 ≤ unnormalized strain < 0.06)
Severely damaged (not easily repairable):	28.6 ≤ normalized strain (0.06 ≤ unnormalized strain)

Table C1.6: Normalized Peak Strain of Concrete Cover at Pier Column Base of 3S Bridges (peak strains are normalized to the crushing strain, 0.005; numbers outside the parentheses are medians, while those inside are median absolute deviations; data of concrete cover at column base of expansion and fixed piers are placed on the left and right sides of the commas, respectively; performance levels in the footnote are defined per Kowalsky (2001) and Revell (2013))

Foundation soil condition			Hard		Soft	
Pier column height (m)			4.57	12.19	4.57	12.19
Longitudinal (0°) ground motions	Bridge skew (°)	0	0.1 (0.0) , 0.4 (0.0)	0.2 (0.0) , 0.2 (0.0)	0.1 (0.0) , 0.5 (0.0)	0.2 (0.0) , 0.2 (0.0)
		15	0.1 (0.0) , 0.5 (0.0)	0.2 (0.0) , 0.2 (0.0)	0.2 (0.0) , 0.6 (0.1)	0.2 (0.0) , 0.3 (0.0)
		30	0.1 (0.0) , 0.5 (0.1)	0.2 (0.0) , 0.2 (0.0)	0.2 (0.0) , 0.7 (0.2)	0.2 (0.0) , 0.3 (0.0)
		45	0.1 (0.0) , 0.4 (0.0)	0.2 (0.0) , 0.3 (0.0)	0.1 (0.0) , 0.3 (0.0)	0.2 (0.0) , 0.3 (0.0)
		60	0.1 (0.0) , 0.2 (0.0)	0.2 (0.0) , 0.3 (0.1)	0.1 (0.0) , 0.2 (0.0)	0.1 (0.0) , 0.2 (0.0)
45° ground motions	Bridge skew (°)	0	0.1 (0.0) , 0.3 (0.0)	0.2 (0.0) , 0.2 (0.0)	0.1 (0.0) , 0.3 (0.0)	0.2 (0.0) , 0.2 (0.0)
		15	0.1 (0.0) , 0.4 (0.0)	0.2 (0.0) , 0.2 (0.0)	0.1 (0.0) , 0.4 (0.0)	0.2 (0.0) , 0.2 (0.0)
		30	0.2 (0.0) , 0.5 (0.1)	0.2 (0.0) , 0.2 (0.0)	0.2 (0.0) , 0.6 (0.1)	0.2 (0.0) , 0.2 (0.0)
		45	0.2 (0.0) , 0.3 (0.0)	0.2 (0.0) , 0.2 (0.0)	0.2 (0.0) , 0.3 (0.0)	0.2 (0.0) , 0.3 (0.1)
		60	0.2 (0.0) , 0.3 (0.0)	0.2 (0.0) , 0.3 (0.1)	0.2 (0.0) , 0.3 (0.0)	0.2 (0.0) , 0.3 (0.1)
Transverse (90°) ground motions	Bridge skew (°)	0	0.1 (0.0) , 0.2 (0.0)	0.3 (0.1) , 0.2 (0.0)	0.1 (0.0) , 0.1 (0.0)	0.3 (0.0) , 0.2 (0.0)
		15	0.2 (0.0) , 0.2 (0.0)	0.3 (0.0) , 0.3 (0.0)	0.1 (0.0) , 0.1 (0.0)	0.3 (0.0) , 0.2 (0.0)
		30	0.2 (0.0) , 0.2 (0.0)	0.3 (0.0) , 0.3 (0.0)	0.1 (0.0) , 0.2 (0.0)	0.3 (0.0) , 0.2 (0.0)
		45	0.2 (0.0) , 0.2 (0.0)	0.2 (0.0) , 0.2 (0.0)	0.2 (0.0) , 0.2 (0.0)	0.2 (0.0) , 0.2 (0.0)
		60	0.2 (0.0) , 0.2 (0.0)	0.3 (0.1) , 0.2 (0.1)	0.2 (0.0) , 0.2 (0.0)	0.3 (0.0) , 0.2 (0.1)
135° ground motions	Bridge skew (°)	0	0.1 (0.0) , 0.4 (0.0)	0.2 (0.0) , 0.2 (0.0)	0.1 (0.0) , 0.4 (0.0)	0.2 (0.0) , 0.2 (0.0)
		15	0.1 (0.0) , 0.3 (0.0)	0.2 (0.0) , 0.2 (0.0)	0.1 (0.0) , 0.4 (0.0)	0.2 (0.0) , 0.2 (0.0)
		30	0.1 (0.0) , 0.3 (0.0)	0.3 (0.0) , 0.3 (0.0)	0.1 (0.0) , 0.4 (0.0)	0.2 (0.0) , 0.2 (0.0)
		45	0.1 (0.0) , 0.2 (0.0)	0.3 (0.0) , 0.3 (0.0)	0.1 (0.0) , 0.2 (0.0)	0.2 (0.0) , 0.2 (0.0)
		60	0.2 (0.0) , 0.2 (0.0)	0.2 (0.0) , 0.3 (0.0)	0.1 (0.0) , 0.2 (0.0)	0.2 (0.0) , 0.2 (0.0)

Undamaged (ultimate strength not mobillized):	normalized strain < 0.4 (unnormalized strain < 0.002)
Lightly damaged (ultimate strength mobilized but uncrushed):	0.4 ≤ normalized strain < 1 (0.002 ≤ unnormalized strain < 0.005)
Moderately damaged (crushed but repairable):	1 ≤ normalized strain < 3.6 (0.005 ≤ unnormalized strain < 0.018)
Severely damaged (not easily repairable):	3.6 ≤ normalized strain (0.018 ≤ unnormalized strain)

Table C1.7: Normalized Peak Strains of Steel H Piles at Piers of 3S Bridges (peak strains are normalized to the yield strain, 0.0017; numbers outside the parentheses are medians, while those inside are median absolute deviations; data for piles supporting expansion and fixed piers are placed on the left and right sides of the commas, respectively)

Foundation soil condition			Hard		Soft	
Pier column height (m)			4.57	12.19	4.57	12.19
Longitudinal (0°) ground motions	Bridge skew (°)	0	0.2 (0.0) , 0.4 (0.0)	0.3 (0.0) , 0.3 (0.0)	0.2 (0.0) , 0.6 (0.0)	0.3 (0.0) , 0.4 (0.0)
		15	0.3 (0.0) , 0.6 (0.0)	0.4 (0.0) , 0.4 (0.0)	0.3 (0.0) , 0.9 (0.1)	0.5 (0.0) , 0.6 (0.0)
		30	0.3 (0.0) , 0.8 (0.0)	0.4 (0.1) , 0.5 (0.1)	0.5 (0.1) , 1.4 (0.1)	0.6 (0.0) , 0.8 (0.1)
		45	0.3 (0.0) , 1.0 (0.1)	0.5 (0.1) , 0.7 (0.1)	0.6 (0.0) , 2.1 (0.5)	0.7 (0.1) , 1.4 (0.3)
		60	0.3 (0.0) , 1.0 (0.1)	0.5 (0.1) , 0.9 (0.2)	0.7 (0.1) , 4.4 (1.1)	0.8 (0.2) , 2.9 (1.2)
45° ground motions	Bridge skew (°)	0	0.6 (0.1) , 0.7 (0.0)	0.6 (0.0) , 0.6 (0.0)	0.8 (0.1) , 1.0 (0.1)	1.1 (0.1) , 0.9 (0.0)
		15	0.5 (0.1) , 0.6 (0.1)	0.6 (0.0) , 0.5 (0.0)	0.8 (0.0) , 0.8 (0.0)	0.9 (0.1) , 0.7 (0.1)
		30	0.4 (0.0) , 0.6 (0.0)	0.5 (0.0) , 0.5 (0.0)	0.6 (0.0) , 0.8 (0.0)	0.6 (0.0) , 0.6 (0.1)
		45	0.4 (0.0) , 0.7 (0.0)	0.4 (0.0) , 0.5 (0.0)	0.5 (0.0) , 0.9 (0.0)	0.5 (0.0) , 0.6 (0.1)
		60	0.3 (0.0) , 0.7 (0.0)	0.3 (0.1) , 0.4 (0.0)	0.4 (0.0) , 0.9 (0.0)	0.4 (0.0) , 0.6 (0.1)
Transverse (90°) ground motions	Bridge skew (°)	0	0.8 (0.1) , 0.9 (0.1)	1.1 (0.3) , 0.8 (0.0)	1.2 (0.1) , 1.3 (0.2)	4.0 (2.8) , 1.7 (0.4)
		15	0.8 (0.1) , 0.9 (0.1)	1.1 (0.2) , 0.8 (0.0)	1.2 (0.1) , 1.2 (0.1)	2.9 (1.6) , 1.6 (0.4)
		30	0.7 (0.1) , 0.8 (0.1)	0.8 (0.1) , 0.7 (0.0)	1.0 (0.1) , 1.0 (0.1)	1.6 (0.5) , 1.4 (0.3)
		45	0.5 (0.1) , 0.8 (0.1)	0.6 (0.0) , 0.7 (0.1)	0.8 (0.0) , 0.9 (0.1)	1.0 (0.2) , 1.3 (0.4)
		60	0.4 (0.0) , 0.6 (0.1)	0.4 (0.0) , 0.6 (0.0)	0.5 (0.0) , 0.7 (0.1)	0.6 (0.1) , 0.9 (0.1)
135° ground motions	Bridge skew (°)	0	0.6 (0.1) , 0.7 (0.1)	0.6 (0.0) , 0.6 (0.0)	0.8 (0.1) , 1.0 (0.1)	1.1 (0.1) , 0.9 (0.1)
		15	0.7 (0.1) , 0.9 (0.0)	0.8 (0.1) , 0.7 (0.1)	1.0 (0.1) , 1.6 (0.1)	1.4 (0.5) , 1.3 (0.2)
		30	0.6 (0.1) , 0.9 (0.1)	0.9 (0.1) , 0.8 (0.1)	1.0 (0.1) , 2.3 (0.4)	1.7 (0.7) , 1.6 (0.5)
		45	0.5 (0.0) , 1.0 (0.1)	0.9 (0.1) , 1.0 (0.1)	1.0 (0.1) , 3.1 (1.0)	1.5 (0.6) , 3.7 (2.2)
		60	0.4 (0.0) , 0.9 (0.1)	0.7 (0.1) , 1.0 (0.1)	0.8 (0.1) , 1.8 (0.5)	1.2 (0.4) , 2.8 (1.7)

Unyielded: normalized strain < 1 (unnormalized strain < 0.0017)

Yielded without signficniant strain hardening: 1 ≤ normalized strain < 10 (0.0017 ≤ unnormalized strain < 0.017)

Yielded and significantly strain hardened: 10 ≤ normalized strain (0.017 ≤ unnormalized strain)

Table C1.8: Occurrences of Limit States at Fixed Piers (Pier 2) of 3S Bridge Variants

Limit state	No. of analyses with occurrence [1]	Skew angle [2] (°)					Foundation soil [2]		Column height [2] (m)		Ground motion incident angle [2] (°)			
		0	15	30	45	60	Hard	Soft	4.57	12.19	0	45	90	135
Rupture of steel fixed bearing anchors (RFA@P2)	71 (4%)	0 (0%)	0 (0%)	0 (0%)	16 (23%)	55 (77%)	65 (92%)	6 (8%)	57 (80%)	14 (20%)	40 (56%)	6 (8%)	0 (0%)	25 (35%)
Unseating of steel fixed bearing (USB@P2)	0 (0%)	0	0	0	0	0	0	0	0	0	0	0	0	0
Yielding of vertical reinforcing steel at column end (YRS@P2)	692 (43%)	134 (19%)	138 (20%)	180 (26%)	133 (19%)	107 (15%)	361 (52%)	331 (48%)	462 (67%)	230 (33%)	220 (32%)	245 (35%)	50 (7%)	177 (26%)
Crushing of concrete cover at column end (CCC@P2)	4 (0%)	0 (0%)	0 (0%)	4 (100%)	0 (0%)	0 (0%)	1 (25%)	3 (75%)	4 (100%)	0 (0%)	4 (100%)	0 (0%)	0 (0%)	0 (0%)
Yielding of pile at pier (YPP@P2)	517 (32%)	79 (15%)	86 (17%)	94 (18%)	132 (26%)	126 (24%)	101 (20%)	416 (80%)	289 (56%)	228 (44%)	130 (25%)	21 (4%)	144 (28%)	222 (43%)

1 The number above the parentheses indicates the number of analyses with occurrences of a limit state.
The percentage inside the parentheses indicates the ratio of the number above the parentheses to all the 1,600 analyses.
2 The number above the parentheses indicates the number of analyses with occurrences of a limit state contributed by a parametric variation.
The percentage inside the parentheses indicates the relative contribution of a parametric variation to the total occurrences of a limit state.

C.2 ADDITIONAL ANALYSIS RESULTS FOR 4S BRIDGES

Table C2.1: Limit state occurrences of each 4S bridge variant under 0° and 45° ground motions (each percentage indicates the number of analyses with occurrences of a limit state out of the 20 analyses with the ground motions applied to a bridge variant in an incident direction)

Ground motion direction	Bridge variant	Critical limit states																																
		Abutment 1 (A1)									Pier 1 (P1, expansion pier)						Pier 2 (P2, fixed pier)					Pier 3 (P3, expansion pier)						Abutment 2 (A2)								
		CEJ	MBU	FBP	RRA	SEB	UBA	UBO	YPW	YPB	RRA	SEB	UEB	YRS	CCC	YPP	RFA	USB	YRS	CCC	YPP	RRA	SEB	UEB	YRS	CCC	YPP	CEJ	MBU	FBP	RRA	SEB	UBO	UBA	YPW	YPB
0°	4S00P15H	100%	0	0	0	50%	0	0	100%	100%	0	0	0	50%	5%	0	0	0	100%	90%	0	0	0	0	55%	5%	0	100%	0	0	0	40%	0	0	100%	100%
	4S15P15H	100%	0	0	0	55%	0	0	100%	100%	0	0	0	65%	5%	0	0	0	100%	100%	0	0	0	0	65%	5%	0	100%	0	0	0	40%	0	0	100%	100%
	4S30P15H	100%	0	0	0	20%	0	0	100%	100%	0	0	0	80%	15%	0	0	0	100%	100%	5%	0	0	0	85%	25%	0	100%	0	0	0	35%	0	0	100%	100%
	4S45P15H	100%	0	0	0	5%	0	0	100%	100%	0	0	0	80%	5%	0	45%	0	100%	100%	100%	0	0	0	75%	20%	0	100%	0	0	0	20%	0	0	100%	100%
	4S60P15H	100%	0	0	0	60%	0	0	100%	65%	0	0	0	0	0	0	100%	0	100%	0	100%	0	0	0	0	0	0	100%	0	0	0	50%	0	0	90%	75%
	4S00P40H	100%	25%	0	0	75%	0	0	100%	100%	0	0	0	65%	0	0	0	0	80%	0	0	0	0	0	65%	0	0	100%	20%	0	0	75%	0	0	100%	100%
	4S15P40H	100%	20%	0	0	75%	0	0	100%	100%	0	0	0	75%	0	0	0	0	80%	0	0	0	0	0	75%	0	0	100%	0	0	0	80%	0	0	100%	100%
	4S30P40H	100%	0	0	25%	75%	0	0	100%	100%	0	0	0	75%	0	0	0	0	80%	0	0	0	0	0	80%	0	0	100%	0	0	10%	80%	0	0	100%	100%
	4S45P40H	100%	0	0	65%	55%	0	0	100%	80%	0	0	0	80%	0	0	0	0	80%	0	55%	0	0	0	75%	0	5%	100%	0	0	70%	70%	0	0	100%	80%
	4S60P40H	100%	0	0	70%	75%	0	0	85%	80%	0	0	0	80%	0	0	65%	0	95%	0	75%	0	0	0	75%	0	0	100%	0	0	70%	65%	0	0	85%	75%
	4S00P15S	100%	0	0	0	50%	0	0	100%	100%	0	0	0	75%	5%	0	0	0	100%	100%	0	0	0	0	75%	5%	0	100%	0	0	0	55%	0	0	100%	100%
	4S15P15S	100%	0	0	0	50%	0	0	100%	100%	0	0	0	75%	0	0	0	0	100%	100%	0	0	0	0	75%	0	0	100%	0	0	0	50%	0	0	100%	100%
	4S30P15S	100%	0	0	0	45%	0	0	100%	100%	0	0	0	80%	10%	0	0	0	100%	100%	100%	0	0	0	85%	5%	5%	100%	0	0	0	45%	0	0	100%	100%
	4S45P15S	100%	0	0	0	35%	0	0	100%	100%	0	0	0	10%	0	45%	0	0	100%	80%	100%	0	0	0	20%	0	40%	100%	0	0	0	40%	0	0	100%	100%
	4S60P15S	100%	0	0	0	45%	0	0	90%	90%	0	0	0	0	0	70%	80%	0	100%	0	100%	0	0	0	0	0	75%	100%	0	0	0	30%	0	0	80%	90%
	4S00P40S	100%	60%	5%	0	75%	0	0	100%	100%	0	0	0	75%	0	0	0	0	80%	5%	0	0	0	0	80%	0	0	100%	70%	5%	0	80%	0	0	100%	100%
	4S15P40S	100%	35%	0	0	80%	0	0	100%	100%	0	0	0	80%	15%	0	0	0	80%	20%	0	0	0	0	80%	15%	0	100%	55%	0	0	80%	0	0	100%	100%
	4S30P40S	100%	25%	0	20%	75%	0	0	100%	100%	0	0	0	75%	15%	25%	0	0	80%	20%	65%	0	0	0	75%	20%	15%	100%	35%	0	20%	80%	0	0	100%	100%
	4S45P40S	100%	0	0	50%	70%	0	0	100%	100%	0	0	0	75%	0	50%	0	0	80%	10%	90%	0	0	0	70%	0	60%	100%	0	0	30%	75%	0	0	100%	100%
	4S60P40S	100%	0	0	55%	80%	0	0	80%	85%	0	0	0	75%	0	60%	0	0	80%	0	100%	0	0	0	65%	0	60%	100%	0	0	25%	65%	0	0	80%	85%
45°	4S00P15H	100%	0	0	0	5%	0	0	100%	100%	0	0	0	5%	0	5%	0	0	100%	75%	50%	0	0	0	5%	0	0	100%	0	0	0	5%	0	0	100%	100%
	4S15P15H	100%	0	0	0	5%	0	0	100%	100%	0	0	0	70%	0	0	0	0	100%	90%	40%	0	0	0	65%	0	0	100%	0	0	0	5%	0	0	100%	100%
	4S30P15H	100%	0	0	0	5%	0	0	100%	100%	0	0	0	90%	15%	0	0	0	100%	100%	50%	0	0	0	90%	5%	0	100%	0	0	0	10%	0	0	100%	100%
	4S45P15H	100%	0	0	0	5%	0	0	100%	95%	0	0	0	80%	5%	0	0	0	100%	95%	100%	0	0	0	85%	10%	0	100%	0	0	0	5%	0	0	100%	95%
	4S60P15H	100%	0	0	0	30%	0	0	95%	75%	0	0	0	80%	0	0	100%	0	100%	65%	100%	0	0	0	65%	0	0	100%	0	0	0	0	0	0	85%	65%
	4S00P40H	100%	0	0	5%	45%	0	0	100%	100%	0	0	0	70%	0	40%	0	0	80%	5%	55%	0	0	0	70%	0	25%	100%	0	0	0	50%	0	0	100%	95%
	4S15P40H	100%	0	0	0	75%	0	0	100%	100%	0	0	0	75%	0	5%	0	0	80%	0	5%	0	0	0	75%	0	5%	100%	0	0	5%	75%	0	0	100%	100%
	4S30P40H	100%	0	0	25%	75%	0	0	100%	100%	0	0	0	80%	0	0	0	0	80%	0	0	0	0	0	80%	0	0	100%	0	0	0	75%	0	0	100%	100%
	4S45P40H	100%	0	0	60%	75%	0	0	100%	90%	0	0	0	80%	0	0	0	0	80%	0	0	0	0	0	80%	0	0	100%	0	0	35%	60%	0	0	100%	90%
	4S60P40H	100%	0	0	75%	75%	0	0	100%	80%	0	0	0	80%	5%	0	0	0	85%	5%	0	0	0	0	80%	20%	0	100%	0	0	75%	70%	0	0	100%	80%
	4S00P15S	100%	0	0	0	5%	0	0	100%	100%	0	0	0	15%	0	80%	0	0	100%	100%	100%	0	0	0	20%	0	80%	100%	0	0	0	5%	0	0	100%	100%
	4S15P15S	100%	0	0	0	10%	0	0	100%	100%	0	0	0	55%	0	55%	0	0	100%	100%	100%	0	0	0	45%	0	70%	100%	0	0	0	5%	0	0	100%	100%
	4S30P15S	100%	0	0	0	10%	0	0	100%	100%	0	0	0	80%	0	40%	0	0	100%	100%	100%	0	0	0	80%	0	70%	100%	0	0	0	15%	0	0	100%	100%
	4S45P15S	100%	0	0	0	10%	0	0	100%	100%	0	0	0	70%	0	45%	0	0	100%	90%	100%	0	0	0	65%	0	55%	100%	0	0	0	5%	0	0	100%	100%
	4S60P15S	100%	0	0	0	0	0	0	65%	80%	0	0	0	65%	0	10%	15%	0	100%	45%	100%	0	0	0	35%	0	5%	100%	0	0	0	0	0	0	70%	80%
	4S00P40S	100%	0	0	0	75%	0	0	95%	90%	0	0	0	55%	0	80%	0	0	80%	0	100%	0	0	0	40%	0	80%	100%	0	0	0	75%	0	0	95%	95%
	4S15P40S	100%	30%	0	0	75%	0	0	100%	100%	0	0	0	75%	0	75%	0	0	80%	0	95%	0	0	0	75%	0	75%	100%	35%	0	0	75%	0	0	100%	100%
	4S30P40S	100%	25%	0	20%	80%	0	0	100%	100%	0	0	0	75%	10%	20%	0	0	80%	20%	75%	0	0	0	75%	20%	15%	100%	35%	0	20%	80%	0	0	100%	100%
	4S45P40S	100%	15%	0	55%	80%	0	0	100%	100%	0	0	0	80%	10%	0	0	0	80%	25%	5%	0	0	0	80%	15%	0	100%	20%	0	20%	80%	0	0	100%	100%
	4S60P40S	100%	0	0	75%	75%	0	0	90%	90%	0	0	0	80%	15%	0	0	0	80%	20%	0	0	0	0	80%	15%	0	100%	0	0	50%	65%	0	0	90%	95%

Preferred limit states:	0	20%	40%	60%	80%	100%
Acceptable limit states:	0	20%	40%	60%	80%	100%
Unacceptable limit states:	0	20%	40%	60%	80%	100%

Table C2.1 Continued: Limit state occurrences of each 4S bridge variant under 90° and 135° ground motions (each percentage indicates the number of analyses with occurrences of a limit state out of the 20 analyses with the ground motions applied to a bridge variant in an incident direction)

Ground motion direction	Bridge variant	Critical limit states																																	
		Abutment 1 (A1)									Pier 1 (P1, expansion pier)						Pier 2 (P2, fixed pier)					Pier 3 (P3, expansion pier)						Abutment 2 (A2)								
		CEJ	MBU	FBP	RRA	SEB	UBA	UBO	YPW	YPB	RRA	SEB	UEB	YRS	CCC	YPP	RFA	USB	YRS	CCC	YPP	RRA	SEB	UEB	YRS	CCC	YPP	CEJ	MBU	FBP	RRA	SEB	UBO	UBA	YPW	YPB
90°	4S00P15H	0	0	0	0	0	0	0	0	75%	0	0	0	0	0	45%	0	0	30%	0	90%	0	0	0	0	0	45%	0	0	0	0	0	0	0	0	70%
	4S15P15H	5%	0	0	0	0	0	0	5%	85%	0	0	0	0	0	45%	0	0	70%	0	100%	0	0	0	0	0	40%	5%	0	0	0	0	0	0	5%	75%
	4S30P15H	90%	0	0	0	0	0	0	40%	85%	0	0	0	25%	0	25%	25%	0	100%	0	100%	0	0	0	20%	0	40%	95%	0	0	0	0	0	0	50%	80%
	4S45P15H	100%	0	0	0	0	0	0	80%	40%	0	0	0	65%	0	0	70%	0	100%	5%	100%	0	0	0	65%	0	0	100%	0	0	0	0	0	0	55%	25%
	4S60P15H	100%	0	0	5%	0	0	0	70%	0	0	0	0	100%	0	0	95%	0	100%	0	100%	0	0	0	100%	0	0	100%	0	0	0	0	0	0	25%	0
	4S00P40H	0	0	0	60%	40%	0	0	0	100%	0	0	0	100%	20%	75%	0	0	100%	50%	90%	0	0	0	100%	15%	75%	0	0	0	60%	25%	0	0	0	100%
	4S15P40H	75%	0	0	55%	20%	0	0	65%	100%	0	0	0	95%	10%	75%	0	0	100%	45%	85%	0	0	0	100%	20%	75%	75%	0	0	65%	35%	0	0	65%	100%
	4S30P40H	100%	0	0	70%	40%	0	0	95%	100%	0	0	0	85%	10%	75%	0	0	100%	70%	85%	0	0	0	80%	25%	75%	100%	0	0	65%	40%	0	0	95%	100%
	4S45P40H	100%	0	0	70%	70%	0	0	80%	85%	0	0	0	75%	0	35%	0	0	100%	35%	95%	0	0	0	70%	20%	50%	100%	0	0	65%	40%	0	0	80%	80%
	4S60P40H	100%	0	0	75%	75%	0	0	85%	80%	0	0	0	75%	0	0	30%	0	100%	20%	75%	0	0	0	75%	20%	0	100%	0	0	70%	45%	0	0	85%	80%
	4S00P15S	0	0	0	0	0	0	0	0	70%	0	0	0	0	0	100%	0	0	0	0	100%	0	0	0	0	0	100%	0	0	0	0	0	0	0	0	60%
	4S15P15S	35%	0	0	0	0	0	0	5%	80%	0	0	0	0	0	100%	0	0	55%	5%	100%	0	0	0	0	0	100%	35%	0	0	0	0	0	0	5%	70%
	4S30P15S	75%	0	0	0	0	0	0	15%	80%	0	0	0	0	0	100%	0	0	85%	5%	100%	0	0	0	15%	0	100%	75%	0	0	0	0	0	0	15%	80%
	4S45P15S	80%	0	0	0	0	0	0	5%	80%	0	0	0	35%	0	95%	0	0	95%	5%	100%	0	0	0	20%	0	90%	55%	0	0	0	0	0	0	0	50%
	4S60P15S	100%	0	0	0	0	0	0	0	70%	0	0	0	100%	0	65%	0	0	100%	0	100%	0	0	0	90%	0	45%	100%	0	0	0	0	0	0	0	45%
	4S00P40S	0	0	0	10%	5%	0	0	0	85%	0	0	0	80%	0	100%	0	0	90%	0	100%	0	0	0	80%	0	100%	0	0	0	10%	0	0	0	0	85%
	4S15P40S	70%	0	0	20%	15%	0	0	40%	85%	0	0	0	80%	0	100%	0	0	100%	0	100%	0	0	0	80%	0	100%	70%	0	0	10%	0	0	0	35%	85%
	4S30P40S	100%	0	0	15%	10%	0	0	80%	100%	0	0	0	80%	0	100%	0	0	100%	5%	100%	0	0	0	80%	15%	100%	100%	0	0	30%	25%	0	0	75%	95%
	4S45P40S	100%	0	0	45%	30%	0	0	80%	85%	0	0	0	75%	0	90%	0	0	80%	0	100%	0	0	0	75%	15%	90%	100%	0	0	35%	35%	0	0	80%	80%
	4S60P40S	100%	0	0	65%	60%	0	0	80%	80%	0	0	0	80%	10%	45%	0	0	80%	20%	100%	0	0	0	80%	20%	40%	100%	0	0	50%	45%	0	5%	80%	80%
135°	4S00P15H	100%	0	0	0	5%	0	0	100%	100%	0	0	0	0	0	5%	0	0	100%	80%	50%	0	0	0	5%	0	0	100%	0	0	0	5%	0	0	100%	100%
	4S15P15H	100%	0	0	0	0	0	0	100%	100%	0	0	0	0	0	5%	5%	0	100%	85%	90%	0	0	0	5%	0	5%	100%	0	0	0	0	0	0	100%	100%
	4S30P15H	100%	0	0	0	0	0	0	100%	100%	0	0	0	55%	0	10%	25%	0	100%	85%	100%	0	0	0	55%	0	0	100%	0	0	0	0	0	0	100%	100%
	4S45P15H	100%	0	0	0	0	0	0	90%	70%	0	0	0	60%	0	0	100%	0	100%	20%	100%	0	0	0	30%	0	0	100%	0	0	0	0	0	0	90%	70%
	4S60P15H	100%	0	0	0	10%	0	0	25%	0	0	0	0	35%	0	0	100%	0	70%	0	100%	0	0	0	25%	0	0	100%	0	0	0	0	0	0	50%	25%
	4S00P40H	100%	0	0	0	50%	0	0	100%	95%	0	0	0	70%	0	35%	0	0	85%	5%	55%	0	0	0	70%	0	30%	100%	0	0	0	45%	0	0	100%	100%
	4S15P40H	100%	0	0	25%	20%	0	0	100%	100%	0	0	0	75%	0	60%	0	0	100%	25%	75%	0	0	0	80%	0	60%	100%	0	0	20%	15%	0	0	100%	95%
	4S30P40H	100%	0	0	50%	40%	0	0	95%	100%	0	0	0	85%	5%	75%	0	0	100%	35%	80%	0	0	0	85%	5%	75%	100%	0	0	60%	40%	0	0	100%	100%
	4S45P40H	80%	0	0	60%	70%	0	0	45%	80%	0	0	0	75%	5%	75%	0	0	100%	50%	100%	0	0	0	75%	0	75%	80%	0	0	75%	50%	0	0	45%	75%
	4S60P40H	75%	0	0	75%	75%	0	0	5%	25%	0	0	0	75%	0	25%	85%	0	100%	25%	100%	0	0	0	75%	0	15%	65%	0	0	65%	40%	0	0	0	30%
	4S00P15S	100%	0	0	0	5%	0	0	100%	100%	0	0	0	20%	0	80%	0	0	100%	100%	100%	0	0	0	15%	0	80%	100%	0	0	0	5%	0	0	100%	100%
	4S15P15S	100%	0	0	0	5%	0	0	100%	100%	0	0	0	0	0	80%	0	0	100%	100%	100%	0	0	0	5%	0	80%	100%	0	0	0	5%	0	0	100%	100%
	4S30P15S	100%	0	0	0	5%	0	0	100%	100%	0	0	0	0	0	85%	0	0	100%	85%	100%	0	0	0	5%	0	80%	100%	0	0	0	0	0	0	100%	100%
	4S45P15S	100%	0	0	0	5%	0	0	85%	90%	0	0	0	0	0	80%	0	0	100%	25%	100%	0	0	0	0	0	80%	100%	0	0	0	0	0	0	100%	100%
	4S60P15S	100%	0	0	0	5%	0	0	75%	75%	0	0	0	0	0	80%	0	0	100%	0	100%	0	0	0	0	0	80%	100%	0	0	0	0	0	0	75%	75%
	4S00P40S	100%	0	0	0	75%	0	0	95%	95%	0	0	0	55%	0	80%	0	0	80%	0	100%	0	0	0	60%	0	80%	100%	0	0	0	75%	0	0	95%	90%
	4S15P40S	100%	0	0	0	55%	0	0	100%	100%	0	0	0	45%	0	100%	0	0	85%	0	100%	0	0	0	45%	0	100%	100%	0	0	0	45%	0	0	95%	100%
	4S30P40S	100%	0	0	10%	40%	0	0	100%	100%	0	0	0	75%	0	100%	0	0	100%	0	100%	0	0	0	80%	0	100%	100%	0	0	0	50%	0	0	95%	100%
	4S45P40S	80%	0	0	10%	35%	0	0	75%	90%	0	0	0	30%	0	100%	0	0	85%	0	100%	0	0	0	45%	0	100%	80%	0	0	0	50%	0	0	80%	80%
	4S60P40S	85%	0	0	25%	45%	0	0	80%	85%	0	0	0	35%	0	85%	0	0	85%	0	100%	0	0	0	35%	0	85%	80%	0	0	15%	15%	0	0	75%	85%

Preferred limit states:	0	20%	40%	60%	80%	100%
Acceptable limit states:	0	20%	40%	60%	80%	100%
Unacceptable limit states:	0	20%	40%	60%	80%	100%

Table C2.2: Occurrences of limit states at abutments (A1 and A2) of 4S bridge variants

Limit state	No. of analyses with occurrence [1]	Skew angle [2] (°)					Foundation soil [2]		Column height [2] (m)		Ground motion incident angle [2] (°)			
		0	15	30	45	60	Hard	Soft	4.57	12.19	0	45	90	135
Closure of expansion joint (CEJ@A1)	1450 (91%)	240 (17%)	277 (19%)	313 (22%)	308 (21%)	312 (22%)	725 (50%)	725 (50%)	717 (49%)	733 (51%)	400 (28%)	400 (28%)	266 (18%)	384 (26%)
Mobilization of backfill ultimate capacity (MBU@A1)	47 (3%)	17 (36%)	17 (36%)	10 (21%)	3 (6%)	0 (0%)	9 (19%)	38 (81%)	0 (0%)	47 (100%)	33 (70%)	14 (30%)	0 (0%)	0 (0%)
Failure of backwall-to-pile-cap connection (FBP@A1)	1 (0%)	1 (100%)	0 (0%)	0 (0%)	0 (0%)	0 (0%)	0 (0%)	1 (100%)	0 (0%)	1 (100%)	1 (100%)	0 (0%)	0 (0%)	0 (0%)
Rupture of retainer anchor (RRA@A1)	269 (17%)	15 (6%)	20 (7%)	47 (17%)	83 (31%)	104 (39%)	174 (65%)	95 (35%)	1 (0%)	268 (100%)	57 (21%)	63 (23%)	98 (36%)	51 (19%)
Sliding of elastomeric bearing (SEB@A1)	575 (36%)	112 (19%)	108 (19%)	104 (18%)	109 (19%)	142 (25%)	291 (51%)	284 (49%)	108 (19%)	467 (81%)	230 (40%)	163 (28%)	73 (13%)	109 (19%)
Unseating of bearing at obtuse corner of deck (UBA@A1)	0 (0%)	0	0	0	0	0	0	0	0	0	0	0	0	0
Unseating of bearing at acute corner of deck (UBO@A1)	0 (0%)	0	0	0	0	0	0	0	0	0	0	0	0	0
Yielding of pile supporting wingwall (YPW@A1)	1279 (80%)	238 (19%)	263 (21%)	285 (22%)	268 (21%)	225 (18%)	652 (51%)	627 (49%)	609 (48%)	670 (52%)	391 (31%)	389 (30%)	165 (13%)	334 (26%)
Yielding of pile supporting backwall (YPB@A1)	1414 (88%)	302 (21%)	310 (22%)	313 (22%)	277 (20%)	212 (15%)	677 (48%)	737 (52%)	681 (48%)	733 (52%)	380 (27%)	380 (27%)	313 (22%)	341 (24%)
Closure of expansion joint (CEJ@A2)	1443 (90%)	240 (17%)	277 (19%)	314 (22%)	303 (21%)	309 (21%)	724 (50%)	719 (50%)	713 (49%)	730 (51%)	400 (28%)	400 (28%)	262 (18%)	381 (26%)
Mobilization of backfill ultimate capacity (MBU@A2)	54 (3%)	18 (33%)	18 (33%)	14 (26%)	4 (7%)	0 (0%)	4 (7%)	50 (93%)	0 (0%)	54 (100%)	36 (67%)	18 (33%)	0 (0%)	0 (0%)
Failure of backwall-to-pile-cap connection (FBP@A2)	1 (0%)	1 (100%)	0 (0%)	0 (0%)	0 (0%)	0 (0%)	0 (0%)	1 (100%)	0 (0%)	1 (100%)	1 (100%)	0 (0%)	0 (0%)	0 (0%)
Rupture of retainer anchor (RRA@A2)	225 (14%)	14 (6%)	20 (9%)	41 (18%)	66 (29%)	84 (37%)	162 (72%)	63 (28%)	0 (0%)	225 (100%)	45 (20%)	41 (18%)	92 (41%)	47 (21%)
Sliding of elastomeric bearing (SEB@A2)	529 (33%)	108 (20%)	102 (19%)	115 (22%)	106 (20%)	98 (19%)	258 (49%)	271 (51%)	95 (18%)	434 (82%)	231 (44%)	152 (29%)	58 (11%)	88 (17%)
Unseating of bearing at obtuse corner of deck (UBO@A2)	0 (0%)	0	0	0	0	0	0	0	0	0	0	0	0	0
Unseating of bearing at acute corner of deck (UBA@A2)	1 (0%)	0 (0%)	0 (0%)	0 (0%)	0 (0%)	1 (100%)	0 (0%)	1 (100%)	0 (0%)	1 (100%)	0 (0%)	0 (0%)	1 (100%)	0 (0%)
Yielding of pile supporting wingwall (YPW@A2)	1265 (79%)	238 (19%)	261 (21%)	286 (23%)	266 (21%)	214 (17%)	641 (51%)	624 (49%)	599 (47%)	666 (53%)	387 (31%)	388 (31%)	150 (12%)	340 (27%)
Yielding of pile supporting backwall (YPB@A2)	1393 (87%)	299 (21%)	305 (22%)	311 (22%)	265 (19%)	213 (15%)	672 (48%)	721 (52%)	666 (48%)	727 (52%)	381 (27%)	379 (27%)	288 (21%)	345 (25%)

1 The number above the parentheses indicates the number of analyses with occurrences of a limit state.
The percentage inside the parentheses indicates the ratio of the number above the parentheses to all the 1,600 analyses.
2 The number above the parentheses indicates the number of analyses with occurrences of a limit state contributed by a parametric variation.
The percentage inside the parentheses indicates the relative contribution of a parametric variation to the total occurrences of a limit state.

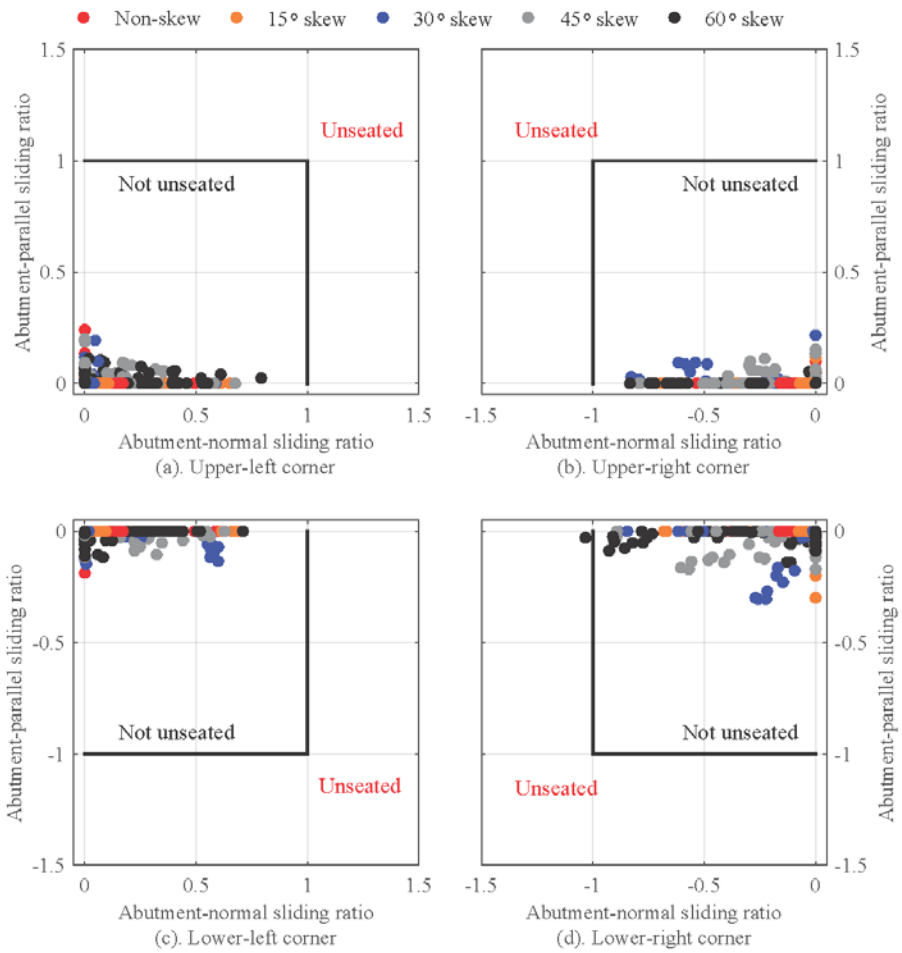

Figure C2.1: Peak sliding ratios of elastomeric bearings at deck corners of 4S bridges.

Table C2.3: Normalized peak strains of steel H piles supporting abutments of 4S bridges (peak strains are normalized to the yield strain of steel piles, 0.0017; numbers outside and inside the parentheses are medians and median absolute deviations, respectively; data for piles supporting backwalls and wingwalls are placed on the left and right sides of the commas, respectively)

Foundation soil condition			Hard				Soft			
Pier column height (m)			4.57		12.19		4.57		12.19	
Longitudinal (0°) ground motions	Bridge skew (°)	0	7.2 (2.2) ,	9.8 (2.5)	16.4 (4.4) ,	20.5 (4.8)	7.3 (2.0) ,	7.3 (2.3)	13.5 (3.3) ,	14.9 (3.7)
		15	12.3 (2.7) ,	13.3 (2.5)	25.7 (4.3) ,	26.6 (4.3)	9.6 (3.0) ,	9.0 (3.1)	17.3 (4.8) ,	17.1 (4.7)
		30	11.3 (3.3) ,	12.0 (3.1)	22.7 (6.6) ,	22.8 (6.2)	10.2 (3.4) ,	9.5 (2.9)	17.5 (8.1) ,	16.4 (7.1)
		45	4.8 (2.1) ,	6.4 (2.4)	6.8 (3.1) ,	8.9 (3.4)	7.8 (3.8) ,	7.9 (3.7)	16.1 (7.2) ,	15.5 (6.5)
		60	1.2 (0.4) ,	1.8 (0.7)	1.3 (0.4) ,	2.3 (1.3)	3.0 (1.6) ,	3.0 (1.7)	6.5 (4.3) ,	7.4 (4.9)
45° ground motions	Bridge skew (°)	0	3.7 (1.2) ,	5.6 (1.2)	8.9 (3.2) ,	11.1 (3.3)	3.3 (0.9) ,	2.5 (0.7)	9.9 (1.7) ,	9.8 (2.0)
		15	6.9 (2.0) ,	8.2 (1.8)	16.7 (4.3) ,	19.2 (3.6)	4.6 (1.3) ,	4.0 (1.2)	12.4 (5.7) ,	12.5 (5.4)
		30	9.1 (3.0) ,	9.7 (2.7)	19.0 (10.1) ,	20.3 (8.6)	5.4 (1.9) ,	4.9 (1.7)	18.4 (6.8) ,	17.3 (6.1)
		45	4.3 (1.7) ,	6.2 (1.7)	12.2 (4.2) ,	15.2 (4.1)	4.1 (1.3) ,	4.1 (1.2)	17.1 (6.2) ,	16.7 (5.2)
		60	1.0 (0.2) ,	1.7 (0.5)	2.4 (0.8) ,	5.9 (1.5)	1.5 (0.5) ,	1.4 (0.4)	9.2 (4.3) ,	9.2 (3.6)
Transverse (90°) ground motions	Bridge skew (°)	0	1.1 (0.1) ,	0.6 (0.0)	2.1 (0.4) ,	1.1 (0.2)	1.1 (0.2) ,	0.7 (0.1)	1.8 (0.8) ,	1.1 (0.4)
		15	1.1 (0.1) ,	0.7 (0.1)	2.0 (0.6) ,	2.1 (0.9)	1.2 (0.2) ,	0.9 (0.2)	2.2 (1.1) ,	1.5 (0.6)
		30	1.1 (0.1) ,	1.0 (0.1)	3.2 (1.3) ,	4.6 (2.3)	1.3 (0.2) ,	1.0 (0.2)	3.6 (2.0) ,	2.3 (1.4)
		45	0.8 (0.1) ,	1.0 (0.3)	2.2 (1.3) ,	4.6 (2.6)	1.0 (0.2) ,	0.9 (0.1)	3.2 (2.3) ,	3.2 (2.4)
		60	0.7 (0.1) ,	0.8 (0.1)	1.7 (0.5) ,	4.4 (1.0)	1.1 (0.2) ,	0.7 (0.2)	4.7 (3.2) ,	5.4 (2.7)
135° ground motions	Bridge skew (°)	0	3.5 (1.1) ,	5.5 (1.1)	8.8 (3.5) ,	11.0 (3.2)	3.3 (1.0) ,	2.5 (0.7)	9.8 (1.8) ,	9.7 (2.1)
		15	4.5 (1.8) ,	5.7 (1.7)	8.2 (3.4) ,	9.0 (3.1)	4.7 (1.7) ,	3.8 (1.3)	11.8 (4.1) ,	10.1 (3.9)
		30	2.8 (1.2) ,	3.9 (1.3)	4.1 (2.5) ,	5.2 (3.4)	5.0 (2.1) ,	4.3 (1.8)	10.0 (6.0) ,	9.0 (5.3)
		45	1.0 (0.2) ,	1.5 (0.3)	1.2 (0.2) ,	1.2 (0.3)	3.3 (1.5) ,	3.2 (1.7)	3.3 (2.4) ,	3.2 (2.3)
		60	0.7 (0.1) ,	0.8 (0.2)	0.9 (0.1) ,	0.8 (0.1)	1.5 (0.5) ,	1.3 (0.5)	1.9 (0.7) ,	1.8 (0.6)

Unyielded: normalized strain < 1 (unnormalized strain < 0.0017)

Yielded without signficniant strain hardening: 1 ≤ normalized strain < 10 (0.0017 ≤ unnormalized strain < 0.017)

Yielded and significantly strain hardened: 10 ≤ normalized strain (0.017 ≤ unnormalized strain)

Table C2.4: Occurrences of limit states at expansion piers (P1 and P3) of 4S bridge variants

Limit state	No. of analyses with occurrence [1]	Skew angle [2] (°)					Foundation soil [2]		Column height [2] (m)		Ground motion incident angle [2] (°)			
		0	15	30	45	60	Hard	Soft	4.57	12.19	0	45	90	135
Rupture of retainer anchor (RRA@P1)	0 (0%)	0	0	0	0	0	0	0	0	0	0	0	0	0
Sliding of elastomeric bearing (SEB@P1)	0 (0%)	0	0	0	0	0	0	0	0	0	0	0	0	0
Unseating of elastomeric bearing (UEB@P1)	0 (0%)	0	0	0	0	0	0	0	0	0	0	0	0	0
Yielding of vertical reinforcing steel at column end (YRS@P1)	918 (57%)	148 (16%)	175 (19%)	209 (23%)	194 (21%)	192 (21%)	504 (55%)	414 (45%)	328 (36%)	590 (64%)	254 (28%)	272 (30%)	231 (25%)	161 (18%)
Crushing of concrete cover at column end (CCC@P1)	39 (2%)	6 (15%)	6 (15%)	16 (41%)	5 (13%)	6 (15%)	21 (54%)	18 (46%)	13 (33%)	26 (67%)	15 (38%)	12 (31%)	10 (26%)	2 (5%)
Yielding of pile at pier (YPP@P1)	627 (39%)	145 (23%)	140 (22%)	131 (21%)	123 (20%)	88 (14%)	143 (23%)	484 (77%)	270 (43%)	357 (57%)	50 (8%)	91 (15%)	254 (41%)	232 (37%)
Rupture of retainer anchor (RRA@P3)	0 (0%)	0	0	0	0	0	0	0	0	0	0	0	0	0
Sliding of elastomeric bearing (SEB@P3)	0 (0%)	0	0	0	0	0	0	0	0	0	0	0	0	0
Unseating of elastomeric bearing (UEB@P3)	0 (0%)	0	0	0	0	0	0	0	0	0	0	0	0	0
Yielding of vertical reinforcing steel at column end (YRS@P3)	898 (56%)	148 (16%)	174 (19%)	214 (24%)	186 (21%)	176 (20%)	269 (30%)	629 (70%)	309 (34%)	589 (66%)	255 (28%)	258 (29%)	226 (25%)	159 (18%)
Crushing of concrete cover at column end (CCC@P3)	68 (4%)	5 (7%)	8 (12%)	24 (35%)	16 (24%)	15 (22%)	39 (57%)	29 (43%)	16 (24%)	52 (76%)	20 (29%)	17 (25%)	30 (44%)	1 (1%)
Yielding of pile at pier (YPP@P3)	626 (39%)	139 (22%)	142 (23%)	135 (22%)	129 (21%)	81 (13%)	139 (22%)	487 (78%)	273 (44%)	353 (56%)	52 (8%)	96 (15%)	253 (40%)	225 (36%)

1 The number above the parentheses indicates the number of analyses with occurrences of a limit state.
The percentage inside the parentheses indicates the ratio of the number above the parentheses to all the 1,600 analyses.

2 The number above the parentheses indicates the number of analyses with occurrences of a limit state contributed by a parametric variation.
The percentage inside the parentheses indicates the relative contribution of a parametric variation to the total occurrences of a limit state.

Table C2.5: Normalized peak strain of vertical reinforcing steel at pier column base of 4S bridges (peak strains are normalized to the yield strain, 0.0021; numbers outside the parentheses are medians, while those inside are median absolute deviations; data of reinforcing steel at column base of expansion and fixed piers are placed on the left and right sides of the commas, respectively; performance levels in the footnote are defined per Kowalsky (2001) and Revell (2013))

Foundation soil condition			Hard				Soft			
Pier column height (m)			4.57		12.19		4.57		12.19	
Longitudinal (0°) ground motions	Bridge skew (°)	0	1.0 (0.4) ,	14.6 (3.1)	1.2 (0.3) ,	1.8 (0.6)	1.2 (0.3) ,	15.2 (3.3)	1.4 (0.8) ,	2.7 (1.5)
		15	1.2 (0.4) ,	16.0 (3.0)	1.3 (0.3) ,	1.9 (0.8)	1.3 (0.4) ,	16.2 (2.8)	1.3 (0.7) ,	2.4 (1.3)
		30	1.7 (0.6) ,	16.7 (2.7)	1.3 (0.3) ,	2.1 (0.8)	1.4 (0.4) ,	16.6 (2.9)	1.6 (0.8) ,	2.9 (1.4)
		45	1.6 (0.6) ,	15.3 (3.6)	1.3 (0.5) ,	2.3 (1.2)	0.7 (0.2) ,	10.1 (3.1)	1.4 (0.8) ,	2.7 (1.6)
		60	0.6 (0.1) ,	3.5 (1.1)	1.3 (0.3) ,	3.6 (0.6)	0.3 (0.1) ,	1.8 (0.2)	1.1 (0.2) ,	2.0 (0.9)
45° ground motions	Bridge skew (°)	0	0.6 (0.1) ,	9.6 (2.3)	1.4 (0.6) ,	2.5 (0.9)	0.7 (0.1) ,	9.7 (1.7)	1.0 (0.1) ,	1.6 (0.4)
		15	1.1 (0.2) ,	12.4 (2.7)	1.5 (0.5) ,	2.5 (0.8)	1.0 (0.1) ,	11.9 (1.4)	1.3 (0.3) ,	2.1 (1.2)
		30	1.9 (0.6) ,	15.1 (2.1)	1.6 (0.5) ,	2.6 (0.6)	1.4 (0.4) ,	12.8 (1.9)	1.5 (1.0) ,	3.1 (1.6)
		45	1.7 (0.5) ,	14.2 (3.0)	1.7 (1.0) ,	3.1 (1.0)	1.1 (0.2) ,	9.8 (1.8)	1.8 (1.2) ,	3.7 (1.8)
		60	1.2 (0.3) ,	9.7 (3.7)	2.7 (1.3) ,	4.1 (1.8)	1.0 (0.2) ,	5.9 (2.4)	2.1 (1.6) ,	4.5 (1.8)
Transverse (90°) ground motions	Bridge skew (°)	0	0.5 (0.1) ,	0.8 (0.2)	2.9 (1.4) ,	5.2 (2.7)	0.4 (0.0) ,	0.5 (0.0)	1.2 (0.2) ,	1.6 (0.3)
		15	0.6 (0.1) ,	1.1 (0.1)	2.9 (1.2) ,	5.3 (1.7)	0.6 (0.1) ,	1.1 (0.4)	1.2 (0.3) ,	1.8 (0.4)
		30	0.9 (0.1) ,	1.7 (0.4)	2.6 (0.8) ,	5.4 (0.9)	0.9 (0.1) ,	3.0 (1.2)	1.4 (0.5) ,	2.2 (1.0)
		45	1.1 (0.1) ,	2.5 (0.5)	1.8 (1.0) ,	4.6 (1.5)	0.9 (0.1) ,	2.1 (0.3)	1.3 (0.8) ,	1.9 (1.0)
		60	1.2 (0.1) ,	2.8 (0.9)	1.6 (1.0) ,	3.1 (1.6)	1.3 (0.2) ,	3.2 (1.2)	1.5 (1.0) ,	2.2 (1.3)
135° ground motions	Bridge skew (°)	0	0.7 (0.1) ,	9.6 (2.4)	1.2 (0.6) ,	2.4 (1.0)	0.7 (0.1) ,	9.9 (1.7)	1.0 (0.1) ,	1.7 (0.4)
		15	0.7 (0.1) ,	9.3 (1.5)	2.0 (0.9) ,	3.9 (1.8)	0.7 (0.1) ,	8.8 (1.0)	1.0 (0.3) ,	1.6 (0.4)
		30	1.0 (0.2) ,	8.3 (0.5)	2.3 (0.7) ,	5.2 (1.3)	0.8 (0.1) ,	7.3 (1.6)	1.1 (0.2) ,	1.6 (0.3)
		45	1.0 (0.1) ,	4.3 (2.2)	1.9 (0.5) ,	5.4 (0.7)	0.7 (0.1) ,	4.4 (1.8)	1.0 (0.1) ,	1.2 (0.1)
		60	0.9 (0.1) ,	1.1 (0.1)	1.3 (0.3) ,	3.4 (0.9)	0.7 (0.1) ,	1.5 (0.2)	0.9 (0.2) ,	1.4 (0.1)

Undamaged (unyielded):	normalized strain < 1 (unnormalized strain < 0.0021)
Lightly damaged (unlikely requiring repair):	1 ≤ normalized strain < 7.1 (0.0021 ≤ unnormalized strain < 0.015)
Moderately damaged (repairable):	7.1 ≤ normalized strain < 28.6 (0.015 ≤ unnormalized strain < 0.06)
Severely damaged (not easily repairable):	28.6 ≤ normalized strain (0.06 ≤ unnormalized strain)

Table C2.6: Normalized peak strain of concrete cover at pier column base of 4S bridges (peak strains are normalized to the crushing strain, 0.005; numbers outside the parentheses are medians, while those inside are median absolute deviations; data of concrete cover at column base of expansion and fixed piers are placed on the left and right sides of the commas, respectively; performance levels in the footnote are defined per Kowalsky (2001) and Revell (2013))

Foundation soil condition			Hard		Soft	
Pier column height (m)			4.57	12.19	4.57	12.19
Longitudinal (0°) ground motions	Bridge skew (°)	0	0.3 (0.1) , 2.5 (0.7)	0.3 (0.0) , 0.4 (0.1)	0.3 (0.1) , 2.6 (0.7)	0.4 (0.1) , 0.5 (0.2)
		15	0.3 (0.1) , 2.9 (0.6)	0.3 (0.0) , 0.4 (0.0)	0.4 (0.1) , 3.0 (0.6)	0.4 (0.1) , 0.5 (0.1)
		30	0.4 (0.1) , 3.1 (0.7)	0.4 (0.0) , 0.5 (0.1)	0.4 (0.1) , 3.1 (0.7)	0.4 (0.1) , 0.5 (0.3)
		45	0.4 (0.1) , 2.7 (0.8)	0.3 (0.1) , 0.4 (0.1)	0.2 (0.0) , 1.8 (0.6)	0.3 (0.1) , 0.5 (0.2)
		60	0.2 (0.0) , 0.6 (0.2)	0.3 (0.0) , 0.6 (0.1)	0.1 (0.0) , 0.4 (0.0)	0.3 (0.0) , 0.4 (0.1)
45° ground motions	Bridge skew (°)	0	0.2 (0.0) , 1.5 (0.4)	0.4 (0.1) , 0.5 (0.2)	0.2 (0.0) , 1.5 (0.3)	0.3 (0.0) , 0.4 (0.1)
		15	0.3 (0.0) , 2.1 (0.6)	0.3 (0.1) , 0.5 (0.1)	0.3 (0.0) , 2.0 (0.3)	0.3 (0.1) , 0.4 (0.2)
		30	0.4 (0.1) , 2.7 (0.4)	0.3 (0.0) , 0.4 (0.1)	0.4 (0.0) , 2.4 (0.4)	0.4 (0.1) , 0.5 (0.2)
		45	0.4 (0.1) , 2.5 (0.6)	0.4 (0.1) , 0.5 (0.1)	0.3 (0.0) , 1.6 (0.2)	0.4 (0.2) , 0.6 (0.2)
		60	0.3 (0.1) , 1.8 (0.6)	0.5 (0.2) , 0.7 (0.2)	0.3 (0.0) , 0.9 (0.4)	0.4 (0.3) , 0.7 (0.2)
Transverse (90°) ground motions	Bridge skew (°)	0	0.2 (0.0) , 0.3 (0.0)	0.6 (0.2) , 1.0 (0.5)	0.2 (0.0) , 0.2 (0.0)	0.3 (0.0) , 0.4 (0.0)
		15	0.2 (0.0) , 0.3 (0.0)	0.6 (0.2) , 0.9 (0.4)	0.2 (0.0) , 0.3 (0.0)	0.4 (0.0) , 0.4 (0.1)
		30	0.2 (0.0) , 0.4 (0.0)	0.6 (0.2) , 1.1 (0.2)	0.2 (0.0) , 0.5 (0.2)	0.4 (0.1) , 0.5 (0.1)
		45	0.3 (0.0) , 0.5 (0.1)	0.4 (0.1) , 0.9 (0.3)	0.2 (0.0) , 0.4 (0.0)	0.3 (0.1) , 0.4 (0.1)
		60	0.3 (0.0) , 0.5 (0.1)	0.3 (0.1) , 0.6 (0.2)	0.3 (0.0) , 0.5 (0.1)	0.3 (0.2) , 0.4 (0.1)
135° ground motions	Bridge skew (°)	0	0.2 (0.0) , 1.8 (0.4)	0.3 (0.1) , 0.4 (0.1)	0.3 (0.0) , 1.8 (0.4)	0.3 (0.0) , 0.4 (0.0)
		15	0.2 (0.0) , 1.7 (0.2)	0.5 (0.1) , 0.7 (0.3)	0.2 (0.0) , 1.7 (0.2)	0.3 (0.0) , 0.4 (0.0)
		30	0.3 (0.0) , 1.6 (0.1)	0.5 (0.1) , 0.9 (0.3)	0.2 (0.0) , 1.3 (0.3)	0.3 (0.0) , 0.4 (0.0)
		45	0.3 (0.0) , 0.7 (0.3)	0.4 (0.1) , 1.0 (0.2)	0.2 (0.0) , 0.8 (0.3)	0.3 (0.0) , 0.3 (0.0)
		60	0.2 (0.0) , 0.3 (0.0)	0.3 (0.0) , 0.6 (0.1)	0.2 (0.0) , 0.4 (0.0)	0.3 (0.0) , 0.4 (0.0)

Undamaged (ultimate strength not mobillized):	normalized strain < 0.4 (unnormalized strain < 0.002)
Lightly damaged (ultimate strength mobilized but uncrushed):	0.4 ≤ normalized strain < 1 (0.002 ≤ unnormalized strain < 0.005)
Moderately damaged (crushed but repairable):	1 ≤ normalized strain < 3.6 (0.005 ≤ unnormalized strain < 0.018)
Severely damaged (not easily repairable):	3.6 ≤ normalized strain (0.018 ≤ unnormalized strain)

Table C2.7: Normalized peak strains of steel H piles at piers of 4S bridges (peak strains are normalized to the yield strain, 0.0017; numbers outside the parentheses are medians, while those inside are median absolute deviations; data for piles supporting expansion and fixed piers are placed on the left and right sides of the commas, respectively)

Foundation soil condition			Hard		Soft	
Pier column height (m)			4.57	12.19	4.57	12.19
Longitudinal (0°) ground motions	Bridge skew (°)	0	0.3 (0.0) , 0.4 (0.0)	0.4 (0.0) , 0.4 (0.0)	0.4 (0.0) , 0.5 (0.0)	0.4 (0.0) , 0.4 (0.0)
		15	0.4 (0.0) , 0.6 (0.0)	0.5 (0.0) , 0.5 (0.0)	0.6 (0.1) , 0.8 (0.0)	0.7 (0.1) , 0.7 (0.0)
		30	0.5 (0.0) , 0.9 (0.0)	0.7 (0.1) , 0.8 (0.1)	0.7 (0.1) , 1.5 (0.1)	0.8 (0.1) , 1.1 (0.1)
		45	0.6 (0.0) , 1.4 (0.1)	0.7 (0.1) , 1.0 (0.1)	0.9 (0.2) , 6.1 (1.4)	1.0 (0.2) , 2.2 (0.7)
		60	0.6 (0.1) , 1.5 (0.1)	0.7 (0.1) , 1.2 (0.1)	1.3 (0.4) , 10.8 (3.2)	1.1 (0.2) , 4.6 (2.5)
45° ground motions	Bridge skew (°)	0	0.7 (0.1) , 1.0 (0.1)	0.9 (0.1) , 1.0 (0.1)	1.1 (0.1) , 1.7 (0.2)	1.4 (0.3) , 2.3 (0.6)
		15	0.7 (0.1) , 0.9 (0.1)	0.8 (0.1) , 0.9 (0.1)	1.0 (0.1) , 1.4 (0.2)	1.1 (0.1) , 1.4 (0.1)
		30	0.7 (0.1) , 1.0 (0.1)	0.6 (0.0) , 0.7 (0.1)	1.0 (0.1) , 1.5 (0.2)	0.8 (0.1) , 1.1 (0.0)
		45	0.6 (0.0) , 1.2 (0.1)	0.5 (0.0) , 0.6 (0.0)	1.0 (0.2) , 3.1 (0.5)	0.6 (0.1) , 0.7 (0.0)
		60	0.5 (0.0) , 1.5 (0.1)	0.5 (0.0) , 0.6 (0.0)	0.8 (0.1) , 5.0 (1.8)	0.6 (0.1) , 0.7 (0.1)
Transverse (90°) ground motions	Bridge skew (°)	0	1.0 (0.1) , 1.3 (0.3)	1.2 (0.1) , 1.2 (0.1)	3.3 (1.4) , 6.7 (2.4)	4.3 (2.4) , 6.9 (3.9)
		15	0.9 (0.1) , 1.4 (0.3)	1.2 (0.1) , 1.2 (0.0)	3.1 (1.3) , 5.8 (1.5)	3.8 (2.0) , 6.8 (3.4)
		30	0.9 (0.1) , 1.9 (0.5)	1.1 (0.1) , 1.2 (0.0)	3.0 (1.2) , 4.5 (1.9)	3.0 (1.6) , 5.6 (2.7)
		45	0.8 (0.1) , 2.2 (0.5)	1.0 (0.1) , 1.3 (0.1)	1.6 (0.3) , 2.4 (0.6)	1.6 (0.5) , 3.7 (1.4)
		60	0.6 (0.0) , 1.5 (0.2)	0.7 (0.1) , 1.1 (0.1)	1.1 (0.2) , 1.6 (0.2)	0.9 (0.1) , 2.5 (0.4)
135° ground motions	Bridge skew (°)	0	0.8 (0.1) , 1.0 (0.1)	0.9 (0.2) , 1.0 (0.1)	1.1 (0.1) , 1.7 (0.2)	1.4 (0.3) , 2.3 (0.6)
		15	0.8 (0.1) , 1.2 (0.1)	1.0 (0.1) , 1.1 (0.1)	1.4 (0.1) , 3.5 (0.8)	1.9 (0.8) , 3.5 (1.9)
		30	0.9 (0.1) , 1.9 (0.5)	1.1 (0.1) , 1.2 (0.1)	2.0 (0.6) , 7.7 (1.7)	2.9 (1.6) , 7.3 (2.4)
		45	0.8 (0.0) , 3.0 (0.7)	1.1 (0.1) , 1.5 (0.1)	1.9 (0.4) , 8.4 (2.7)	2.9 (1.3) , 11.4 (3.1)
		60	0.6 (0.0) , 2.0 (0.3)	0.9 (0.1) , 1.3 (0.1)	1.1 (0.2) , 8.8 (1.9)	1.8 (0.7) , 11.0 (2.0)

Unyielded: normalized strain < 1 (unnormalized strain < 0.0017)

Yielded without signficniant strain hardening: 1 ≤ normalized strain < 10 (0.0017 ≤ unnormalized strain < 0.017)

Yielded and significantly strain hardened: 10 ≤ normalized strain (0.017 ≤ unnormalized strain)

Table C2.8: Occurrences of limit states at fixed piers (Pier 2) of 4S bridge variants

Limit state	No. of analyses with occurrence [1]	Skew angle [2] (°)					Foundation soil [2]		Column height [2] (m)		Ground motion incident angle [2] (°)			
		0	15	30	45	60	Hard	Soft	4.57	12.19	0	45	90	135
Rupture of fixed bearing anchor (RFA@P2)	188 (12%)	0 (0%)	1 (1%)	10 (5%)	43 (23%)	134 (71%)	169 (90%)	19 (10%)	152 (81%)	36 (19%)	58 (31%)	23 (12%)	44 (23%)	63 (34%)
Unseating of steel fixed bearing (USB@P2)	0 (0%)	0	0	0	0	0	0	0	0	0	0	0	0	0
Yielding of vertical reinforcing steel at column end (YRS@P2)	1439 (90%)	261 (18%)	286 (20%)	301 (21%)	296 (21%)	295 (21%)	735 (51%)	704 (49%)	735 (51%)	704 (49%)	363 (25%)	361 (25%)	337 (23%)	378 (26%)
Crushing of concrete cover at column end (CCC@P2)	549 (34%)	122 (22%)	134 (24%)	145 (26%)	108 (20%)	40 (7%)	292 (53%)	257 (47%)	446 (81%)	103 (19%)	165 (30%)	187 (34%)	53 (10%)	144 (26%)
Yielding of pile at pier (YPP@P2)	1167 (73%)	198 (17%)	198 (17%)	232 (20%)	269 (23%)	270 (23%)	501 (43%)	666 (57%)	655 (56%)	512 (44%)	178 (15%)	235 (20%)	384 (33%)	370 (32%)

1 The number above the parentheses indicates the number of analyses with occurrences of a limit state.
The percentage inside the parentheses indicates the ratio of the number above the parentheses to all the 1,600 analyses.
2 The number above the parentheses indicates the number of analyses with occurrences of a limit state contributed by a parametric variation.
The percentage inside the parentheses indicates the relative contribution of a parametric variation to the total occurrences of a limit state.

C.3 ADDITIONAL ANALYSIS RESULTS FOR 3C BRIDGES

Table C3.1: Limit state occurrences of each 3C bridge variant under 0° and 45° ground motions (each percentage indicates the number of analyses with occurrences of a limit state out of the 20 analyses with the ground motions applied to a bridge variant in an incident direction)

Ground motion direction	Bridge variant	Critical limit states																													
		Abutment 1 (A1)									Pier 1 (P1, expansion pier)						Pier 2 (P2, fixed pier)					Abutment 2 (A2)								
		CEJ	MBU	FBP	RRA	SEB	UBA	UBO	YPW	YPB	RRA	SEB	UEB	YRS	CCC	YPP	RRA	RSD	YRS	CCC	YPP	CEJ	MBU	FBP	RRA	SEB	UBO	UBA	YPW	YPB
0°	3C00P15H	100%	0	0	0	0	0	0	100%	95%	0	0	0	0	0	0	0	0	100%	25%	0	100%	0	0	0	0	0	0	100%	100%
	3C15P15H	100%	0	0	0	0	0	0	100%	100%	0	0	0	0	0	0	0	0	100%	65%	0	100%	0	0	0	0	0	0	100%	100%
	3C30P15H	100%	0	0	0	0	0	0	100%	100%	0	0	0	0	0	0	0	5%	100%	80%	25%	100%	0	0	0	0	0	0	100%	100%
	3C45P15H	100%	0	0	0	0	0	0	100%	100%	0	0	0	0	0	0	0	100%	100%	0	25%	100%	0	0	0	0	0	0	100%	100%
	3C60P15H	100%	0	0	0	0	0	0	100%	80%	0	0	0	0	0	0	0	100%	0	0	10%	100%	0	0	0	0	0	0	100%	75%
	3C00P40H	100%	0	0	0	35%	0	0	100%	100%	0	0	0	40%	0	0	0	0	35%	0	0	100%	10%	5%	0	35%	0	0	100%	100%
	3C15P40H	100%	0	0	0	10%	0	0	100%	100%	0	0	0	35%	0	0	0	0	45%	0	0	100%	5%	0	0	10%	0	0	100%	100%
	3C30P40H	100%	0	0	20%	20%	0	0	100%	100%	0	10%	0	45%	0	0	0	0	65%	0	5%	100%	0	0	65%	20%	0	0	100%	100%
	3C45P40H	100%	0	0	70%	5%	0	0	100%	100%	0	5%	0	20%	0	0	0	5%	70%	0	40%	100%	0	0	80%	35%	0	0	100%	100%
	3C60P40H	100%	0	0	30%	0	0	0	100%	100%	0	0	0	0	0	0	0	95%	85%	0	35%	100%	0	0	65%	5%	0	0	100%	100%
	3C00P15S	100%	0	0	0	5%	0	0	100%	95%	0	5%	0	10%	0	0	0	0	100%	55%	0	100%	5%	0	0	0	0	0	100%	95%
	3C15P15S	100%	0	0	0	5%	0	0	100%	100%	0	15%	0	30%	15%	5%	0	0	100%	75%	70%	100%	0	0	0	5%	0	0	100%	100%
	3C30P15S	100%	0	0	0	5%	0	0	100%	100%	0	5%	0	5%	0	25%	0	5%	100%	80%	100%	100%	0	0	0	0	0	0	100%	100%
	3C45P15S	100%	0	0	0	0	0	0	100%	100%	0	0	0	0	0	70%	0	90%	100%	0	100%	100%	0	0	0	0	0	0	100%	100%
	3C60P15S	100%	0	0	0	0	0	0	80%	85%	0	0	0	0	0	75%	0	100%	5%	0	100%	100%	0	0	0	0	0	0	75%	80%
	3C00P40S	100%	30%	0	0	55%	0	0	100%	100%	0	15%	0	55%	0	0	0	0	65%	0	0	100%	20%	5%	0	55%	0	0	100%	100%
	3C15P40S	100%	35%	5%	0	55%	0	0	100%	100%	0	5%	0	75%	0	0	0	0	80%	0	0	100%	50%	0	0	60%	0	0	100%	100%
	3C30P40S	100%	35%	0	0	55%	0	0	100%	100%	0	40%	0	75%	0	55%	0	0	80%	0	75%	100%	40%	0	20%	60%	0	0	100%	100%
	3C45P40S	100%	0	0	0	25%	0	0	100%	100%	0	10%	0	20%	0	65%	0	0	75%	0	100%	100%	0	0	20%	35%	0	0	100%	100%
	3C60P40S	100%	0	0	0	5%	0	0	100%	100%	0	0	0	0	0	70%	0	40%	60%	0	100%	100%	0	0	0	0	0	0	100%	100%
45°	3C00P15H	100%	0	0	0	0	0	0	100%	100%	0	0	0	0	0	0	0	0	100%	0	15%	100%	0	0	0	0	0	0	100%	95%
	3C15P15H	100%	0	0	0	0	0	0	100%	100%	0	0	0	0	0	0	0	0	100%	5%	10%	100%	0	0	0	0	0	0	100%	100%
	3C30P15H	100%	0	0	0	0	0	0	100%	100%	0	0	0	0	0	0	0	0	100%	65%	5%	100%	0	0	0	0	0	0	100%	100%
	3C45P15H	100%	0	0	0	0	0	0	100%	90%	0	0	0	5%	0	0	0	30%	100%	5%	5%	100%	0	0	5%	0	0	0	100%	100%
	3C60P15H	100%	0	0	0	0	0	0	100%	85%	0	0	0	0	0	0	0	100%	75%	0	0	100%	0	0	15%	0	0	0	100%	100%
	3C00P40H	100%	0	0	5%	0	0	0	100%	100%	0	0	0	5%	0	0	0	0	5%	0	0	100%	0	0	0	0	0	0	100%	100%
	3C15P40H	100%	0	0	5%	5%	0	0	100%	100%	0	0	0	15%	0	0	0	0	10%	0	0	100%	0	0	0	5%	0	0	100%	100%
	3C30P40H	100%	0	0	30%	5%	0	0	100%	100%	0	0	0	30%	0	0	0	0	35%	0	0	100%	0	0	45%	5%	0	0	100%	100%
	3C45P40H	100%	0	0	75%	35%	0	0	100%	100%	0	5%	0	40%	0	0	0	0	60%	0	0	100%	0	0	95%	35%	0	0	100%	100%
	3C60P40H	100%	10%	10%	80%	40%	0	0	100%	100%	0	0	0	75%	0	0	0	0	80%	10%	0	100%	0	0	100%	40%	0	0	100%	100%
	3C00P15S	100%	0	0	0	0	0	0	75%	90%	0	0	0	0	0	60%	0	0	100%	0	100%	100%	0	0	0	0	0	0	85%	95%
	3C15P15S	100%	0	0	0	0	0	0	95%	95%	0	0	0	0	0	60%	0	0	100%	45%	75%	100%	0	0	0	0	0	0	95%	95%
	3C30P15S	100%	0	0	0	0	0	0	100%	100%	0	0	0	35%	5%	20%	0	0	100%	75%	75%	100%	0	0	0	0	0	0	100%	100%
	3C45P15S	100%	0	0	0	0	0	0	80%	85%	0	0	0	5%	0	0	0	0	100%	10%	95%	100%	0	0	0	0	0	0	90%	90%
	3C60P15S	100%	0	0	0	0	0	0	80%	80%	0	0	0	10%	0	0	0	55%	85%	0	90%	100%	0	0	0	0	0	0	80%	80%
	3C00P40S	100%	0	0	5%	15%	0	0	95%	100%	0	0	0	30%	0	75%	0	0	20%	0	75%	100%	0	0	0	15%	0	0	95%	95%
	3C15P40S	100%	10%	0	25%	25%	0	0	100%	100%	0	0	0	35%	0	70%	0	0	30%	0	55%	100%	10%	0	0	20%	0	0	95%	100%
	3C30P40S	100%	30%	0	70%	50%	0	0	100%	100%	0	0	0	65%	0	10%	0	0	60%	0	5%	100%	20%	0	35%	35%	0	0	100%	100%
	3C45P40S	100%	30%	0	75%	50%	0	0	100%	100%	0	0	0	65%	0	0	0	0	70%	0	0	100%	25%	0	80%	35%	0	0	100%	100%
	3C60P40S	100%	15%	10%	80%	40%	0	0	100%	100%	0	5%	0	75%	5%	0	0	0	85%	20%	5%	100%	10%	5%	100%	35%	0	10%	100%	100%

Preferred limit states:	0	20%	40%	60%	80%	100%
Acceptable limit states:	0	20%	40%	60%	80%	100%
Unacceptable limit states:	0	20%	40%	60%	80%	100%

Table C3.1 Continued: Limit state occurrences of each 3C bridge variant under 90° and 135° ground motions (each percentage indicates the number of analyses with occurrences of a limit state out of the 20 analyses with the ground motions applied to a bridge variant in an incident direction)

Ground motion direction	Bridge variant	Critical limit states																												
		Abutment 1 (A1)									Pier 1 (P1, expansion pier)						Pier 2 (P2, fixed pier)					Abutment 2 (A2)								
		CEJ	MBU	FBP	RRA	SEB	UBA	UBO	YPW	YPB	RRA	SEB	UEB	YRS	CCC	YPP	RRA	RSD	YRS	CCC	YPP	CEJ	MBU	FBP	RRA	SEB	UBO	UBA	YPW	YPB
90°	3C00P15H	0	0	0	0	0	0	0	0	60%	0	0	0	0	0	45%	0	0	0	0	60%	0	0	0	0	0	0	0	0	10%
	3C15P15H	50%	0	0	0	0	0	0	0	80%	0	0	0	0	0	70%	0	0	0	0	90%	5%	0	0	0	0	0	0	0	20%
	3C30P15H	100%	0	0	5%	0	0	0	65%	95%	0	0	0	5%	0	10%	0	10%	75%	0	75%	100%	0	0	0	0	0	0	0	35%
	3C45P15H	100%	0	0	20%	0	0	0	100%	55%	0	0	0	15%	0	0	0	35%	50%	0	70%	100%	0	0	5%	0	0	0	35%	15%
	3C60P15H	100%	0	0	30%	0	0	0	75%	50%	0	0	0	35%	0	0	0	65%	75%	0	35%	100%	0	0	5%	0	0	0	25%	10%
	3C00P40H	0	0	0	95%	80%	0	0	0	100%	0	0	0	95%	0	95%	0	0	75%	0	40%	0	0	0	45%	10%	0	0	0	100%
	3C15P40H	95%	0	0	100%	75%	0	0	75%	100%	0	0	0	95%	0	95%	0	0	70%	0	55%	100%	0	0	55%	5%	0	0	65%	95%
	3C30P40H	100%	0	0	100%	70%	0	0	95%	100%	0	0	0	100%	10%	75%	0	0	80%	0	40%	100%	0	0	70%	10%	0	0	95%	100%
	3C45P40H	100%	0	0	90%	55%	0	0	100%	100%	0	0	0	75%	0	50%	5%	40%	75%	0	55%	100%	0	0	80%	25%	0	0	100%	85%
	3C60P40H	100%	5%	10%	100%	55%	0	0	100%	95%	0	0	0	75%	0	0	0	30%	70%	0	5%	100%	5%	5%	90%	25%	0	0	100%	85%
	3C00P15S	0	0	0	5%	5%	0	0	0	80%	0	0	0	0	0	100%	0	0	0	0	100%	0	0	0	0	0	0	0	0	15%
	3C15P15S	40%	0	0	5%	5%	0	0	5%	80%	0	0	0	0	0	100%	0	0	0	0	100%	35%	0	0	0	0	0	0	0	25%
	3C30P15S	95%	0	0	5%	0	0	0	5%	80%	0	0	0	0	0	100%	0	0	55%	0	100%	65%	0	0	0	0	0	0	0	40%
	3C45P15S	100%	0	0	5%	0	0	0	0	75%	0	0	0	0	0	85%	0	0	50%	0	95%	95%	0	0	0	0	0	0	0	10%
	3C60P15S	100%	0	0	25%	0	0	0	0	70%	0	0	0	30%	0	15%	0	0	90%	0	55%	100%	0	0	0	0	0	0	0	10%
	3C00P40S	15%	0	0	75%	70%	0	0	0	100%	0	0	0	60%	0	100%	0	0	20%	0	100%	0	0	0	15%	0	0	0	0	85%
	3C15P40S	90%	0	0	80%	70%	0	0	35%	100%	0	0	0	70%	0	100%	0	0	50%	0	100%	80%	0	0	25%	10%	0	0	5%	85%
	3C30P40S	100%	0	0	80%	75%	0	0	75%	100%	0	0	0	75%	0	100%	0	0	65%	0	100%	100%	0	0	65%	25%	0	0	60%	90%
	3C45P40S	100%	0	0	90%	65%	0	0	90%	100%	0	0	0	65%	0	90%	0	0	45%	0	100%	100%	0	0	85%	20%	0	0	80%	100%
	3C60P40S	100%	0	0	100%	65%	0	0	100%	100%	0	0	0	75%	0	35%	0	0	65%	15%	75%	100%	0	0	95%	25%	0	0	95%	100%
135°	3C00P15H	100%	0	0	0	0	0	0	100%	100%	0	0	0	0	0	0	0	0	100%	0	15%	100%	0	0	0	0	0	0	100%	85%
	3C15P15H	100%	0	0	0	0	0	0	100%	100%	0	0	0	0	0	20%	0	5%	100%	0	100%	100%	0	0	0	0	0	0	100%	100%
	3C30P15H	100%	0	0	0	0	0	0	85%	75%	0	0	0	0	0	5%	0	70%	100%	0	100%	100%	0	0	0	0	0	0	100%	100%
	3C45P15H	100%	0	0	0	0	0	0	100%	60%	0	0	0	0	0	5%	0	100%	0	0	100%	100%	0	0	0	0	0	0	100%	55%
	3C60P15H	100%	0	0	10%	0	0	0	40%	10%	0	0	0	5%	0	0	0	100%	0	0	45%	100%	0	0	0	0	0	0	15%	10%
	3C00P40H	100%	0	0	0	0	0	0	100%	100%	0	0	0	5%	0	0	0	0	5%	0	0	100%	0	0	0	0	0	0	100%	100%
	3C15P40H	100%	0	0	45%	0	0	0	100%	100%	0	0	0	50%	0	40%	0	0	55%	0	25%	100%	0	0	10%	5%	0	0	100%	100%
	3C30P40H	100%	0	0	100%	40%	0	0	100%	100%	0	0	0	90%	0	55%	0	0	80%	5%	75%	100%	0	0	75%	10%	0	0	100%	100%
	3C45P40H	100%	0	0	95%	30%	0	0	60%	90%	0	0	0	75%	0	70%	10%	75%	85%	0	80%	100%	0	0	65%	5%	0	0	75%	55%
	3C60P40H	100%	0	0	100%	20%	0	0	60%	90%	0	5%	0	60%	0	25%	5%	100%	100%	0	35%	100%	0	0	55%	0	0	0	5%	15%
	3C00P15S	100%	0	0	0	0	0	0	90%	95%	0	0	0	0	0	70%	0	0	100%	0	100%	100%	0	0	0	0	0	0	75%	80%
	3C15P15S	100%	0	0	0	0	0	0	80%	100%	0	0	0	0	0	90%	0	0	100%	25%	100%	100%	0	0	0	0	0	0	90%	100%
	3C30P15S	100%	0	0	0	0	0	0	75%	80%	0	0	0	0	0	85%	0	10%	100%	20%	100%	100%	0	0	5%	0	0	0	90%	100%
	3C45P15S	100%	0	0	5%	0	0	0	75%	75%	0	0	0	0	0	80%	0	80%	75%	0	100%	100%	0	0	10%	0	0	0	75%	75%
	3C60P15S	100%	0	0	0	0	0	0	45%	50%	0	0	0	0	0	80%	0	95%	0	0	100%	100%	0	0	5%	0	0	0	50%	60%
	3C00P40S	100%	0	0	10%	10%	0	0	95%	100%	0	0	0	25%	0	80%	0	0	25%	0	70%	100%	0	0	0	10%	0	0	95%	100%
	3C15P40S	100%	0	0	45%	0	0	0	95%	100%	0	0	0	20%	0	80%	0	0	30%	0	80%	100%	0	0	5%	0	0	0	95%	100%
	3C30P40S	100%	0	0	70%	15%	0	0	80%	100%	0	0	0	70%	0	85%	0	0	75%	0	80%	100%	0	0	0	0	0	0	80%	85%
	3C45P40S	100%	0	0	80%	15%	0	0	85%	100%	0	0	0	55%	0	85%	0	0	75%	0	100%	100%	0	0	15%	0	0	0	80%	85%
	3C60P40S	100%	0	0	85%	15%	0	0	75%	100%	0	0	0	40%	0	75%	0	5%	35%	0	100%	100%	0	0	40%	0	0	0	50%	80%

Preferred limit states:	0	20%	40%	60%	80%	100%
Acceptable limit states:	0	20%	40%	60%	80%	100%
Unacceptable limit states:	0	20%	40%	60%	80%	100%

Table C3.2: Occurrences of limit states at abutments (A1 and A2) of 3C bridge variants

Limit state	No. of analyses with occurrence [1]	Skew angle [2] (°)					Foundation soil [2]		Column height [2] (m)		Ground motion incident angle [2] (°)			
		0	15	30	45	60	Hard	Soft	4.57	12.19	0	45	90	135
Closure of expansion joint (CEJ@A1)	1497 (94%)	243 (16%)	295 (20%)	319 (21%)	320 (21%)	320 (21%)	749 (50%)	748 (50%)	737 (49%)	760 (51%)	400 (27%)	400 (27%)	297 (20%)	400 (27%)
Mobilization of backfill ultimate capacity (MBU@A1)	41 (3%)	6 (15%)	10 (24%)	13 (32%)	6 (15%)	6 (15%)	3 (7%)	38 (93%)	1 (2%)	40 (98%)	21 (51%)	19 (46%)	1 (2%)	0 (0%)
Failure of backwall-to-pile-cap connection (FBP@A1)	7 (0%)	0 (0%)	1 (14%)	0 (0%)	0 (0%)	6 (86%)	4 (57%)	3 (43%)	0 (0%)	7 (100%)	1 (14%)	4 (57%)	2 (29%)	0 (0%)
Rupture of retainer anchor (RRA@A1)	446 (28%)	39 (9%)	61 (14%)	96 (22%)	122 (27%)	128 (29%)	241 (54%)	205 (46%)	23 (5%)	423 (95%)	25 (6%)	90 (20%)	202 (45%)	129 (29%)
Sliding of elastomeric bearing (SEB@A1)	276 (17%)	55 (20%)	50 (18%)	67 (24%)	56 (20%)	48 (17%)	116 (42%)	160 (58%)	5 (2%)	271 (98%)	56 (20%)	53 (19%)	138 (50%)	29 (11%)
Unseating of bearing at obtuse corner of deck (UBA@A1)	0 (0%)	0	0	0	0	0	0	0	0	0	0	0	0	0
Unseating of bearing at acute corner of deck (UBO@A1)	0 (0%)	0	0	0	0	0	0	0	0	0	0	0	0	0
Yielding of pile supporting wingwall (YPW@A1)	1293 (81%)	231 (18%)	257 (20%)	276 (21%)	278 (22%)	251 (19%)	691 (53%)	602 (47%)	590 (46%)	703 (54%)	396 (31%)	385 (30%)	184 (14%)	328 (25%)
Yielding of pile supporting backwall (YPB@A1)	1465 (92%)	303 (21%)	311 (21%)	306 (21%)	286 (20%)	259 (18%)	722 (49%)	743 (51%)	670 (46%)	795 (54%)	391 (27%)	385 (26%)	344 (23%)	345 (24%)
Closure of expansion joint (CEJ@A2)	1479 (92%)	243 (16%)	284 (19%)	313 (21%)	319 (22%)	320 (22%)	741 (50%)	738 (50%)	720 (49%)	759 (51%)	400 (27%)	400 (27%)	279 (19%)	400 (27%)
Mobilization of backfill ultimate capacity (MBU@A2)	40 (3%)	7 (18%)	13 (33%)	12 (30%)	5 (13%)	3 (8%)	4 (10%)	36 (90%)	1 (3%)	39 (97%)	26 (65%)	13 (33%)	1 (3%)	0 (0%)
Failure of backwall-to-pile-cap connection (FBP@A2)	4 (0%)	2 (50%)	0 (0%)	0 (0%)	0 (0%)	2 (50%)	2 (50%)	2 (50%)	0 (0%)	4 (100%)	2 (50%)	1 (25%)	1 (25%)	0 (0%)
Rupture of retainer anchor (RRA@A2)	329 (21%)	12 (4%)	19 (6%)	76 (23%)	108 (33%)	114 (35%)	205 (62%)	124 (38%)	10 (3%)	319 (97%)	50 (15%)	95 (29%)	127 (39%)	57 (17%)
Sliding of elastomeric bearing (SEB@A2)	146 (9%)	25 (17%)	24 (16%)	33 (23%)	38 (26%)	26 (18%)	57 (39%)	89 (61%)	1 (1%)	145 (99%)	64 (44%)	45 (31%)	31 (21%)	6 (4%)
Unseating of bearing at obtuse corner of deck (UBO@A2)	0 (0%)	0	0	0	0	0	0	0	0	0	0	0	0	0
Unseating of bearing at acute corner of deck (UBA@A2)	2 (0%)	0 (0%)	0 (0%)	0 (0%)	0 (0%)	2 (100%)	0 (0%)	2 (100%)	0 (0%)	2 (100%)	0 (0%)	2 (100%)	0 (0%)	0 (0%)
Yielding of pile supporting wingwall (YPW@A2)	1230 (77%)	230 (19%)	249 (20%)	265 (22%)	267 (22%)	219 (18%)	643 (52%)	587 (48%)	556 (45%)	674 (55%)	395 (32%)	388 (32%)	132 (11%)	315 (26%)
Yielding of pile supporting backwall (YPB@A2)	1320 (83%)	271 (21%)	284 (22%)	290 (22%)	254 (19%)	221 (17%)	649 (49%)	671 (51%)	572 (43%)	748 (57%)	390 (30%)	390 (30%)	223 (17%)	317 (24%)

1 The number above the parentheses indicates the number of analyses with occurrences of a limit state.
The percentage inside the parentheses indicates the ratio of the number above the parentheses to all the 1,600 analyses.
2 The number above the parentheses indicates the number of analyses with occurrences of a limit state contributed by a parametric variation.
The percentage inside the parentheses indicates the relative contribution of a parametric variation to the total occurrences of a limit state.

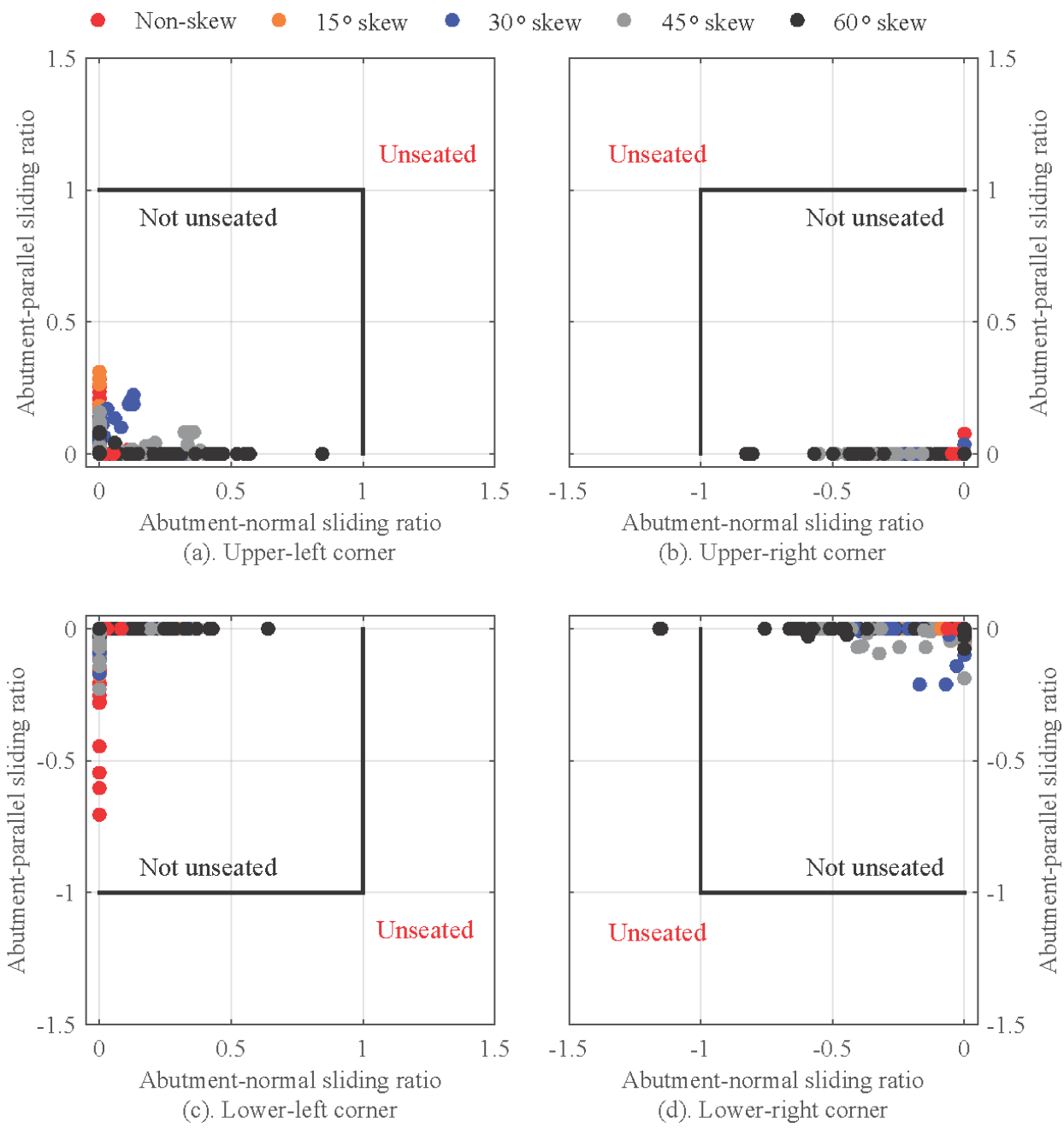

Figure C3.1: Peak sliding ratios of elastomeric bearings at deck corners of 3C bridges.

Table C3.3: Normalized peak strains of steel H piles supporting abutments of 3C bridges (peak strains are normalized to the yield strain of steel piles, 0.0017; numbers outside and inside the parentheses are medians and median absolute deviations, respectively; data for piles supporting backwalls and wingwalls are placed on the left and right sides of the commas, respectively)

Foundation soil condition			Hard				Soft			
Pier column height (m)			4.57		12.19		4.57		12.19	
Longitudinal (0°) ground motions	Bridge skew (°)	0	2.3 (0.9) ,	3.8 (1.2)	8.9 (3.4) ,	11.3 (3.9)	3.8 (1.5) ,	3.0 (1.3)	8.3 (1.9) ,	8.2 (2.6)
		15	5.7 (1.4) ,	6.9 (1.4)	12.5 (3.0) ,	13.4 (2.9)	6.3 (2.5) ,	5.5 (2.5)	11.5 (4.0) ,	10.9 (3.8)
		30	5.9 (2.4) ,	7.0 (2.1)	13.4 (3.7) ,	14.0 (4.9)	6.1 (2.8) ,	5.2 (2.7)	14.8 (3.1) ,	13.8 (3.0)
		45	3.8 (2.0) ,	5.3 (2.5)	5.6 (2.7) ,	7.8 (2.9)	3.7 (2.1) ,	3.5 (2.1)	10.9 (2.8) ,	10.7 (2.8)
		60	1.2 (0.2) ,	1.5 (0.4)	2.9 (1.2) ,	4.4 (1.5)	2.5 (1.5) ,	2.5 (1.5)	7.2 (2.5) ,	7.5 (2.2)
45° ground motions	Bridge skew (°)	0	1.5 (0.3) ,	2.3 (0.5)	4.7 (1.8) ,	6.3 (1.9)	2.1 (0.6) ,	1.6 (0.4)	4.7 (2.2) ,	3.6 (1.8)
		15	2.5 (0.5) ,	3.8 (0.8)	8.2 (2.7) ,	9.3 (2.6)	2.9 (0.9) ,	2.1 (0.8)	6.2 (2.1) ,	5.7 (2.4)
		30	4.1 (1.8) ,	5.2 (1.7)	11.2 (4.4) ,	12.1 (4.1)	3.8 (1.5) ,	2.9 (1.4)	9.7 (3.9) ,	9.1 (4.2)
		45	2.0 (0.5) ,	3.0 (0.8)	7.9 (3.6) ,	9.9 (4.2)	2.7 (0.8) ,	2.6 (0.9)	9.1 (3.9) ,	8.5 (3.9)
		60	1.3 (0.2) ,	1.9 (0.3)	2.7 (1.3) ,	4.5 (2.1)	1.8 (0.7) ,	1.7 (0.7)	6.6 (3.0) ,	6.0 (2.6)
Transverse (90°) ground motions	Bridge skew (°)	0	0.9 (0.1) ,	0.5 (0.0)	1.6 (0.2) ,	0.9 (0.1)	1.0 (0.2) ,	0.6 (0.1)	1.8 (0.7) ,	1.1 (0.4)
		15	1.0 (0.1) ,	0.6 (0.1)	1.7 (0.4) ,	1.4 (0.4)	1.0 (0.2) ,	0.7 (0.1)	2.3 (0.9) ,	1.5 (0.3)
		30	1.1 (0.1) ,	1.0 (0.3)	2.6 (1.5) ,	3.1 (1.4)	1.0 (0.2) ,	0.8 (0.1)	4.3 (2.1) ,	2.1 (1.0)
		45	0.9 (0.1) ,	1.1 (0.2)	2.2 (0.8) ,	4.0 (1.6)	1.0 (0.1) ,	0.8 (0.1)	4.0 (2.1) ,	2.7 (1.2)
		60	0.8 (0.2) ,	0.9 (0.2)	2.1 (1.0) ,	4.2 (1.8)	0.9 (0.1) ,	0.7 (0.2)	4.8 (2.8) ,	3.6 (1.8)
135° ground motions	Bridge skew (°)	0	1.6 (0.3) ,	2.4 (0.4)	4.8 (1.8) ,	6.2 (2.0)	2.0 (0.5) ,	1.7 (0.4)	5.7 (2.0) ,	4.5 (1.6)
		15	1.9 (0.6) ,	2.7 (0.8)	3.9 (1.2) ,	5.1 (1.4)	3.7 (1.8) ,	3.0 (1.3)	6.9 (3.2) ,	5.5 (2.7)
		30	1.7 (0.7) ,	2.3 (0.9)	3.5 (1.8) ,	4.4 (2.4)	3.4 (1.5) ,	2.8 (1.3)	6.3 (3.3) ,	5.6 (2.7)
		45	1.1 (0.2) ,	1.5 (0.4)	1.1 (0.2) ,	1.2 (0.2)	1.9 (1.1) ,	1.8 (1.0)	2.2 (0.9) ,	1.9 (0.9)
		60	0.8 (0.1) ,	0.8 (0.1)	1.1 (0.4) ,	1.0 (0.4)	1.1 (0.3) ,	1.0 (0.2)	1.5 (0.5) ,	1.3 (0.4)

Unyielded: normalized strain < 1 (unnormalized strain < 0.0017)

Yielded without signficniant strain hardening: 1 ≤ normalized strain < 10 (0.0017 ≤ unnormalized strain < 0.017)

Yielded and significantly strain hardened: 10 ≤ normalized strain (0.017 ≤ unnormalized strain)

Table C3.4: Occurrences of limit states at expansion piers (Pier 1) of 3C bridge variants

Limit state	No. of analyses with occurrence [1]	Skew angle[2] (°)					Foundation soil [2]		Column height [2] (m)		Ground motion incident angle [2] (°)			
		0	15	30	45	60	Hard	Soft	4.57	12.19	0	45	90	135
Rupture of retainer anchor (RRA@P1)	0 (0%)	0	0	0	0	0	0	0	0	0	0	0	0	0
Sliding of elastomeric bearing (SEB@P1)	25 (2%)	4 (16%)	4 (16%)	11 (44%)	4 (16%)	2 (8%)	5 (20%)	20 (80%)	5 (20%)	20 (80%)	22 (88%)	2 (8%)	0 (0%)	1 (4%)
Unseating of elastomeric bearing (UEB@P1)	0 (0%)	0	0	0	0	0	0	0	0	0	0	0	0	0
Yielding of vertical reinforcing steel at column end (YRS@P1)	453 (28%)	65 (14%)	85 (19%)	119 (26%)	88 (19%)	96 (21%)	218 (48%)	235 (52%)	38 (8%)	415 (92%)	82 (18%)	98 (22%)	174 (38%)	99 (22%)
Crushing of concrete cover at column end (CCC@P1)	7 (0%)	0 (0%)	3 (43%)	3 (43%)	0 (0%)	1 (14%)	7 (100%)	0 (0%)	4 (57%)	3 (43%)	3 (43%)	2 (29%)	2 (29%)	0 (0%)
Yielding of pile at pier (YPP@P1)	591 (37%)	125 (21%)	146 (25%)	125 (21%)	120 (20%)	75 (13%)	132 (22%)	459 (78%)	255 (43%)	336 (57%)	73 (12%)	59 (10%)	253 (43%)	206 (35%)

1 The number above the parentheses indicates the number of analyses with occurrences of a limit state.
The percentage inside the parentheses indicates the ratio of the number above the parentheses to all the 1,600 analyses.

2 The number above the parentheses indicates the number of analyses with occurrences of a limit state contributed by a parametric variation.
The percentage inside the parentheses indicates the relative contribution of a parametric variation to the total occurrences of a limit state.

Table C3.5: Normalized peak strain of vertical reinforcing steel at pier column base of 3C bridges (peak strains are normalized to the yield strain, 0.0021; numbers outside the parentheses are medians, while those inside are median absolute deviations; data of reinforcing steel at column base of expansion and fixed piers are placed on the left and right sides of the commas, respectively; performance levels in the footnote are defined per Kowalsky (2001) and Revell (2013))

Foundation soil condition			Hard				Soft			
Pier column height (m)			4.57		12.19		4.57		12.19	
Longitudinal (0°) ground motions	Bridge skew (°)	0	0.5 (0.1) ,	5.2 (1.3)	0.9 (0.2) ,	0.9 (0.2)	0.6 (0.1) ,	6.8 (2.4)	1.2 (0.5) ,	1.1 (0.3)
		15	0.6 (0.1) ,	7.0 (1.0)	0.9 (0.2) ,	1.0 (0.1)	0.8 (0.3) ,	10.3 (3.2)	1.4 (0.5) ,	1.4 (0.5)
		30	0.6 (0.1) ,	7.8 (1.2)	0.9 (0.3) ,	1.1 (0.3)	0.8 (0.1) ,	10.0 (3.4)	1.5 (0.6) ,	1.7 (0.7)
		45	0.4 (0.1) ,	1.5 (0.1)	0.7 (0.2) ,	1.3 (0.5)	0.5 (0.1) ,	1.4 (0.1)	0.7 (0.2) ,	1.1 (0.2)
		60	0.3 (0.0) ,	0.7 (0.1)	0.6 (0.2) ,	1.1 (0.1)	0.3 (0.1) ,	0.8 (0.1)	0.6 (0.1) ,	1.0 (0.1)
45° ground motions	Bridge skew (°)	0	0.3 (0.0) ,	2.6 (0.4)	0.7 (0.1) ,	0.7 (0.1)	0.5 (0.1) ,	2.8 (0.7)	0.8 (0.3) ,	0.8 (0.1)
		15	0.6 (0.1) ,	4.3 (0.6)	0.6 (0.1) ,	0.7 (0.1)	0.7 (0.1) ,	6.2 (1.4)	0.9 (0.3) ,	0.9 (0.2)
		30	0.8 (0.1) ,	6.6 (1.1)	0.8 (0.3) ,	0.9 (0.3)	0.9 (0.2) ,	8.6 (1.5)	1.3 (0.7) ,	1.3 (0.6)
		45	0.8 (0.1) ,	3.2 (1.2)	0.9 (0.4) ,	1.0 (0.3)	0.8 (0.1) ,	3.4 (0.9)	1.4 (0.7) ,	1.2 (0.4)
		60	0.7 (0.1) ,	1.2 (0.2)	1.2 (0.6) ,	1.3 (0.5)	0.8 (0.1) ,	1.5 (0.5)	1.2 (0.7) ,	1.2 (0.3)
Transverse (90°) ground motions	Bridge skew (°)	0	0.4 (0.1) ,	0.5 (0.1)	1.9 (0.6) ,	1.1 (0.2)	0.3 (0.0) ,	0.3 (0.0)	1.1 (0.2) ,	0.9 (0.1)
		15	0.5 (0.1) ,	0.6 (0.1)	2.3 (0.7) ,	1.3 (0.4)	0.4 (0.0) ,	0.7 (0.1)	1.2 (0.2) ,	1.0 (0.1)
		30	0.7 (0.1) ,	1.1 (0.1)	3.2 (0.5) ,	1.6 (0.9)	0.6 (0.1) ,	1.0 (0.1)	1.7 (0.5) ,	1.1 (0.3)
		45	0.9 (0.1) ,	1.0 (0.1)	1.3 (0.6) ,	1.6 (0.5)	0.7 (0.1) ,	1.0 (0.1)	1.1 (0.4) ,	0.9 (0.3)
		60	1.0 (0.1) ,	1.3 (0.2)	1.5 (0.5) ,	1.2 (0.4)	1.0 (0.1) ,	1.2 (0.1)	1.8 (0.9) ,	1.2 (0.4)
135° ground motions	Bridge skew (°)	0	0.3 (0.0) ,	2.6 (0.4)	0.7 (0.1) ,	0.7 (0.1)	0.5 (0.1) ,	2.8 (0.8)	0.8 (0.2) ,	0.8 (0.1)
		15	0.4 (0.1) ,	2.8 (0.5)	1.0 (0.2) ,	1.0 (0.2)	0.5 (0.1) ,	3.7 (1.7)	0.8 (0.2) ,	0.9 (0.1)
		30	0.7 (0.1) ,	2.2 (0.3)	1.5 (0.5) ,	2.5 (1.0)	0.5 (0.1) ,	3.4 (0.8)	1.1 (0.2) ,	1.3 (0.2)
		45	0.6 (0.1) ,	0.8 (0.0)	1.8 (0.9) ,	2.0 (0.6)	0.5 (0.0) ,	1.1 (0.2)	1.0 (0.1) ,	1.0 (0.1)
		60	0.7 (0.1) ,	0.6 (0.1)	1.0 (0.3) ,	1.2 (0.1)	0.6 (0.1) ,	0.8 (0.0)	0.9 (0.2) ,	0.9 (0.1)

Undamaged (unyielded):	normalized strain < 1 (unnormalized strain < 0.0021)
Lightly damaged (unlikely requiring repair):	1 ≤ normalized strain < 7.1 (0.0021 ≤ unnormalized strain < 0.015)
Moderately damaged (repairable):	7.1 ≤ normalized strain < 28.6 (0.015 ≤ unnormalized strain < 0.06)
Severely damaged (not easily repairable):	28.6 ≤ normalized strain (0.06 ≤ unnormalized strain)

Table C3.6: Normalized peak strain of concrete cover at pier column base of 3C bridges (peak strains are normalized to the crushing strain, 0.005; numbers outside the parentheses are medians, while those inside are median absolute deviations; data of concrete cover at column base of expansion and fixed piers are placed on the left and right sides of the commas, respectively; performance levels in the footnote are defined per Kowalsky (2001) and Revell (2013))

Foundation soil condition			Hard		Soft	
Pier column height (m)			4.57	12.19	4.57	12.19
Longitudinal (0°) ground motions	Bridge skew (°)	0	0.2 (0.0) , 0.8 (0.2)	0.3 (0.0) , 0.3 (0.0)	0.2 (0.0) , 1.1 (0.4)	0.3 (0.1) , 0.3 (0.1)
		15	0.2 (0.0) , 1.2 (0.2)	0.3 (0.0) , 0.3 (0.0)	0.3 (0.1) , 1.8 (0.6)	0.4 (0.1) , 0.4 (0.1)
		30	0.2 (0.0) , 1.4 (0.2)	0.3 (0.1) , 0.3 (0.1)	0.3 (0.0) , 1.8 (0.6)	0.4 (0.1) , 0.4 (0.1)
		45	0.2 (0.0) , 0.4 (0.0)	0.2 (0.0) , 0.3 (0.1)	0.2 (0.0) , 0.4 (0.0)	0.2 (0.1) , 0.3 (0.0)
		60	0.1 (0.0) , 0.2 (0.0)	0.2 (0.0) , 0.3 (0.0)	0.1 (0.0) , 0.2 (0.0)	0.2 (0.0) , 0.2 (0.0)
45° ground motions	Bridge skew (°)	0	0.2 (0.0) , 0.5 (0.0)	0.2 (0.0) , 0.2 (0.0)	0.2 (0.0) , 0.5 (0.1)	0.2 (0.0) , 0.2 (0.0)
		15	0.2 (0.0) , 0.7 (0.1)	0.2 (0.0) , 0.2 (0.0)	0.2 (0.0) , 0.9 (0.2)	0.2 (0.0) , 0.2 (0.0)
		30	0.2 (0.0) , 1.1 (0.2)	0.2 (0.0) , 0.2 (0.1)	0.2 (0.0) , 1.4 (0.3)	0.3 (0.1) , 0.3 (0.1)
		45	0.2 (0.0) , 0.6 (0.2)	0.2 (0.1) , 0.3 (0.1)	0.2 (0.0) , 0.6 (0.1)	0.3 (0.1) , 0.3 (0.1)
		60	0.2 (0.0) , 0.3 (0.0)	0.3 (0.1) , 0.3 (0.1)	0.2 (0.0) , 0.4 (0.1)	0.3 (0.1) , 0.3 (0.0)
Transverse (90°) ground motions	Bridge skew (°)	0	0.2 (0.0) , 0.2 (0.0)	0.4 (0.1) , 0.3 (0.0)	0.1 (0.0) , 0.1 (0.0)	0.3 (0.0) , 0.3 (0.0)
		15	0.2 (0.0) , 0.2 (0.0)	0.5 (0.1) , 0.4 (0.1)	0.2 (0.0) , 0.2 (0.0)	0.3 (0.0) , 0.3 (0.0)
		30	0.2 (0.0) , 0.3 (0.0)	0.6 (0.1) , 0.4 (0.2)	0.2 (0.0) , 0.3 (0.0)	0.4 (0.1) , 0.3 (0.1)
		45	0.2 (0.0) , 0.3 (0.0)	0.3 (0.1) , 0.4 (0.1)	0.2 (0.0) , 0.3 (0.0)	0.3 (0.0) , 0.2 (0.0)
		60	0.3 (0.0) , 0.3 (0.0)	0.3 (0.1) , 0.3 (0.1)	0.3 (0.0) , 0.3 (0.0)	0.4 (0.1) , 0.3 (0.1)
135° ground motions	Bridge skew (°)	0	0.2 (0.0) , 0.5 (0.1)	0.2 (0.0) , 0.2 (0.0)	0.2 (0.0) , 0.6 (0.1)	0.3 (0.0) , 0.3 (0.0)
		15	0.2 (0.0) , 0.6 (0.1)	0.3 (0.0) , 0.3 (0.0)	0.2 (0.0) , 0.7 (0.2)	0.2 (0.0) , 0.2 (0.0)
		30	0.2 (0.0) , 0.5 (0.0)	0.4 (0.1) , 0.5 (0.1)	0.2 (0.0) , 0.6 (0.1)	0.3 (0.0) , 0.3 (0.0)
		45	0.2 (0.0) , 0.3 (0.0)	0.4 (0.1) , 0.4 (0.1)	0.2 (0.0) , 0.3 (0.0)	0.3 (0.0) , 0.2 (0.0)
		60	0.2 (0.0) , 0.2 (0.0)	0.3 (0.1) , 0.3 (0.0)	0.2 (0.0) , 0.2 (0.0)	0.3 (0.0) , 0.3 (0.0)

Undamaged (ultimate strength not mobillized):	normalized strain < 0.4 (unnormalized strain < 0.002)
Lightly damaged (ultimate strength mobilized but uncrushed):	0.4 ≤ normalized strain < 1 (0.002 ≤ unnormalized strain < 0.005)
Moderately damaged (crushed but repairable):	1 ≤ normalized strain < 3.6 (0.005 ≤ unnormalized strain < 0.018)
Severely damaged (not easily repairable):	3.6 ≤ normalized strain (0.018 ≤ unnormalized strain)

Table C3.7: Normalized peak strains of steel H piles at piers of 3C bridges (peak strains are normalized to the yield strain, 0.0017; numbers outside the parentheses are medians, while those inside are median absolute deviations; data for piles supporting expansion and fixed piers are placed on the left and right sides of the commas, respectively)

Foundation soil condition			Hard		Soft	
Pier column height (m)			4.57	12.19	4.57	12.19
Longitudinal (0°) ground motions	Bridge skew (°)	0	0.3 (0.0) , 0.5 (0.0)	0.4 (0.0) , 0.4 (0.0)	0.4 (0.0) , 0.7 (0.1)	0.4 (0.1) , 0.4 (0.0)
		15	0.4 (0.0) , 0.8 (0.0)	0.4 (0.0) , 0.5 (0.0)	0.5 (0.1) , 1.1 (0.1)	0.7 (0.1) , 0.7 (0.1)
		30	0.4 (0.0) , 1.0 (0.1)	0.5 (0.1) , 0.6 (0.1)	0.9 (0.2) , 1.9 (0.5)	1.0 (0.2) , 1.2 (0.1)
		45	0.6 (0.1) , 0.9 (0.1)	0.6 (0.1) , 1.0 (0.1)	1.4 (0.6) , 2.5 (0.4)	1.1 (0.3) , 2.3 (0.8)
		60	0.6 (0.1) , 0.8 (0.1)	0.7 (0.1) , 0.9 (0.1)	1.3 (0.5) , 4.7 (1.2)	1.4 (0.2) , 6.9 (2.2)
45° ground motions	Bridge skew (°)	0	0.8 (0.1) , 0.9 (0.1)	0.8 (0.0) , 0.7 (0.0)	1.0 (0.1) , 1.3 (0.1)	1.4 (0.5) , 1.1 (0.1)
		15	0.7 (0.1) , 0.8 (0.1)	0.7 (0.0) , 0.6 (0.0)	1.0 (0.1) , 1.0 (0.1)	1.1 (0.2) , 1.0 (0.1)
		30	0.6 (0.0) , 0.7 (0.0)	0.5 (0.0) , 0.5 (0.1)	0.9 (0.1) , 1.1 (0.0)	0.8 (0.1) , 0.9 (0.1)
		45	0.5 (0.0) , 0.9 (0.0)	0.5 (0.0) , 0.6 (0.0)	0.8 (0.1) , 1.3 (0.1)	0.7 (0.1) , 0.8 (0.1)
		60	0.5 (0.0) , 0.8 (0.0)	0.4 (0.1) , 0.5 (0.0)	0.7 (0.1) , 1.3 (0.1)	0.6 (0.1) , 0.9 (0.1)
Transverse (90°) ground motions	Bridge skew (°)	0	1.0 (0.1) , 1.1 (0.1)	1.4 (0.3) , 1.0 (0.1)	2.7 (1.0) , 2.5 (0.8)	8.9 (3.6) , 4.0 (2.2)
		15	1.0 (0.1) , 1.1 (0.1)	1.4 (0.3) , 1.0 (0.1)	3.1 (1.3) , 2.0 (0.5)	9.1 (3.6) , 4.7 (2.1)
		30	0.9 (0.1) , 1.2 (0.1)	1.2 (0.1) , 0.9 (0.1)	1.7 (0.3) , 1.4 (0.1)	4.2 (1.8) , 2.4 (0.8)
		45	0.7 (0.1) , 1.2 (0.2)	1.0 (0.2) , 1.1 (0.1)	1.3 (0.1) , 1.1 (0.1)	2.0 (0.8) , 1.8 (0.7)
		60	0.5 (0.0) , 0.9 (0.1)	0.6 (0.1) , 0.8 (0.1)	0.9 (0.0) , 1.0 (0.1)	0.9 (0.2) , 1.3 (0.3)
135° ground motions	Bridge skew (°)	0	0.8 (0.1) , 0.9 (0.1)	0.7 (0.0) , 0.6 (0.0)	1.0 (0.1) , 1.3 (0.1)	1.5 (0.5) , 1.1 (0.2)
		15	0.8 (0.1) , 1.2 (0.1)	1.0 (0.1) , 0.9 (0.1)	1.4 (0.3) , 2.6 (0.8)	2.9 (1.8) , 2.1 (1.2)
		30	0.8 (0.0) , 1.3 (0.1)	1.0 (0.2) , 1.1 (0.1)	1.8 (0.5) , 5.2 (1.8)	3.0 (2.1) , 4.1 (3.0)
		45	0.7 (0.0) , 1.5 (0.2)	1.1 (0.2) , 1.2 (0.1)	1.7 (0.8) , 7.2 (2.0)	3.9 (2.8) , 7.6 (3.6)
		60	0.6 (0.0) , 1.0 (0.1)	0.9 (0.1) , 0.9 (0.0)	1.3 (0.3) , 5.7 (2.4)	1.9 (1.1) , 7.3 (3.2)

Unyielded: normalized strain < 1 (unnormalized strain < 0.0017)

Yielded without signficniant strain hardening: 1 ≤ normalized strain < 10 (0.0017 ≤ unnormalized strain < 0.017)

Yielded and significantly strain hardened: 10 ≤ normalized strain (0.017 ≤ unnormalized strain)

Table C3.8: Occurrences of limit states at fixed piers (Pier 2) of 3C bridge variants

Limit state	No. of analyses with occurrence [1]	Skew angle [2] (°)					Foundation soil [2]		Column height [2] (m)		Ground motion incident angle [2] (°)			
		0	15	30	45	60	Hard	Soft	4.57	12.19	0	45	90	135
Rupture of retainer anchor (RRA@P2)	4 (0%)	0 (0%)	0 (0%)	0 (0%)	3 (75%)	1 (25%)	4 (100%)	0 (0%)	0 (0%)	4 (100%)	0 (0%)	0 (0%)	1 (25%)	3 (75%)
Rupture of steel dowel connection (RSD@P2)	309 (19%)	0 (0%)	1 (0%)	20 (6%)	111 (36%)	177 (57%)	213 (69%)	96 (31%)	231 (75%)	78 (25%)	108 (35%)	37 (12%)	36 (12%)	128 (41%)
Yielding of vertical reinforcing steel at column end (YRS@P2)	1026 (64%)	170 (17%)	194 (19%)	254 (25%)	226 (22%)	182 (18%)	512 (50%)	514 (50%)	567 (55%)	459 (45%)	293 (29%)	283 (28%)	202 (20%)	248 (24%)
Crushing of concrete cover at column end (CCC@P2)	136 (9%)	16 (12%)	43 (32%)	65 (48%)	3 (2%)	9 (7%)	52 (38%)	84 (62%)	126 (93%)	10 (7%)	76 (56%)	47 (35%)	3 (2%)	10 (7%)
Yielding of pile at pier (YPP@P2)	870 (54%)	135 (16%)	172 (20%)	192 (22%)	213 (24%)	158 (18%)	255 (29%)	615 (71%)	508 (58%)	362 (42%)	157 (18%)	122 (14%)	290 (33%)	301 (35%)

1 The number above the parentheses indicates the number of analyses with occurrences of a limit state.
The percentage inside the parentheses indicates the ratio of the number above the parentheses to all the 1,600 analyses.
2 The number above the parentheses indicates the number of analyses with occurrences of a limit state contributed by a parametric variation.
The percentage inside the parentheses indicates the relative contribution of a parametric variation to the total occurrences of a limit state.

C.4 ADDITIONAL ANALYSIS RESULTS FOR 4C BRIDGES

Table C4.1: Limit state occurrences of each 4C bridge variant under 0° and 45° ground motions (each percentage indicates the number of analyses with occurrences of a limit state out of the 20 analyses with the ground motions applied to a bridge variant in an incident direction)

Ground motion direction	Bridge variant	Critical limit states																																
		Abutment 1 (A1)									Pier 1 (P1, expansion pier)						Pier 2 (P2, fixed pier)					Pier 3 (P3, expansion pier)						Abutment 2 (A2)								
		CEJ	MBU	FBP	RRA	SEB	UBA	UBO	YPW	YPB	RRA	SEB	UEB	YRS	CCC	YPP	RRA	RSD	YRS	CCC	YPP	RRA	SEB	UEB	YRS	CCC	YPP	CEJ	MBU	FBP	RRA	SEB	UBO	UBA	YPW	YPB
0°	4C00P15H	100%	15%	0	0	10%	0	0	100%	100%	0	45%	0	90%	50%	0	0	0	100%	100%	0	0	30%	0	95%	65%	0	100%	0	0	0	20%	0	0	100%	100%
	4C15P15H	100%	5%	0	0	15%	0	0	100%	100%	0	50%	0	100%	75%	0	0	0	100%	100%	0	0	50%	0	100%	65%	0	100%	5%	0	0	10%	0	0	100%	100%
	4C30P15H	100%	10%	0	0	0	0	0	100%	100%	0	45%	0	100%	80%	25%	0	25%	100%	100%	10%	0	40%	0	100%	90%	20%	100%	0	0	0	15%	0	0	100%	100%
	4C45P15H	100%	0	0	0	0	0	0	100%	100%	0	5%	0	75%	10%	40%	0	100%	100%	20%	30%	0	5%	0	75%	15%	25%	100%	0	0	0	0	0	0	100%	100%
	4C60P15H	100%	0	0	0	0	0	0	100%	100%	0	0	0	25%	0	55%	0	100%	50%	0	60%	0	0	0	25%	0	70%	100%	0	0	0	0	0	0	100%	100%
	4C00P40H	100%	45%	0	0	75%	0	0	100%	100%	0	20%	0	80%	20%	0	0	0	80%	15%	0	0	25%	0	80%	25%	0	100%	50%	0	0	65%	0	0	100%	100%
	4C15P40H	100%	40%	0	0	60%	0	0	100%	100%	0	25%	0	80%	25%	0	0	0	80%	20%	0	0	30%	0	80%	30%	0	100%	35%	0	0	55%	0	0	100%	100%
	4C30P40H	100%	20%	0	40%	50%	0	0	100%	100%	0	25%	0	80%	25%	0	0	0	80%	20%	0	0	25%	0	80%	25%	0	100%	25%	0	35%	40%	0	0	100%	100%
	4C45P40H	100%	0	0	60%	30%	0	0	100%	100%	0	25%	0	80%	25%	25%	0	0	95%	25%	45%	0	30%	0	80%	40%	25%	100%	0	0	65%	55%	0	0	100%	100%
	4C60P40H	100%	0	0	45%	25%	0	0	100%	80%	0	20%	0	75%	25%	55%	0	100%	100%	15%	90%	0	25%	0	75%	25%	60%	100%	0	0	60%	30%	0	0	100%	90%
	4C00P15S	100%	30%	0	0	30%	0	0	100%	100%	0	65%	0	95%	75%	0	0	0	100%	100%	0	0	65%	0	90%	75%	0	100%	15%	0	0	30%	0	0	100%	100%
	4C15P15S	100%	45%	0	0	40%	0	0	100%	100%	0	60%	0	90%	80%	60%	0	0	100%	100%	15%	0	70%	0	90%	80%	50%	100%	15%	0	0	45%	0	0	100%	100%
	4C30P15S	100%	25%	0	0	25%	0	0	100%	100%	0	65%	0	100%	80%	80%	0	40%	100%	100%	85%	0	70%	0	95%	80%	75%	100%	15%	0	0	25%	0	0	100%	100%
	4C45P15S	100%	0	0	0	0	0	0	100%	100%	0	0	0	70%	0	80%	0	100%	100%	70%	100%	0	5%	0	75%	0	80%	100%	0	0	0	0	0	0	100%	100%
	4C60P15S	100%	0	0	0	0	0	0	95%	100%	0	0	0	0	0	90%	0	100%	90%	0	100%	0	10%	0	0	0	90%	100%	0	0	0	0	0	0	100%	95%
	4C00P40S	100%	65%	5%	0	70%	0	0	100%	100%	0	30%	0	80%	30%	0	0	0	80%	20%	0	0	35%	0	80%	30%	0	100%	50%	0	0	70%	0	0	100%	100%
	4C15P40S	100%	55%	0	0	65%	0	0	100%	100%	0	25%	0	75%	30%	0	0	0	80%	25%	0	0	15%	0	80%	30%	0	100%	50%	0	0	65%	0	0	100%	100%
	4C30P40S	100%	30%	0	20%	60%	0	0	100%	100%	0	20%	0	75%	25%	25%	0	0	85%	25%	35%	0	15%	0	75%	25%	25%	100%	40%	0	20%	45%	0	0	100%	100%
	4C45P40S	100%	20%	0	30%	35%	0	0	100%	100%	0	20%	0	75%	25%	70%	0	0	80%	30%	100%	0	25%	0	70%	30%	75%	100%	20%	0	55%	30%	0	0	100%	100%
	4C60P40S	100%	20%	0	0	20%	0	0	90%	95%	0	20%	0	60%	10%	80%	0	20%	80%	20%	100%	0	25%	0	60%	30%	80%	100%	10%	0	45%	20%	0	0	100%	100%
45°	4C00P15H	100%	0	0	0	0	0	0	100%	100%	0	0	0	20%	15%	5%	0	25%	100%	100%	50%	0	5%	0	30%	15%	5%	100%	0	0	0	0	0	0	100%	100%
	4C15P15H	100%	0	0	0	0	0	0	100%	100%	0	25%	0	90%	30%	5%	0	15%	100%	100%	35%	0	15%	0	75%	30%	0	100%	0	0	0	0	0	0	100%	100%
	4C30P15H	100%	0	0	0	0	0	0	100%	100%	0	5%	0	100%	65%	0	0	50%	100%	100%	55%	0	25%	0	100%	70%	0	100%	0	0	0	0	0	0	100%	100%
	4C45P15H	100%	0	0	0	0	0	0	100%	100%	0	0	0	100%	45%	20%	0	100%	100%	70%	85%	0	0	0	100%	55%	25%	100%	0	0	0	0	0	0	100%	100%
	4C60P15H	100%	0	0	0	0	0	0	100%	85%	0	0	0	95%	30%	10%	0	100%	100%	40%	5%	0	0	0	90%	45%	5%	100%	0	0	5%	0	0	0	100%	75%
	4C00P40H	100%	0	0	10%	15%	0	0	100%	100%	0	0	0	75%	0	5%	0	0	100%	35%	0	0	0	0	75%	0	0	100%	0	0	0	10%	0	0	100%	100%
	4C15P40H	100%	30%	0	0	30%	0	0	100%	100%	0	15%	0	80%	20%	0	0	0	85%	10%	0	0	10%	0	75%	15%	0	100%	15%	0	5%	30%	0	0	100%	100%
	4C30P40H	100%	20%	0	20%	40%	0	0	100%	100%	0	10%	0	80%	25%	0	0	0	80%	25%	0	0	20%	0	80%	20%	0	100%	25%	0	20%	40%	0	0	100%	100%
	4C45P40H	100%	10%	0	55%	20%	0	0	100%	100%	0	20%	0	80%	20%	0	0	0	80%	20%	0	0	5%	0	80%	25%	0	100%	15%	0	25%	25%	0	5%	100%	100%
	4C60P40H	100%	20%	20%	60%	20%	0	0	100%	80%	0	0	0	80%	20%	0	0	0	80%	50%	0	0	0	0	80%	45%	0	100%	5%	0	70%	55%	0	10%	100%	85%
	4C00P15S	100%	0	0	0	0	0	0	100%	100%	0	10%	0	55%	15%	80%	0	5%	100%	100%	100%	0	10%	0	45%	15%	80%	100%	0	0	0	0	0	0	100%	100%
	4C15P15S	100%	0	0	0	0	0	0	100%	100%	0	45%	0	80%	75%	85%	0	0	100%	100%	100%	0	30%	0	80%	70%	80%	100%	0	0	0	0	0	0	100%	100%
	4C30P15S	100%	0	0	0	0	0	0	100%	100%	0	30%	0	85%	75%	85%	0	0	100%	100%	100%	0	40%	0	80%	75%	80%	100%	0	0	0	0	0	0	100%	100%
	4C45P15S	100%	0	0	0	0	0	0	100%	100%	0	40%	0	85%	65%	95%	0	65%	100%	90%	100%	0	20%	0	85%	50%	90%	100%	0	0	0	0	0	0	100%	100%
	4C60P15S	100%	0	0	0	0	0	0	90%	95%	0	0	0	85%	20%	100%	0	100%	100%	45%	100%	0	5%	0	90%	35%	100%	100%	0	0	10%	0	0	0	95%	95%
	4C00P40S	100%	35%	0	0	35%	0	0	100%	100%	0	25%	0	80%	25%	90%	0	0	80%	20%	100%	0	15%	0	80%	20%	85%	100%	25%	0	0	35%	0	0	100%	100%
	4C15P40S	100%	45%	0	0	55%	0	0	100%	100%	0	20%	0	75%	20%	80%	0	0	80%	20%	90%	0	20%	0	75%	20%	70%	100%	30%	0	0	55%	0	0	100%	100%
	4C30P40S	100%	25%	0	0	50%	0	0	100%	100%	0	5%	0	75%	20%	50%	0	0	80%	25%	45%	0	10%	0	75%	25%	35%	100%	40%	0	20%	35%	0	0	100%	100%
	4C45P40S	100%	25%	0	20%	40%	0	0	100%	100%	0	15%	0	75%	25%	10%	0	0	85%	40%	15%	0	15%	0	75%	25%	0	100%	30%	0	25%	30%	0	0	100%	100%
	4C60P40S	100%	0	0	40%	20%	0	0	100%	100%	0	15%	0	75%	35%	35%	0	0	100%	45%	45%	0	10%	0	75%	45%	30%	100%	30%	0	60%	40%	0	10%	100%	100%

Preferred limit states:	0	20%	40%	60%	80%	100%
Acceptable limit states:	0	20%	40%	60%	80%	100%
Unacceptable limit states:	0	20%	40%	60%	80%	100%

Table C4.1 Continued: Limit state occurrences of each 4C bridge variant under 90° and 135° ground motions (each percentage indicates the number of analyses with occurrences of a limit state out of the 20 analyses with the ground motions applied to a bridge variant in an incident direction)

Ground motion direction	Bridge variant	Critical limit states																																	
		Abutment 1 (A1)									Pier 1 (P1, expansion pier)						Pier 2 (P2, fixed pier)					Pier 3 (P3, expansion pier)						Abutment 2 (A2)								
		CEJ	MBU	FBP	RRA	SEB	UBA	UBO	YPW	YPB	RRA	SEB	UEB	YRS	CCC	YPP	RRA	RSD	YRS	CCC	YPP	RRA	SEB	UEB	YRS	CCC	YPP	CEJ	MBU	FBP	RRA	SEB	UBO	UBA	YPW	YPB
90°	4C00P15H	0	0	0	0	0	0	0	0	100%	0	0	0	20%	0	75%	0	75%	70%	0	100%	0	0	0	10%	0	70%	0	0	0	0	0	0	0	0	100%
	4C15P15H	25%	0	0	0	0	0	0	10%	95%	0	0	0	40%	0	75%	5%	75%	80%	0	90%	0	0	0	35%	0	65%	25%	0	0	0	0	0	0	10%	85%
	4C30P15H	95%	0	0	0	0	0	0	70%	100%	0	0	0	90%	5%	90%	30%	100%	100%	5%	100%	0	0	0	90%	5%	85%	90%	0	0	5%	0	0	0	70%	100%
	4C45P15H	100%	0	0	20%	0	0	0	80%	100%	0	0	0	100%	40%	95%	50%	100%	100%	10%	100%	0	0	0	100%	30%	95%	95%	0	0	25%	0	0	0	90%	100%
	4C60P15H	100%	0	0	50%	0	0	0	95%	100%	0	0	0	100%	65%	45%	60%	100%	100%	35%	85%	0	0	0	100%	70%	70%	100%	0	0	45%	10%	0	0	100%	95%
	4C00P40H	0	0	0	65%	20%	0	0	0	100%	0	0	0	100%	35%	25%	0	0	100%	65%	15%	0	0	0	100%	45%	15%	0	0	0	65%	25%	0	0	0	100%
	4C15P40H	85%	0	0	70%	20%	0	0	55%	100%	0	0	0	100%	70%	0	0	0	100%	70%	0	0	0	0	100%	70%	0	90%	0	0	70%	10%	0	0	60%	100%
	4C30P40H	100%	0	0	70%	15%	0	0	100%	100%	0	0	0	100%	65%	0	0	0	100%	80%	0	0	0	0	100%	60%	0	100%	0	0	75%	35%	0	0	100%	100%
	4C45P40H	100%	0	0	70%	30%	0	0	100%	100%	0	0	0	95%	30%	65%	0	40%	100%	50%	95%	0	0	0	95%	20%	60%	100%	0	0	70%	20%	0	0	100%	100%
	4C60P40H	100%	5%	5%	75%	20%	0	0	90%	85%	0	0	0	80%	15%	60%	0	100%	100%	20%	80%	0	0	0	80%	25%	35%	100%	0	0	75%	25%	0	10%	100%	85%
	4C00P15S	0	0	0	0	0	0	0	0	80%	0	0	0	0	0	100%	0	0	0	0	100%	0	0	0	0	0	100%	0	0	0	0	0	0	0	0	85%
	4C15P15S	65%	0	0	0	0	0	0	20%	80%	0	0	0	10%	0	100%	0	5%	75%	0	100%	0	0	0	5%	0	100%	70%	0	0	0	0	0	0	20%	85%
	4C30P15S	80%	0	0	0	0	0	0	60%	90%	0	0	0	60%	0	100%	0	15%	95%	40%	100%	0	0	0	70%	0	100%	75%	0	0	0	0	0	0	55%	90%
	4C45P15S	100%	0	0	0	0	0	0	60%	100%	0	0	0	80%	0	100%	0	65%	100%	60%	100%	0	0	0	85%	10%	100%	100%	0	0	20%	0	0	0	70%	100%
	4C60P15S	100%	0	0	15%	0	0	0	45%	100%	0	0	0	95%	25%	100%	25%	60%	100%	80%	100%	0	0	0	100%	65%	100%	100%	0	0	50%	15%	0	0	90%	100%
	4C00P40S	0	0	0	30%	0	0	0	20%	100%	0	0	0	85%	5%	100%	0	0	95%	15%	100%	0	0	0	85%	15%	100%	0	0	0	25%	0	0	0	20%	100%
	4C15P40S	65%	0	0	30%	10%	0	0	75%	100%	0	0	0	85%	15%	100%	0	0	100%	30%	100%	0	0	0	85%	20%	100%	65%	0	0	25%	10%	0	0	75%	100%
	4C30P40S	100%	0	0	35%	10%	0	0	80%	100%	0	0	0	85%	20%	100%	0	0	100%	55%	100%	0	0	0	85%	25%	95%	100%	0	0	35%	20%	0	0	85%	100%
	4C45P40S	100%	0	0	50%	20%	0	0	90%	100%	0	0	0	80%	15%	95%	0	0	95%	20%	100%	0	0	0	80%	20%	100%	100%	5%	0	55%	35%	0	0	100%	100%
	4C60P40S	100%	0	0	65%	25%	0	0	85%	100%	0	0	0	80%	20%	80%	0	0	85%	20%	100%	0	0	0	80%	25%	80%	100%	20%	0	75%	30%	5%	15%	100%	95%
135°	4C00P15H	100%	0	0	0	0	0	0	100%	100%	0	5%	0	40%	15%	10%	0	20%	100%	95%	45%	0	0	0	35%	15%	5%	100%	0	0	0	0	0	0	100%	100%
	4C15P15H	100%	0	0	0	0	0	0	100%	100%	0	5%	0	60%	10%	15%	0	75%	100%	75%	90%	0	0	0	45%	15%	15%	100%	0	0	0	0	0	0	100%	100%
	4C30P15H	100%	0	0	5%	0	0	0	100%	100%	0	10%	0	100%	40%	75%	0	100%	100%	60%	100%	0	5%	0	100%	40%	85%	100%	0	0	0	0	0	0	100%	100%
	4C45P15H	100%	0	0	0	0	0	0	100%	100%	0	0	0	100%	10%	80%	20%	100%	100%	0	95%	0	0	0	100%	20%	80%	100%	0	0	0	0	0	0	100%	100%
	4C60P15H	100%	0	0	0	0	0	0	100%	85%	0	0	0	100%	5%	75%	45%	100%	100%	0	100%	0	0	0	100%	10%	75%	100%	0	0	5%	0	0	0	100%	70%
	4C00P40H	100%	0	0	5%	10%	0	0	100%	100%	0	0	0	80%	0	0	0	0	100%	0	0	0	0	0	75%	0	5%	100%	0	0	15%	10%	0	0	100%	100%
	4C15P40H	100%	0	0	25%	10%	0	0	100%	100%	0	0	0	100%	15%	5%	0	0	100%	15%	0	0	0	0	100%	0	0	100%	0	0	5%	0	0	0	100%	100%
	4C30P40H	100%	0	0	55%	10%	0	0	100%	100%	0	0	0	100%	25%	0	0	0	100%	70%	0	0	0	0	100%	30%	5%	100%	0	0	55%	5%	0	0	100%	100%
	4C45P40H	100%	0	0	65%	10%	0	0	85%	100%	0	0	0	100%	25%	75%	35%	65%	100%	50%	100%	0	0	0	100%	50%	80%	95%	0	0	75%	10%	0	0	100%	100%
	4C60P40H	100%	0	0	75%	0	0	0	65%	90%	0	0	0	80%	20%	75%	70%	100%	100%	0	100%	0	0	0	85%	20%	75%	100%	0	0	55%	0	0	0	55%	80%
	4C00P15S	100%	0	0	0	0	0	0	100%	100%	0	10%	0	65%	15%	80%	0	5%	100%	100%	100%	0	10%	0	60%	15%	85%	100%	0	0	0	0	0	0	100%	100%
	4C15P15S	100%	0	0	0	0	0	0	100%	100%	0	10%	0	75%	25%	90%	0	15%	100%	100%	100%	0	10%	0	70%	30%	85%	100%	0	0	0	0	0	0	100%	95%
	4C30P15S	100%	0	0	0	0	0	0	100%	100%	0	0	0	65%	20%	90%	0	45%	100%	100%	100%	0	0	0	80%	30%	90%	100%	0	0	0	0	0	0	100%	90%
	4C45P15S	100%	0	0	0	0	0	0	95%	95%	0	0	0	55%	5%	100%	0	80%	100%	40%	100%	0	0	0	65%	5%	95%	100%	0	0	0	0	0	0	100%	95%
	4C60P15S	100%	0	0	0	0	0	0	80%	85%	0	0	0	85%	0	100%	0	100%	100%	0	100%	0	0	0	85%	5%	100%	100%	0	0	5%	0	0	0	100%	90%
	4C00P40S	100%	35%	0	0	40%	0	0	100%	100%	0	20%	0	80%	25%	90%	0	0	85%	25%	100%	0	20%	0	80%	30%	90%	100%	30%	0	0	35%	0	0	100%	100%
	4C15P40S	100%	25%	0	0	40%	0	0	100%	100%	0	20%	0	80%	20%	95%	0	0	95%	20%	100%	0	20%	0	80%	25%	100%	100%	15%	0	5%	30%	0	0	100%	100%
	4C30P40S	100%	0	0	5%	20%	0	0	100%	100%	0	10%	0	80%	20%	95%	0	0	100%	25%	100%	0	20%	0	80%	20%	95%	100%	20%	0	25%	10%	0	0	100%	100%
	4C45P40S	100%	0	0	0	20%	0	0	85%	100%	0	20%	0	80%	0	95%	0	0	100%	0	100%	0	0	0	80%	0	100%	100%	0	0	10%	0	0	0	100%	100%
	4C60P40S	80%	0	0	15%	10%	0	0	80%	90%	0	0	0	80%	0	95%	0	30%	85%	0	100%	0	0	0	80%	0	95%	80%	0	0	30%	5%	0	0	80%	85%

Preferred limit states:	0	20%	40%	60%	80%	100%
Acceptable limit states:	0	20%	40%	60%	80%	100%
Unacceptable limit states:	0	20%	40%	60%	80%	100%

Table C4.2: Occurrences of limit states at abutments (A1 and A2) of 4C bridge variants

Limit state	No. of analyses with occurrence [1]	Skew angle [2] (°)					Foundation soil [2]		Column height [2] (m)		Ground motion incident angle [2] (°)			
		0	15	30	45	60	Hard	Soft	4.57	12.19	0	45	90	135
Closure of expansion joint (CEJ@A1)	1479 (92%)	240 (16%)	288 (19%)	315 (21%)	320 (22%)	316 (21%)	741 (50%)	738 (50%)	733 (50%)	746 (50%)	400 (27%)	400 (27%)	283 (19%)	396 (27%)
Mobilization of backfill ultimate capacity (MBU@A1)	140 (9%)	45 (32%)	49 (35%)	26 (19%)	11 (8%)	9 (6%)	44 (31%)	96 (69%)	26 (19%)	114 (81%)	85 (61%)	42 (30%)	1 (1%)	12 (9%)
Failure of backwall-to-pile-cap connection (FBP@A1)	6 (0%)	1 (100%)	0 (0%)	0 (0%)	0 (0%)	5 (83%)	5 (83%)	1 (17%)	0 (0%)	6 (100%)	1 (17%)	4 (67%)	1 (17%)	0 (0%)
Rupture of retainer anchor (RRA@A1)	259 (16%)	22 (8%)	25 (10%)	50 (19%)	74 (29%)	88 (34%)	188 (73%)	71 (27%)	18 (7%)	241 (93%)	39 (15%)	41 (16%)	129 (50%)	50 (19%)
Sliding of elastomeric bearing (SEB@A1)	255 (16%)	61 (24%)	69 (27%)	56 (22%)	41 (16%)	28 (11%)	107 (42%)	148 (58%)	24 (9%)	231 (91%)	122 (48%)	65 (25%)	34 (13%)	34 (13%)
Unseating of bearing at obtuse corner of deck (UBA@A1)	0 (0%)	0	0	0	0	0	0	0	0	0	0	0	0	0
Unseating of bearing at acute corner of deck (UBO@A1)	0 (0%)	0	0	0	0	0	0	0	0	0	0	0	0	0
Yielding of pile supporting wingwall (YPW@A1)	1400 (88%)	244 (17%)	272 (19%)	302 (22%)	299 (21%)	283 (20%)	710 (51%)	690 (49%)	680 (49%)	720 (51%)	397 (28%)	398 (28%)	227 (16%)	378 (27%)
Yielding of pile supporting backwall (YPB@A1)	1562 (98%)	316 (20%)	315 (20%)	318 (20%)	319 (20%)	294 (19%)	780 (50%)	782 (50%)	778 (50%)	784 (50%)	395 (25%)	392 (25%)	386 (25%)	389 (25%)
Closure of expansion joint (CEJ@A2)	1477 (92%)	240 (16%)	290 (20%)	313 (21%)	318 (22%)	316 (21%)	739 (50%)	738 (50%)	731 (49%)	746 (51%)	400 (27%)	400 (27%)	282 (19%)	395 (27%)
Mobilization of backfill ultimate capacity (MBU@A2)	127 (8%)	34 (27%)	33 (26%)	33 (26%)	14 (11%)	13 (10%)	35 (28%)	92 (72%)	10 (8%)	117 (92%)	66 (52%)	43 (34%)	5 (4%)	13 (10%)
Failure of backwall-to-pile-cap connection (FBP@A2)	0 (0%)	0	0	0	0	0	0	0	0	0	0	0	0	0
Rupture of retainer anchor (RRA@A2)	304 (19%)	21 (7%)	22 (7%)	58 (19%)	85 (28%)	118 (39%)	185 (61%)	119 (39%)	34 (11%)	270 (89%)	56 (18%)	48 (16%)	143 (47%)	57 (19%)
Sliding of elastomeric bearing (SEB@A2)	263 (16%)	60 (23%)	62 (24%)	54 (21%)	41 (16%)	46 (17%)	120 (46%)	143 (54%)	34 (13%)	229 (87%)	124 (47%)	71 (27%)	47 (18%)	21 (8%)
Unseating of bearing at obtuse corner of deck (UBO@A2)	1 (0%)	0 (0%)	0 (0%)	0 (0%)	0 (0%)	1 (100%)	0 (0%)	1 (100%)	0 (0%)	1 (100%)	0 (0%)	0 (0%)	1 (100%)	0 (0%)
Unseating of bearing acute corner of deck (UBA@A2)	10 (0%)	0 (0%)	0 (0%)	0 (0%)	1 (10%)	9 (90%)	5 (50%)	5 (50%)	0 (0%)	10 (100%)	0 (0%)	5 (50%)	5 (50%)	0 (0%)
Yielding of pile supporting wingwall (YPW@A2)	1435 (90%)	244 (17%)	273 (19%)	302 (21%)	312 (22%)	304 (21%)	717 (50%)	718 (50%)	700 (49%)	735 (51%)	400 (28%)	399 (28%)	249 (17%)	387 (27%)
Yielding of pile supporting backwall (YPB@A2)	1553 (97%)	317 (20%)	313 (20%)	316 (20%)	319 (21%)	288 (19%)	773 (50%)	780 (50%)	769 (50%)	784 (50%)	397 (26%)	391 (25%)	384 (25%)	381 (25%)

1 The number above the parentheses indicates the number of analyses with occurrences of a limit state.
The percentage inside the parentheses indicates the ratio of the number above the parentheses to all the 1,600 analyses.
2 The number above the parentheses indicates the number of analyses with occurrences of a limit state contributed by a parametric variation.
The percentage inside the parentheses indicates the relative contribution of a parametric variation to the total occurrences of a limit state.

Table C4.3: Normalized peak strains of steel H piles supporting abutments of 4C bridges (peak strains are normalized to the yield strain of steel piles, 0.0017; numbers outside and inside the parentheses are medians and median absolute deviations, respectively; data for piles supporting backwalls and wingwalls are placed on the left and right sides of the commas, respectively)

Foundation soil condition		Hard								Soft							
Pier column height (m)		4.57				12.19				4.57				12.19			
Longitudinal (0°) ground motions	Bridge skew (°) 0	6.9	(3.2) ,	12.3	(3.7)	17.0	(7.8) ,	25.5	(6.6)	7.5	(3.4) ,	10.3	(3.8)	13.3	(5.7) ,	16.5	(5.3)
	15	9.2	(3.2) ,	14.4	(4.8)	24.0	(11.3) ,	28.1	(9.5)	13.5	(5.8) ,	14.0	(6.3)	18.4	(8.4) ,	19.6	(6.4)
	30	13.5	(5.2) ,	17.2	(6.4)	22.4	(12.3) ,	24.5	(11.2)	14.7	(6.4) ,	15.8	(6.3)	18.0	(7.7) ,	19.0	(7.2)
	45	13.5	(5.1) ,	15.1	(4.7)	9.0	(5.5) ,	14.0	(6.1)	11.6	(4.1) ,	12.4	(4.4)	12.9	(7.7) ,	13.8	(8.5)
	60	3.4	(1.8) ,	5.5	(2.4)	3.2	(2.3) ,	6.1	(4.9)	8.3	(4.5) ,	8.6	(4.6)	8.7	(6.9) ,	9.9	(7.5)
45° ground motions	Bridge skew (°) 0	3.9	(2.2) ,	6.6	(1.7)	9.2	(4.3) ,	14.2	(4.1)	4.2	(1.7) ,	4.6	(1.3)	11.9	(5.9) ,	12.7	(5.3)
	15	7.1	(3.2) ,	10.0	(3.1)	14.1	(8.0) ,	19.3	(7.8)	5.8	(3.4) ,	6.5	(3.2)	12.2	(8.4) ,	14.9	(6.8)
	30	8.3	(3.3) ,	10.6	(3.4)	23.6	(12.2) ,	26.2	(11.7)	8.5	(5.0) ,	9.9	(3.8)	18.1	(7.6) ,	18.4	(7.7)
	45	7.7	(4.3) ,	9.8	(3.9)	19.7	(7.4) ,	24.4	(7.7)	7.6	(2.4) ,	9.1	(3.3)	16.9	(8.2) ,	20.0	(6.7)
	60	2.3	(0.7) ,	4.7	(1.8)	5.0	(2.7) ,	10.2	(6.0)	5.2	(2.8) ,	6.8	(3.3)	6.4	(3.9) ,	10.3	(4.0)
Transverse (90°) ground motions	Bridge skew (°) 0	1.2	(0.1) ,	0.7	(0.1)	4.0	(1.5) ,	2.3	(0.8)	1.5	(0.5) ,	1.0	(0.4)	4.8	(3.1) ,	2.9	(1.7)
	15	1.3	(0.2) ,	0.9	(0.2)	4.3	(1.4) ,	2.9	(1.4)	1.7	(0.8) ,	1.2	(0.5)	5.9	(3.3) ,	3.8	(1.9)
	30	1.6	(0.3) ,	1.6	(0.4)	4.2	(1.7) ,	5.8	(2.6)	2.0	(0.9) ,	1.5	(0.6)	6.0	(3.6) ,	4.5	(2.3)
	45	2.1	(0.7) ,	2.4	(0.8)	5.9	(4.0) ,	10.4	(6.1)	2.1	(0.8) ,	1.5	(0.5)	7.4	(3.9) ,	7.2	(4.4)
	60	1.6	(0.4) ,	2.6	(0.7)	2.9	(1.6) ,	6.8	(4.4)	1.8	(0.5) ,	1.9	(0.6)	5.5	(3.0) ,	8.4	(4.0)
135° ground motions	Bridge skew (°) 0	3.3	(1.0) ,	6.8	(1.5)	10.3	(4.7) ,	15.1	(4.1)	2.9	(1.3) ,	4.4	(1.2)	10.5	(6.0) ,	11.9	(5.7)
	15	4.4	(1.2) ,	8.2	(2.2)	10.1	(7.9) ,	14.1	(7.9)	5.3	(2.9) ,	6.5	(2.5)	11.8	(8.6) ,	14.1	(6.7)
	30	6.0	(3.6) ,	7.3	(3.0)	5.0	(3.1) ,	8.4	(5.2)	6.3	(4.4) ,	6.8	(4.0)	8.4	(6.0) ,	9.6	(6.7)
	45	2.3	(1.0) ,	3.4	(1.0)	2.9	(1.1) ,	2.5	(0.9)	8.1	(3.9) ,	7.9	(3.5)	6.7	(3.5) ,	5.9	(3.8)
	60	1.3	(0.3) ,	1.8	(0.3)	1.7	(0.3) ,	1.4	(0.4)	3.2	(1.9) ,	3.9	(2.2)	4.3	(3.0) ,	3.1	(2.1)

Unyielded: normalized strain < 1 (unnormalized strain < 0.0017)

Yielded without signficniant strain hardening: 1 ≤ normalized strain < 10 (0.0017 ≤ unnormalized strain < 0.017)

Yielded and significantly strain hardened: 10 ≤ normalized strain (0.017 ≤ unnormalized strain)

Table C4.4: Occurrences of limit states at expansion piers (Piers 1 and 3) of 4C bridge variants

Limit state	No. of analyses with occurrence [1]	Skew angle[2] (°)					Foundation soil [2]		Column height [2] (m)		Ground motion incident angle [2] (°)			
		0	15	30	45	60	Hard	Soft	4.57	12.19	0	45	90	135
Rupture of retainer anchor (RRA@P1)	0 (0%)	0	0	0	0	0	0	0	0	0	0	0	0	0
Sliding of elastomeric bearing (SEB@P1)	169 (11%)	46 (27%)	60 (36%)	45 (27%)	29 (17%)	11 (7%)	71 (42%)	98 (58%)	106 (63%)	63 (37%)	113 (67%)	56 (33%)	0 (0%)	22 (13%)
Unseating of elastomeric bearing (UEB@P1)	0 (0%)	0	0	0	0	0	0	0	0	0	0	0	0	0
Yielding of vertical reinforcing steel at column end (YRS@P1)	1227 (77%)	209 (17%)	244 (20%)	275 (22%)	266 (22%)	239 (19%)	654 (53%)	579 (47%)	576 (47%)	657 (53%)	301 (25%)	314 (26%)	297 (24%)	321 (26%)
Crushing of concrete cover at column end (CCC@P1)	411 (26%)	65 (16%)	102 (25%)	118 (29%)	68 (17%)	58 (14%)	219 (53%)	192 (47%)	233 (57%)	178 (43%)	138 (34%)	129 (31%)	85 (21%)	59 (14%)
Yielding of pile at pier (YPP@P1)	857 (54%)	132 (15%)	142 (17%)	163 (19%)	209 (24%)	211 (25%)	237 (28%)	620 (72%)	502 (59%)	355 (41%)	137 (16%)	151 (18%)	301 (35%)	268 (31%)
Rupture of retainer anchor (RRA@P3)	0 (0%)	0	0	0	0	0	0	0	0	0	0	0	0	0
Sliding of elastomeric bearing (SEB@P3)	187 (12%)	43 (23%)	54 (29%)	54 (29%)	21 (11%)	15 (8%)	69 (37%)	118 (63%)	104 (56%)	83 (44%)	119 (64%)	51 (27%)	0 (0%)	17 (9%)
Unseating of elastomeric bearing (USB@P3)	0 (0%)	0	0	0	0	0	0	0	0	0	0	0	0	0
Yielding of vertical reinforcing steel at column end (YRS@P3)	1227 (77%)	204 (17%)	235 (19%)	278 (23%)	269 (22%)	241 (20%)	315 (26%)	912 (74%)	571 (47%)	656 (53%)	301 (25%)	309 (25%)	297 (24%)	320 (26%)
Crushing of concrete cover at column end (CCC@P3)	465 (29%)	73 (16%)	100 (22%)	124 (27%)	79 (17%)	89 (19%)	245 (53%)	220 (47%)	259 (56%)	206 (44%)	152 (33%)	140 (30%)	101 (22%)	72 (15%)
Yielding of pile at pier (YPP@P3)	838 (52%)	128 (15%)	133 (16%)	158 (19%)	206 (25%)	213 (25%)	231 (28%)	607 (72%)	495 (59%)	343 (41%)	135 (16%)	137 (16%)	294 (35%)	272 (32%)

1 The number above the parentheses indicates the number of analyses with occurrences of a limit state.
The percentage inside the parentheses indicates the ratio of the number above the parentheses to all the 1,600 analyses.

2 The number above the parentheses indicates the number of analyses with occurrences of a limit state contributed by a parametric variation.
The percentage inside the parentheses indicates the relative contribution of a parametric variation to the total occurrences of a limit state.

Table C4.5: Normalized peak strain of vertical reinforcing steel at pier column base of 4C bridges (peak strains are normalized to the yield strain, 0.0021; numbers outside the parentheses are medians, while those inside are median absolute deviations; data of reinforcing steel at column base of expansion and fixed piers are placed on the left and right sides of the commas, respectively; performance levels in the footnote are defined per Kowalsky (2001) and Revell (2013))

Foundation soil condition			Hard								Soft							
Pier column height (m)			4.57				12.19				4.57				12.19			
Longitudinal (0°) ground motions	Bridge skew (°)	0	8.9	(7.9) ,	16.0	(3.0)	2.8	(1.4) ,	3.0	(1.3)	22.2	(5.0) ,	22.0	(3.9)	3.1	(2.2) ,	3.4	(1.9)
		15	18.5	(7.8) ,	16.4	(3.5)	2.9	(1.8) ,	2.7	(1.8)	24.2	(4.2) ,	23.5	(2.9)	3.7	(2.6) ,	3.6	(2.1)
		30	20.0	(5.4) ,	19.4	(3.9)	2.8	(1.8) ,	3.0	(1.7)	21.1	(3.9) ,	24.3	(0.9)	3.0	(1.8) ,	3.5	(2.1)
		45	1.3	(0.4) ,	2.4	(0.5)	3.6	(2.5) ,	3.7	(2.2)	1.2	(0.3) ,	5.5	(1.1)	3.0	(2.2) ,	4.0	(2.4)
		60	0.9	(0.1) ,	1.0	(0.1)	1.5	(0.8) ,	2.2	(0.4)	0.6	(0.1) ,	1.2	(0.1)	1.9	(1.4) ,	3.4	(2.1)
45° ground motions	Bridge skew (°)	0	0.9	(0.1) ,	9.8	(1.8)	2.1	(1.2) ,	3.0	(1.7)	1.0	(0.1) ,	11.0	(1.4)	2.0	(1.4) ,	2.1	(1.1)
		15	1.4	(0.4) ,	12.3	(2.7)	2.0	(1.2) ,	2.6	(1.5)	14.5	(7.7) ,	18.3	(3.6)	2.6	(1.6) ,	2.8	(1.8)
		30	13.4	(7.8) ,	14.6	(3.4)	2.8	(2.0) ,	3.3	(1.7)	18.0	(6.2) ,	20.5	(2.1)	2.7	(1.7) ,	3.7	(2.2)
		45	4.9	(3.5) ,	6.9	(1.9)	3.5	(2.0) ,	4.3	(1.9)	8.5	(6.7) ,	17.3	(4.0)	3.1	(2.2) ,	4.7	(3.0)
		60	4.4	(2.4) ,	4.1	(1.3)	4.0	(2.6) ,	5.9	(2.9)	2.6	(1.5) ,	5.3	(1.7)	4.2	(3.3) ,	5.8	(3.2)
Transverse (90°) ground motions	Bridge skew (°)	0	0.8	(0.1) ,	1.1	(0.2)	4.2	(1.6) ,	5.8	(2.1)	0.6	(0.1) ,	0.7	(0.1)	2.5	(0.5) ,	3.4	(0.6)
		15	0.9	(0.2) ,	1.3	(0.2)	5.2	(1.9) ,	7.0	(2.3)	0.8	(0.1) ,	1.9	(0.7)	2.9	(0.7) ,	3.9	(0.9)
		30	1.6	(0.6) ,	1.6	(0.4)	5.2	(2.3) ,	6.8	(2.3)	1.1	(0.3) ,	4.2	(2.3)	3.2	(1.1) ,	4.5	(1.3)
		45	3.4	(2.0) ,	1.7	(0.5)	3.3	(1.3) ,	5.0	(1.7)	1.7	(0.8) ,	7.2	(2.7)	2.7	(1.2) ,	3.3	(1.0)
		60	7.6	(4.2) ,	4.1	(1.4)	2.9	(1.6) ,	3.3	(1.7)	4.8	(3.2) ,	10.5	(3.2)	3.2	(1.8) ,	4.0	(2.2)
135° ground motions	Bridge skew (°)	0	0.9	(0.1) ,	9.8	(2.0)	2.2	(1.1) ,	2.8	(1.6)	1.1	(0.2) ,	11.3	(1.5)	1.8	(1.2) ,	2.1	(1.1)
		15	1.0	(0.1) ,	7.3	(2.7)	2.7	(1.0) ,	3.6	(1.3)	1.1	(0.2) ,	11.7	(1.6)	2.1	(1.2) ,	3.0	(1.4)
		30	1.8	(0.7) ,	5.1	(2.1)	4.1	(1.1) ,	6.4	(1.4)	1.4	(0.5) ,	9.1	(2.7)	2.5	(0.8) ,	3.8	(1.1)
		45	1.6	(0.4) ,	1.6	(0.1)	4.3	(1.8) ,	4.9	(1.9)	1.0	(0.2) ,	5.0	(0.7)	1.7	(0.4) ,	2.2	(0.4)
		60	2.1	(0.5) ,	1.6	(0.1)	3.0	(1.4) ,	1.9	(0.3)	1.7	(0.4) ,	2.6	(0.6)	1.4	(0.2) ,	1.6	(0.2)

Undamaged (unyielded):	normalized strain < 1 (unnormalized strain < 0.0021)
Lightly damaged (unlikely requiring repair):	1 ≤ normalized strain < 7.1 (0.0021 ≤ unnormalized strain < 0.015)
Moderately damaged (repairable):	7.1 ≤ normalized strain < 28.6 (0.015 ≤ unnormalized strain < 0.06)
Severely damaged (not easily repairable):	28.6 ≤ normalized strain (0.06 ≤ unnormalized strain)

Table C4.6: Normalized peak strain of concrete cover at pier column base of 4C bridges (peak strains are normalized to the crushing strain, 0.005; numbers outside the parentheses are medians, while those inside are median absolute deviations; data of concrete cover at column base of expansion and fixed piers are placed on the left and right sides of the commas, respectively; performance levels in the footnote are defined per Kowalsky (2001) and Revell (2013))

Foundation soil condition			Hard				Soft			
Pier column height (m)			4.57		12.19		4.57		12.19	
Longitudinal (0°) ground motions	Bridge skew (°)	0	2.0 (1.7) ,	3.1 (0.6)	0.6 (0.2) ,	0.6 (0.2)	5.1 (1.4) ,	4.4 (0.9)	0.6 (0.4) ,	0.6 (0.2)
		15	4.3 (2.0) ,	3.4 (0.8)	0.6 (0.3) ,	0.5 (0.2)	5.8 (1.3) ,	5.1 (0.9)	0.7 (0.4) ,	0.7 (0.3)
		30	4.5 (1.4) ,	4.2 (0.9)	0.5 (0.3) ,	0.6 (0.3)	4.9 (1.0) ,	5.5 (0.4)	0.6 (0.3) ,	0.7 (0.3)
		45	0.4 (0.1) ,	0.5 (0.1)	0.6 (0.4) ,	0.7 (0.3)	0.4 (0.1) ,	1.2 (0.3)	0.6 (0.4) ,	0.8 (0.4)
		60	0.3 (0.0) ,	0.3 (0.0)	0.4 (0.1) ,	0.4 (0.1)	0.2 (0.0) ,	0.3 (0.0)	0.4 (0.3) ,	0.6 (0.3)
45° ground motions	Bridge skew (°)	0	0.3 (0.0) ,	1.9 (0.3)	0.5 (0.2) ,	0.7 (0.3)	0.3 (0.0) ,	2.0 (0.3)	0.4 (0.2) ,	0.5 (0.2)
		15	0.4 (0.1) ,	2.5 (0.6)	0.4 (0.2) ,	0.5 (0.2)	3.1 (1.8) ,	3.9 (1.0)	0.5 (0.3) ,	0.6 (0.2)
		30	2.9 (1.8) ,	2.9 (0.7)	0.6 (0.3) ,	0.5 (0.2)	4.1 (1.6) ,	4.4 (0.6)	0.6 (0.3) ,	0.7 (0.3)
		45	1.0 (0.6) ,	1.3 (0.3)	0.6 (0.3) ,	0.7 (0.3)	1.6 (1.3) ,	3.4 (0.9)	0.6 (0.4) ,	0.8 (0.4)
		60	0.8 (0.4) ,	0.8 (0.3)	0.7 (0.4) ,	1.0 (0.4)	0.5 (0.2) ,	1.0 (0.3)	0.8 (0.5) ,	0.9 (0.4)
Transverse (90°) ground motions	Bridge skew (°)	0	0.3 (0.0) ,	0.4 (0.0)	0.9 (0.3) ,	1.2 (0.5)	0.2 (0.0) ,	0.3 (0.0)	0.6 (0.1) ,	0.7 (0.1)
		15	0.3 (0.0) ,	0.4 (0.0)	1.2 (0.5) ,	1.5 (0.5)	0.3 (0.0) ,	0.4 (0.1)	0.7 (0.1) ,	0.9 (0.2)
		30	0.4 (0.1) ,	0.4 (0.0)	1.2 (0.5) ,	1.6 (0.5)	0.3 (0.0) ,	0.7 (0.4)	0.7 (0.2) ,	1.0 (0.2)
		45	0.6 (0.3) ,	0.4 (0.1)	0.6 (0.2) ,	1.0 (0.4)	0.4 (0.1) ,	1.2 (0.6)	0.5 (0.1) ,	0.6 (0.2)
		60	1.4 (0.8) ,	0.8 (0.3)	0.5 (0.2) ,	0.6 (0.2)	0.9 (0.5) ,	1.9 (0.7)	0.5 (0.3) ,	0.6 (0.3)
135° ground motions	Bridge skew (°)	0	0.3 (0.0) ,	2.0 (0.5)	0.5 (0.2) ,	0.6 (0.2)	0.4 (0.0) ,	2.4 (0.3)	0.5 (0.2) ,	0.5 (0.2)
		15	0.3 (0.0) ,	1.5 (0.7)	0.6 (0.2) ,	0.7 (0.2)	0.4 (0.1) ,	2.5 (0.4)	0.5 (0.2) ,	0.6 (0.2)
		30	0.5 (0.1) ,	1.1 (0.5)	0.9 (0.2) ,	1.3 (0.2)	0.4 (0.1) ,	2.0 (0.7)	0.6 (0.1) ,	0.8 (0.2)
		45	0.4 (0.0) ,	0.4 (0.0)	0.9 (0.3) ,	1.0 (0.3)	0.3 (0.0) ,	0.9 (0.2)	0.4 (0.0) ,	0.5 (0.1)
		60	0.4 (0.0) ,	0.4 (0.0)	0.6 (0.2) ,	0.5 (0.0)	0.4 (0.1) ,	0.5 (0.1)	0.4 (0.0) ,	0.4 (0.0)

Undamaged (ultimate strength not mobillized):	normalized strain < 0.4 (unnormalized strain < 0.002)
Lightly damaged (ultimate strength mobilized but uncrushed):	0.4 ≤ normalized strain < 1 (0.002 ≤ unnormalized strain < 0.005)
Moderately damaged (crushed but repairable):	1 ≤ normalized strain < 3.6 (0.005 ≤ unnormalized strain < 0.018)
Severely damaged (not easily repairable):	3.6 ≤ normalized strain (0.018 ≤ unnormalized strain)

Table C4.7: Normalized peak strains of steel H piles at piers of 4C bridges (peak strains are normalized to the yield strain, 0.0017; numbers outside the parentheses are medians, while those inside are median absolute deviations; data for piles supporting expansion and fixed piers are placed on the left and right sides of the commas, respectively)

Foundation soil condition			Hard				Soft			
Pier column height (m)			4.57		12.19		4.57		12.19	
Longitudinal (0°) ground motions	Bridge skew (°)	0	0.4 (0.0) ,	0.4 (0.0)	0.4 (0.0) ,	0.4 (0.0)	0.6 (0.0) ,	0.5 (0.0)	0.4 (0.0) ,	0.4 (0.0)
		15	0.6 (0.1) ,	0.6 (0.0)	0.5 (0.0) ,	0.5 (0.0)	1.0 (0.2) ,	0.9 (0.1)	0.6 (0.1) ,	0.6 (0.0)
		30	0.9 (0.1) ,	0.9 (0.0)	0.6 (0.1) ,	0.7 (0.0)	1.9 (0.6) ,	1.7 (0.6)	0.9 (0.1) ,	0.9 (0.1)
		45	0.9 (0.2) ,	0.9 (0.0)	0.9 (0.1) ,	1.0 (0.1)	3.6 (2.3) ,	2.2 (0.2)	1.5 (0.7) ,	1.9 (0.5)
		60	1.1 (0.2) ,	1.1 (0.1)	1.0 (0.2) ,	1.2 (0.1)	6.0 (3.9) ,	6.3 (1.7)	2.6 (1.7) ,	8.2 (4.3)
45° ground motions	Bridge skew (°)	0	0.9 (0.0) ,	1.0 (0.1)	0.9 (0.1) ,	0.9 (0.0)	1.5 (0.2) ,	1.9 (0.4)	1.4 (0.2) ,	1.5 (0.3)
		15	0.8 (0.1) ,	0.9 (0.1)	0.7 (0.0) ,	0.8 (0.0)	1.4 (0.2) ,	1.4 (0.2)	1.1 (0.2) ,	1.2 (0.1)
		30	0.8 (0.0) ,	1.0 (0.0)	0.6 (0.0) ,	0.6 (0.0)	1.6 (0.2) ,	1.6 (0.2)	1.0 (0.1) ,	1.0 (0.1)
		45	0.9 (0.1) ,	1.1 (0.0)	0.5 (0.1) ,	0.6 (0.0)	1.9 (0.6) ,	2.7 (0.6)	0.8 (0.1) ,	0.9 (0.1)
		60	0.9 (0.1) ,	0.8 (0.1)	0.6 (0.1) ,	0.7 (0.1)	1.8 (0.3) ,	3.1 (0.3)	0.9 (0.2) ,	0.9 (0.2)
Transverse (90°) ground motions	Bridge skew (°)	0	1.1 (0.2) ,	1.4 (0.2)	0.9 (0.0) ,	0.9 (0.0)	5.2 (3.2) ,	7.7 (3.8)	4.9 (2.9) ,	6.9 (1.9)
		15	1.1 (0.1) ,	1.3 (0.2)	0.9 (0.0) ,	0.9 (0.0)	5.2 (3.4) ,	7.2 (4.5)	4.7 (2.7) ,	6.4 (1.9)
		30	1.2 (0.2) ,	1.4 (0.1)	0.9 (0.0) ,	0.9 (0.0)	4.8 (2.7) ,	6.7 (3.7)	3.0 (1.0) ,	4.5 (0.5)
		45	1.5 (0.4) ,	1.3 (0.1)	1.1 (0.1) ,	1.1 (0.0)	4.4 (2.4) ,	3.8 (2.1)	3.2 (1.9) ,	6.6 (2.3)
		60	1.0 (0.1) ,	1.1 (0.1)	1.0 (0.1) ,	1.1 (0.0)	2.0 (0.7) ,	2.1 (0.5)	1.8 (0.7) ,	3.6 (1.8)
135° ground motions	Bridge skew (°)	0	0.9 (0.1) ,	1.0 (0.1)	0.9 (0.1) ,	0.9 (0.0)	1.5 (0.2) ,	1.9 (0.4)	1.4 (0.2) ,	1.5 (0.3)
		15	0.9 (0.1) ,	1.2 (0.1)	0.9 (0.1) ,	0.9 (0.0)	2.6 (0.8) ,	4.5 (1.3)	2.3 (0.9) ,	2.6 (1.1)
		30	1.1 (0.1) ,	1.1 (0.1)	0.9 (0.0) ,	0.9 (0.0)	4.4 (2.9) ,	7.4 (4.1)	3.1 (1.2) ,	4.8 (0.9)
		45	1.4 (0.2) ,	1.3 (0.1)	1.2 (0.1) ,	1.2 (0.0)	7.4 (4.9) ,	10.1 (3.8)	6.5 (3.2) ,	12.8 (2.7)
		60	1.3 (0.2) ,	1.2 (0.0)	1.3 (0.2) ,	1.3 (0.1)	7.8 (5.0) ,	10.4 (2.7)	6.0 (3.7) ,	15.3 (5.2)

Unyielded: normalized strain < 1 (unnormalized strain < 0.0017)

Yielded without signficniant strain hardening: 1 ≤ normalized strain < 10 (0.0017 ≤ unnormalized strain < 0.017)

Yielded and significantly strain hardened: 10 ≤ normalized strain (0.017 ≤ unnormalized strain)

Table C4.8: Occurrences of limit states at fixed piers (Pier 2) of 4C bridge variants

Limit state	No. of analyses with occurrence [1]	Skew angle [2] (°)					Foundation soil [2]		Column height [2] (m)		Ground motion incident angle [2] (°)			
		0	15	30	45	60	Hard	Soft	4.57	12.19	0	45	90	135
Rupture of retainer anchor (RRA@P2)	68 (4%)	0 (0%)	1 (1%)	6 (9%)	21 (31%)	40 (59%)	63 (93%)	5 (7%)	47 (69%)	21 (31%)	0 (0%)	0 (0%)	34 (50%)	34 (50%)
Rupture of steel dowel connection (RSD@P2)	523 (33%)	26 (5%)	37 (7%)	75 (14%)	163 (31%)	222 (42%)	353 (67%)	170 (33%)	432 (83%)	91 (17%)	117 (22%)	92 (18%)	147 (28%)	167 (32%)
Yielding of vertical reinforcing steel at column end (YRS@P2)	1478 (92%)	278 (19%)	295 (20%)	304 (21%)	307 (21%)	294 (20%)	752 (51%)	726 (49%)	752 (51%)	726 (49%)	356 (24%)	370 (25%)	359 (24%)	393 (27%)
Crushing of concrete cover at column end (CCC@P2)	694 (43%)	158 (23%)	157 (23%)	186 (27%)	119 (17%)	74 (11%)	333 (48%)	361 (52%)	467 (67%)	227 (33%)	181 (26%)	227 (33%)	131 (19%)	155 (22%)
Yielding of pile at pier (YPP@P2)	1018 (64%)	162 (16%)	164 (16%)	186 (18%)	253 (25%)	253 (25%)	352 (35%)	666 (65%)	607 (60%)	411 (40%)	154 (15%)	205 (20%)	333 (33%)	326 (32%)

1 The number above the parentheses indicates the number of analyses with occurrences of a limit state.
The percentage inside the parentheses indicates the ratio of the number above the parentheses to all the 1,600 analyses.
2 The number above the parentheses indicates the number of analyses with occurrences of a limit state contributed by a parametric variation.
The percentage inside the parentheses indicates the relative contribution of a parametric variation to the total occurrences of a limit state.

APPENDIX D: ADDITIONAL RESULTS FOR CHAPTER 5

D.1 ADDITIONAL ANALYSIS RESULTS FOR SECTION 5.1

D.1.1 4S60P40S Bridge Variant

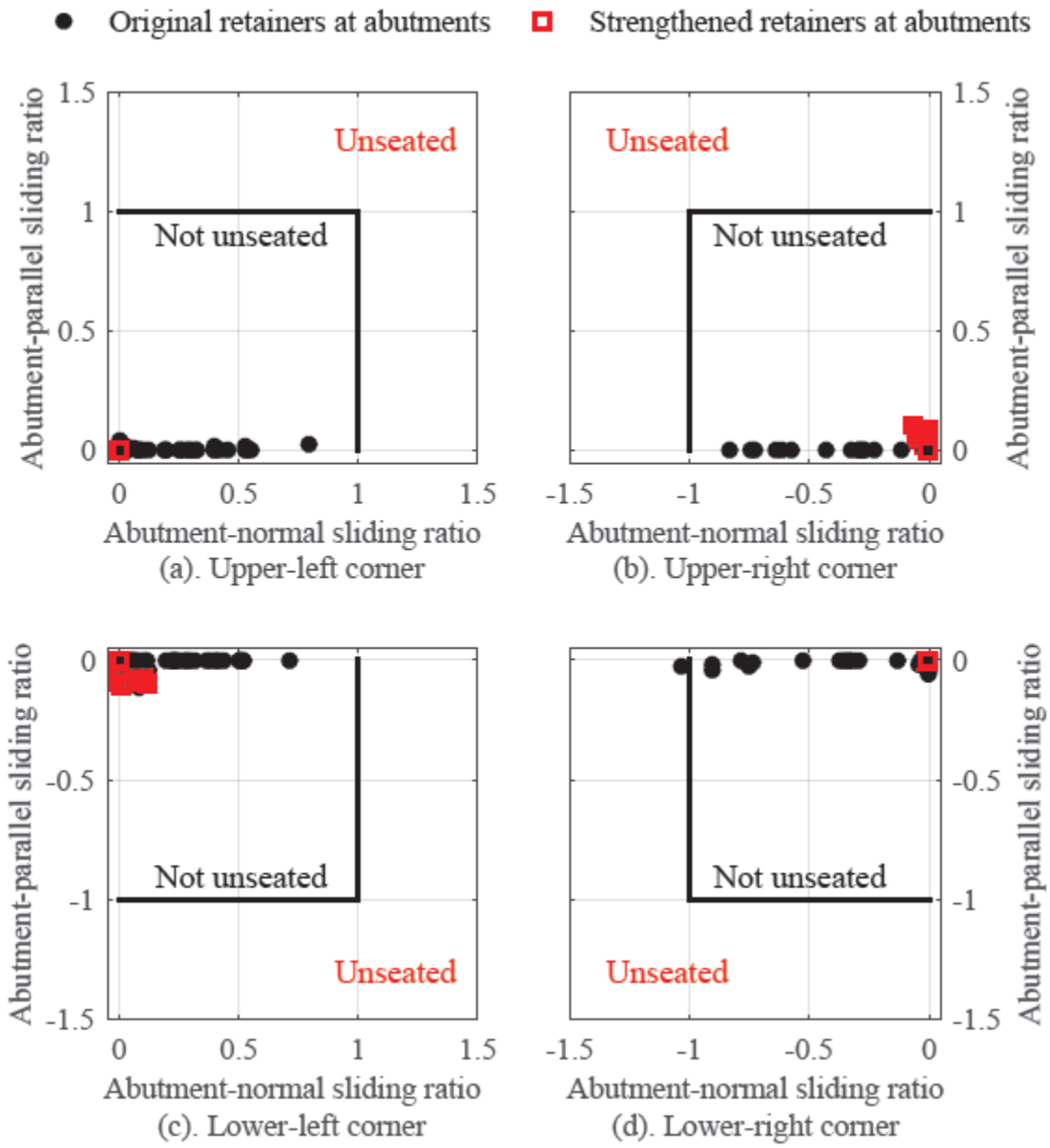

Figure D.1: Comparison of peak sliding distance of elastomeric bearings at deck corners of 4S60P40S bridge variant with original and strengthened retainer anchorage at abutments.

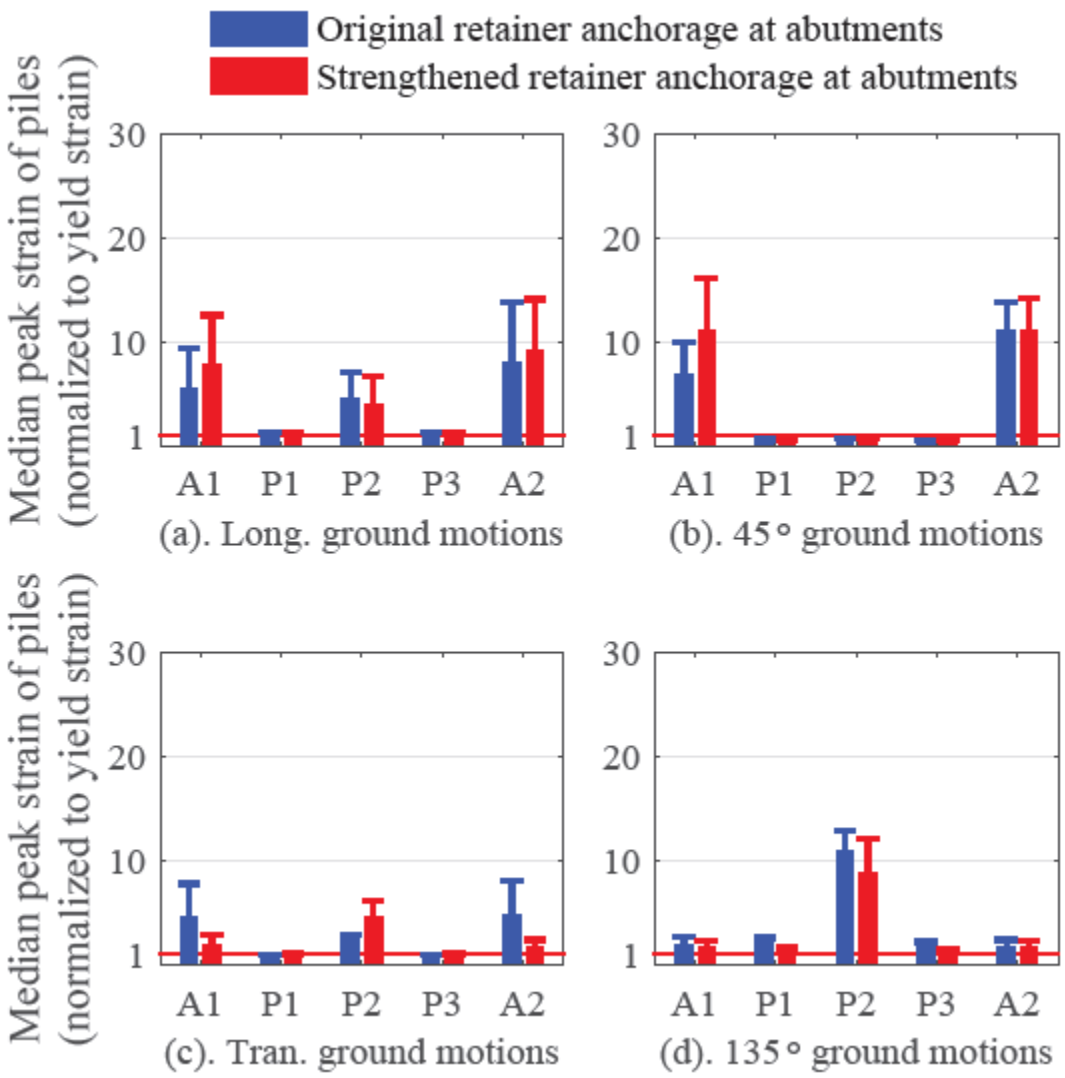

Figure D.2: Comparison of peak pile strain (median + median absolute deviation) of 4S60P40S bridge variant with original and strengthened retainer anchorage at abutments.

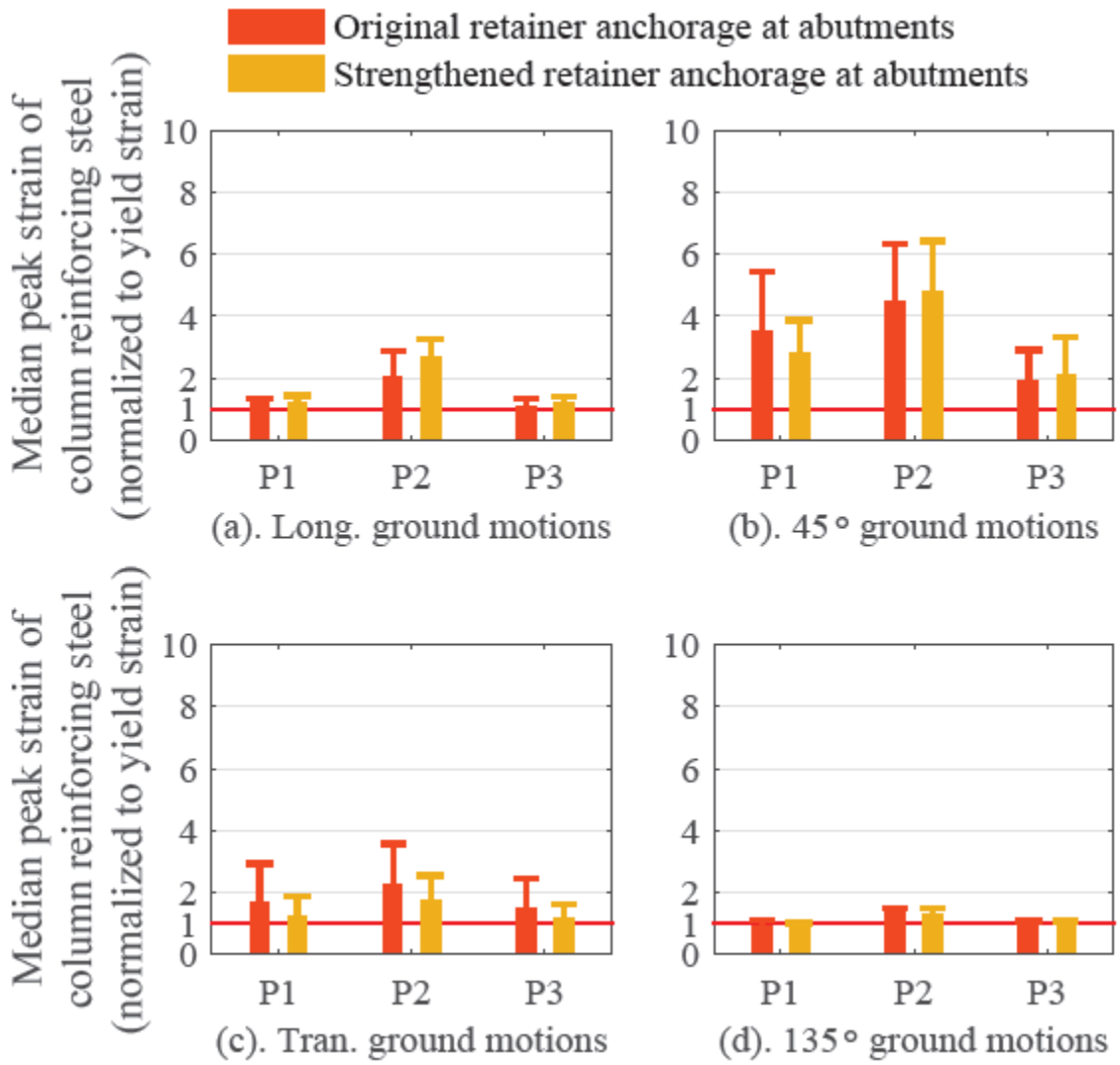

Figure D.3: Comparison of peak strain (median + median absolute deviation) of reinforcing steel at pier column bases of 4S60P40S bridge variant with original and strengthened retainer anchorage at abutments.

D.1.2 3C60P40S Bridge Variant

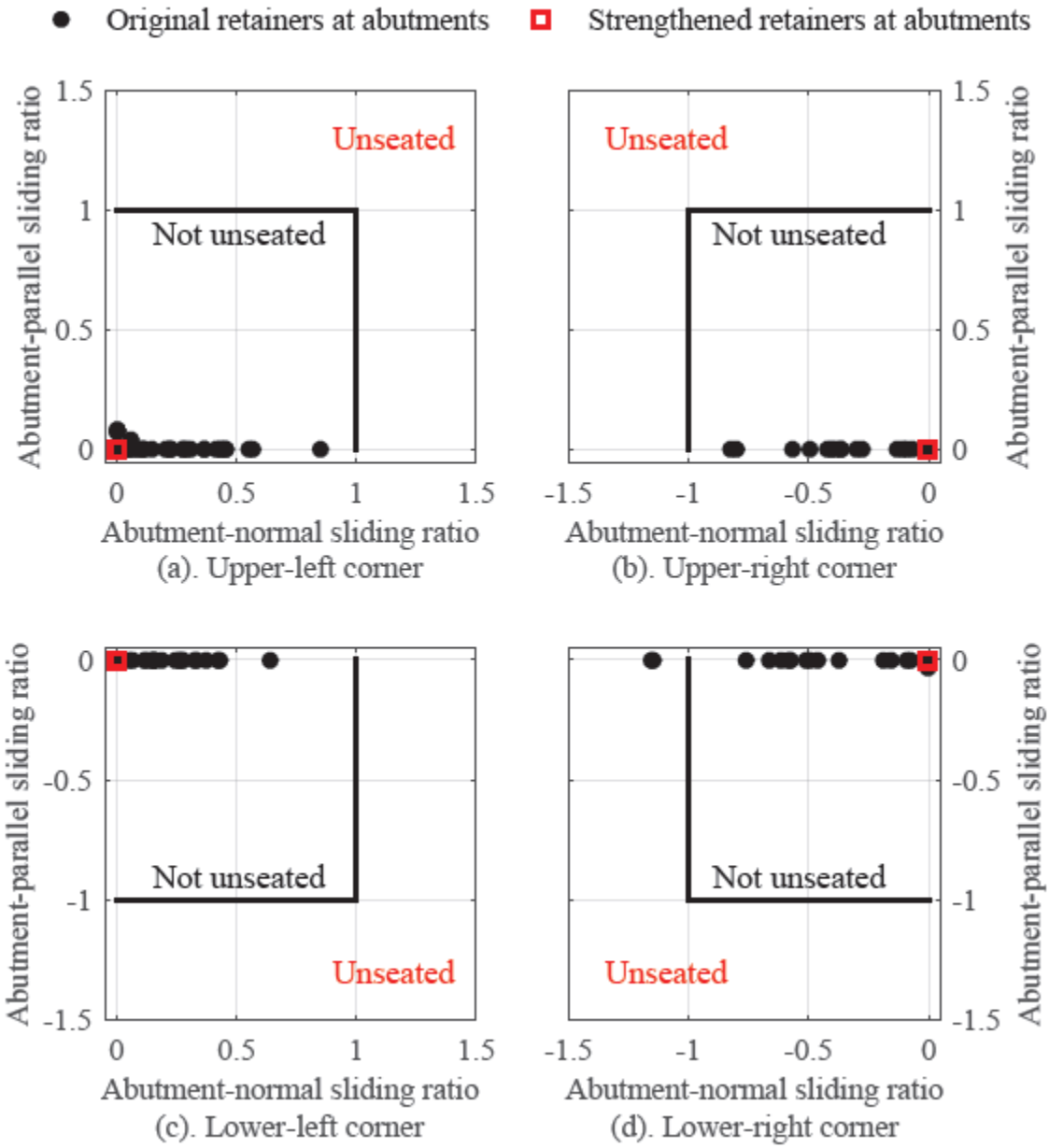

Figure D.4: Comparison of peak sliding distance of elastomeric bearings at deck corners of 3C60P40S bridge variant with original and strengthened retainer anchorage at abutments.

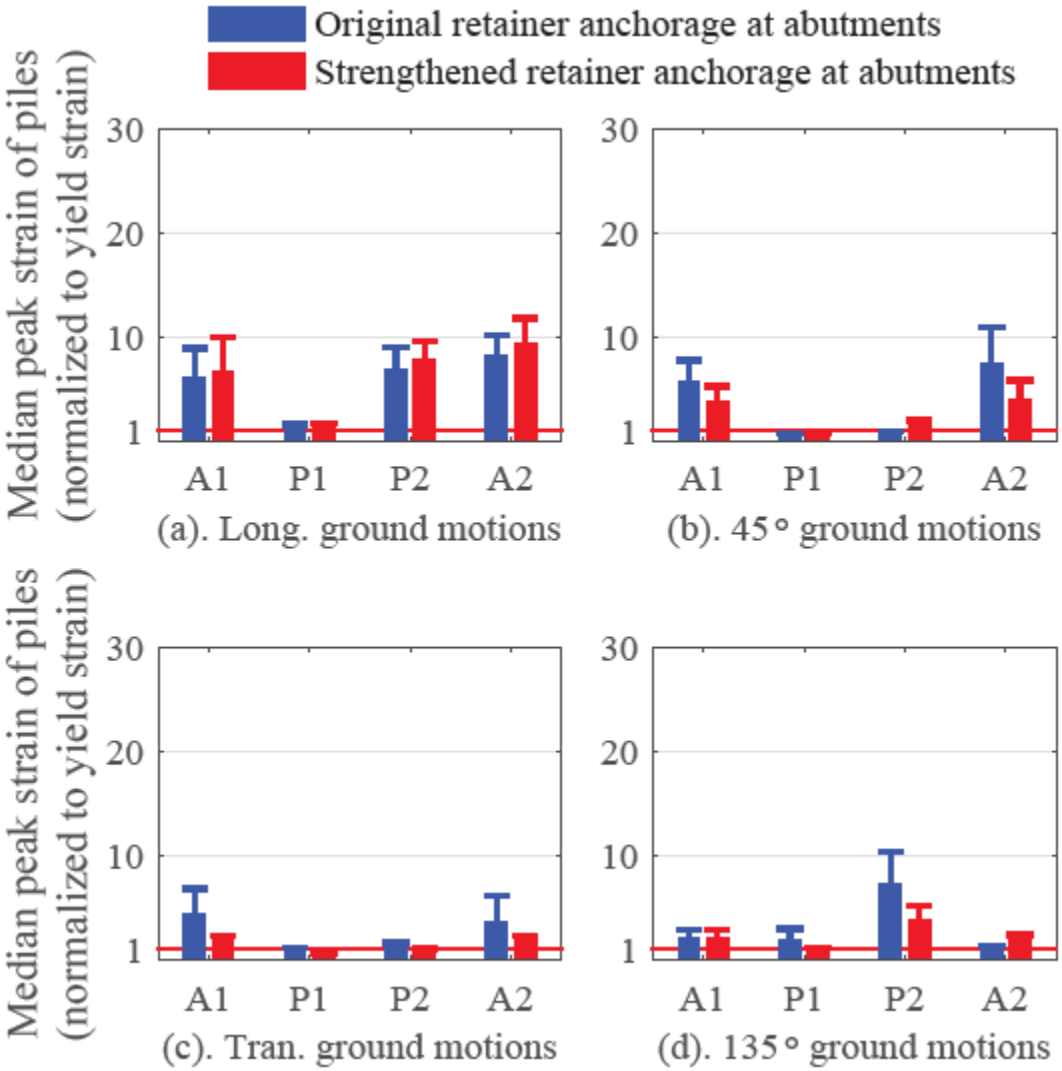

Figure D.5: Comparison of peak pile strain (median + median absolute deviation) of 3C60P40S bridge variant with original and strengthened retainer anchorage at abutments.

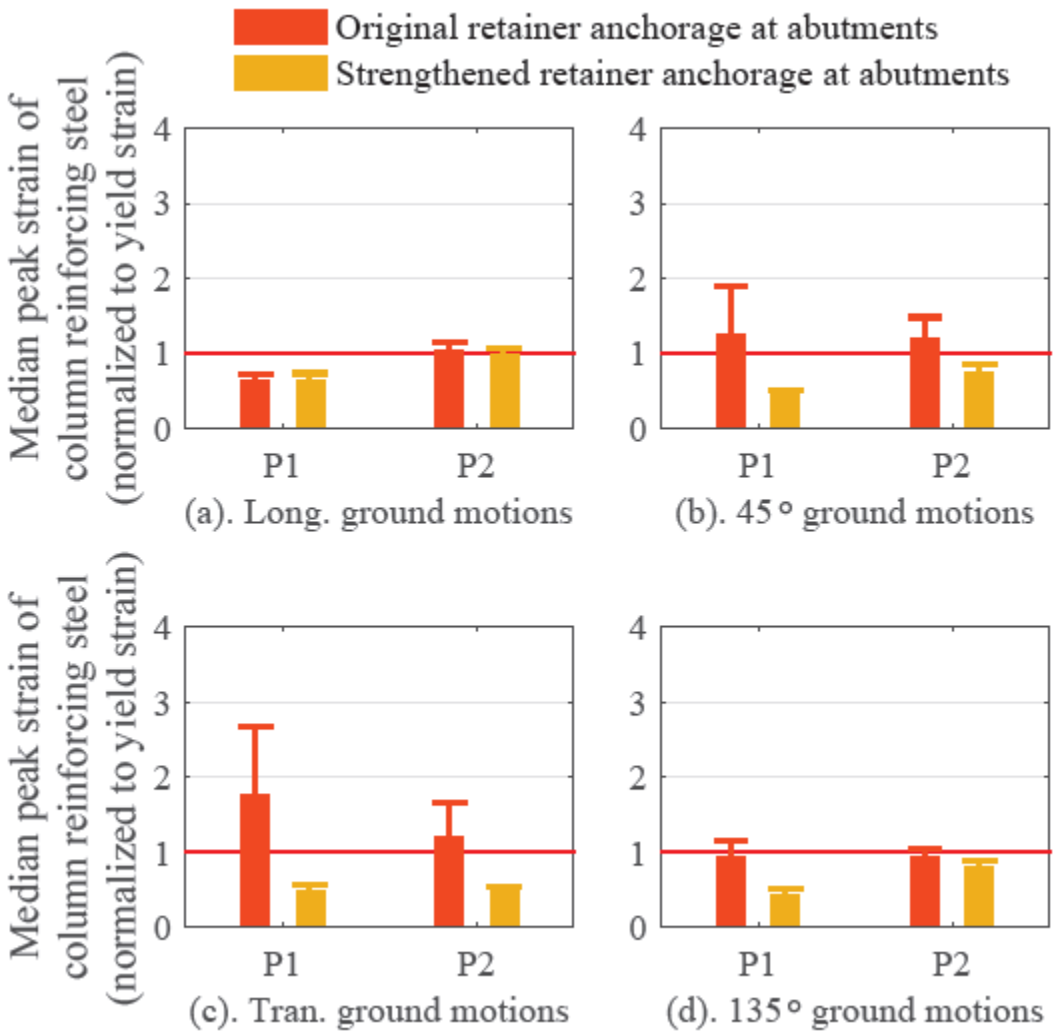

Figure D.6: Comparison of peak strain (median + median absolute deviation) of reinforcing steel at pier column bases of 3C60P40S bridge variant with original and strengthened retainer anchorage at abutments.

D.1.3 4C45P40H Bridge Variant

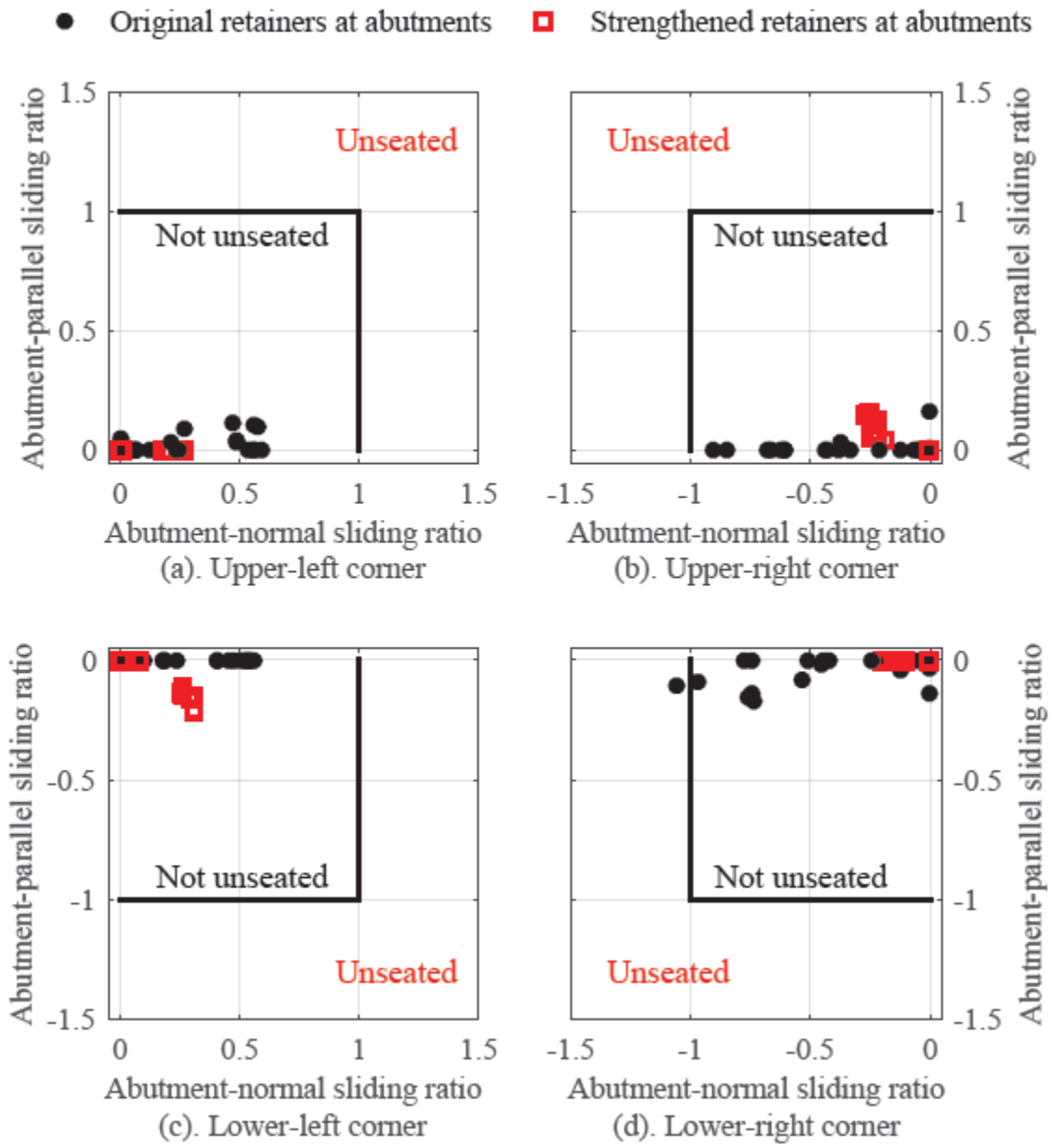

Figure D.7: Comparison of peak sliding distance of elastomeric bearings at deck corners of 4C45P40H bridge variant with original and strengthened retainer anchorage at abutments.

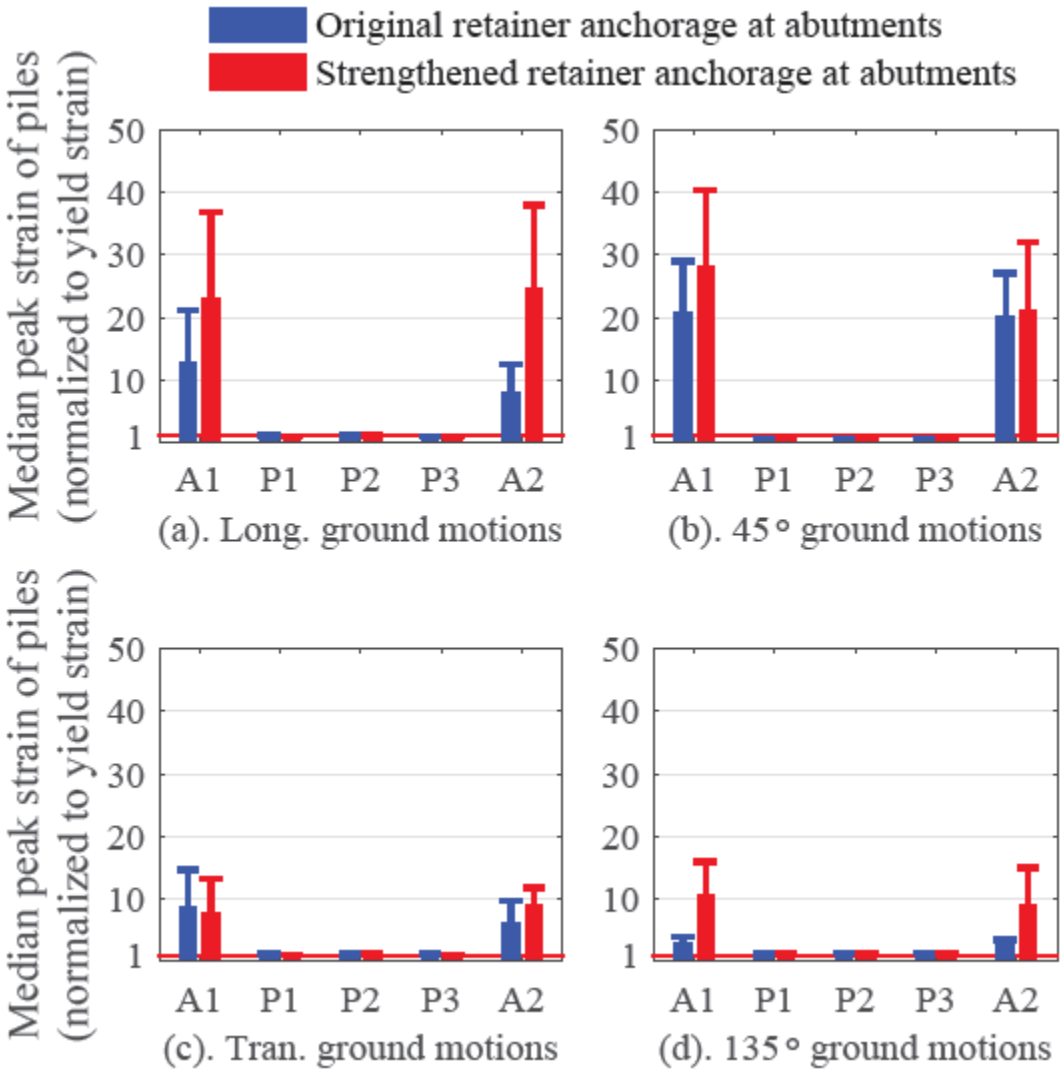

Figure D.8: Comparison of peak pile strain (median + median absolute deviation) of 4C45P40H bridge variant with original and strengthened retainer anchorage at abutments.

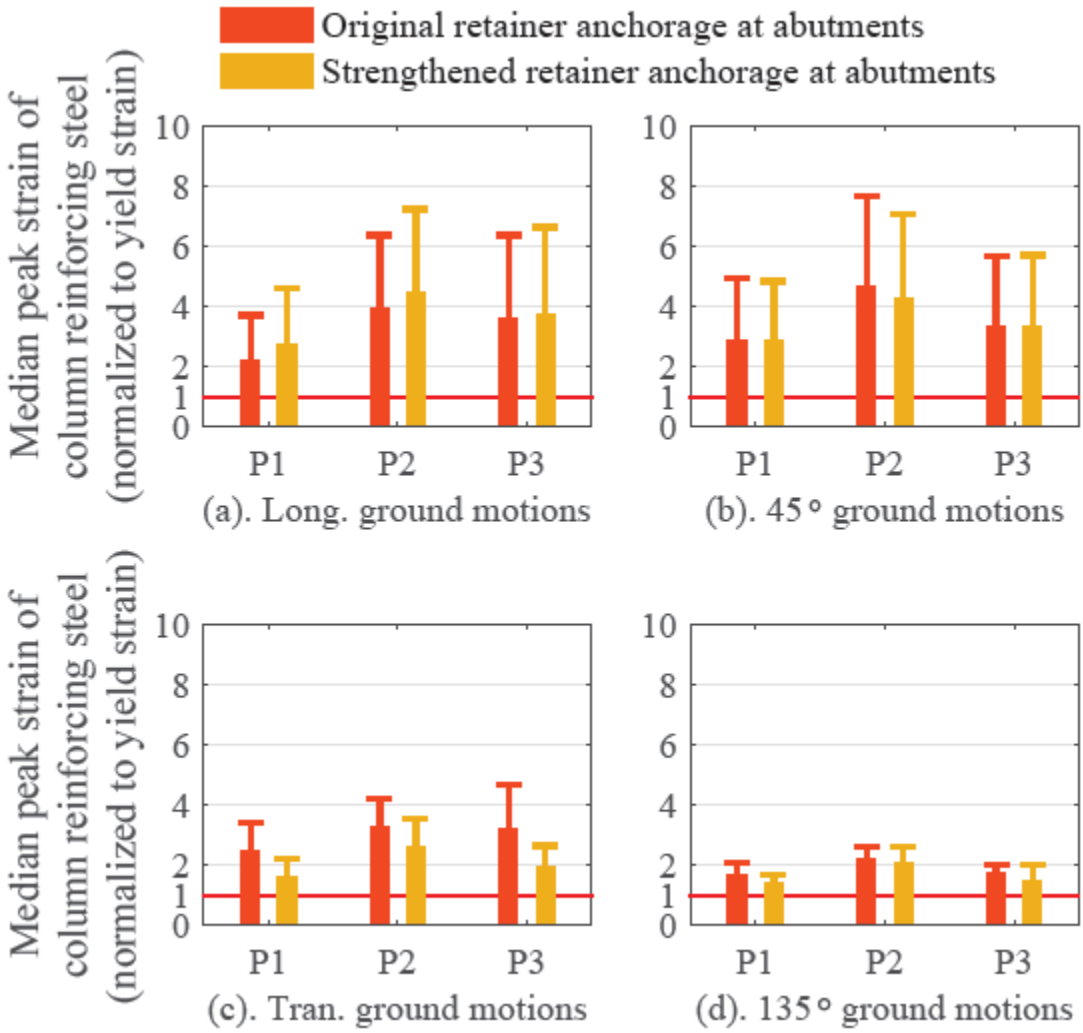

Figure D.9: Comparison of peak strain (median + median absolute deviation) of reinforcing steel at pier column bases of 4C45P40H bridge variant with original and strengthened retainer anchorage at abutments.

D.1.4 4C60P40H Bridge Variant

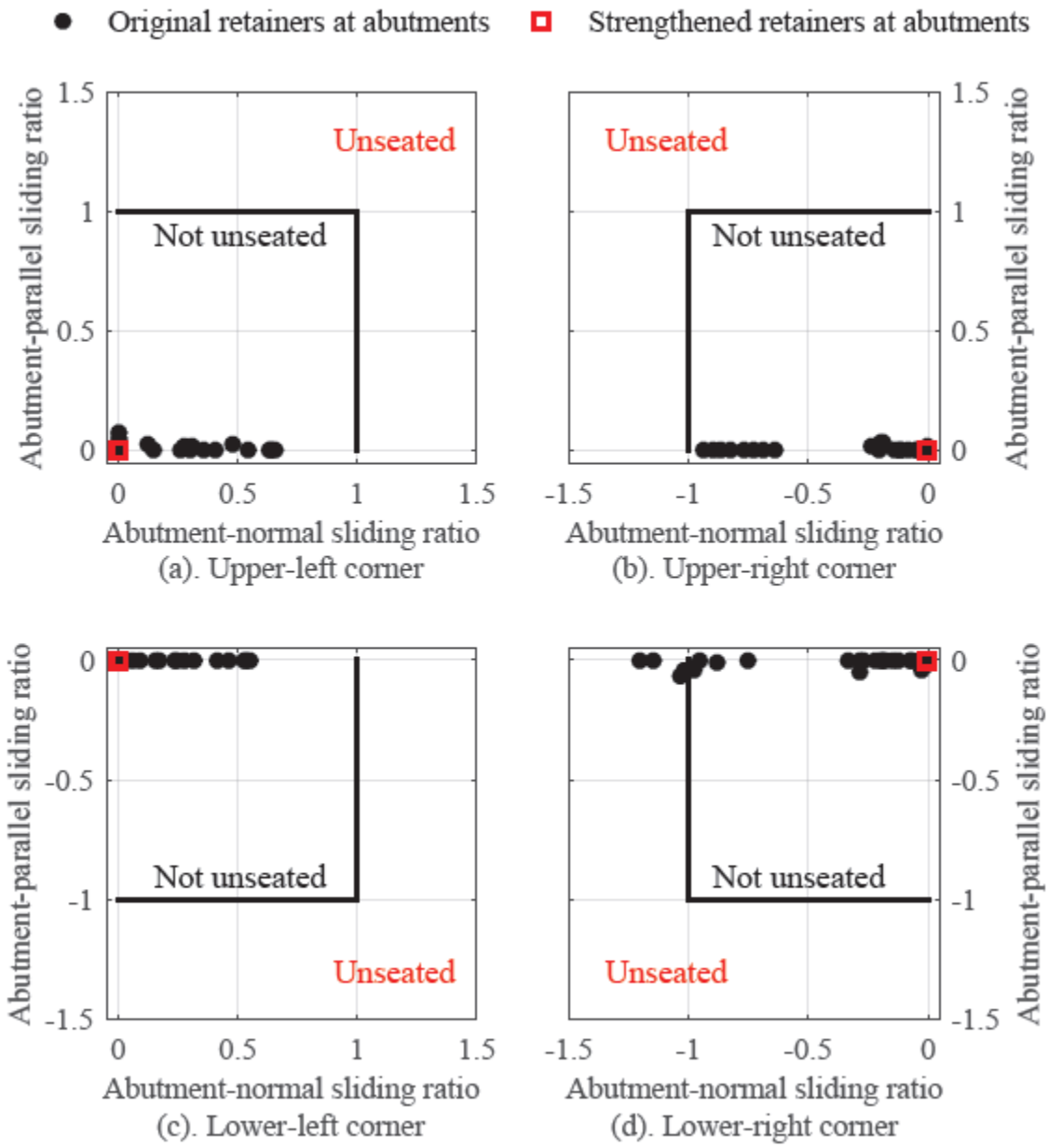

Figure D.10: Comparison of peak sliding distance of elastomeric bearings at deck corners of 4C60P40H bridge variant with original and strengthened retainer anchorage at abutments.

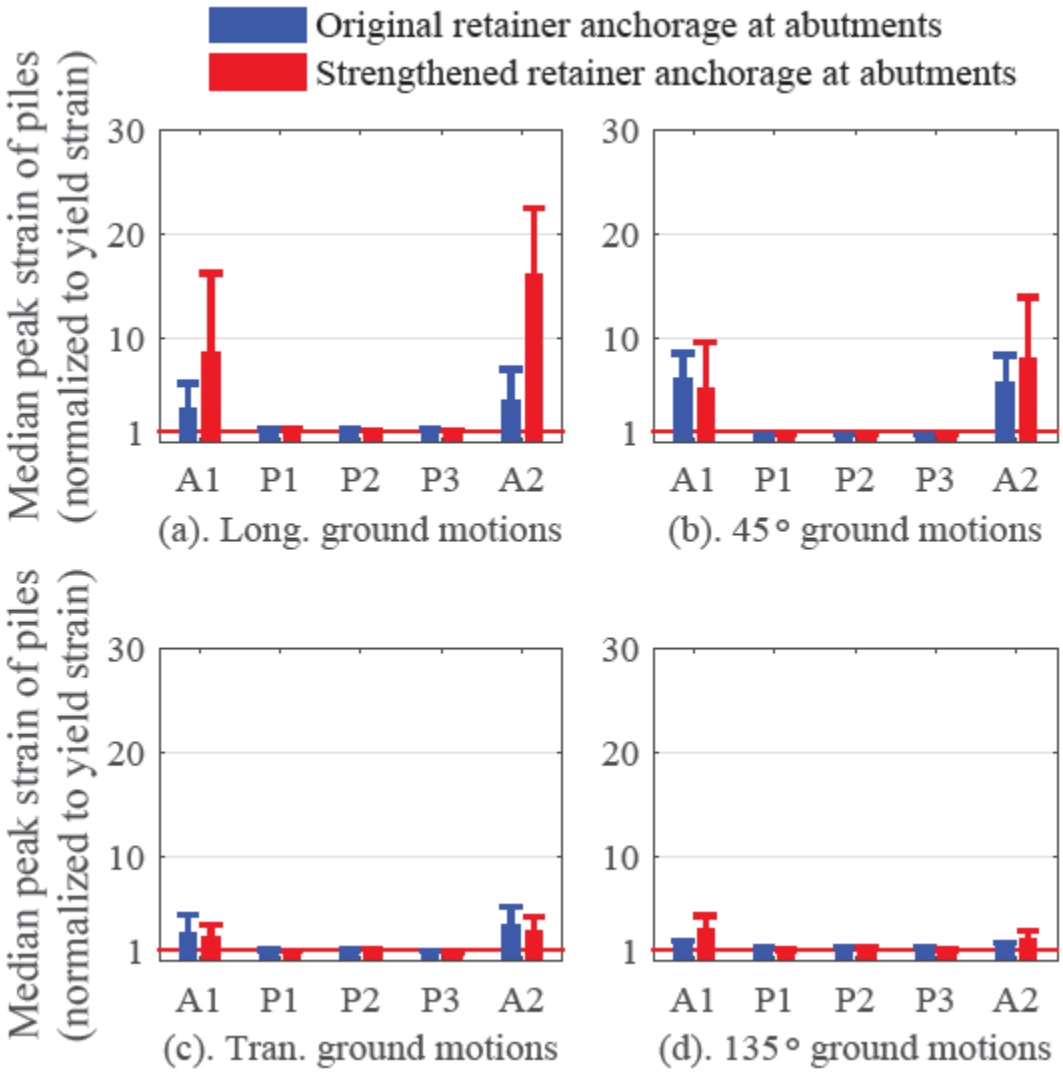

Figure D.11: Comparison of peak pile strain (median + median absolute deviation) of 4C60P40H bridge variant with original and strengthened retainer anchorage at abutments.

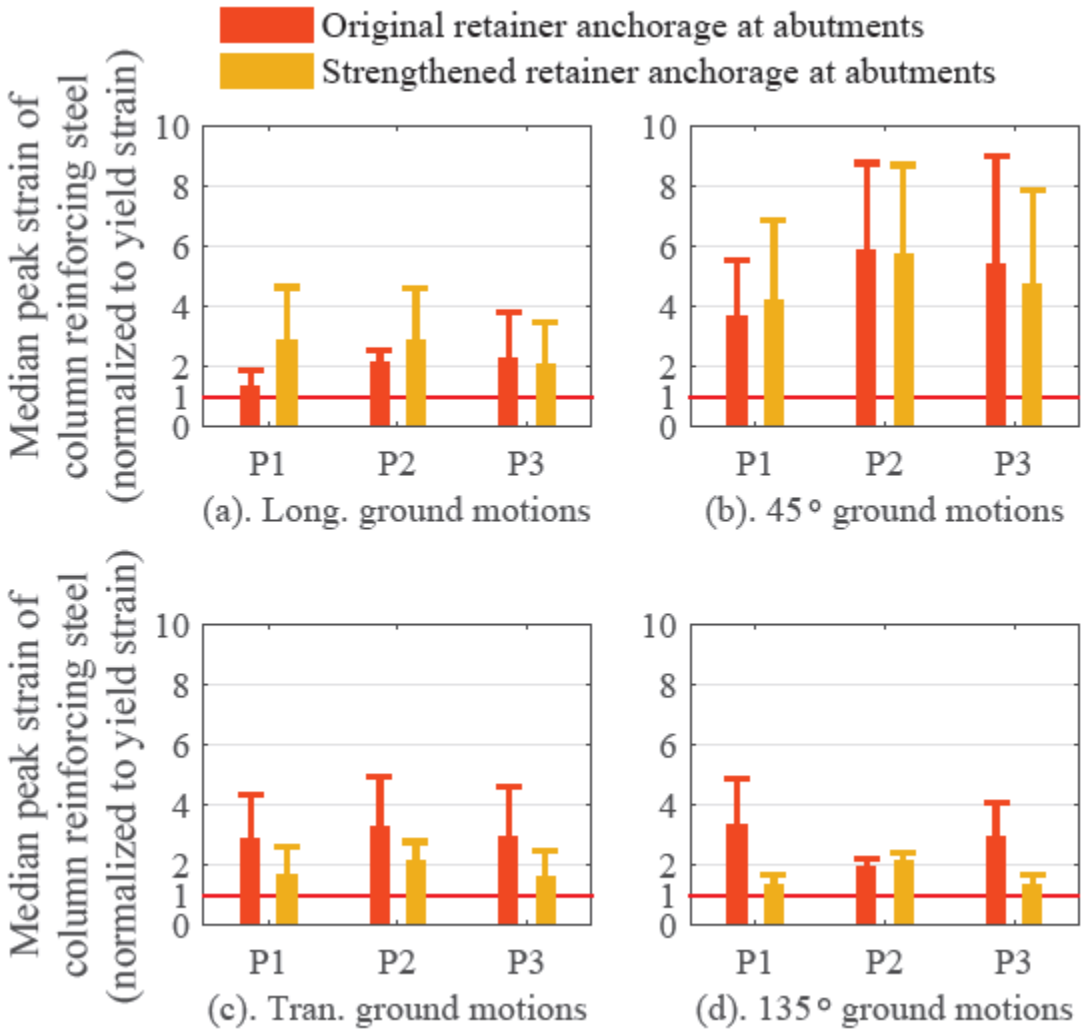

Figure D.12: Comparison of peak strain (median + median absolute deviation) of reinforcing steel at pier column bases of 4C60P40H bridge variant with original and strengthened retainer anchorage at abutments.

D.2 ADDITIONAL ANALYSIS RESULTS FOR SECTION 5.2

D.2.1 3S00P15S Bridge Variant

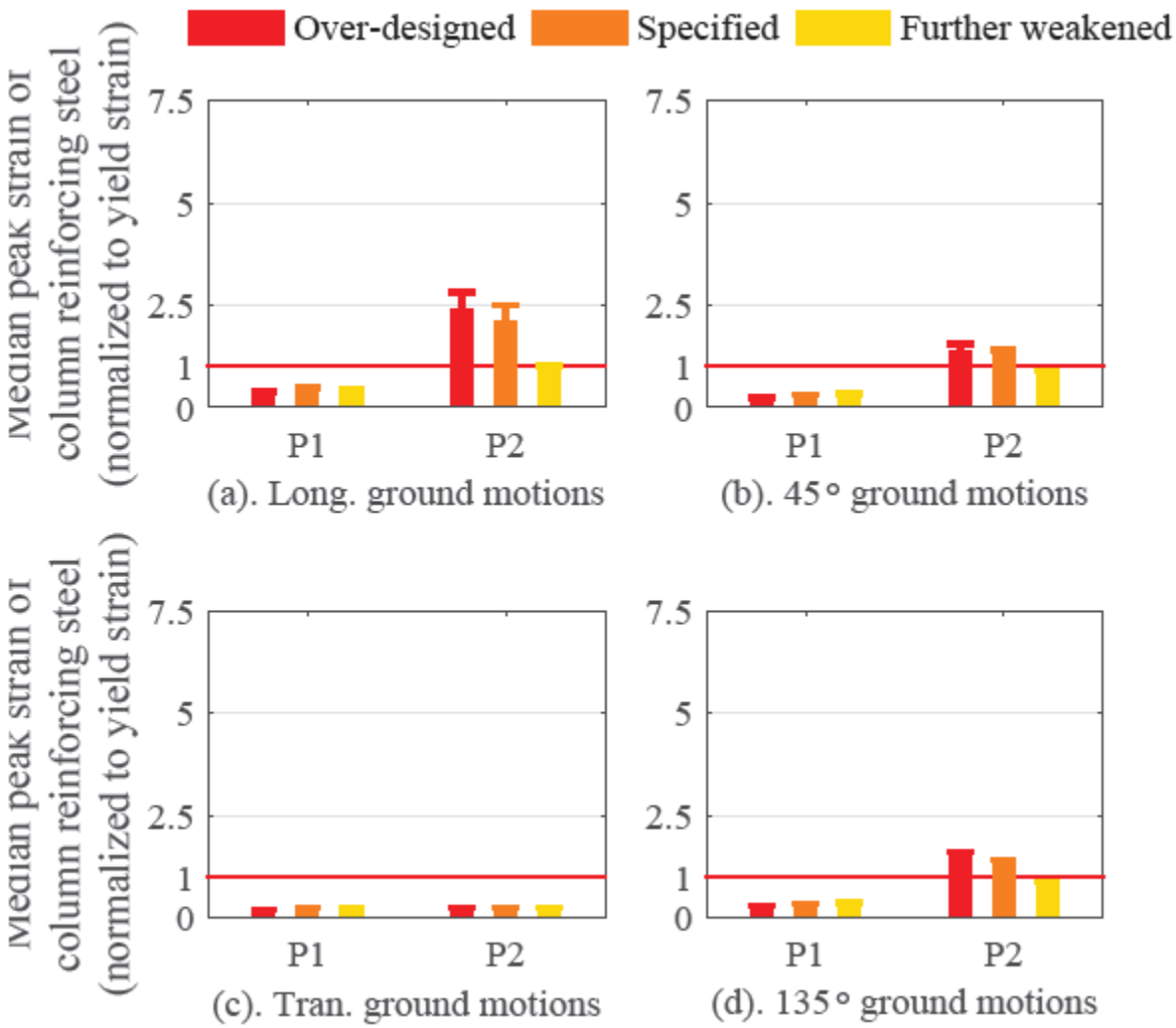

Figure D.13: Comparison of peak strain (median + median absolute deviation) of reinforcing steel at pier column bases of 3S00P15S bridge variant with different designs of steel fixed bearing anchorage.

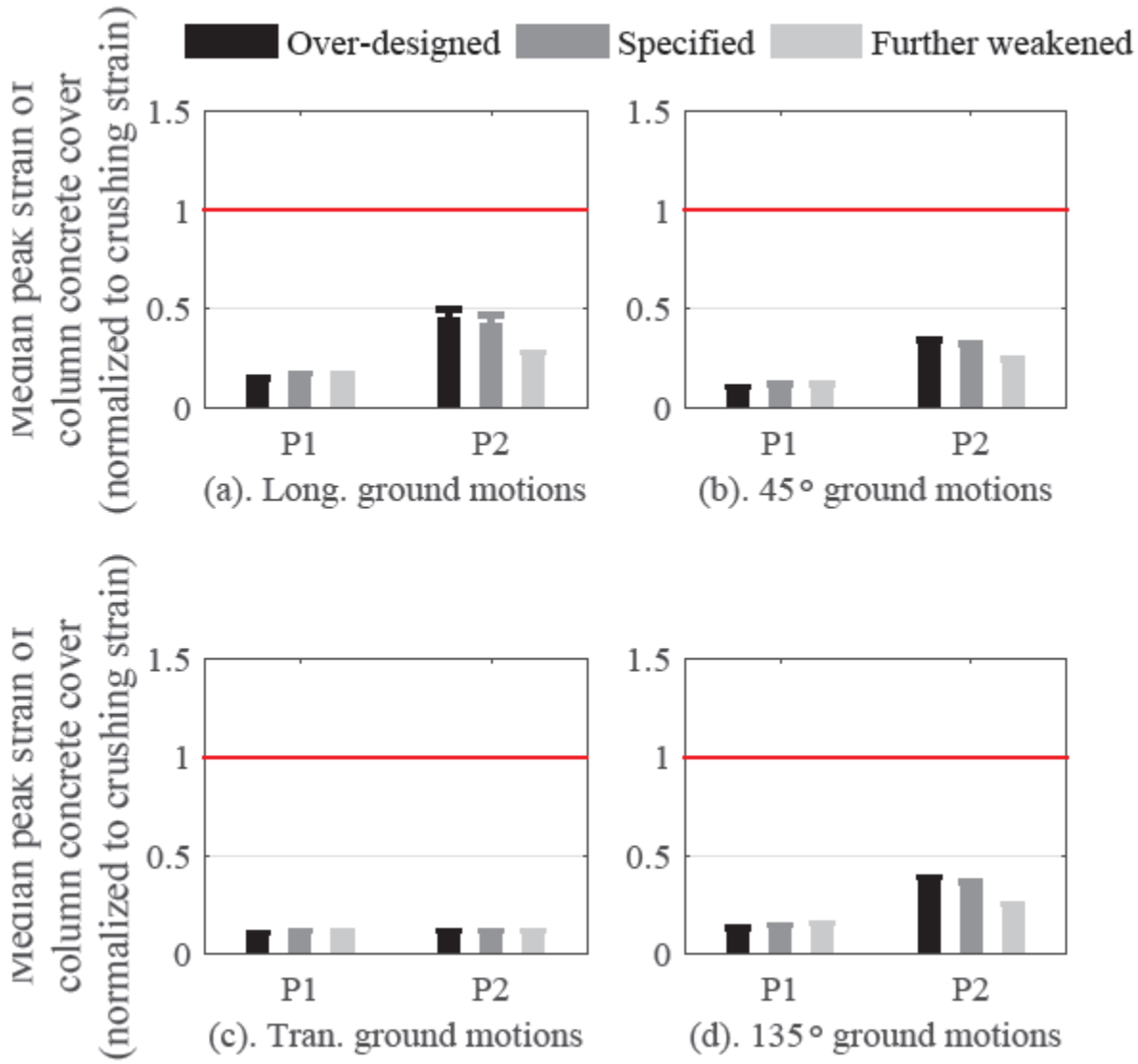

Figure D.14: Comparison of peak strain (median + median absolute deviation) of concrete cover at pier column bases of 3S00P15S bridge variant with different designs of steel fixed bearing anchorage.

D.2.2 3S15P15S Bridge Variant

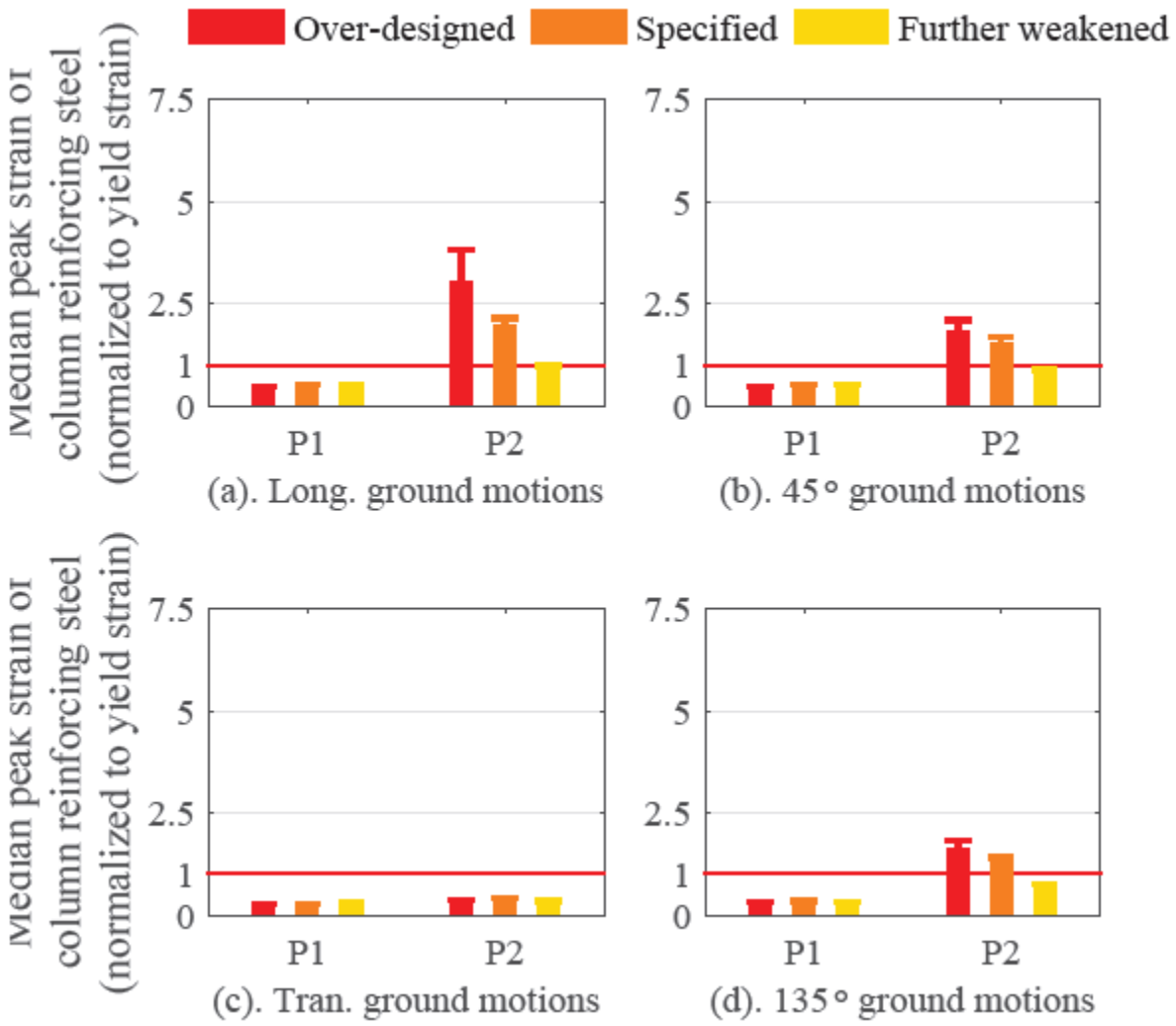

Figure D.15: Comparison of peak strain (median + median absolute deviation) of reinforcing steel at pier column bases of 3S15P15S bridge variant with different designs of steel fixed bearing anchorage.

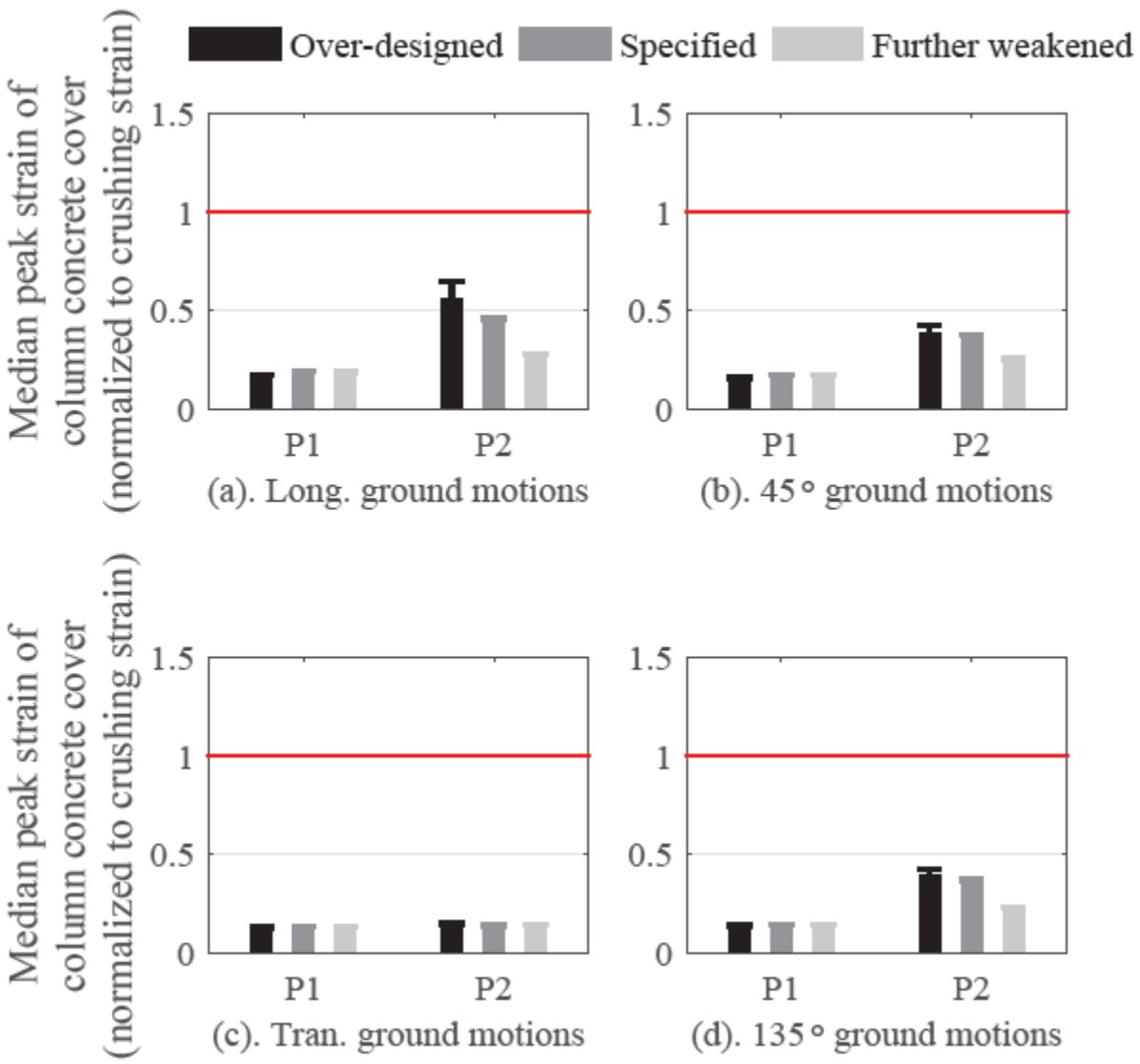

Figure D.16: Comparison of peak strain (median + median absolute deviation) of concrete cover at pier column bases of 3S15P15S bridge variant with different designs of steel fixed bearing anchorage.

D.2.3 3C00P15S Bridge Variant

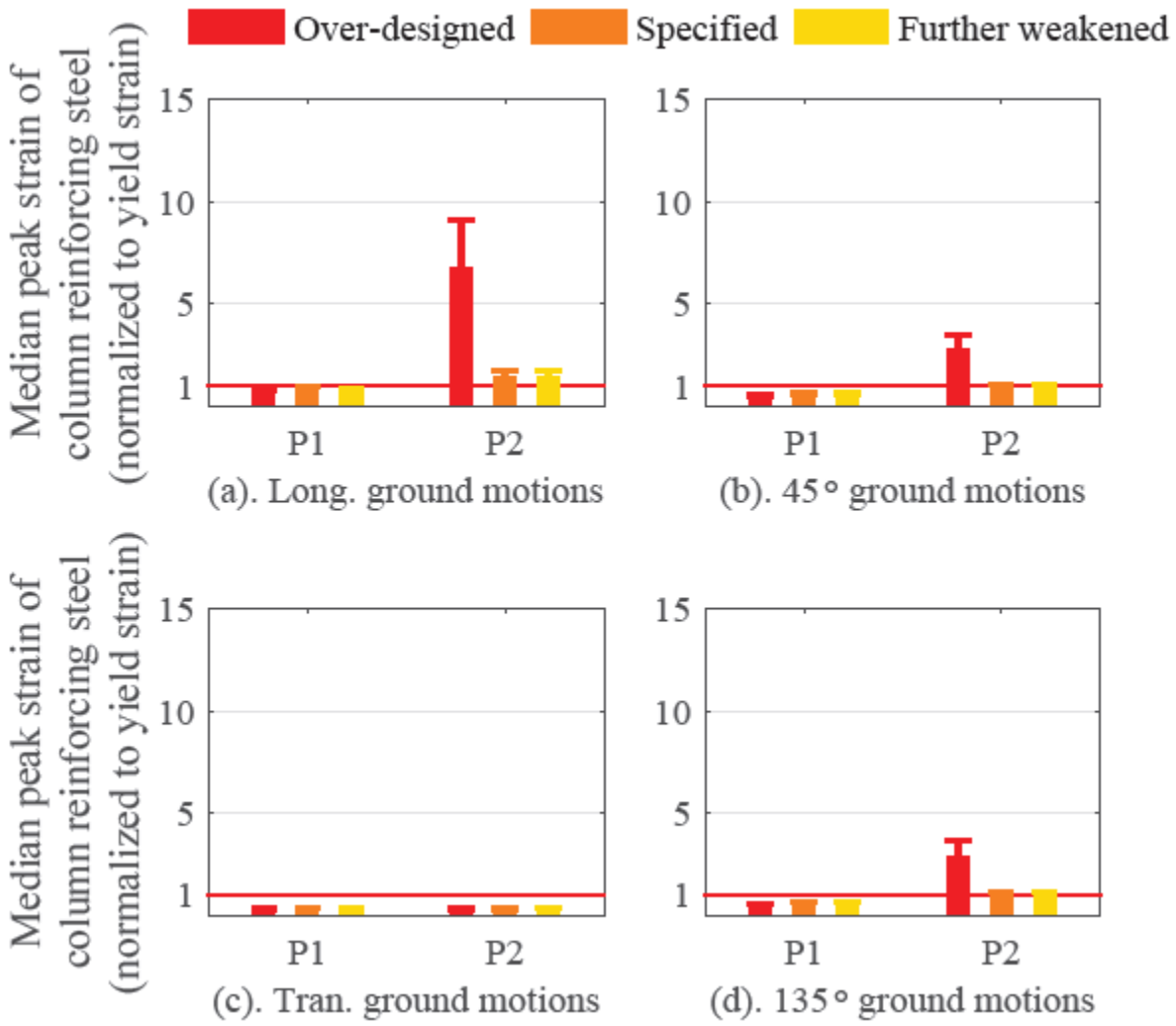

Figure D.17: Comparison of peak strain (median + median absolute deviation) of reinforcing steel at pier column bases of 3C00P15S bridge variant with different designs of steel fixed bearing anchorage.

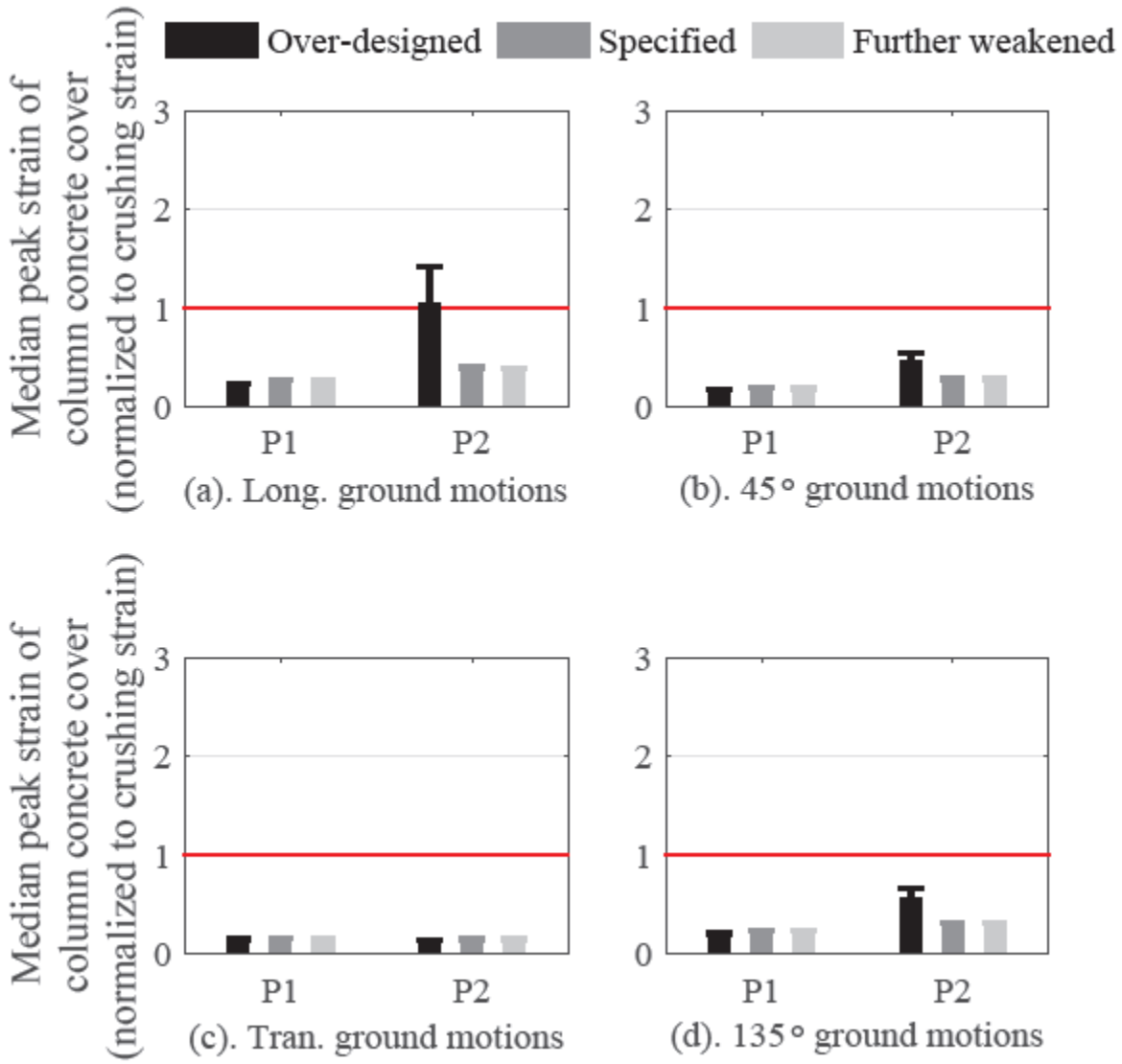

Figure D.18: Comparison of peak strain (median + median absolute deviation) of concrete cover at pier column bases of 3C00P15S bridge variant with different designs of steel fixed bearing anchorage.

D.2.4 3C15P15S Bridge Variant

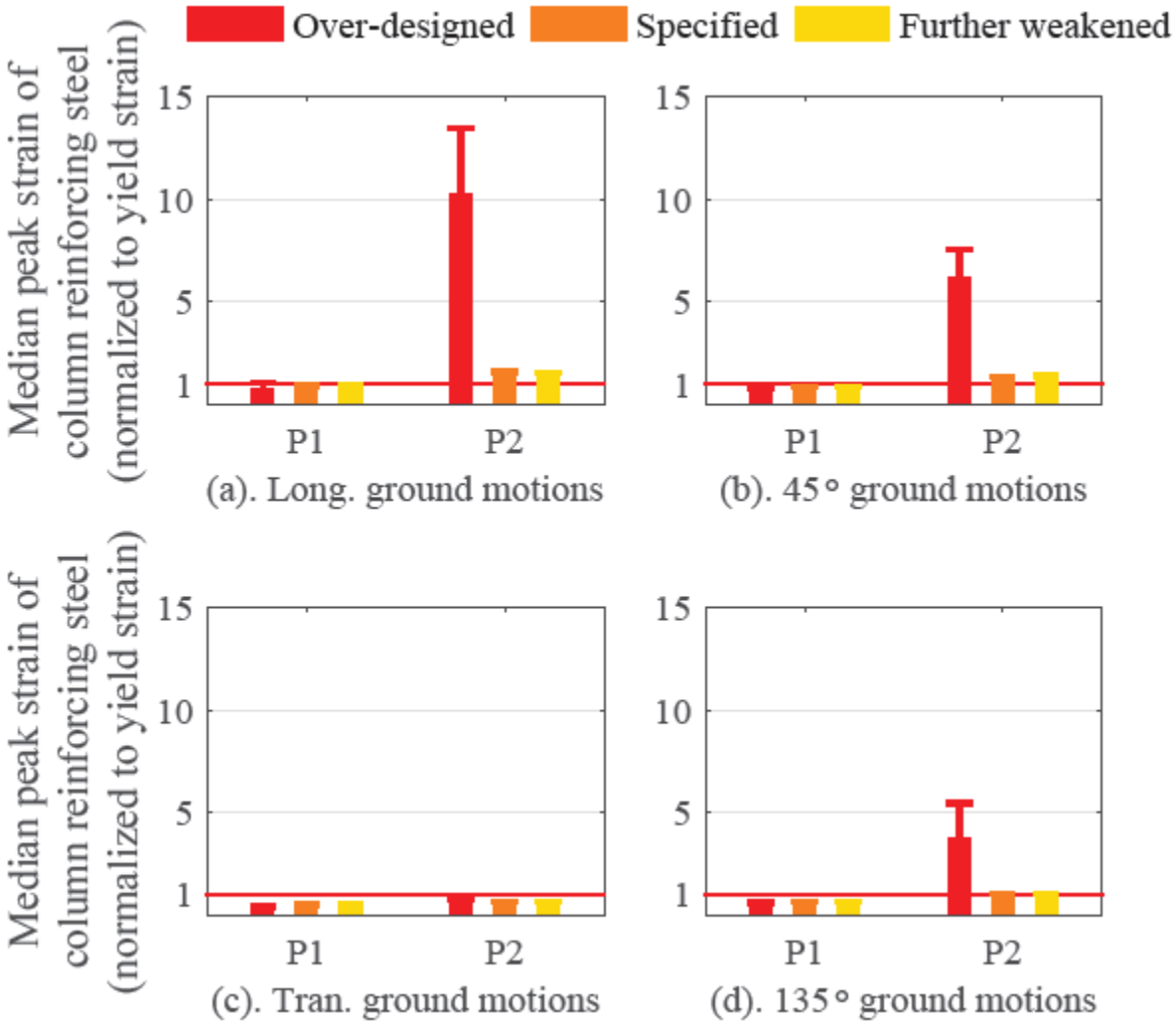

Figure D.19: Comparison of peak strain (median + median absolute deviation) of reinforcing steel at pier column bases of 3C15P15S bridge variant with different designs of steel fixed bearing anchorage.

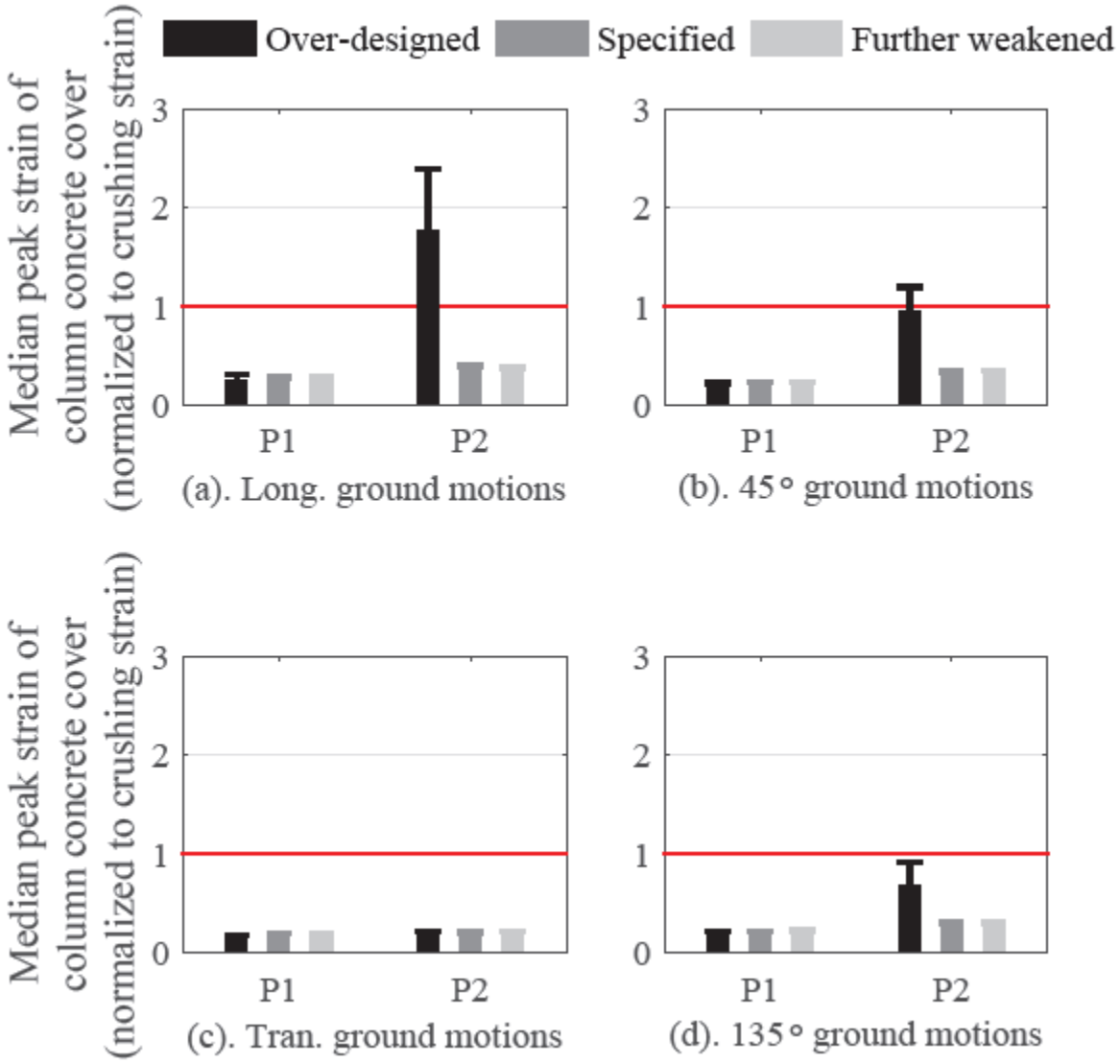

Figure D.20: Comparison of peak strain (median + median absolute deviation) of concrete cover at pier column bases of 3C15P15S bridge variant with different designs of steel fixed bearing anchorage.

D.2.5 3C30P15S Bridge Variant

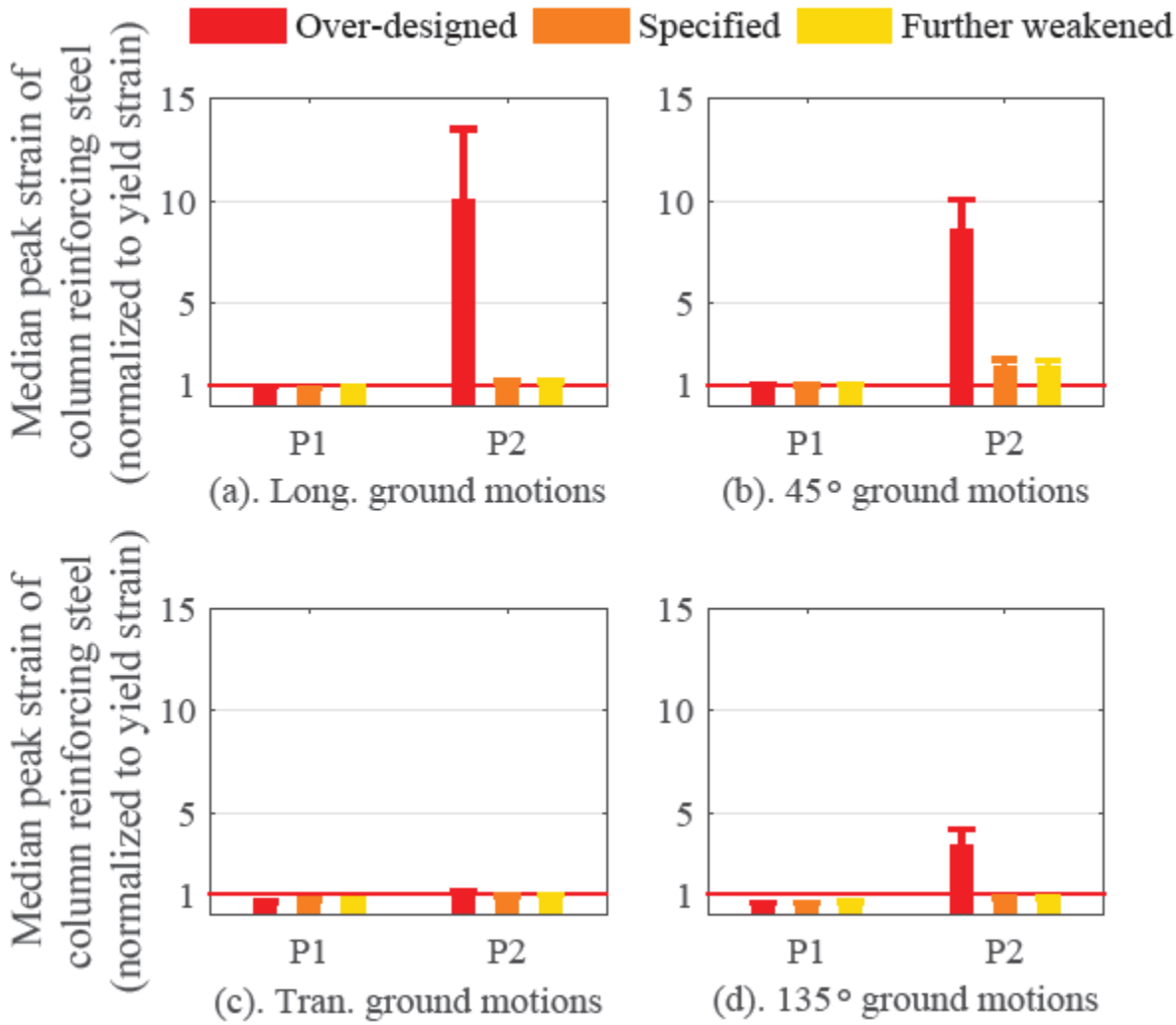

Figure D.21: Comparison of peak strain (median + median absolute deviation) of reinforcing steel at pier column bases of 3C30P15S bridge variant with different designs of steel fixed bearing anchorage.

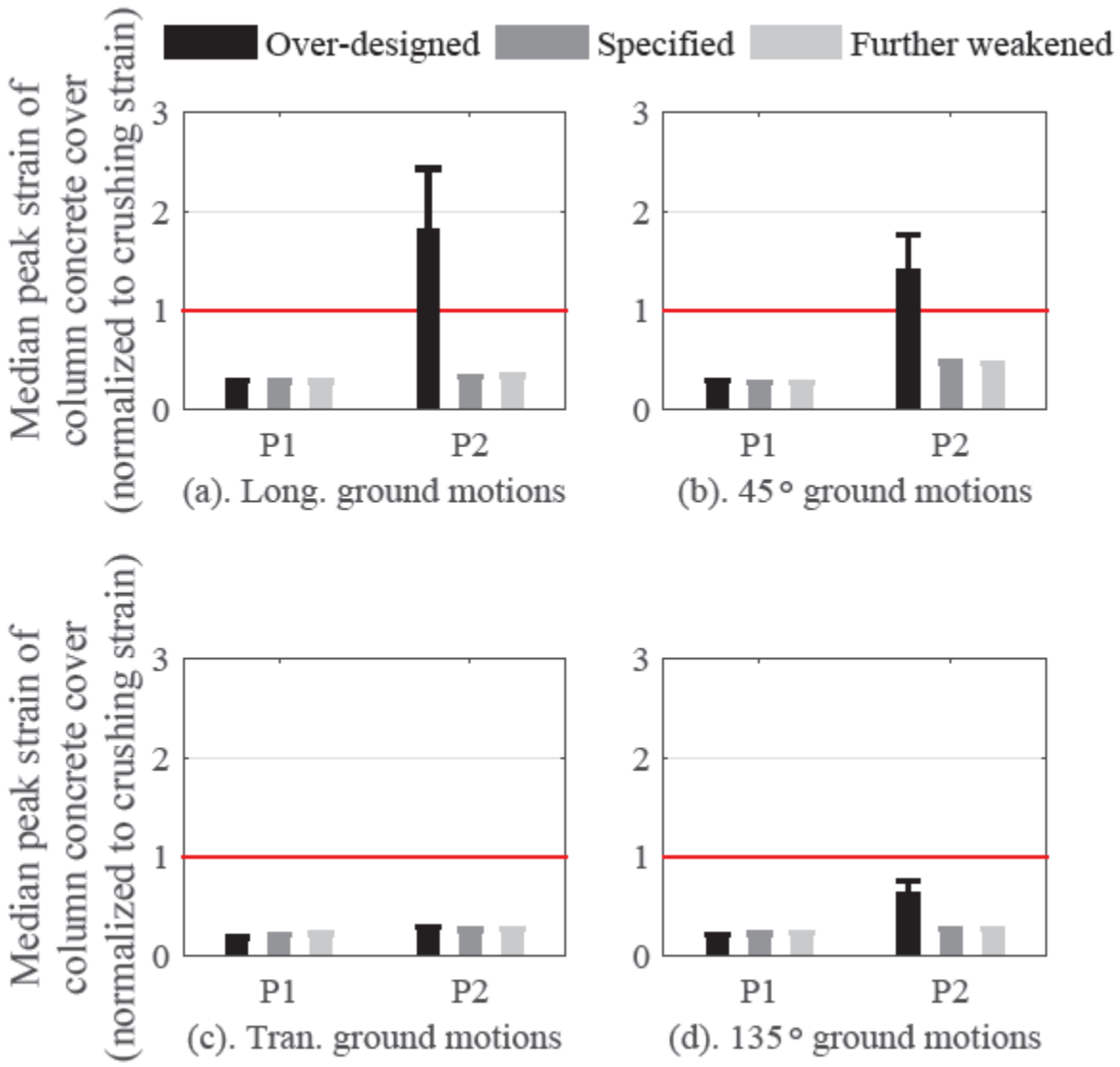

Figure D.22: Comparison of peak strain (median + median absolute deviation) of concrete cover at pier column bases of 3C30P15S bridge variant with different designs of steel fixed bearing anchorage.

D.2.6 4S00P15S Bridge Variant

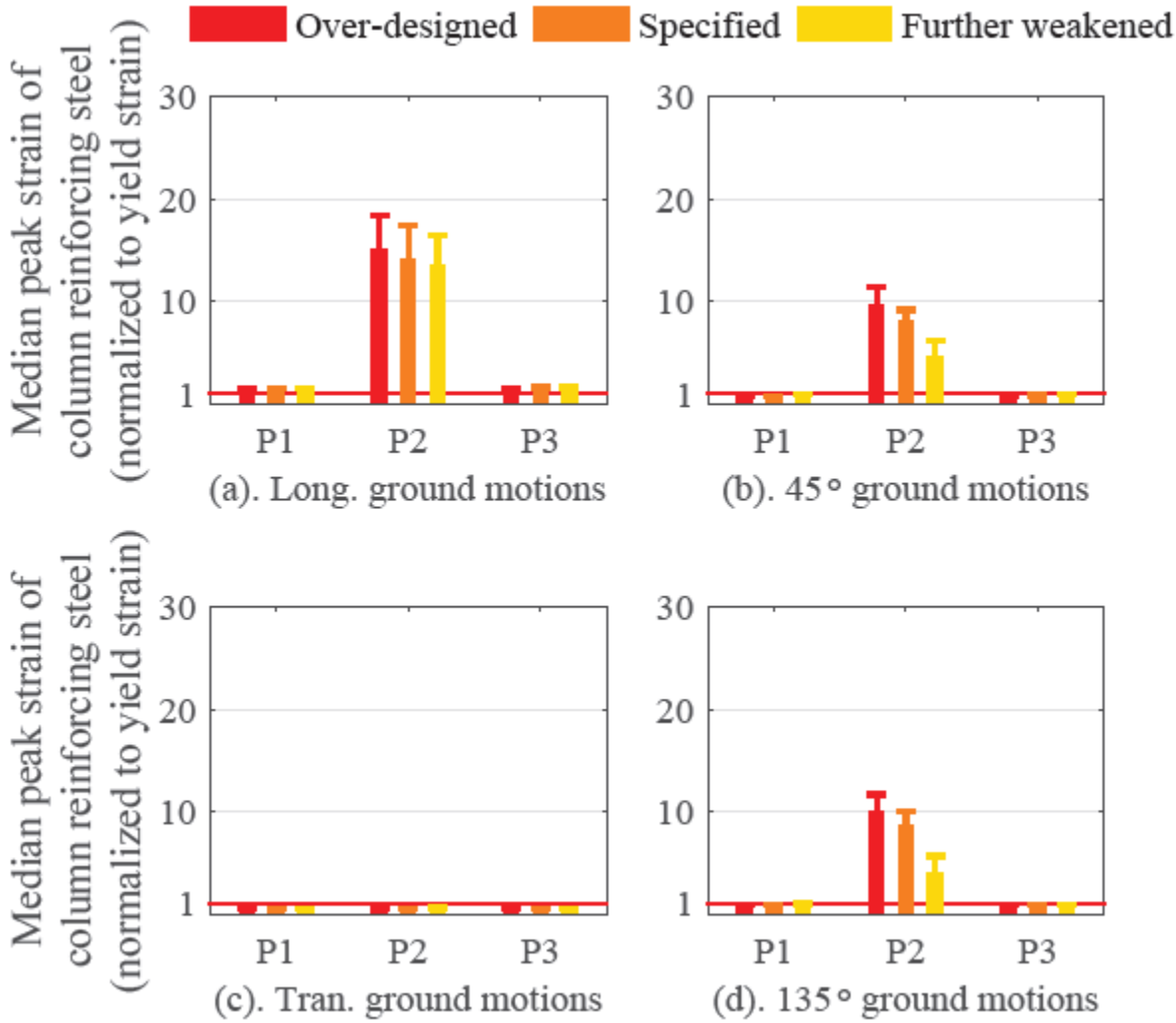

Figure D.23: Comparison of peak strain (median + median absolute deviation) of reinforcing steel at pier column bases of 4S00P15S bridge variant with different designs of steel fixed bearing anchorage.

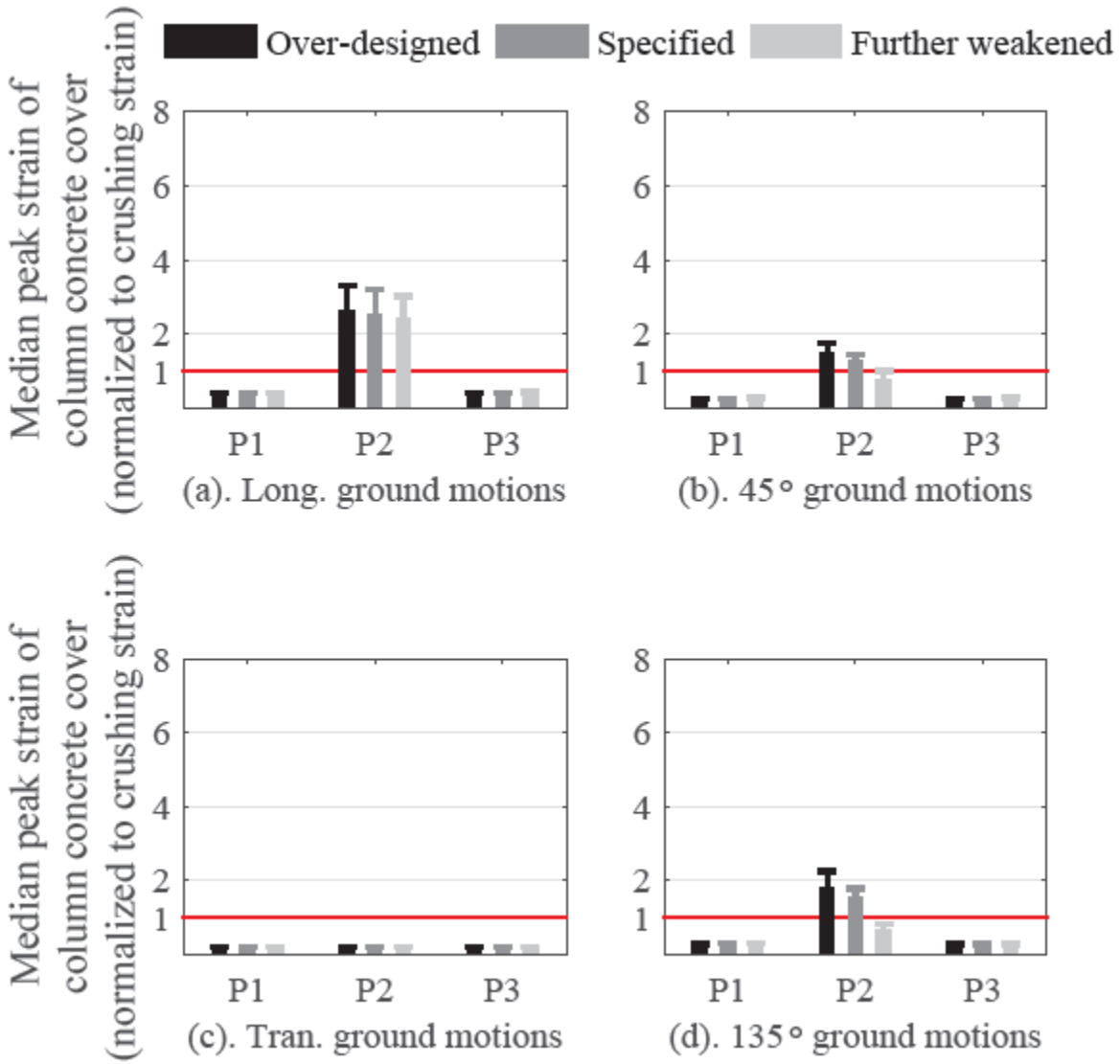

Figure D.24: Comparison of peak strain (median + median absolute deviation) of concrete cover at pier column bases of 4S00P15S bridge variant with different designs of steel fixed bearing anchorage.

D.2.7 4S15P15S Bridge Variant

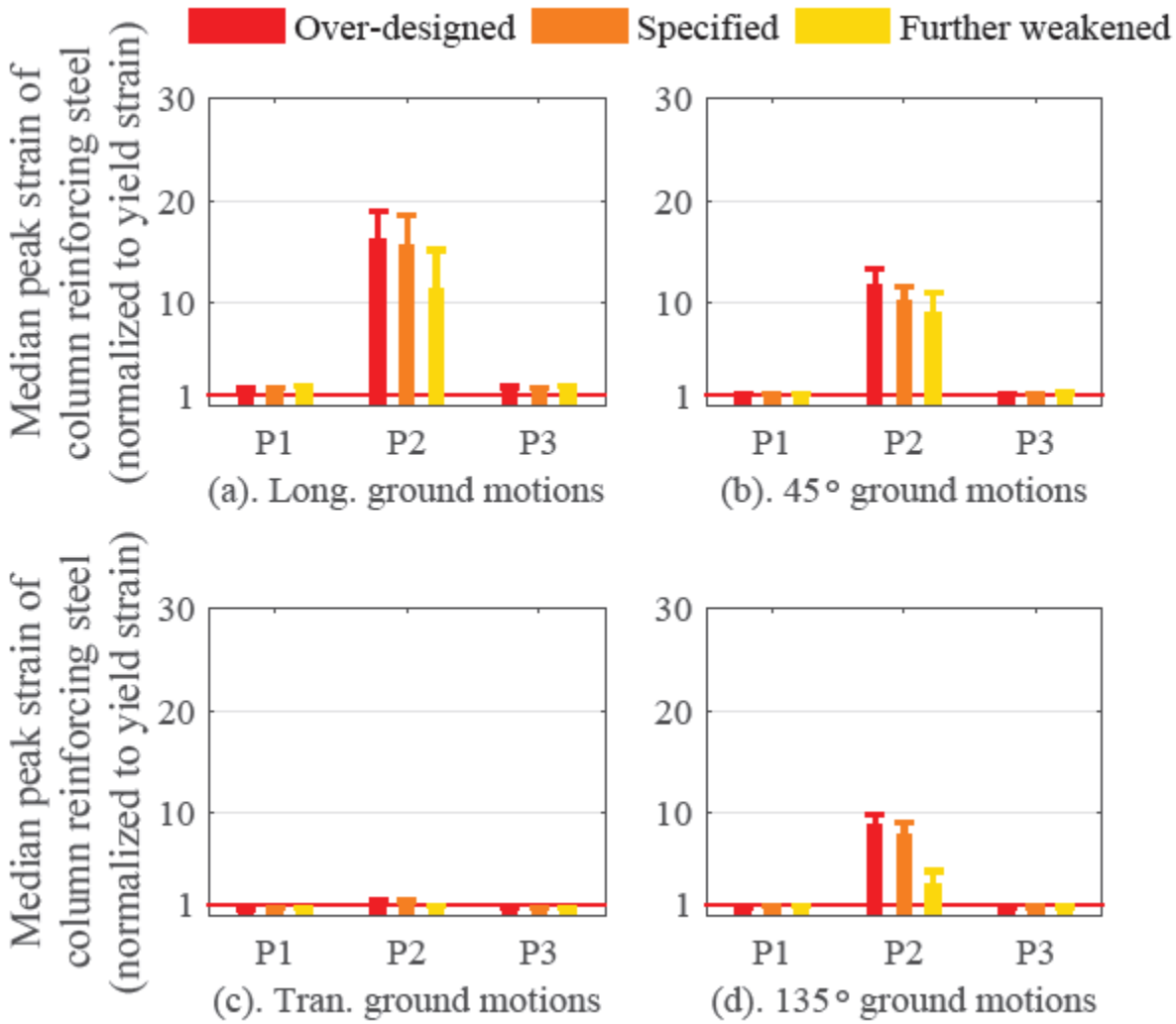

Figure D.25: Comparison of peak strain (median + median absolute deviation) of reinforcing steel at pier column bases of 4S15P15S bridge variant with different designs of steel fixed bearing anchorage.

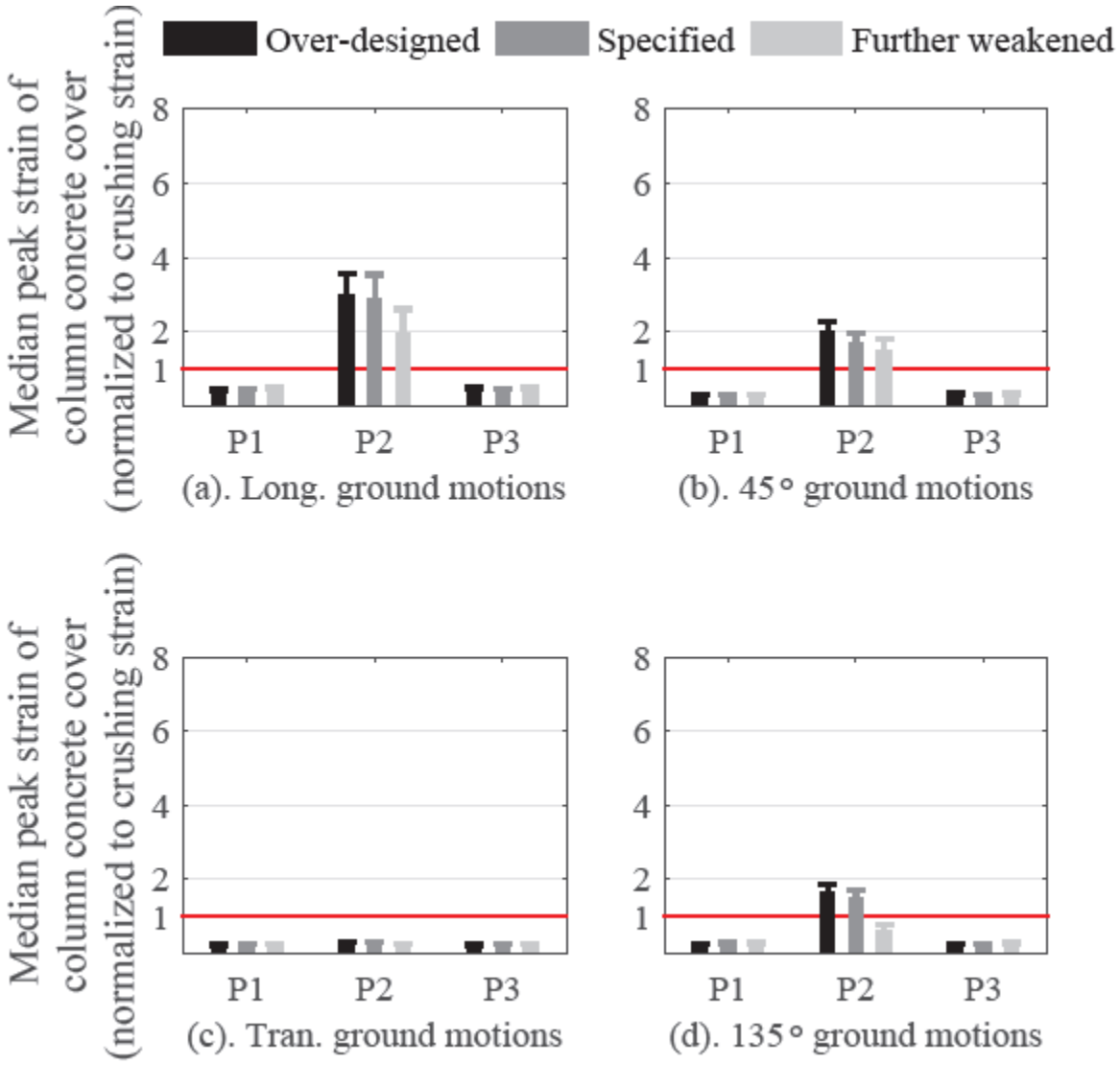

Figure D.26: Comparison of peak strain (median + median absolute deviation) of concrete cover at pier column bases of 4S15P15S bridge variant with different designs of steel fixed bearing anchorage.

D.2.8 4S30P15S Bridge Variant

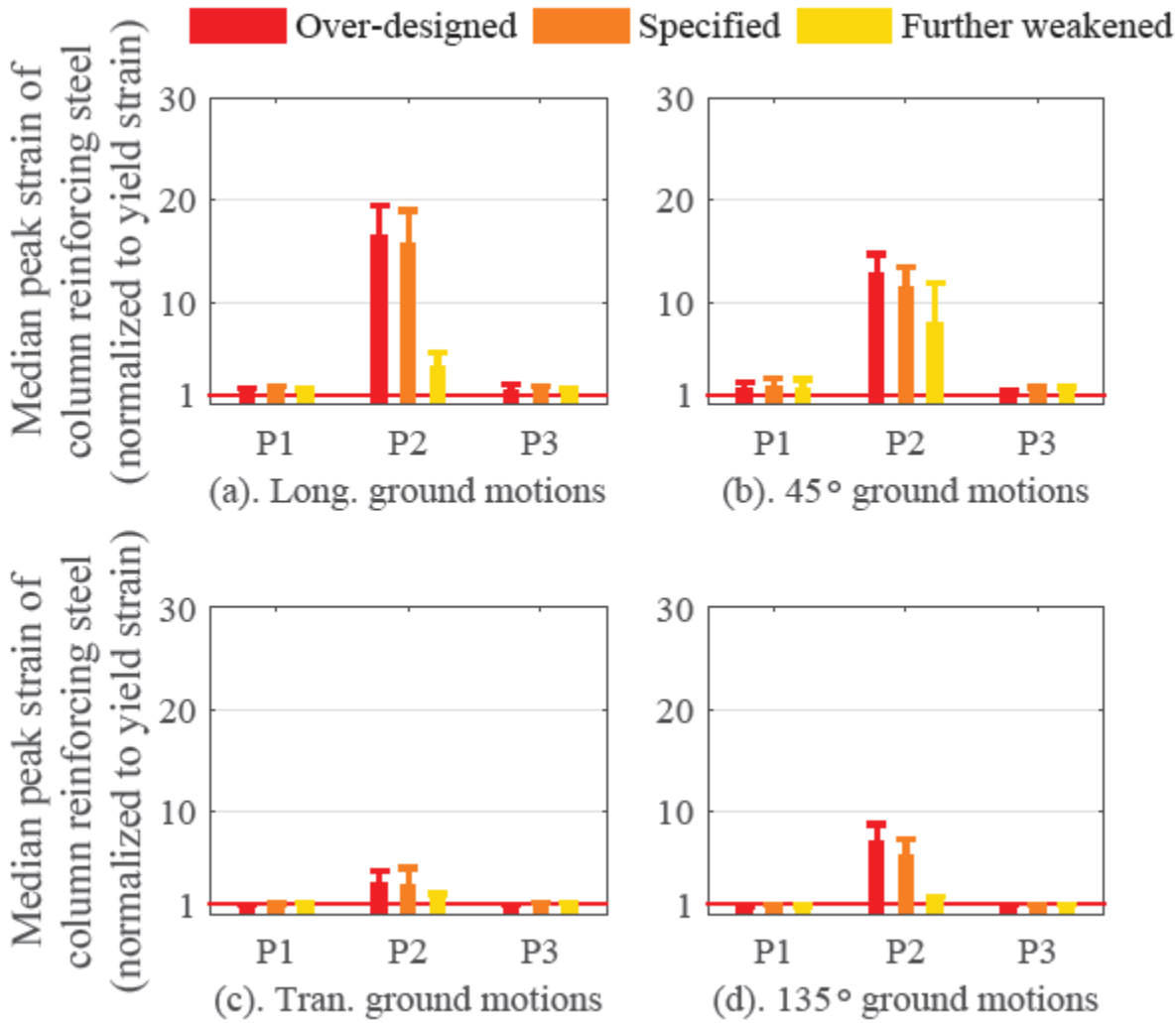

Figure D.27: Comparison of peak strain (median + median absolute deviation) of reinforcing steel at pier column bases of 4S30P15S bridge variant with different designs of steel fixed bearing anchorage.

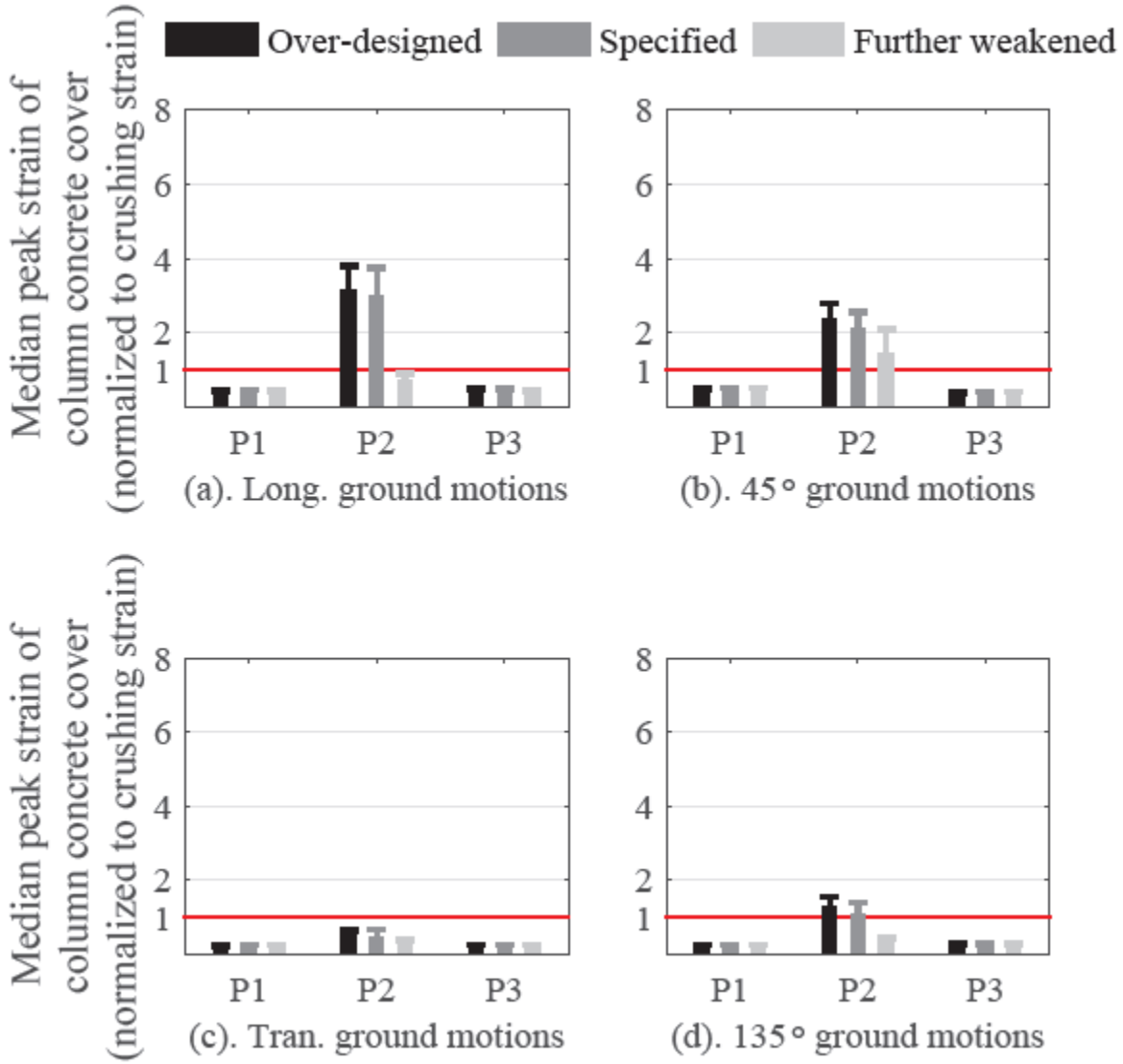

Figure D.28: Comparison of peak strain (median + median absolute deviation) of concrete cover at pier column bases of 4S30P15S bridge variant with different designs of steel fixed bearing anchorage.

D.2.9 4C00P15S Bridge Variant

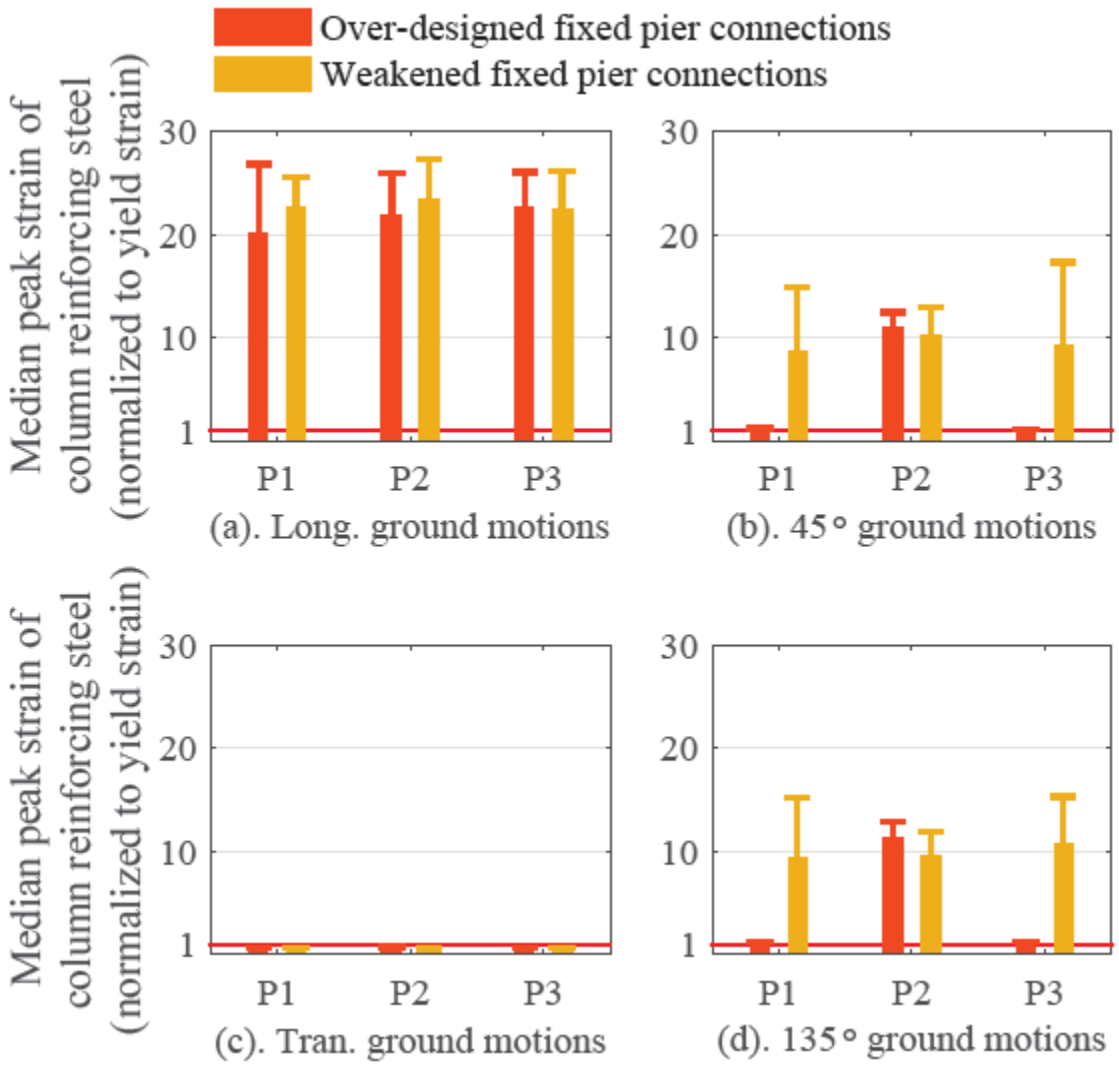

Figure D.29: Comparison of peak strain (median + median absolute deviation) of reinforcing steel at pier column bases of 4C00P15S bridge variant with different designs of steel fixed bearing anchorage.

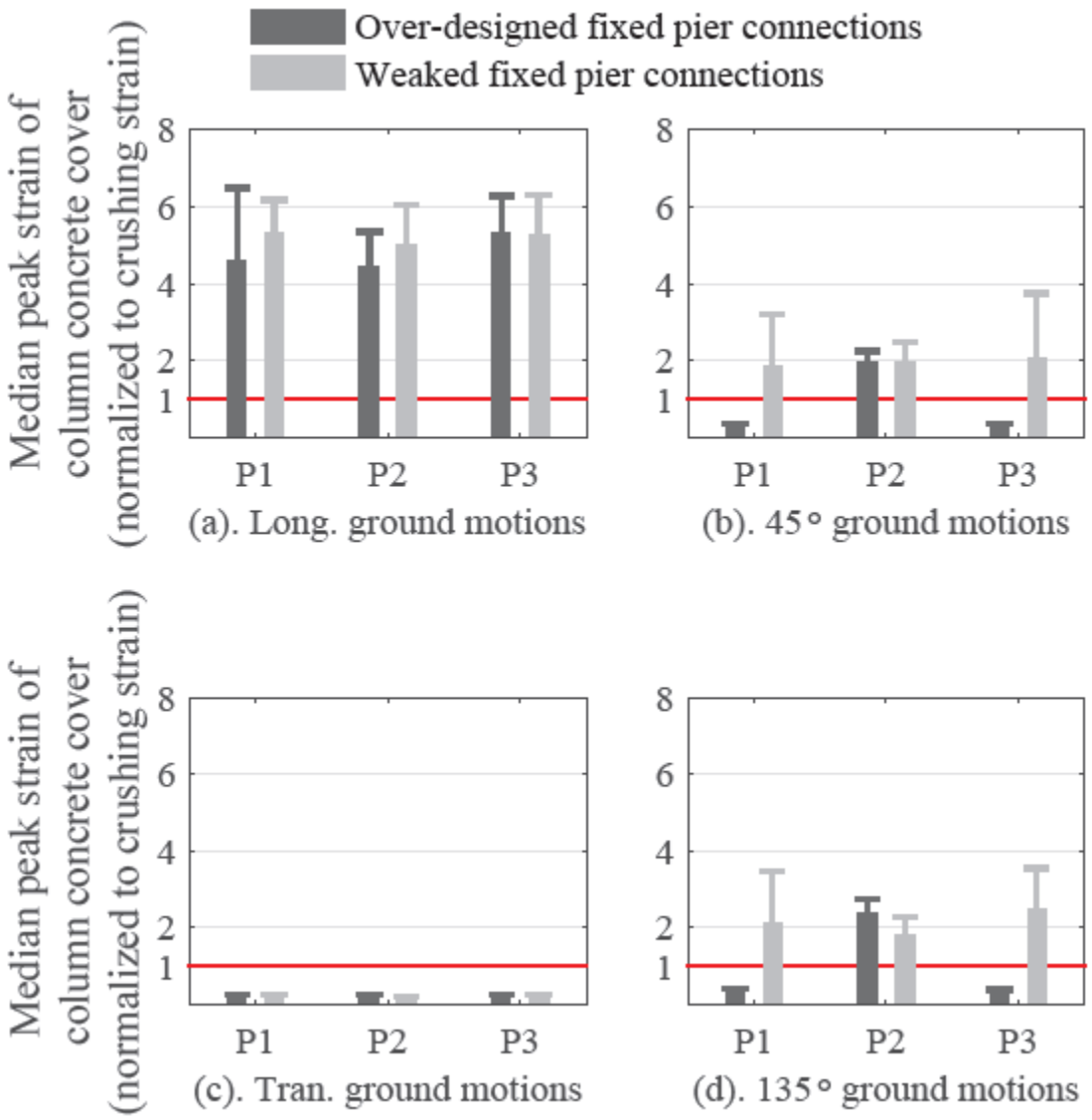

Figure D.30: Comparison of peak strain (median + median absolute deviation) of concrete cover at pier column bases of 4C00P15S bridge variant with different designs of steel fixed bearing anchorage.

D.2.10 4C15P15S Bridge Variant

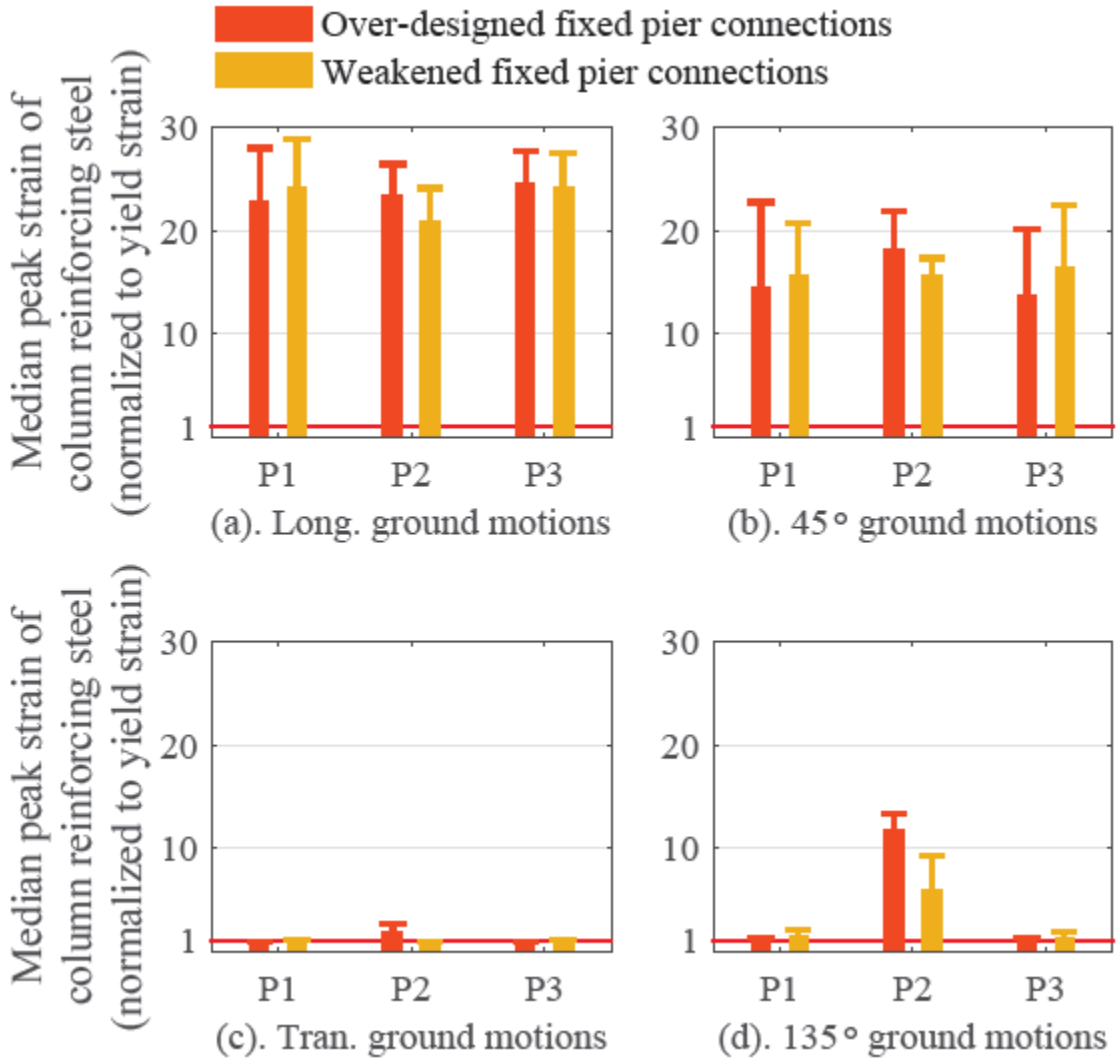

Figure D.31: Comparison of peak strain (median + median absolute deviation) of reinforcing steel at pier column bases of 4C15P15S bridge variant with different designs of steel fixed bearing anchorage.

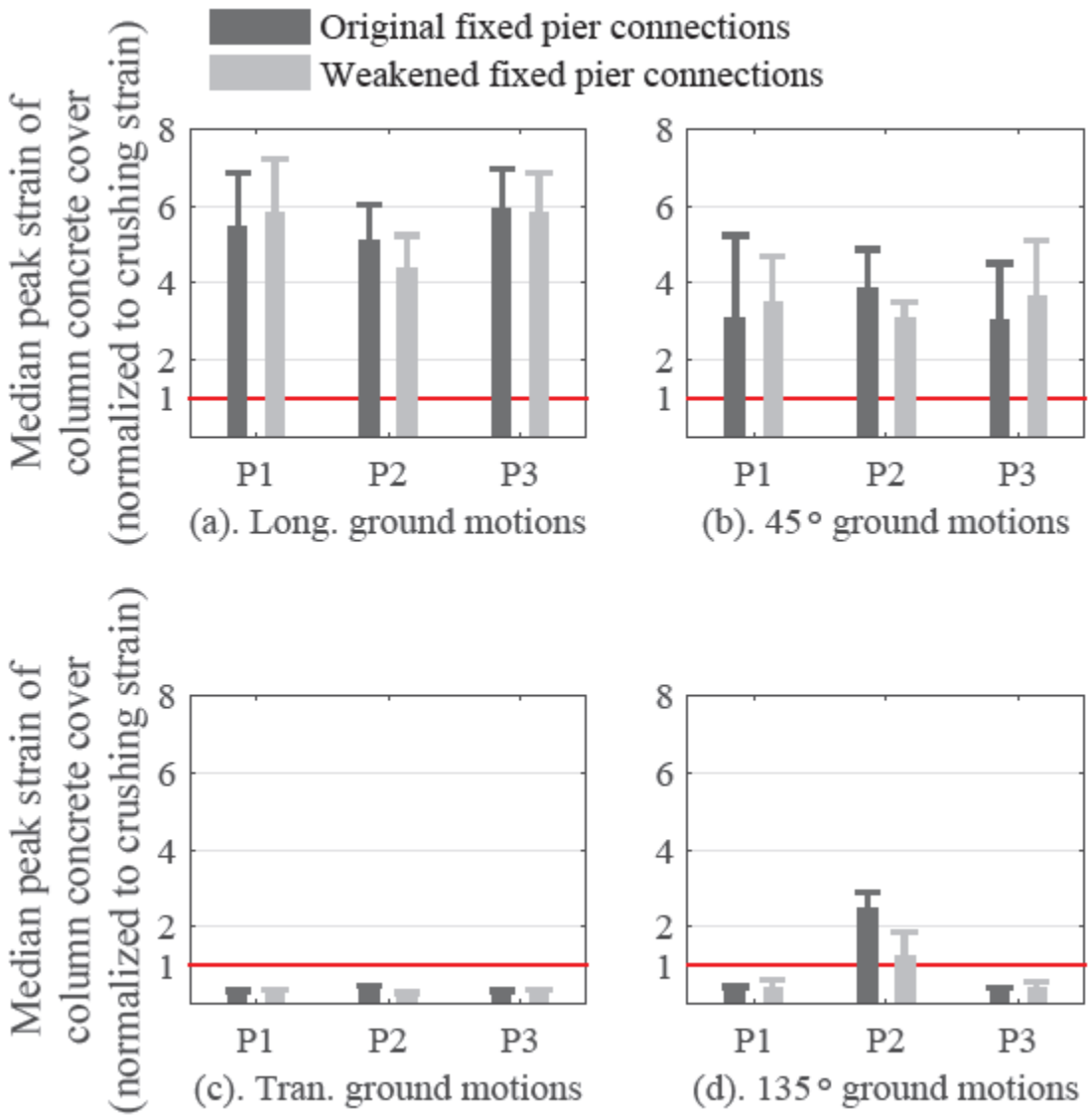

Figure D.32: Comparison of peak strain (median + median absolute deviation) of concrete cover at pier column bases of 4C15P15S bridge variant with different designs of steel fixed bearing anchorage.

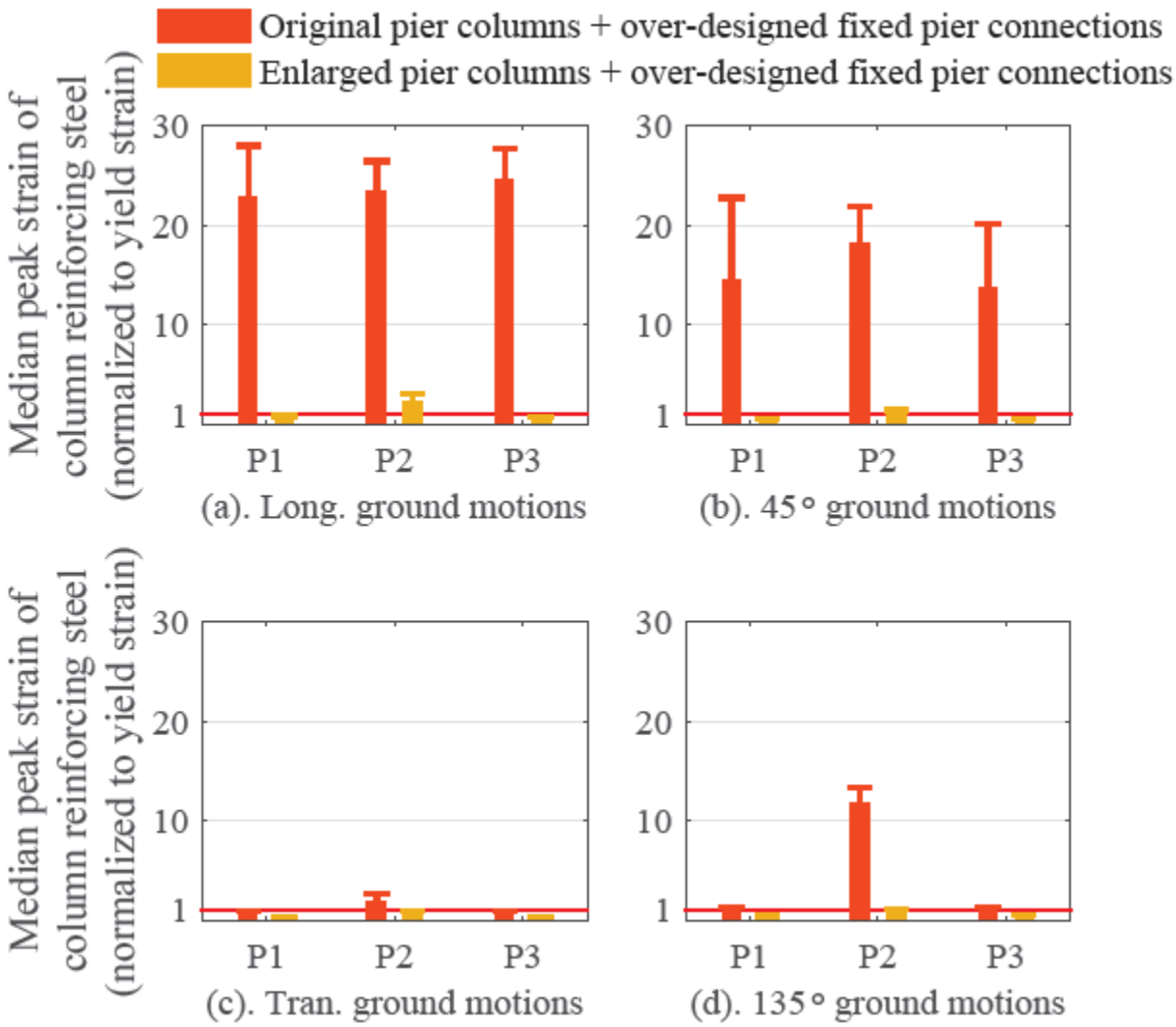

Figure D.33: Comparison of peak strain (median + median absolute deviation) of reinforcing steel at pier column bases of 4C15P15S bridge between Cases 1 and 2 of Table 5.5.

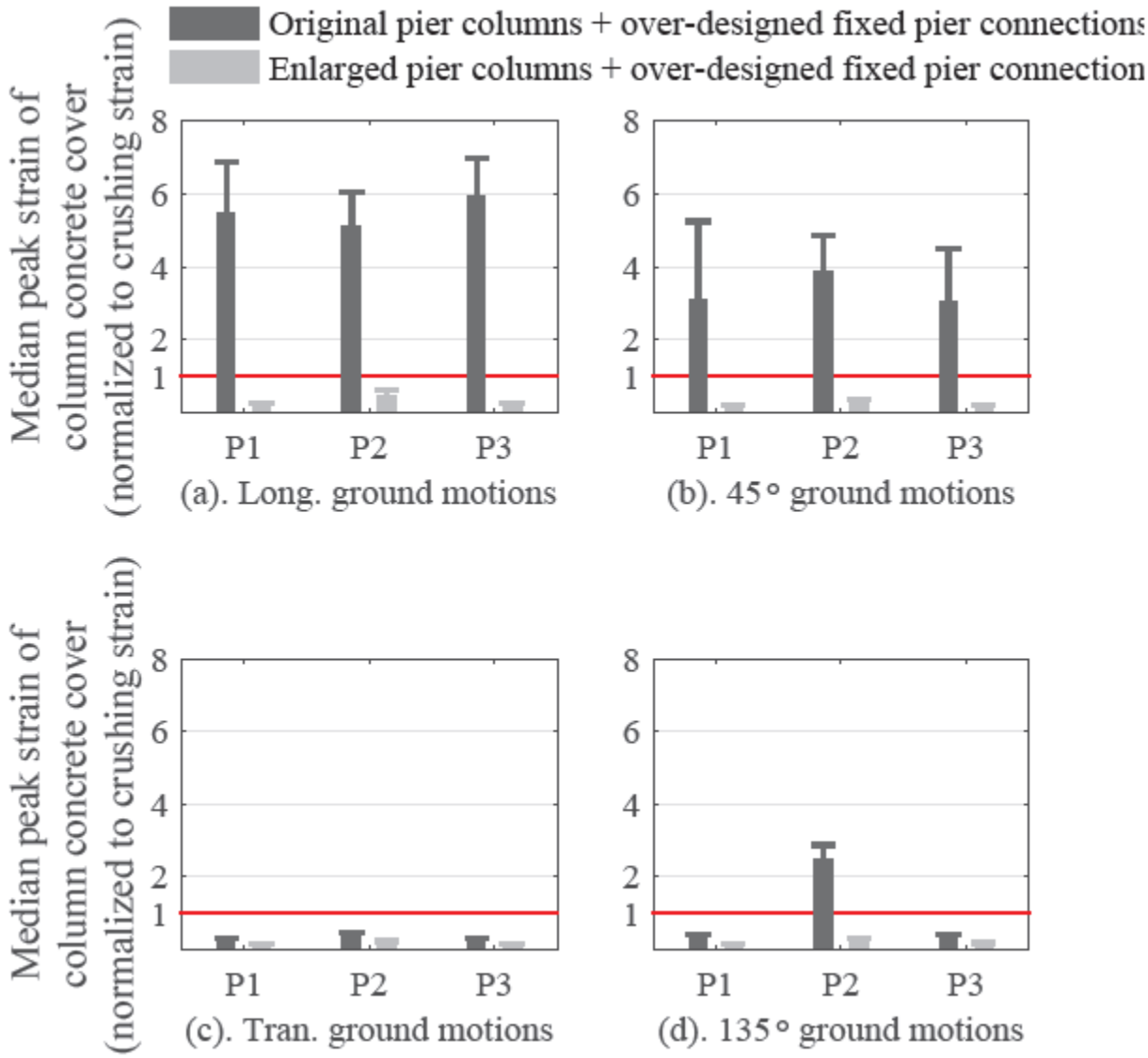

Figure D.34: Comparison of peak strain (median + median absolute deviation) of concrete cover at pier column bases of 4C15P15S bridge between Cases 1 and 2 of Table 5.5.

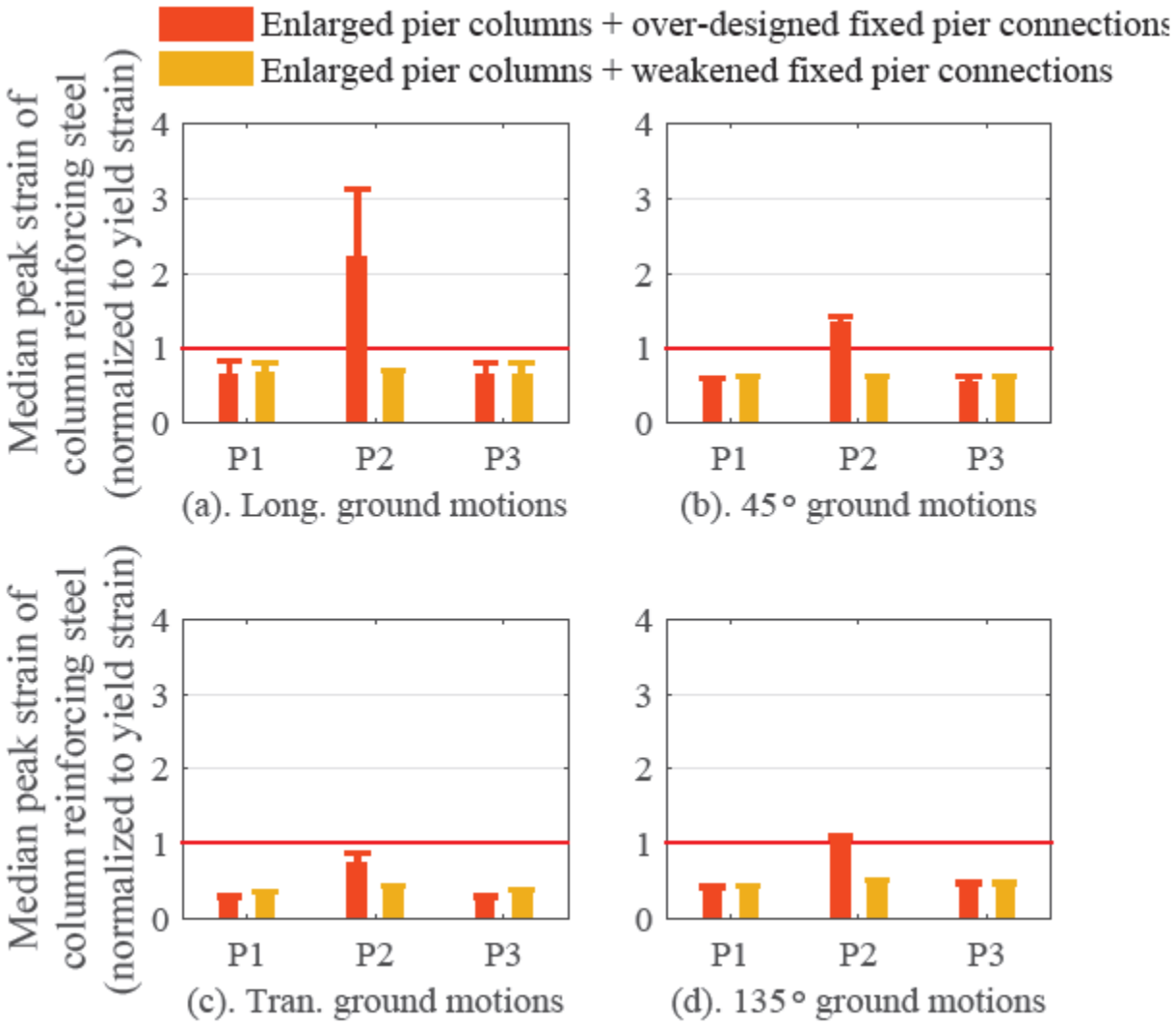

Figure D.35: Comparison of peak strain (median + median absolute deviation) of reinforcing steel at pier column bases of 4C15P15S bridge between Cases 2 and 3 of Table 5.5.

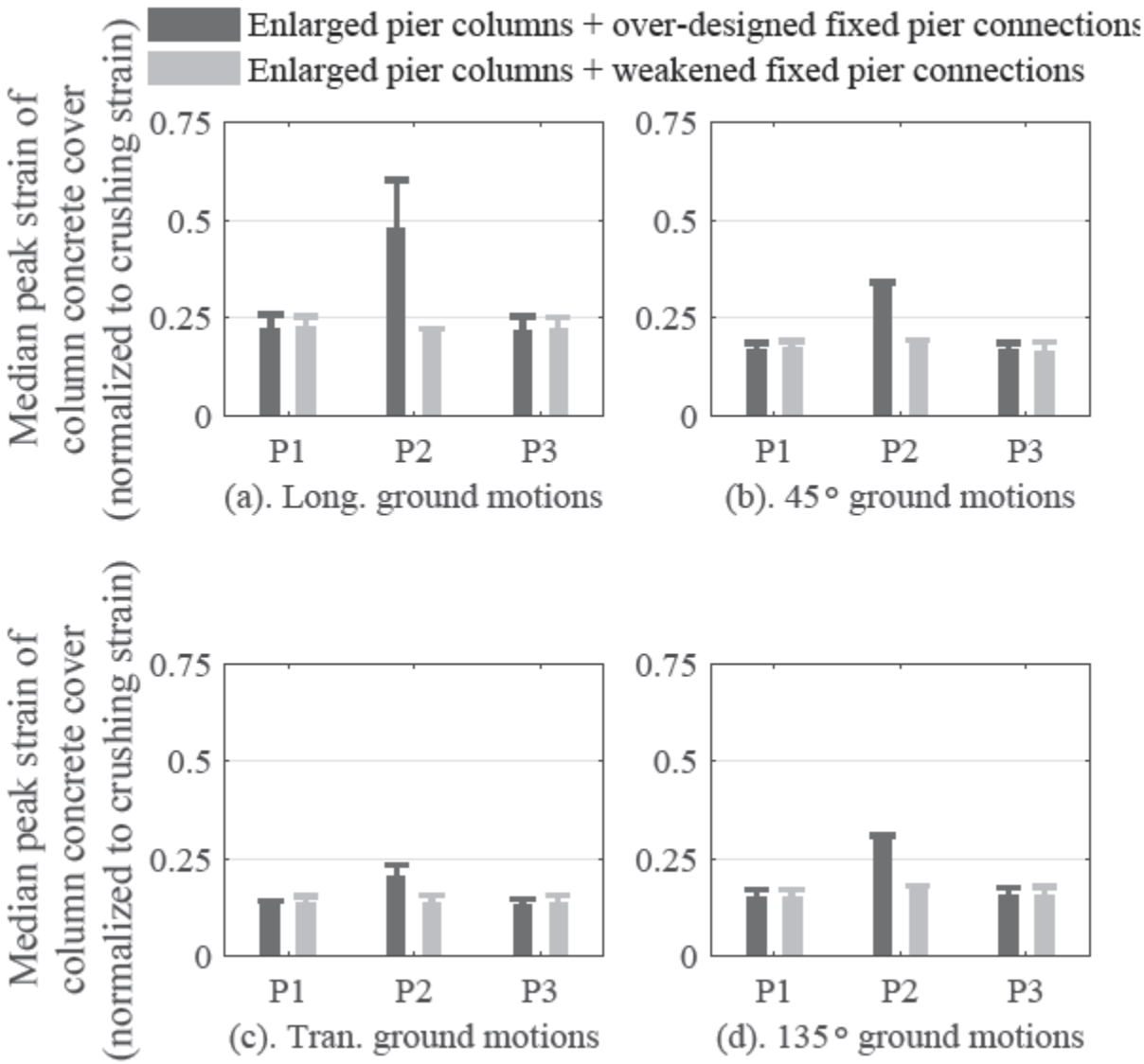

Figure D.36: Comparison of peak strain (median + median absolute deviation) of concrete cover at pier column bases of 4C15P15S bridge between Cases 2 and 3 of Table 5.5.

D2.11 4C30P15S Bridge Variant

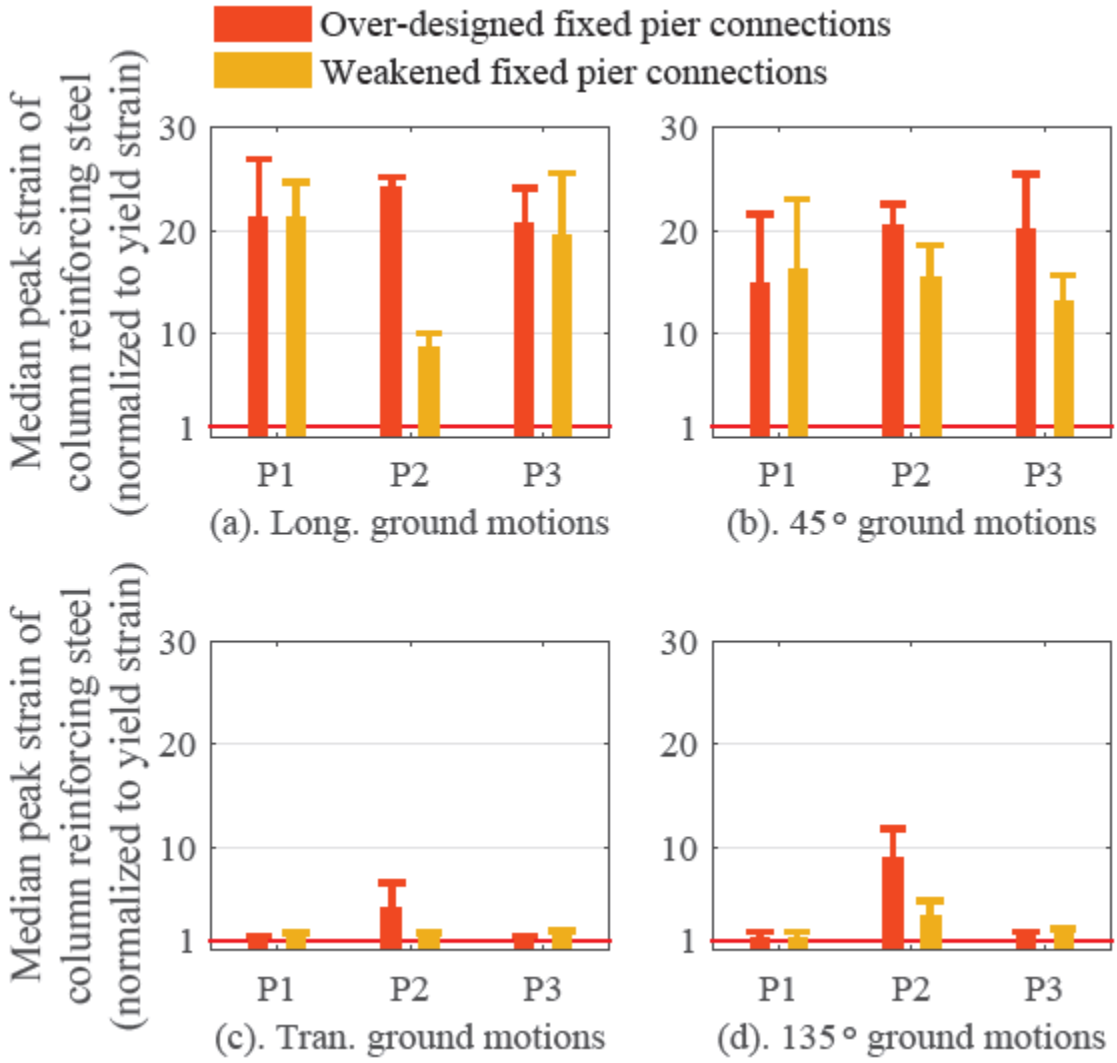

Figure D.37: Comparison of peak strain (median + median absolute deviation) of reinforcing steel at pier column bases of 4C30P15S bridge variant with different designs of steel fixed bearing anchorage.

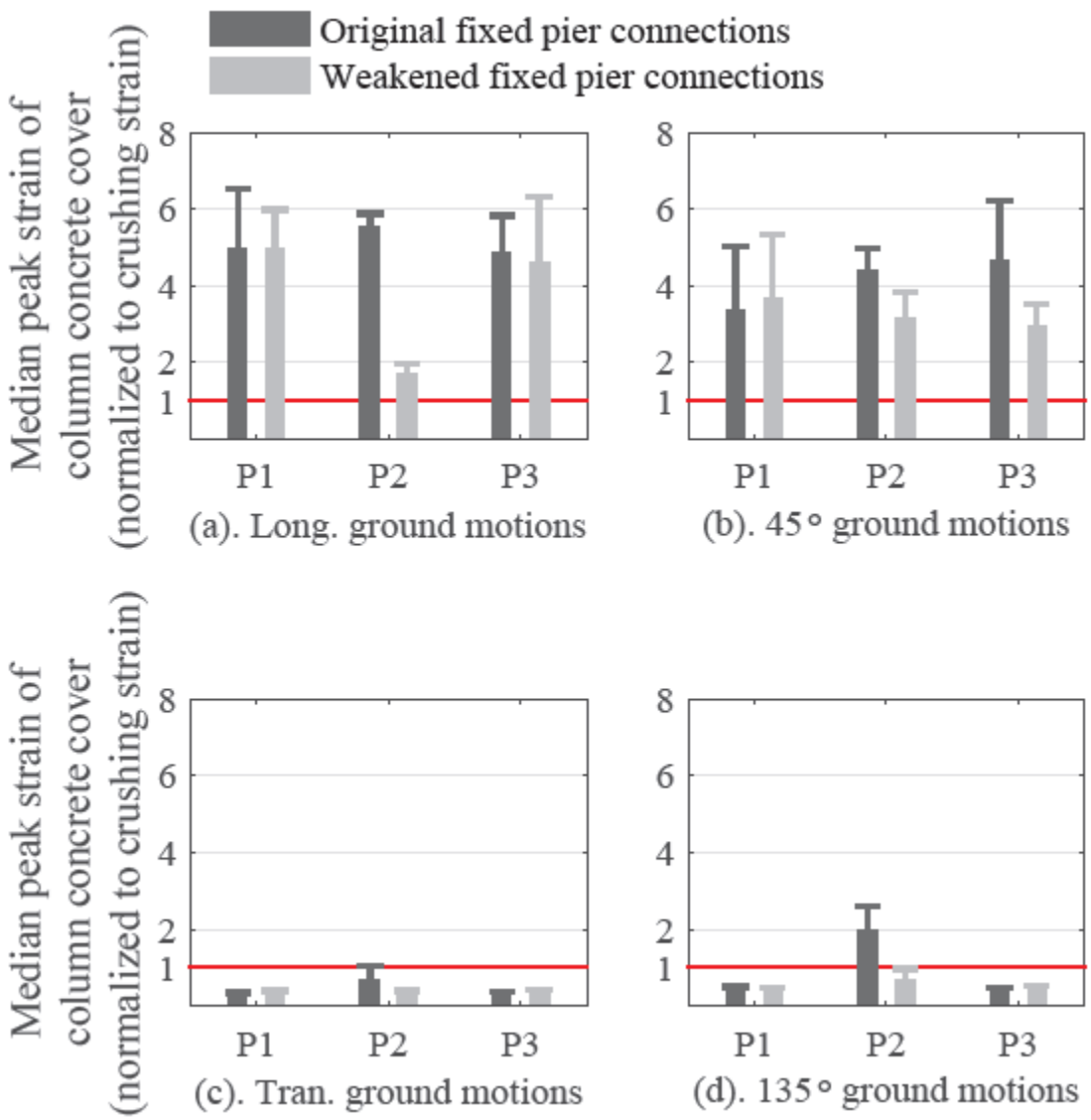

Figure D.38: Comparison of peak strain (median + median absolute deviation) of concrete cover at pier column bases of 4C30P15S bridge variant with different designs of steel fixed bearing anchorage.

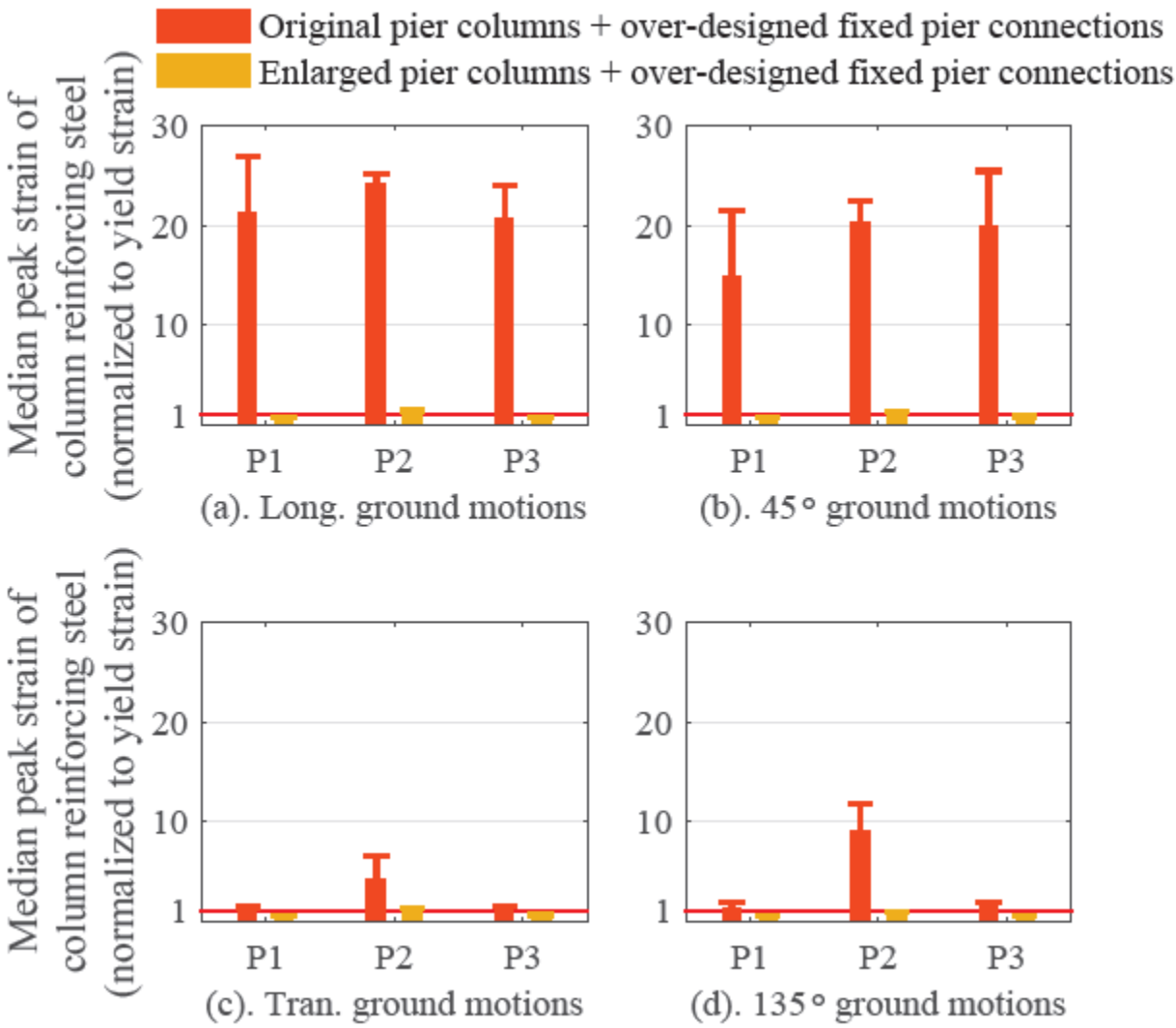

Figure D.39: Comparison of peak strain (median + median absolute deviation) of reinforcing steel at pier column bases of 4C30P15S bridge between Cases 1 and 2 of Table 5.5.

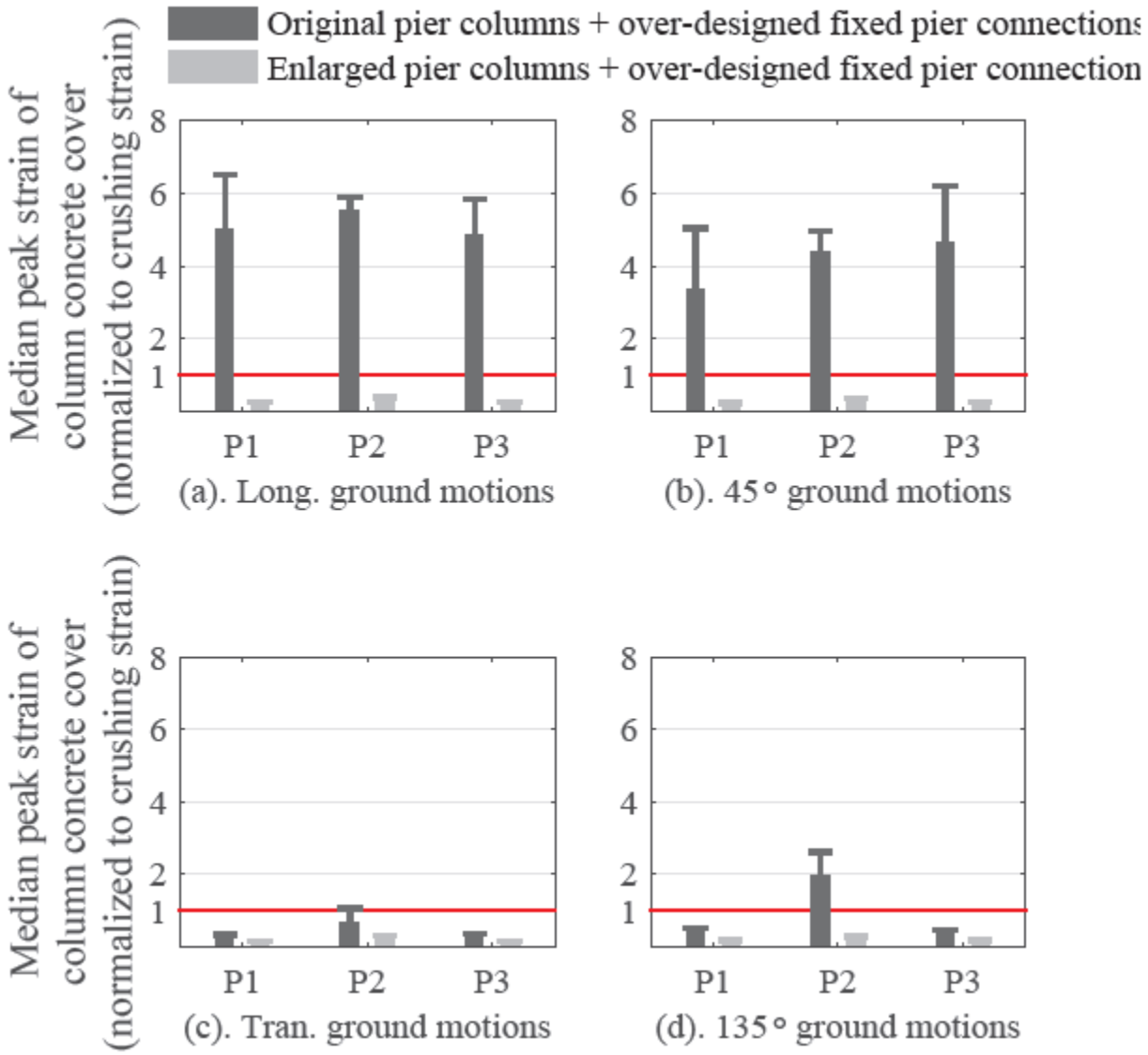

Figure D.40: Comparison of peak strain (median + median absolute deviation) of concrete cover at pier column bases of 4C30P15S bridge between Cases 1 and 2 of Table 5.5.

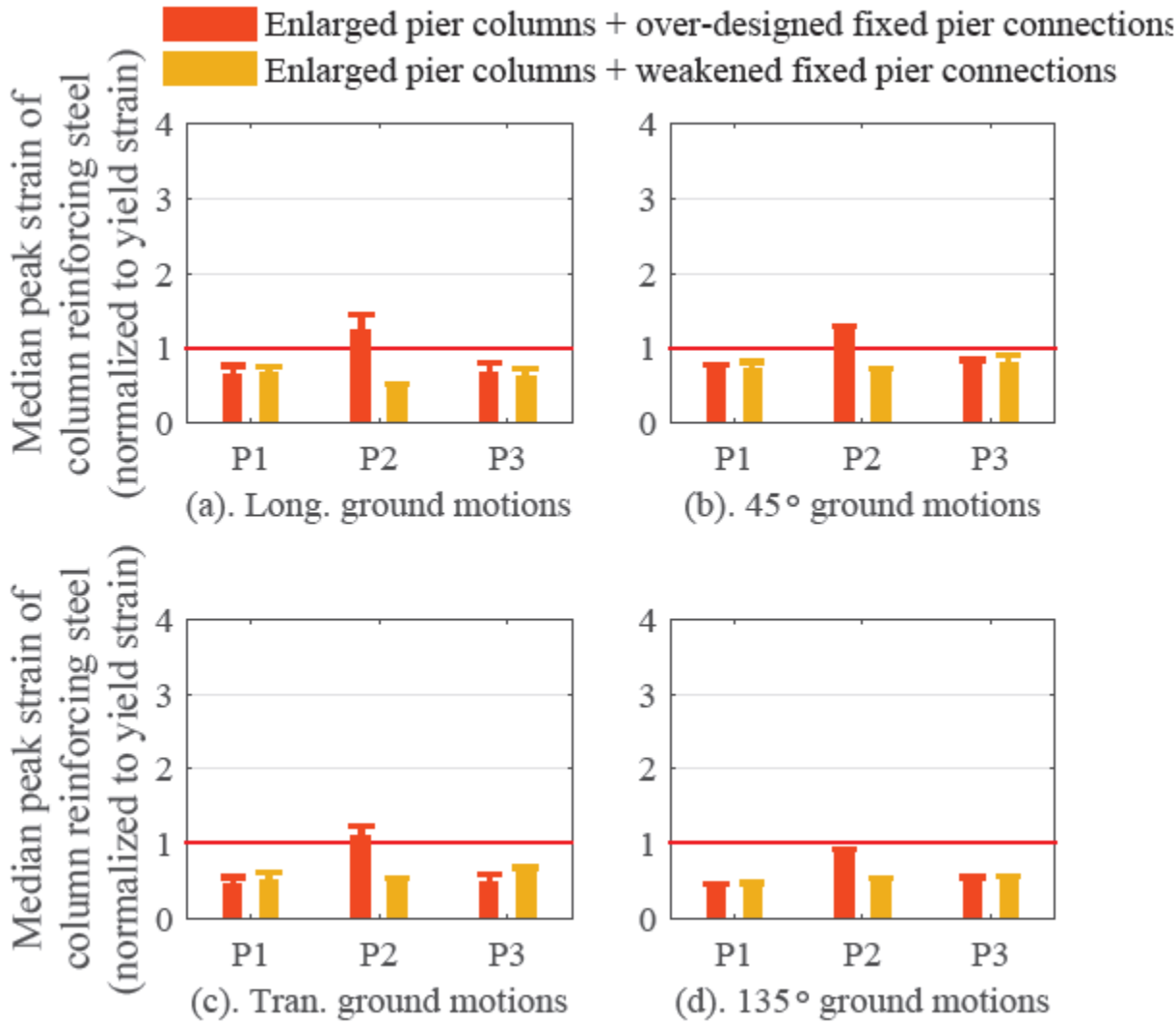

Figure D.41: Comparison of peak strain (median + median absolute deviation) of reinforcing steel at pier column bases of 4C30P15S bridge between Cases 2 and 3 of Table 5.5.

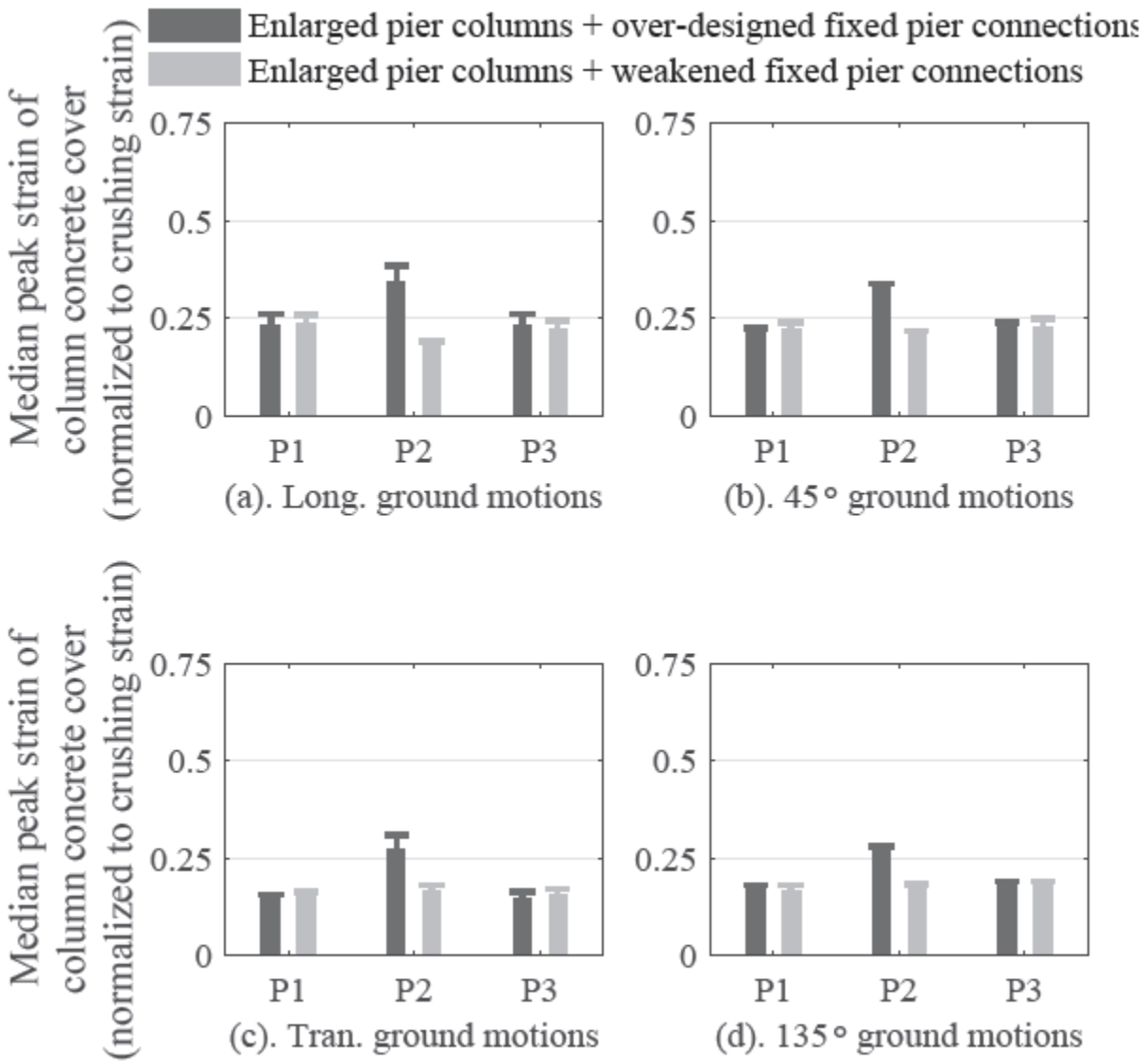

Figure D.42: Comparison of peak strain (median + median absolute deviation) of concrete cover at pier column bases of 4C30P15S bridge between Cases 2 and 3 of Table 5.5.

Illinois Department of Transportation

ILLINOIS